

UNIVERSITY OF OKLAHOMA

GRADUATE COLLEGE

CONVERSION OF OXYGENATES FROM BIOMASS-DERIVED COMPOUNDS
OVER SUPPORTED METAL CATALYSTS

A DISSERTATION

SUBMITTED TO THE GRADUATE FACULTY

in partial fulfillment of the requirements for the

Degree of

DOCTOR OF PHILOSOPHY

By

SURAPAS SITTHISA
Norman, Oklahoma
2012

CONVERSION OF OXYGENATES FROM BIOMASS-DERIVED COMPOUNDS
OVER SUPPORTED METAL CATALYSTS

A DISSERTATION APPROVED FOR THE
SCHOOL OF CHEMICAL, BIOLOGICAL AND MATERIALS ENGINEERING

BY

Dr. Daniel E. Resasco, Chair

Dr. Richard G. Mallinson

Dr. Lance L. Lobban

Dr. Rolf E. Jentoft

Dr. Kenneth M. Nicholas

© Copyright by SURAPAS SITTHISA 2012
All Rights Reserved.

ACKNOWLEDGEMENTS

First, I would like to record my sincerest gratitude to my Ph.D. thesis advisor, Dr. Daniel Resasco, for his guidance, encouragement, and patience. I would also like to thank him for being very inspirational, giving me this opportunity and allowing me the independence in designing the framework of the research work. It is a great pleasure working in his group, and will always be my best memory and treasure in my future career.

I would especially like to thank Dr. Richard Mallinson, Dr. Lance Lobban, Dr. Rolf Jentoft and Dr. Kenneth Nicholas for serving as my dissertation committees.

I would like to express my appreciation to my M.S. thesis advisor, Dr. Siriporn Jongpatiwut at the Petroleum and Petrochemical College, for introducing and giving me an opportunity to pursue my Ph.D. at OU. It is truly considered as the first important stepping stone to my future achievement.

I wish to express my gratefulness to Dr. Tawan Sooknoi at the King Mongkut's Institute of Technology Ladkrabang for being very flexible and understanding some tough situations that I faced during my time at the

beginning here. Without his personal and academic supports, I could not have made it this far.

I would like to thank Dr. Sundararajan Uppili, Dr. Tushar V. Choudhary and Dr. Walter Alvarez for the guidance and encouragement during my internship at ConocoPhillips. I enjoy very much the knowledge and wisdom of industrial practice that they have given me as well as the supportive opportunities. My experiences with ConocoPhillips have been very positive and rewarding and I believe that I have become a better scientist and person as a result of it.

I would like to thank all of faculty, my fellow students and post-docs which I have met and worked with during my time at OU. Moreover, I want to thank Dr. Wei An for his computational expertise and performing DFT calculations. I also would like to thank Pilar, Veronica, Sunya, Jimmy, Air and Mink for their warm support and friendship through different phases of my graduate study.

Most of all, I really want to express my great thankfulness to my parents and sister for their endless love, support and encouragement.

TABLE OF CONTENTS

1. Introduction and Background	1
1.1 Introduction	2
1.2 Biomass conversion to fuels	3
1.3 Pyrolysis of biomass and bio-oil	7
1.4 Bio-oil upgrading	9
1.5 Conversion of components derived from lignocellulose	13
1.5.1 Lignin conversion	13
1.5.2 Furfural conversion	15
1.6 Conversion of furfural to fuels and chemicals	18
1.6.1 Aldol-condensation	18
1.6.2 Hydrogenation of furfural to furfuryl alcohol	21
1.6.3 Decarbonylation	25
1.7 Surface study of oxygenates on metal surfaces	27
2. Experimental Setup	38
2.1 Catalyst preparation	38
2.2 Catalyst characterization	39
2.2.1 Temperature programmed reduction (TPR)	39
2.2.2 Carbon monoxide chemisorption	39
2.2.3 DRIFT of adsorbed CO	40
2.2.4 DRIFT of adsorbed furfural on copper catalyst	41
2.2.5 X-ray powder diffraction	41
2.2.6 Transmission electron microscopy	42
2.2.7 BET surface area	42
2.3 Catalytic activity testing	43
3. Comparative Study of the Furfural Conversion over Cu, Pd and Ni monometallic catalysts	45
3.1 Introduction	45
3.2 Catalyst characterization	46
3.3 Conversion of furfural over Cu/SiO ₂	48
3.4 Conversion of furfural over Pd/SiO ₂	52
3.5 Conversion of furfural over Ni/SiO ₂	56
3.6 Comparative analysis of the furfural	63

conversion on Cu, Pd and Ni catalysts	
3.7 Conclusion	69
4. Kinetics and mechanism of hydrogenation of Furfural on Copper Catalyst	74
4.1 Introduction	74
4.2 Cu/SiO ₂ Catalyst characterization	75
4.3 Furfural reaction over Cu/SiO ₂ catalyst	77
4.4 Kinetics of furfural conversion on Cu/SiO ₂	80
4.5 DRIFT spectra of furfural adsorbed on Cu	97
4.6 DFT calculations of furfural on Cu surfaces	101
4.7 Discussion	103
4.8 Conclusion	106
5. Conversion of Aldehydes on Pd/SiO ₂ and Bimetallic Pd-Cu/SiO ₂ Catalysts	110
5.1 Introduction	110
5.2 Catalyst characterization	111
5.2.1 Temperature Programmed Reduction (TPR)	111
5.2.2 DRIFTS of adsorbed CO	113
5.2.3 CO Chemisorption	116
5.2.4 X-Ray Photoelectron Spectroscopy (XPS)	117
5.3 Reaction of aldehydes on monometallic Pd/SiO ₂	119
5.4 Reactions of aldehydes on bimetallic Pd-Cu/SiO ₂	126
5.5 DFT calculations of 2-methylpentanal (MPAL) and furfural (FAL) adsorption on Pd(111) and PdCu(111) slabs	130
5.6 Discussion	139
5.6.1 Reaction of aldehydes on Pd/SiO ₂	139
5.6.2 Effect of Cu loading on Pd/SiO ₂	145
5.7 Conclusion	148
6. Conversion of Furfural on Bimetallic Pd-Fe Catalyst	153
6.1 Introduction	153
6.2 Conversion of furfural over Pd/SiO ₂ and Pd-Fe/SiO ₂ catalysts	154
6.3 Adsorption of furfural and furfuryl alcohol on Pd(111) and PdFe(111) surfaces	164
6.4 Mechanism of hydrogenolysis of furfuryl alcohol on Pd-Fe/SiO ₂ catalyst	169
6.5 Effect of supports on the 2-methylfuran	173

selectivity	
6.6 Conclusion	179
7. Conversion of Furfural on Bimetallic Ni-Fe Catalysts	181
7.1 Introduction	181
7.2 Catalyst characterization	183
7.3 Conversion of furfural over monometallic Ni catalyst	190
7.4 Conversion of furfural over Ni-Fe bimetallic catalysts	194
7.5 Conversion of furfuryl alcohol (FOL) over Ni-Fe bimetallic catalysts	201
7.6 Conversion of tetrahydrofurfuryl alcohol (HFOL) over Ni-Fe bimetallic catalysts	203
7.7 Conversion of benzyl alcohol (BZOL) over Ni-Fe bimetallic catalysts	204
7.8 Adsorption of furfural on Ni(111) and NiFe(111) surfaces	206
7.9 Discussion	213
7.10 Conclusion	218
8. Conversion of Catechol on Bimetallic Ni-Fe Catalysts	221
8.1 Introduction	221
8.2 Conversion of catechol over Ni/SiO ₂ and Ni-Fe/SiO ₂ catalysts	223
8.3 Mechanistic studies of catechol conversion on bimetallic Ni-Fe catalyst	225
8.4 Theoretical analysis of the proposed mechanism	234
8.5 Conclusion	236

APPENDICES

A Adsorption and Hydrogenation of Furfural on Cu Surface	239
B DFT Calculation on Reaction Pathway on Pd(111) and PdFe(111) surfaces	263
C Conversion of Furfural over Pd/TiO ₂	276

LIST OF TABLES

Table 3.1	Conversion and yield of products from the reaction of furfural over 10%Cu/SiO ₂ catalyst	49
Table 3.2	Conversion and yield of products from the reaction of furfural over 1%Pd/SiO ₂ catalyst. Reaction conditions: H ₂ /Feed ratio = 25, H ₂ pressure = 1 atm, TOS = 15 min	53
Table 3.3	Conversion and yield of products from the reaction of furfural over 5%Ni/SiO ₂ catalyst. Reaction conditions: H ₂ /Feed ratio = 25, H ₂ pressure = 1 atm, TOS = 15 min, FOL: furfuryl alcohol, HFOL: tetra hydrofurfuryl alcohol, BAL:butanal, BOL: butanol	58
Table 3.4	Selectivity of products from the reaction of furfural over 10%Cu/SiO ₂ , 1%Pd/SiO ₂ and 5%Ni/SiO ₂ catalysts. Reaction conditions, Temp = 230°C, H ₂ /Feed ratio = 25, H ₂ pressure = 1atm, TOS = 5 min	64
Table 4.1	Properties of the 10 wt% Cu/SiO ₂ catalyst	77
Table 4.2	Kinetic and thermodynamic parameters obtained from fitting the experimental data of with the kinetic model at various temperatures	87
Table 5.1	Characteristics of the catalysts investigated	116
Table 5.2	Adsorption energies (kJ/mol) and optimized bond lengths (Å) of 2-methylpentanal on Pd(111) and PdCu(111) slabs	133
Table 5.3	Adsorption energies (kJ/mol) and optimized Bond lengths (Å) of furfural on Pd(111) and PdCu(111)slabs	136
Table 6.1	Conversion and yield of products from the reaction of furfural and furfuryl alcohol over 1%Pd/SiO ₂ and	160

1%Pd-0.5%Fe/SiO₂ catalysts

Table 6.2	Comparison of bond lengths (Å) of furfural/furfuryl alcohol in gas-phase and adsorbed on Pd (111) and PdFe (111) surfaces. See Figure 6.4,6.5 and 6.6 for adsorption configurations and for the assignment of each C, O, and H atom. Adsorption energies (E_{ads}) in Kcal/mol are included.	168
Table 7.1	Physical properties of catalysts	186
Table 7.2	Conversion and yield of products from the reaction of furfural over 5wt.%Ni/SiO ₂ and 5wt.%Ni-2wt.%Fe/SiO ₂ catalysts	195
Table 7.3	Comparison of bond lengths of furfural in gas-phase and adsorbed on Ni (111) and NiFe (111) surfaces. See Figure 1 (a)-(e) for adsorption configurations and (f) for the assignment of C, O, and H atoms. Adsorption energies (E_{ads}) also included	209
Table 8.1	Conversion and product distribution for the reaction of catechol over Ni/SiO ₂ and Ni-Fe/SiO ₂ catalysts	233
Table 8.2	Bond lengths of catechol species on the surface. Adsorbed initial state (IS), transition state (TS1), and metastable (final) state	236
Table A.1	Calculated bond lengths (Å), bond angle (degree) and surface adsorption energy (eV), E_{ads} , for furfural adsorption on Cu(111).	246
Table A.2	Calculated bond lengths (Å), bond angles (degree) and surface adsorption energies (kcal/mol), E_{ads} , for furfural adsorption on Cu(110).	254
Table B.1	Comparison of characteristic bond lengths Of furfural/furfuryl alcohol in gas-phase and adsorbed on Pd (111) and PdFe (111) surfaces. See Figure B.1 and B.2 for adsorption configurations and for the	268

assignment of atoms. Adsorption energies
(E_{ads}) are included

LIST OF FIGURES

Figure 1.1	Figure 1.1 Summary of pathways for Cellulosic biomass conversion to liquid fuels	4
Figure 1.2	Proposed pathways for conversion of furfural to fuel components and chemical	20
Figure 1.3	Important oxygenate intermediates observed on transition metal surfaces	29
Figure 3.1	Temperature programmed reduction profiles (TPR) of 1%Pd/SiO ₂ , 5%Ni/SiO ₂ and 10%Cu/SiO ₂ catalysts	48
Figure 3.2	Selectivity of products from decarbonylation (Furan+THF) and hydrogenation (FOL+HFOL) reactions at difference temperatures. W/F = 9.6 g.cat.mol ⁻¹ .h, H ₂ /Feed ratio = 25, H ₂ pressure = 1atm, TOS = 15 min	56
Figure 3.3	Selectivity of products from decarbonylation (Furan), and hydrogenation (FOL+HFOL) and ring opening (BAL+BOL+Butane) reactions at difference temperatures. W/F = 4.8 g.cat.mol ⁻¹ .h, H ₂ /Feed ratio = 25, H ₂ pressure = 1atm, TOS = 15 min	59
Figure 3.4	Possible reaction pathways for furfural conversion over Cu, Pd and Ni catalysts	61
Figure 3.5	Selectivity of products from hydrogenation (FOL) over 1%Pd/SiO ₂ Ni/SiO ₂ and 10%Cu/SiO ₂ at different conversions. H ₂ /Feed ratio = 25, H ₂ pressure = 1atm, TOS = 15 min	65
Figure 3.6	Selectivity of products from decarbonylation (Furan), and ring opening (BAL+BOL+Butane) reactions (RO) over 1%Pd/SiO ₂ and 5%Ni/SiO ₂ at different conversions. H ₂ /Feed ratio = 25, H ₂ pressure = 1atm, TOS = 15 min	66

Figure 4.1	TEM micrograph of the 10% Cu/SiO ₂ catalysts, showing ~3-4 nm Cu clusters dispersed on the silica support particles (~ 50nm)	76
Figure 4.2	Yield of products from the reaction of (a) furfural (FAL) and (b) furfuryl alcohol (FOL) over 10 wt%Cu/SiO ₂ . Temp=290°C, H ₂ /feed ratio = 25, H ₂ Pressure = 1 atm, TOS = 15 min.	78
Figure 4.3	Partial pressures of the reactant and products from the reaction of furfural on the 10 %Cu/SiO ₂ catalyst at (a) 230°C, (b) 270°C and (c) 290°C. The points are experimental data and the lines are calculated from the kinetics model.	84
Figure 4.4	Partial pressures of the reactant and products from the reaction of furfuryl alcohol on the 10 wt%Cu/SiO ₂ catalyst at (a) 270°C and (b) 290°C. The points are experimental data and the lines are calculated from the kinetics model.	85
Figure 4.5	Partial pressures of the reactant and products from the reaction of a mixture of 50 mol% furfural and 50 mol% of furfuryl alcohol on the 10 wt%Cu/SiO ₂ catalyst at 270°C. The points are experimental data and the lines are calculated from the kinetics model.	86
Figure 4.6	Rate constants, k_i , a) and adsorption equilibrium constants, K_{ads} , b) as a function of inverse temperature.	89
Figure 4.7	Partial pressures of the reactant and products from the reaction of the following mixtures a). 50% FAL-50% MF b). 50% FOL-50% MF c). 30% FAL - 35% FOL-35% MF	92
Figure 4.8	Partial pressures of the reactant and products from the reaction of furfural in the presence of water at (a) 230°C (b) 270°C and (c) 290°C. Feed mole composition	95

-furfural:water, 1:20. The points are experimental data and the lines are calculated from the kinetics model.

- Figure 4.9** Conversion of furfural over 10 wt%Cu/SiO₂. 96
Temp=290°C, H₂/feed ratio = 25,
H₂ Pressure = 1 atm, TOS = 15 min.
- Figure 4.10** DRIFT spectra of 10 Cu/SiO₂ at 30°C 99
recorded before and after adsorption of (a);
and at increasing temperatures following
adsorption.
- Figure 4.11** DRIFT spectra of furfural adsorbed on 101
pure Cu metal powder at 30°C after
pretreatment in H₂ at 350°C for 1 h.
- Figure 4.12** The most stable configuration of furfural 102
on Cu(111)
- Figure 5.1** Temperature programmed reduction profiles 112
(TPR) of Pd and Pd-Cu catalysts.
- Figure 5.2** Infrared spectra of CO adsorbed on (a) 115
0.5Pd/SiO₂, (b) 0.25Cu-0.5Pd/SiO₂, (c)
0.5Cu-0.5Pd/SiO₂, (d) 2Cu-0.5Pd/SiO₂
and (e) 0.5Cu/SiO₂.
- Figure 5.3** X-Ray Photoelectron Spectroscopy (XPS) 118
of Pd_{3d} for different loadings of Cu in
Pd/SiO₂ catalysts.
- Figure 5.4** Conversion and product distribution 119
from furfural over 0.5%Pd/SiO₂ as a function
of W/F. Temp = 230°C, H₂/Feed ratio = 25,
H₂ pressure = 1atm, TOS = 15 min.
- Figure 5.5** (a) Yield and (b) selectivity of products 121
from furfural conversion over 0.5%Pd/SiO₂
catalyst as a function of reaction
temperature. W/F = 0.2 h, H₂/Feed ratio
= 25, H₂ pressure = 1atm, TOS = 15 min
- Figure 5.6** Conversion and product distribution from 123
2-methyl-pentanal over 5%Pd/SiO₂ catalyst.
Temp = 125°C, H₂/Feed ratio = 12,
H₂ pressure = 1atm, TOS = 15 min.

Figure 5.7	(a) Yield and (b) selectivity of products from the reaction of furfural on Pd/SiO ₂ as a function of Cu loading. W/F = 0.1 h, Temp = 230°C, H ₂ /Feed ratio = 25, H ₂ pressure = 1 atm, TOS = 15 min	127
Figure 5.8	(a) Yield of products from the reaction of 2-methyl-pentanal on Pd/SiO ₂ as a function of Cu loading. W/F = 3 h, Temp = 125°C, H ₂ /Feed ratio = 12, H ₂ pressure = 1 atm, TOS = 15 min (b) Ether/C5 ratio as a function of conversion for Pd/SiO ₂ and Pd-Cu/SiO ₂ catalysts	128
Figure 5.9	Yield of hydrogenation products on 0.5Pd/SiO ₂ , 0.5Pd-0.5Cu/SiO ₂ and 0.5Cu/SiO ₂ catalysts. W/F = 0.2 h, Temp = 250°C, H ₂ /Feed ratio = 25, H ₂ pressure = 1atm, TOS = 15 min.	129
Figure 5.10	DFT optimized structures of 2-methylpentanal (MPAL) in gas phase (a), and its adsorption on Pd(111) (b) and PdCu(111)(c-e) slabs. The corresponding bond lengths are given in Table 5.2	132
Figure 5.11	DFT optimized structures of furfural (FAL) in gas phase (a), and its adsorption on Pd(111) (b) and PdCu(111) (c-e) slabs. The corresponding bond lengths are given in Table 5.3.	135
Figure 6.1	Product distribution from the reaction of furfural over a monometallic 1%Pd/SiO ₂ catalyst, at 250°C, H ₂ /Feed ratio = 25, pressure = 1atm.	155
Figure 6.2	Possible surface species on the Pd surface during conversion of furfural	156
Figure 6.3	Product distribution from the reaction of furfural over a bimetallic 1%Pd-0.5%Fe/SiO ₂ catalyst, at 250°C, H ₂ /Feed ratio = 25, pressure = 1atm.	158
Figure 6.4	Optimized structures of gas phase	166

a) furfural and b) furfuryl alcohol

Figure 6.5	Optimized structures of furfural and furfuryl alcohol on Pd(111) surface	166
Figure 6.6	Optimized structures of furfural and furfuryl alcohol on PdFe(111) surface	167
Figure 6.7	Proposed reaction mechanisms for the conversion of furfuryl alcohol on Pd-Fe catalyst.	170
Figure 6.8	MS spectrum after the reaction of furfuryl alcohol with D ₂ on Pd-Fe/SiO ₂ catalyst.	172
Figure 6.9	2-Methyfurane selectivity as a function of furfural conversion over supported Pd-Fe catalysts at 250°C, H ₂ /Feed ratio = 25, pressure = 1atm.	174
Figure 6.10	X-ray photoelectron spectroscopy (XPS) of Pd _{3d} for Pd and Pd-Fe catalysts with different supports	176
Figure 6.11	XRD patterns of Pd and Pd-Fe catalysts with different supports	178
Figure 7.1	XRD patterns of monometallic Ni, Fe and bimetallic Ni-Fe catalysts reduced at 450°C for 1h.	185
Figure 7.2	TEM images of 5%Ni/SiO ₂ , 5%Ni-5%Fe/SiO ₂ , and 5%Fe/SiO ₂ catalysts after H ₂ pretreatment at 450°C for 1 h.	187
Figure 7.3	Temperature programmed reduction (TPR) of monometallic Ni, Fe and bimetallic Ni-Fe catalysts.	187
Figure 7.4	Product distribution from the reaction of furfural over a monometallic 5 wt.%Ni/SiO ₂ catalyst, at 210°C, H ₂ /Feed Ratio = 25, pressure = 1atm.	191
Figure 7.5	Yield of products from the reaction of	193

furfural over a monometallic 5 wt.%Ni/SiO₂ catalyst as a function of temperature. Reaction conditions: W/F = 0.1 h, H₂/Feed ratio = 25, pressure = 1atm.

- Figure 7.6** a) Yield and b) selectivity of products from the reaction of furfural over bimetallic Ni-Fe catalysts as a function of Fe loading. Reaction conditions: Temp. = 250°C, W/F = 0.1 h, H₂/Feed ratio = 25, pressure = 1atm. 197
- Figure 7.7** Product distributions from furfural conversion over various types of catalysts. Reaction conditions: Temp. = 250°C, W/F = 0.1 h, H₂/Feed ratio = 25, pressure = 1atm 198
- Figure 7.8** Product distribution as a function of temperature from the reaction of furfural over 5 wt.%Ni-2 wt.%Fe/SiO₂. Reaction conditions: Temp. = 250°C, W/F = 0.1 h, H₂/Feed ratio = 25, pressure = 1atm. 200
- Figure 7.9** Yield of products from the reaction of furfuryl alcohol over Ni-Fe bimetallic catalysts as a function of Fe loading. Reaction conditions: Temp. = 250°C, W/F = 0.1 h, H₂/Feed ratio = 25, pressure = 1atm. 202
- Figure 7.10** Yield of products from the reaction of benzyl alcohol over Ni-Fe bimetallic catalysts as a function of Fe loading. Reaction conditions: Temp. = 250°C, W/F = 0.1 h, H₂/Feed ratio = 25, pressure = 1atm. 205
- Figure 7.11** Optimized furfural structures of a) gas-phase b) adsorbed on Ni (111) and c) adsorbed NiFe(111) surfaces with a upright configuration 207
- Figure 7.12** Optimized structures of furfural adsorbed on a) Ni (111) surface and NiFe(111) surface b), c), d), and side view e) with a planar configuration 208

Figure 7.13	Calculated PDOS for furfural adsorbed on Ni(111) and NiFe(111) surface, corresponding to the adsorption configuration in Figure 7.12 (a)-(d), respectively. PDOS for clean surface (e) and gas-phase furfural (f) also included for comparison.	213
Figure 8.1	The m/z of catechol after the exchange on a) Ni-Fe and b) Ni catalysts	227
Figure 8.2	Proposed reaction pathways for conversion of catechol to phenol	228
Figure 8.3	The m/z of phenol product after the reaction of catechol over Ni-Fe/SiO ₂ catalyst.	229
Figure 8.4	The m/z of phenol after the H/D exchange over Ni-Fe/SiO ₂ catalyst.	230
Figure 8.5	Proposed reaction pathways for conversion of catechol to phenol via internal H transfer without incorporation of external H (or D)	231
Figure 8.6	Calculated structures along minimum-energy pathway for H-transfer step of catechol on NiFe(111)	234
Figure A.1	a) DFT optimized geometry of furfural in gas phase. Red, yellow and light blue spheres represent oxygen, carbon and hydrogen atoms, respectively. b). DFT optimized geometry of Cu(111) slab. Cu atoms are denoted by bluish grey spheres. Bond angles, bond lengths and some important distances (Å) are labeled.	242
Figure A.2	Plausible adsorption configurations of Furfural on Cu(111) in parallel modes	244
Figure A.3	Plausible adsorption configurations of furfural on Cu(111) in the parallel C=O modes.	244
Figure A.4	Plausible adsorption configurations of	245

furfural on Cu(111) in perpendicular modes.

- Figure A.5** Optimized geometries for plausible adsorption in parallel modes. The distances shown in the figure are in Å. 248
- Figure A.6** Optimized geometries for plausible adsorption in the parallel C=O modes. The distances shown in the figure are in Å. 249
- Figure A.7** Optimized geometries for plausible adsorption in the perpendicular modes. The distances shown in the figure are in Å. 252
- Figure A.8** DFT optimized surface layer geometry of Cu(110) slab. Cu atoms on top layer are denoted by bluish grey spheres, those in the second layer are denoted by brown spheres. Bond angles, bond lengths and some important distances (Å) are labeled. 253
- Figure A.9** Optimized geometries for adsorption configuration on Cu(110). The distances shown in the figure are in Å. 255
- Figure A.10** Optimized geometries of the adsorbed furfural molecules, transition states and intermediates Cu(111) via Mechanisms (a) and (b). The distances shown in the figure are in Å. 259
- Figure B.1** Optimized adsorption structures of furfural, furfuryl alcohol, methylfuran, and furan on Pd (111) and PdFe(111) surface and corresponding adsorption energies. (a) FAL/Pd; (b) FAL/PdFe; (c) FOL/Pd; (d) FOL/PdFe; (e) Furan/Pd; (f) Furan/PdFe. Additional adsorption structures see IS and FS in Figure B.2. For comparison, optimized structures of gas-phase furfural and furfuryl alcohol are displayed in (g) and (h). Characteristic bond length and binding distance (in Å) as well as adsorption energy are labeled. 267

- Figure B.2** Calculated structures along minimum-
Energy pathway for C-O bond scission
(a and b) and H-addition (c and d) in
furfural hydrogenolysis via furfuryl
alcohol route on Pd (111) and PdFe(111)
surface. IS: initial state; TS:
transition state; MS:metastable state;
FS: final state. Characteristic bond
length and binding distance (in Å)
as well as adsorption energy are labeled. 270
- Figure B.3** Energy profile for furfural hydrogenolysis 271
via furfuryl alcohol route on Pd (111)
surface (blue, $E_{a1}/E_{a2} = 36.0/19.5$ kcal/mol)
and PdFe(111) surface (red, $E_{a1}/E_{a2} =$
 $12.1/23.2$ kcal/mol). The zero line
represents the gas-phase furfuryl alcohol
and a clean slab.
- Figure B.4** Calculated PDOS for gas-phase FOL (a) 273
Clean surface (b) and FOL adsorbed on
Pd(111) surface (c) and on PdFe(111)
surface (d). Calculated d-band center for
pure Pd(111) surface and PdFe(111) surface
is -1.56 and -2.01eV, respectively.
- Figure C.1** Yield of products as a function W/F from 276
the conversion of furfural over 1%Pd/TiO₂.
Reaction condition: Temp. = 250°C, H₂/Feed
ratio = 25, pressure = 1 atm
- Figure C.2** Selectivity of products (conv. ~80%) 277
as a function of Pd loading from the
conversion of furfural. Reaction condition:
Temp. = 250°C, H₂/Feed ratio = 25, pressure
= 1 atm
- Figure C.3** Proposed reaction mechanism for 278
Conversion of furfural over Pd/TiO₂
catalysts

ABSTRACT

The increasing consumption and phase-out of conventional fuels has caused the tremendous interest of our society in making use of renewable energy resources such as biomass. In response to this interest, bio-oil produced from biomass feed stocks has been gradually making its contribution as a part of normal fuels. However, since the bio-oil is not stable due to its high oxygen content, upgrading is necessary to improve its performance. Since the high oxygen content of bio-oils has limited its storage ability and lowered its heating content, in some cases, removing oxygen or deoxygenating bio-oil molecules has been proposed as a recommended catalytic reaction. However, the role of the bio-oil upgrading process is not only to eliminate oxygen, but also to retain carbon in the liquid, preferably by the cleavage of C-O bonds. In the scope of this dissertation, the author will present how a detailed knowledge of the nature of adsorbed species on different metal surfaces leads to tailored catalysts with the desired properties for conversion of oxygenates derived from bio-oils.

In the first part of the dissertation, the author will focus on the deoxygenation reaction of furfural, which can be derived from biomass feed stocks and contain the aldehyde functional group, on different monometallic catalysts. Within this context, copper, palladium and nickel catalysts have been selected to study their activity, selectivity, and possible reaction pathways. The study of the behavior of different metals may be useful in designing catalytic strategies towards the production of fuel components with specific characteristics. For the second part of the dissertation, bimetallic alloy catalysts have been used for the conversion of furfural. In this regard, the product with minimal reduction of carbon yield has been achieved. For example, monometallic Pd catalyst is highly active for decarbonylation of furfural by C-C bond cleavage yielding furan and CO as the dominant product. However, the addition of Fe to Pd forming Pd-Fe alloy, making the C-O bond cleavage more favorable, can dramatically change the product selectivity from furan to 2-methylfuran.

CHAPTER 1

Introduction and Background

1.1 Introduction

The increasing consumption and phase-out of conventional fuels has derived the tremendous interest of our society in making uses of renewable energy resources such as biomass to generate renewable, bio-derived fuels, which offer lower net green house gas (GHG) effects on global warming. The biomass-derived fuels can be produced from lignocellulosic, carbohydrate, and lipid feedstocks. Among them, bio-oil obtained by fast pyrolysis has a good potential as a second-generation bio-derived fuel because it can be produced in high volumes without threatening food supplies and biodiversity [1,2]. Depending on their origin, these feedstocks can contain different concentrations of oxygen (up to 50 wt%) and varying oxygenated compounds. For example digestion of cellulose produces sugars, which can be dehydrated into furfurals, or decomposition of lignin fractions produces phenolic compounds (guaiacols, anisoles, cresols)[3,4]. The poor properties of bio-oils such as low heating value,

immiscibility with hydrocarbon fuels, chemical instability, high viscosity, corrosiveness, result from their oxygen-rich composition [5]. Therefore, bio-oil upgrading is a requirement to transform the oxygenate compounds into fungible fuels. The upgrading of bio-oils primarily involves hydrodeoxygenation (HDO), because oxygen enhances the reactivity of the bio-oil components, resulting in the mentioned undesirable properties. Furfural, being one of the oxygenates commonly found in bio-oil, this research work mainly focuses on the study of furfural conversion as a main aromatic aldehyde derived from bio-oil. The objective of this dissertation is to study the reaction chemistry of furfural and its related compounds and optimize the transformation of these feeds into valuable chemicals and fuel compounds. Although a great deal of work has been done on the performances of different catalysts in reactions of furfural, there are still open fundamental questions on how the furfural molecule adsorb and react on metal surfaces. From the knowledge obtained from studies of other oxygenates, it is possible that the furfural adsorption modes and reaction routes might change from one metal to another and from metal to oxide surfaces. In addition, the adsorption configurations and reaction pathways also change as one

varies the metal composition from mono-metallic to bimetallic catalysts. These changes will eventually affect the product distribution of the furfural reaction. Finally, all of this information will be gathered and processed to provide the complete strategy to optimize the production of desirable chemicals and fuel compounds from furfural and other oxygenates derived from bio-oil.

1.2 Biomass conversion to fuels

Although biomass can be utilized in its raw state as an energy source, for example, by co-combustion with fossil fuels for electricity generation, there are compelling reasons to find ways of converting biomass into liquid fuels. In the case of lignocellulosic biomass (Figure 1.4), there are three main approaches that can be considered [6,7].

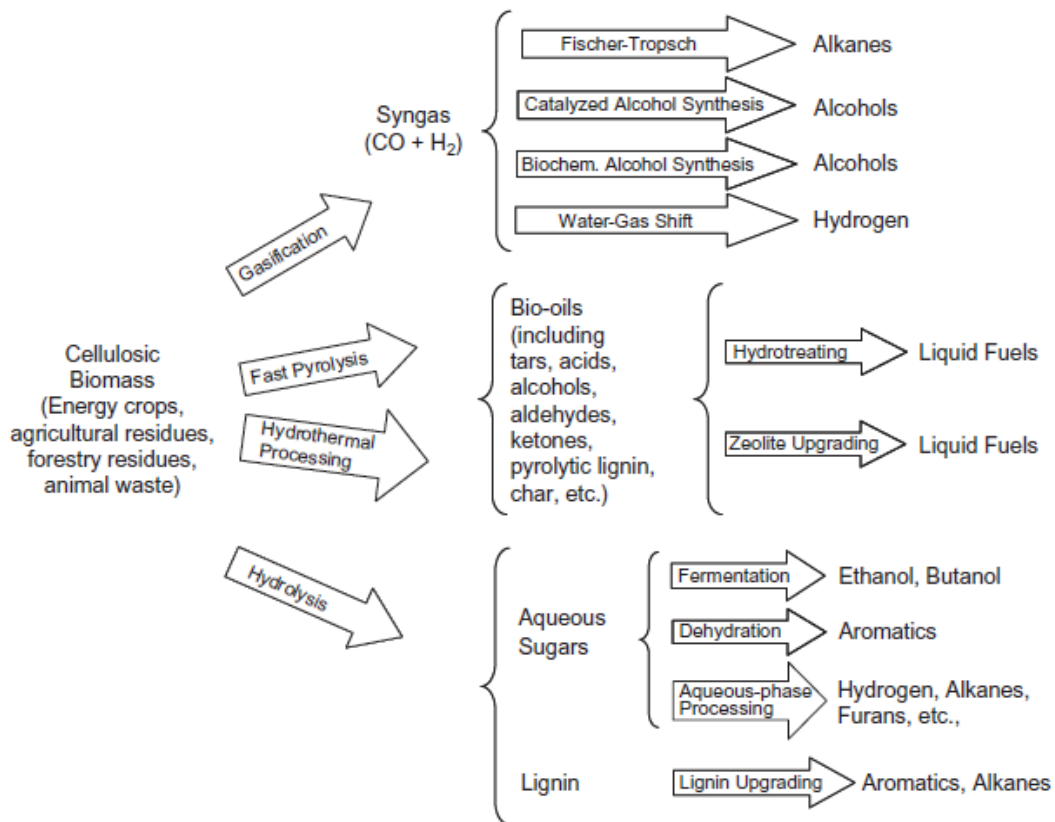


Figure 1.1 Summary of pathways for cellulosic biomass conversion to liquid fuels [7]

In the first of these, biomass is gasified to produce syngas, which after treatment to remove tars and other impurities, can be catalytically converted to hydrocarbons (via the Fischer-Tropsch synthesis) or to alcohols. Other options include syngas conversion to ethanol using certain types of anaerobic bacteria, or treatment with water-gas shift catalysts to generate additional hydrogen from the water and carbon monoxide present. The resulting hydrogen

can be used in a variety of refinery and chemical processes, as a fuel for PEM fuel cells, etc. A second approach involves the use of direct thermochemical conversion processes, in which biomass is heated in the absence of air to produce a crude bio-oil. One such process is fast pyrolysis, in which the production of liquids is maximized by the use of short residence times (1-2 s) and high processing temperatures (ca. 500°C) [8]. In solvolysis, which is often referred to as hydrothermal upgrading when the solvent used is water, biomass is typically treated for 5-20 min with water under subcritical conditions (300-350°C, 10-18 MPa) [9]. A third option is high-pressure liquefaction. This is also a single step process, which utilizes longer residence times and lower temperatures than fast pyrolysis (ca. 300-400°C), hydrogen pressures of up to 20 MPa, and typically requires the addition of a catalyst [10]. Due to the hydrogen requirement, the economics of this process are generally considered to be inferior to those of fast pyrolysis or solvolysis [11]. A commonality of the crude bio-oils resulting from these direct conversion processes is that they cannot be used as transportation fuels without subsequent upgrading due to their high oxygen content (up to 40 wt% on a dry basis) and water content

(up to 25 wt%). Upgrading typically requires either hydrotreating or catalytic cracking to eliminate the oxygen functionalities present in the oil [12,13]. The third approach to lignocellulosic biomass conversion to liquid fuels involves the use of enzymes or acid- or base-catalyzed hydrolysis to decompose the sugar polymers present into their constituent monomers. These sugars can then be fermented to alcohols, dehydrated over acid catalysts to give aromatics, [14] subjected to catalytic aqueous phase processing to give a variety of fuel-type products such as furans, alkanes and hydrogen (depending on the process), [15,16] or converted to a variety of chemicals. Efficient processes for utilization of the lignin remaining after removal of the sugars have yet to be found, although catalytic conversion of lignin to aromatics and alkanes by hydrotreating) or aromatics and coke (by catalytic cracking) has been demonstrated [17].

1.3 Pyrolysis of biomass and bio-oil

During the past decade, there have been numerous studies dedicated to the pyrolysis of biomass. It is conceivable that high heating rates and short reaction times in the pyrolysis process (i.e. so-called fast or flash pyrolysis) afford high yields of liquid products. Biomass is rapidly heated up to 500-600 °C in the absence of air/oxygen, which leads to decomposition of the biomass to a mixture of vapors and aerosols. Subsequently, the rapid cooling/condensation produce gases, char, and a dark viscous liquid, the bio-oil. Yields and properties of corresponding vapor, liquids, and solid products obtained from pyrolysis processes strongly depend upon various variables such as the nature of the feedstock, heating rate, and reaction temperature. Generally, pyrolysis is a purely thermal process; however, some catalysts may be used during the conventional process [18-23].

Again, the amount of bio-oil, gas, and char produced from pyrolysis of wood depends on the chosen conditions [24]. For examples, charcoal, CO₂ and water are predominant product for a pyrolysis at lower temperature (< 400 °C) and heating rates (0.01-2 °C/s). This reaction path is shifted to liquid bio-oil production at higher temperature

(400-800°C) and heating rate (10-1000 °C/s). As the pyrolysis temperature increased further, biomass can be cracked to mainly gaseous products such as CO, H₂ and CH₄.

Bio-oil is a complex mixture containing carbon, hydrogen and oxygen. It is composed of different species of oxygenated compounds including carboxylic acids, alcohols, aldehydes, esters, ketones, sugars, phenols, guaiacols, syringols, and furans [25,26]. In addition to these organic compounds, the as-received bio-oil contains a lot of water, practically therefore, it can be divided into four fractions: namely aliphatic, aromatic, polar and non-volatile parts, by using solvent extraction and liquid chromatography techniques [27]. Analysis revealed a high concentration of small polar components such as acetic acids and hydroxyacetones in the aqueous phase; and the highly oxygenated aromatic component in the oil phase.

Bio-oil is mainly composed of levoglucosan, furfural, phenols (with methyl, methoxy and/or propenyl groups), aldehydes (including benzaldehyde with methyl and/or hydroxyl) and vanillin, and also observed that these compositions are similar regardless of the species of wood [23,28]. In addition, it is noted that phenol and furan

derivatives are the predominating compounds existing in the organic fraction of bio-oils.

1.4 Bio-oil upgrading

Bio-oils must be upgraded if they are to be used as a replacement for diesel and gasoline fuels. As was said in the previous section, the properties that most negatively affect bio-oil fuel quality are low heating value, incompatibility with conventional fuels, solids contents, high viscosity, incomplete volatility, and chemical instability. These problems are mainly contributed from the presence of oxygen content in the bio-oil. Hence, upgrading processes are required to remove the oxygen. Different approaches can be applied for the upgrading of bio-oils. Heterogeneous catalysts can be employed during the pyrolysis process in order to modify the vapor composition; otherwise, they can be used with bio-oils in order to modify the type and amount of functional groups in the oils. There are several techniques, both physical and chemical methods have been studied.

Since the late 1980s, vapor phase catalytic reactions during the pyrolysis of biomass, in which zeolite

materials were used as catalysts have been studied [29-36]. In 1997, Katikaneri *et al.* combined catalytic approach into a fluidized bed reactor during the pyrolysis [37]. They used the solid catalyst (i.e., HZSM-5) as fluidizing material in the reactor. The liquid and gaseous products were separated and collected. In addition, they also studied the catalytic upgrading of pyrolysis oil produced from maple wood by the RTP™ process from ENSYN Technologies Inc [38]. Zeolites and silica-alumina catalysts were employed for these investigations. It is remarkable that the silica-alumina catalyst exhibited the highest selectivity for aliphatic hydrocarbons, whereas the HZSM-5 catalyst afforded the highest selectivity toward aromatic hydrocarbons and the highest yield of organic liquid product. Another similar work on zeolites was reported by Williams *et al.* [39,40]. The objective was to investigate the effect of the presence of zeolites on formation of hazardous polycyclic aromatic hydrocarbons. It was noted that using zeolite catalyst for vapor phase upgrading during the pyrolysis resulted in an increased heavy aromatic compound production. At the same time, the yield of pyrolysis oil decreased, while char and gaseous formation increased. Adjaye *et al.* [41,42] exhibited that HZSM-5 was the most effective catalyst for producing the

organic distillate fraction, overall hydrocarbons and aromatic hydrocarbons and the least coke formation. Reaction pathways were proposed that bio-oil conversion proceeded through the thermal decomposition and then followed by thermocatalytic conversion. The former step converted the bio-oil into light and heavy organics, as well as chars from polymerization of the bio-oil; while the later produced gas, water, coke, tar, and the desired organic fraction.

Oxygen existing in bio-oils can be removed catalytically as H_2O , CO_2 , or CO . Nokkosmaki *et al.* [43] claimed that using ZnO catalyst in the pyrolysis vapor reaction can minimize the loss of liquid yields and improve the stability of the bio-oils. Adam *et al.* [28] showed the effects and catalytic properties of the mesopore structured MCM-41 based catalysts on bio-oil upgrading. It was found that the catalyst enhanced the production of acetic acid, furfural and furans, while the yields of phenolic compounds reduced.

Another promising approach to obtain high quality bio oils is the hydrotreating processes. Generally, the reaction was performed by the catalysts of Co-Mo, Ni-Mo and their oxides on the Al_2O_3 supports under elevated

pressure of hydrogen and/or CO. Oxygen is basically eliminated in the forms of H₂O and CO₂, in which the energy concentration of the bio-oils is enhanced. Pindoria *et al.* [44,45] hydrotreated the vapor from fast pyrolysis and indicated that that the catalyst deactivation resulted from the strong adsorption of the organic components themselves, which poisoned the acid sites, rather than the coke deposition. Elloit *et al.* [46] examined the effect of the flow directions on the conversion of bio-oils in a fixed bed reactor. They showed that the down-flow configuration brought about higher conversion as compared with the up-flow configuration. In addition, a two-fold conversion increase was observed over NiMo/ γ -Al₂O₃, in comparison to CoMo/spinel catalysts.

The upgrading reaction using sulfided catalysts (i.e., sulfided Co-Mo-P/Al₂O₃) was investigated by Zhang *et al.* [47]. This liquid phase reaction was operated at high pressure (2 MPa) of hydrogen and temperature of 360°C with the hydrogen donor solvent tetralin. It was marked that the oxygen content was reduced by 39%, and consequently the corresponding upgraded bio-oil was soluble in the hydrocarbon solvent. Boocock *et al.* studied the elimination of methoxy groups of phenol derivatives in

bio-oils [48]. Sulfided and unsulfided forms of $\text{Mo}_x\text{O}_y/\text{Co}_x\text{O}_y/\gamma\text{-Al}_2\text{O}_3$ and $\text{Mo}_x\text{O}_y/\text{Ni}_x\text{O}_y/\gamma\text{-Al}_2\text{O}_3$ were used as catalysts. It was claimed that the sulfided cobalt oxide catalyst gave a higher loss of methoxy groups in the bio-oils. A commercial $\text{Ru}/\gamma\text{-Al}_2\text{O}_3$ catalyst and a copper chromite (CuCr_2O_4) catalyst were also tested by Gagnon *et al.*, [49] which suggested the optimum temperature for hydrodeoxygenation is as low as 80°C .

1.5 Conversion of components derived from lignocellulose

All components of lignocellulose should be utilized in fuel or chemical production in an integrated biorefinery. A number of non-carbohydrates can be selectively produced from lignocellulose, including lignin, furfural (from xylose), and levulinic acid (from cellulose). All of these compounds can be converted into fuels or chemicals.

1.5.1 Lignin conversion

Lignin, which consists of coniferyl alcohol, sinapyl alcohol, and coumaryl alcohol polymers, represents a major

fraction of biomass (10-30 wt %) and is currently used as a low-grade fuel to provide heat in the pulp and paper industry. Designs of ethanol production in a lignocellulosic plant also show lignin being used to provide process heat [50]. However, it would be ideal to convert the lignin into a higher value fuel or chemical. This would also require the development of alternative ways of providing process heat to the biorefinery or developing less energy intensive processes. Lignin can be used as a replacement for phenol-acetone resins, and other uses are being developed [51]. Lignin also can be converted into a transportation fuel by hydrodeoxygenation or zeolite upgrading. These are the same methods used to upgrade bio-oils, that contain a large fraction of lignin products. Previous hydrodeoxygenation experiments of lignin feedstocks have used sulfided NiMo and CoMo catalysts supported on alumina, chromium, and zeolites at 250-450°C [52,53,54,55]. The major products from hydrodeoxygenation include phenols, cyclohexane, benzene, naphthalene, and phenanthrene with liquid oil yields of 61% the original lignin. It is likely that coking reactions occur under reaction conditions and deactivation due to water, similar to what was observed by Delmon and co-workers for hydrodeoxygenation of guaiacol [56,57,58].

The reactions that occur during hydrodeoxygenation include hydrogenation of C=C bonds, hydrogenation of aromatics, and deoxygenation of C-O bonds.

1.5.2 Furfural conversion

Over the past couple of years, several research groups have described approaches to converting six-carbon sugars such as glucose and fructose into a chemical called hydroxymethylfurfural or HMF. This molecule represents a renewable building block for the synthesis of plastics, and industrial and household chemicals. Now, a sister chemical to HMF, furfural, is beginning to gain the attention of cellulosic ethanol producers and academic researchers. Furfural is an almond-scented, oily, colorless liquid that turns yellow to dark brown when exposed to air. It is used as a solvent for refining lubricating oils, as a fungicide and weed killer and in the production of tetrahydrofuran, an important industrial solvent. In addition, furfural along with its sister molecule HMF, can serve as a building block for other potential transportation fuels including dimethylfuran and ethyl levulinate [59]. Furfural is the triple dehydration product of xylose and is an important chemical obtained from the hemicellulose biomass fraction. Industrially,

more than 300,000 metric tons/year of furfural are produced [60]. Furfural is currently too expensive for use as a fuel; however, future production of furfural in an integrated biorefinery where all fractions of biomass are used could significantly decrease the cost. The Quaker Oat Company in 1922 developed the first commercial process for production of furfural from oat hulls using acid catalyst [61]. During the production of furfural, superheated steam passes through a reactor containing the biomass to provide heat for the reaction and remove the furfural product. Furfural is reactive under these conditions, so it is vital to remove the furfural before it undergoes undesired reactions. Typical reaction conditions for furfural production are 3 wt % sulfuric acid, 2:1 to 3:1 acid solution to lignocellulosic mass ratios, 170-185°C, and 3 h retention time [60].

Sulfuric acid is not necessary if the temperature is raised high enough. This is because acetic acid in the hemicellulose reaction is released and can catalyze the dehydration reaction [61]. Typical furfural yields are around 45-50% [60]. Higher yields of up to 60% can be obtained by acid-catalyzed dehydration of pure xylose [62]. According to Zeitsch, the principle yield loss of

furfural is due to reactions between furfural and xylose, and by eliminating this problem by proper reactor design, significantly better yields can be obtained [63,64]. Another new method, tested at the pilot-plant scale, appears to be promising for producing furfural at yields as high as 70%. This method involves using a continuous tubular reactor at high temperature (250°C), short residence time (5-60 s), acid concentrations from 0.3 to 2.0 wt %, and steam injection to rapidly remove the furfural [60]. The mechanism for formation of furfural from xylose appears to go through a 2,5-anhydride intermediate [62]. Furfural can also be produced from xylose using heterogeneous catalysts including MCM functionalized sulfonic acid catalysts [65], heteropolyacids [66], faujasite, and mordenite [67]. However, furfural by itself can not be used as a motor fuel because of its tendency to polymerize.

1.6 Conversion of furfural to fuels and chemicals

Several pathways have been proposed for conversion of furfural to fuel components and chemical as shown in Figure 1.2.

1.6.1 Aldol-condensation

Biomass-derived sugars can be upgraded to conventional fuels through the combination of aldol-condensation reactions and hydrogenation/dehydration reactions. Dumesic et al. [68,69] have done seminal work in this area, applying molecular engineering concepts to formulate refining strategies for the production of renewable fuels.

The aldol-condensation reaction is initiated by the abstraction of the α -hydrogen from aldehydes and ketones, in the presence of a basic catalyst. The resulting enolate reacts with the carbonyl carbon of another molecule to form the aldol-product that, after dehydration, forms an α,β -unsaturated carbonyl molecule.

Although furfural molecules do not have α -hydrogens, it is possible to perform cross-condensation reactions with other aldehydes and ketones, like acetone and propanal. In this approach, diesel and jet fuel can be produced by the coupling of C5-C6 furfural molecules with C3 aldehydes and ketones. The cross-condensed products, ranging from C8 to C15, can be hydrogenated at low temperatures (100-150°C) to decrease their solubility in the aqueous phase and their oxygen content. High temperatures and bifunctional catalysts (acid and metal) are required to perform dehydration and hydrogenation reactions in order to remove the residual oxygen and produce C8 to C15 alkanes. Another route proposed by these authors was based on the partial hydrogenation of the aromatic ring in the furfural molecules, in which an α -hydrogen is generated and 5-hydroxymethyl-tetrahydrofurfural (HMTHFA) and tetrahydro-2-furfural (THF2A) are formed as products. These molecules can then react by self aldol-condensation to generate C10 to C12 products.

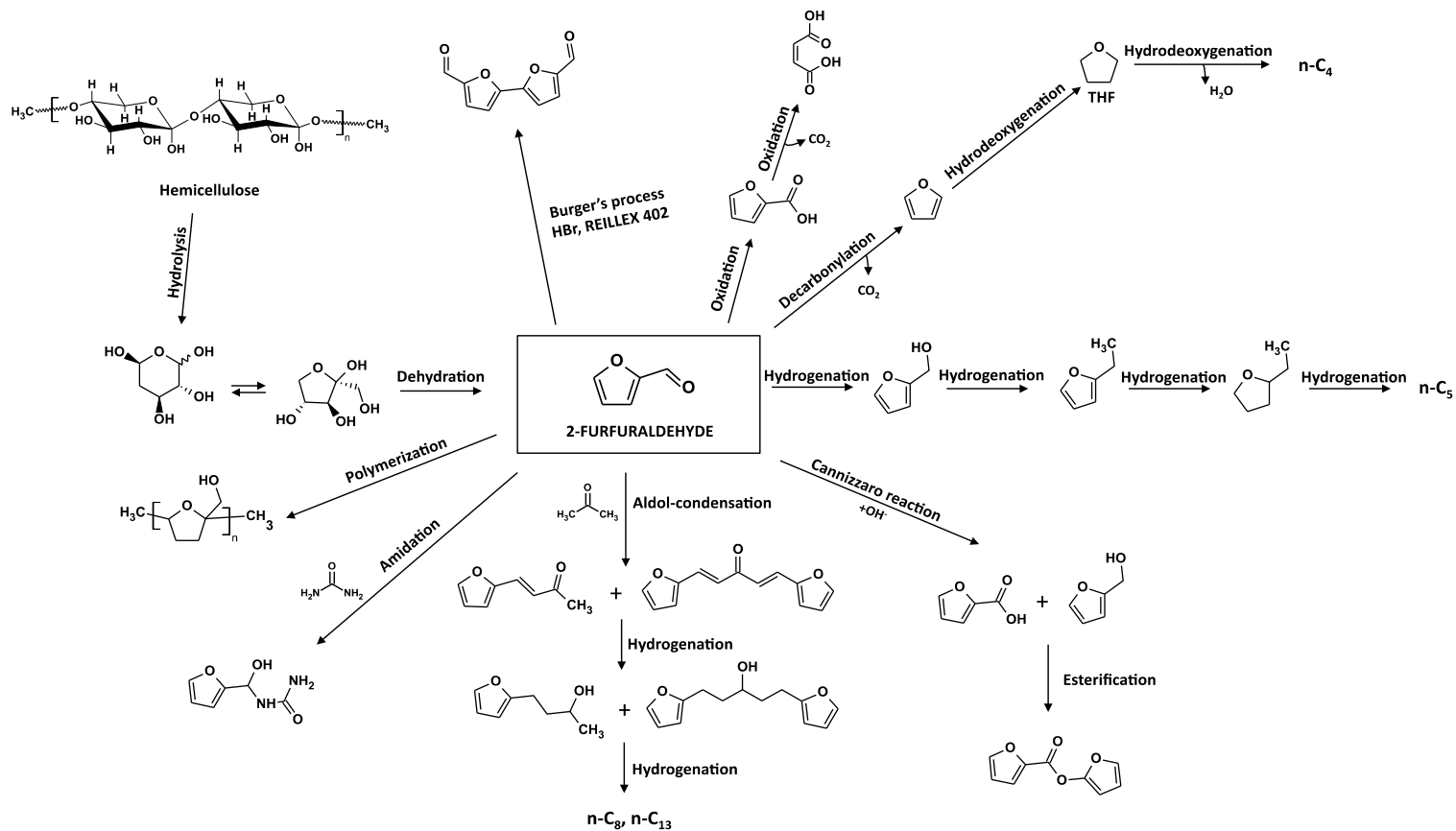


Figure 1.2 Proposed pathways for conversion of furfural to fuel components and chemical

The aldol-condensation reactions are carried out in polar solvents, such as water or water-methanol, and usually catalyzed by homogeneous bases like NaOH or $\text{Ca}(\text{OH})_2$. However, in homogeneous catalysis, for every 10 parts of product formed, 1 part of spent catalyst is generated, which increases up to 13 % the selling price of the product due to required purification, recovery, and waste treatments [70]. In contrast, heterogeneous catalysts are readily separated by filtration methods and, depending on the reactor configuration, they can be used for vapor phase [71,72], liquid-phase [73,74], or biphasic liquid, [75] systems.

1.6.2 Hydrogenation of furfural to furfuryl alcohol

Hydrogenation of furfural with hydrogen gas on metal catalysts produces mainly furfuryl alcohol. This alcohol finds uses as a solvent, but is primarily used as an ingredient in the manufacture of chemical products such as foundry resins, adhesives, and wetting agents [74]. The catalysts most typically used in furfural hydrogenation are metals because they are able to dissociate hydrogen, thus making hydrogenation possible. The choice of catalyst

support is based on its ability to disperse and stabilize metal particles enhancing the active surface area. Compared to other aldehydes, in addition to the carbonyl group, furfural contains an aromatic furanyl ring that could be also hydrogenated. While carbonyl hydrogenation is usually preferred due to the high stability of the aromatic ring, metal catalysts that have strong interactions with the unsaturated C=C bonds can still saturate the ring. Therefore, the selectivity toward aromatic alcohols is strongly dependent on the metal catalyst used. Furthermore, the geometric and electronic properties of different metals can affect both hydrogenation activity and selectivity by influencing the type of adsorption intermediates. In this section we will primarily discuss the differences observed in furfural hydrogenation on group IB and VIII metals.

Among the group IB metals, Cu has been the most intensively investigated as a catalyst for furfural hydrogenation [76-82]. Silver has been used in a few studies while there is no report on Au catalysts [83]. The group IB metals are significantly less active than other metals. However, they exhibit a remarkable selectivity towards hydrogenation of the carbonyl group leaving the

C=C double bonds in the furanyl ring unreacted. In this sense, Cu has been found to be the most selective among all tested metal catalysts. Selectivities above 98 % to furfuryl alcohol have been achieved over monometallic Cu/SiO₂ catalysts [82]. Also, monometallic Ag catalysts have been found to be able to hydrogenate the C=O group of furfural with relatively good selectivity, but not as high as that of Cu. For example, 80 % selectivity was obtained over a Ag/SiO₂ catalyst prepared by the sol-gel method [84].

The group VIII metals (Ni, Pd, and Pt) have also been used for furfural hydrogenation in both vapor and liquid phases on different supports; they all exhibit significant activity and selectivity [83], particularly at low temperatures (i.e., below 200°C). For example, Ni catalysts have been used at low temperatures (100°C) in liquid phase, exhibiting > 95 % selectivity to furfuryl alcohol [85,86]. Likewise, supported Pt catalysts doped with transition metal oxides have exhibited high selectivity, e.g., Pt/TiO₂/SiO₂ (selectivity = 94%) and Pt/ZrO₂/TiO₂ (selectivity = 95%) [87]. However, at higher temperatures (> 200°C) the selectivity to alcohols on group VIII metals drops significantly upon the appearance

of other reactions. For example, over a Ni/SiO₂ catalyst at 230°C and excess of hydrogen (H₂/feed ratio = 25), only 25% selectivity to furfuryl alcohol was observed [88]. On Pd catalysts, it is even lower, e.g., a Pd/SiO₂ catalyst at 230°C yielded 14 % selectivity [89] and a Pd-Y catalysts at 350°C rendered only 1% selectivity to furfuryl alcohol [90]. The lower selectivities observed at high temperatures on group VIII metals can be ascribed to the emergence of decarbonylation and ring opening reactions. In addition, hydrogenation of the furanyl ring yielding the saturated alcohol is also observed over group VIII metal catalysts due to a stronger interaction of the furanyl ring with the metal surface than that obtained with group IB metals [91]. As a result, Cu and Ag should be the preferred catalysts if high selectivity to furfuryl alcohol is desirable, particularly at high temperatures. However, the intrinsic activity for furfural hydrogenation is lower on group IB metals than on group VIII metals, which is typically explained by the difference in extent of d-orbital filling. That is, the d-orbitals are filled in group IB, reducing the bond strength.

1.6.3 Decarbonylation

The decarbonylation of furfural results in the production of furan, which could be utilized as a fuel component, but also as a chemical intermediate. For example, furan can be subsequently hydrogenated to tetrahydrofuran, which is commonly used as solvent and as a starting material for polyurethane manufacture [74]. While decarbonylation of furfural can be carried out in both the vapor and liquid phases, [92-94] the former is generally preferred due to the advantage of simpler operation and the possibility of easier catalyst regeneration and reuse. Different catalysts have been tested for this reaction. They include metal oxides such as Mn, Zn, Cd, Sr, K, Fe, Mo, and Cr oxides [95-97] or group VIII metals such as Pd, Pt, Rh, Ni [98,99]. The latter are known to be effective catalysts and to result in high yields at rather mild conditions. By contrast, the former require more severe operating conditions and promote formation of heavy products that may cause catalyst deactivation.

Among the group VIII metals, Pd has been the most intensively investigated as the active metal in furfural decarbonylation, [100,101] while Pt and Ni have been used

less often. It has been found that the high decarbonylation activity of Pd may be modified by the incorporation of a second metal (alloy formation) [89] or additives such as alkali and alkaline-earth metals [102]. Although Pd catalysts are relatively more active than other catalysts, the yield of furan decreases sharply with time on stream. For example, after 3 h on stream a Pd/C catalyst was found to lose most of its decarbonylation activity. An even faster deactivation was observed on a Pd/Al₂O₃ catalyst [103,104]. Among the various possible reasons for the observed deactivation, the most commonly proposed is carbon deposition, which could be due to side reactions, such as condensation and/or decomposition of furfural. Earlier studies demonstrated that a rapid loss in the activity of Pd/Al₂O₃ was observed in the absence of hydrogen, but the activity could be partially recovered by increasing the hydrogen partial pressure [100].

1.7 Surface study of oxygenates on metal surfaces

The literature of oxygenate surface chemistry and catalysis on transition metal surfaces has grown enormously over the past 20 years, with an increasingly large proportion focusing on fundamental mechanistic studies employing surface science techniques. The majority of surface studies mainly focus on the reaction mechanisms of these molecules on transition metals of group VIII and IB. The reaction pathways and product selectivities observed during the decomposition of aldehydes and alcohols on clean transition metal surfaces appear at first glance to be quite diverse and strongly dependent on the identity of the metal and the detailed molecular structure of the reactants [105]. Nevertheless, spectroscopic identification of surface-bound reaction intermediates provides evidence for the fundamental similarities in the reaction mechanisms of aldehydes and alcohols on many transition metal surfaces. For example, the typical reaction sequence characteristic of alcohol decomposition on group VIII metals involves formation of an alkoxide intermediate via hydroxyl-hydrogen elimination, followed by α -H abstraction leading to an aldehyde intermediate bonded to the surface either via

both carbon and oxygen atoms of its carbonyl function (designated as $\eta^2(\text{C},\text{O})$ -coordination) or via its oxygen atom only ($\eta^1(\text{O})$ -coordination). Oxygen precovered surfaces promote the $\eta^1(\text{O})$ -coordination of aldehyde intermediates, which tend to desorb rather than decompose further, as is the case with the $\eta^2\text{-C},\text{O}$ configuration of aldehyde intermediates. The latter route leads to acyl intermediate formation followed by CO elimination and the release of volatile hydrocarbons. Carboxylates may also be formed from aldehydes in the presence of surface oxygen or by dissociative adsorption of carboxylic acids. Thus the roster of surface intermediates needed to account for oxygenate chemistry includes alkoxides, η^1 - and η^2 -aldehydes, acyls, and carboxylates, shown schematically in Figure 1.3. Considerable spectroscopic evidence for each of these species has been developed on a number of metal surfaces and much, but not all, surface oxygenate chemistry can be explained in terms of their formation and reaction. One advantage of establishing the framework of surface oxygenate chemistry around these common intermediates is that it permits one to identify examples of chemistry that they cannot explain, leading to the

proposal of new surface intermediates and reaction pathways.

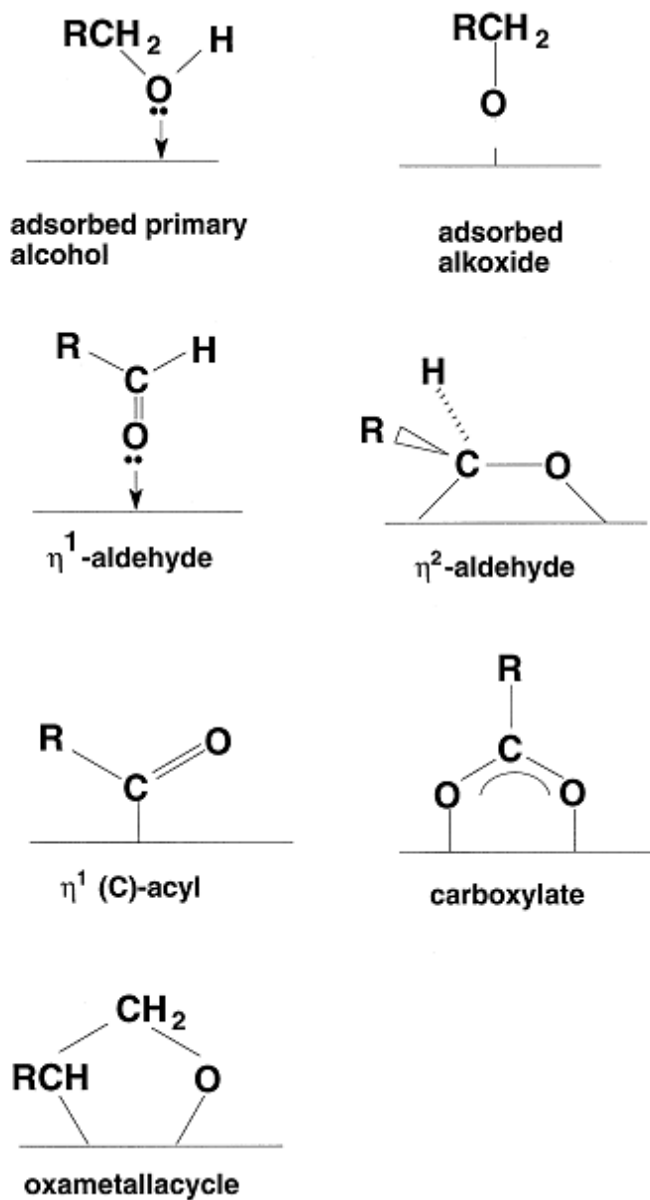


Figure 1.3 Important oxygenate intermediates observed on transition metal surfaces [105]

References

-
- [1] A. Zabaniotou, O. Ioannidou, V. Skoulou, *Fuel* 87 (2008) 1492
- [2] R.E.H. Sims, W. Mabee, J.N. Saddler, M. Taylor, *Bioresour. Technol.* 10 (2010) 1570
- [3] Furimsky, E. *Appl. Catal. A: General* 2000, 199, 147
- [4] Maggi, R.; Delmon, B. *Biomass Bioenergy* 1994, 7, 245
- [5] Oasmaa, A.; Czernik, S. *Energy Fuels* 1999, 13, 914
- [6] G. W. Huber, S. Iborra and A. Corma, *Chem Rev.*, 2006, 106, 4044
- [7] G. W. Huber and J. A. Dumesic, *Catal. Today*, 2006, 111, 119.
- [8] A. V. Bridgwater, *Chem. Eng. J.*, 2003, 91, 87.
- [9] Z. Srokol, A.-G. Bouche, A. van Estrik, R. C. J. Strik, T. Maschmeyer and J. A. Peters, *Carb. Res.*, 2004, 339, 1717.
- [10] F. Behrendt, Y. Neubauer, M. Oevermann, B. Wilmes and N. Zobel, *Chem. Eng. Technol.*, 2008, 31, 667.
- [11] D. C. Elliott, D. Beckman, A. V. Bridgwater, J. P. Diebold, S. B. Gevert and Y. Solantausta, *Energy & Fuels*, 1991, 5, 399.
- [12] S. Czernik, R. Maggi and G. V. C. Peacocke, in: *Fast Pyrolysis of Biomass: A Handbook, Vol. 2*, A. V. Bridgwater, (ed.), CPL Press, Newbury, UK, 2002, Chapter 8.
- [13] D. C. Elliott, *Energy & Fuels*, 2007, 21, 1792.
- [14] T. R. Carlson, T. P. Vispute and G. W. Huber, *ChemSusChem.*, 2008, 1, 397.

-
- [15] J. N. Chheda, G. W. Huber and J. A. Dumesic, *Angew. Chem. Int.*, 2007, 46, 7164.
- [16] R. M. West, E. Kunkes, D. A. Simonetti and J. A. Dumesic, *Catal. Today*, 2009, 147, 115.
- [17] L. Montague, *Lignin Process Design Confirmation and Capital Cost Evaluation*, Report No. NREL/SR-510-31579, National Renewable Energy Laboratory, Golden CO, 2003.
- [18] A. Demirbas, *Fuel Proc. Technol.* 88 (2007) 591
- [19] V.R. Wiggers, A. Wisniewski, L.A.S. Madureira, A.A. Chivanga Barros and H.F. Meier, *Fuel Proc. Technol.* 88 (2009) 2135
- [20] M.G. Perez, J. Shen, X.S. Wang, C.Z Li, *Fuel Proc. Technol.* 91 (2010) 296
- [21] J. Lede, F. Broust, F.T. Ndiaye, M. Ferrer, *Fuel* 86 (2007) 1800
- [22] M. Asadullah, M.A. Rahman, M.M. Ali, M.S. Rahman, M.A. Motin, M.B. Sultan, M.R. Alam, *Fuel* 86 (2007) 2514
- [23] O. Onay, O.M. Kockar, *Fuel* 85 (2006) 1921
- [24] D. Radlein, J. Piskorz, D.S. Scott *J An App Pyrolysis* 1991,19,41.
- [25] Y. Guo, Y. Wang, F. Wei, et al. *Chem Ind Eng Progr.* 2001,8,13.
- [26] W.M. Peng. Q.Y. Wu *New Energy Sour.* 2000,22,39.
- [27] S.P. Zhang, Y.J. Yan, Z.W. Ren, et al. *J Chin Sci Technol.* 2001,27,666.
- [28] J. Adam, M. Blazsó, E. Mészáros, et al. *Fuel.* 2005,84,1494.
- [29] R. Maggi, E. Laurent, P. Grange, B. Delmon, In: *Biomass Energy, Ind. Environ, G, Grassi, A. Collina, H. Zibetta (Eds.)*, Elsevier, London, 1992,2,657.

-
- [30] M.C. Samolada, I.A. Vasalos, In: Advance Thermochemical Biomass Conversion, A.V. Bridgwater, (Ed.), Blackie, 1994,2,859.
- [31] M.C. Samolada, E.D. Grigoriadou, I.A. Vasalos, In: Biomass Energy, Ind. Environ, G, Grassi, A. Collina, H. Zibetta (Eds.), Elsevier, London, 1992,2,731.
- [32] A.V. Bridgwater, M.L. Cottam Energy Biomass Wastes. 1993,16,689.
- [33] A.V. Bridgwater, M.L. Cottam Energy Fuels. 1992,6,113.
- [34] D.S. Scott, J. Piskorz, M.A. Bergougnou, R. Graham, R.P. Overend Ind Eng Chem Res. 1988,27,8.
- [35] D.S. Scott, S. Czernik, J. Piskorz, D. Radlein Energy Biomass Wastes. 1990,13,1349.
- [36] D.S. Scott, J. Piskorz, D. Radlein Energy Biomass Wastes. 1993,16,797.
- [37] S.P.R. Katikaneni, J.D. Adjaye, R.O. Idem, N.N. Bakhshi, In: Developments in Thermochemical Biomass Conversion, Blackie Academic & Professional London, A.V. Bridgwater and D.G.B. Boocock (Eds.) 1997,1,633.
- [38] S.P.R. Katikaneni, R.O. Idem, N.N. Bakhshi, In: Biomass Gasification and Pyrolysis, State of the Art and Future Prospects, M. Kaltschmitt and A.V. Bridgwater (Eds.), CPL Scientific, Newbury, 1997,411.
- [39] P.T. Williams, P.A. Horne J Anal Appl Pyrolysis. 1995,31,39.
- [40] P.T. Williams, N. Nugranad, P.A. Horne In: Biomass Gasification and Pyrolysis, State of the Art and Future Prospects, M. Kaltschmitt and A.V. Bridgwater (Eds.), CPL Scientific, Newbury, 1997,422.
- [41] J.D. Adjaye, N.N. Bakhshi Fuel Process Technol. 1995,45,185.

-
- [42] J.D. Adjaye, N.N. Bakhshi Fuel Process Technol. 1995,45,161.
- [43] M.I. Nokkosmaki, E.T. Kuoppala, E.A. Leppamaki, et al. J Anal Appl Pyrol. 2000,55,119.
- [44] R.V. Pindoria, A. Megaritis, A.A. Herod, et al. Fuel. 1998,77,1715.
- [45] R.V. Pindoria, J.-Y. Lim, J.E. Hawkes, et al. Fuel. 1997,76,1013.
- [46] D.C. Elliott, G.G. Neuenschwander Liquid fuel by low-severity hydrotreating of biocrude. Developments in thermochemical biomass conversion. London: Blackie Academic and Professional, 1996,611.
- [47] S.P. Zhang, Y. Yongjie, T. Li, et al. Bioresour Technol. 2005,96,545.
- [48] D.G.B. Boocock, S.G. Allen, A. Chrowdhury, R. Fruchtl, In: Pyrolysis Oils from Biomass, Producing, Analyzing, and Upgrading; E.J. Soltes and T.A. Milne (Eds.), ACS Symposium Series #376, American Chemical Society, Washington, DC, 1988,92.
- [49] J. Gagnon, S. Kaliaguine, Ind Eng Chem Res. 1988,27,1783.
- [50] Aden, A.; Ruth, M.; Ibsen, K.; Jechura, J.; Neeves, K.; Sheehan, J.; Wallace, B.; Montague, L.; Slayton, A.; Lukas, J. Lignocellulosic Biomass to Ethanol Process Design and Economics Utilizing Co-Current Dilute Acid Prehydrolysis and Enzymatic Hydrolysis for Corn Stover; Report No. NREL/TP-510-32438; National Renewable Energy Laboratory: Golden, CO, 2002; <http://www.osti.gov/bridge>.
- [51] Gosselink, R. J. A.; Jong, E. d.; Guran, B.; Abacherli, A. Ind. Crop. Prod. 2004, 20, 121.
- [52] Piskorz, J.; Majerski, P.; Radlein, D.; Scott, D. S. Energy Fuels 1989, 3, 723.
- [53] Train, P. M.; Klein, M. T. Fuel Sci. Technol. 1991, 9, 193.

-
- [54] Ratcliff, M. A.; Johnson, D. K.; Posey, F. L.; Chum, H. L. *Appl. Biochem. Biotechnol.* 1988, 17, 151.
- [55] Oasmaa, A.; Alen, R.; Meier, D. *Bioresour. Technol.* 1993, 45, 189.
- [56] Laurent, E.; Delmon, B. *Appl. Catal. A* 1994, 109, 77.
- [57] Laurent, E.; Delmon, B. *Appl. Catal. A* 1994, 109, 97.
- [58] Laurent, E.; Delmon, B. *J. Catal.* 1994, 146, 281.
- [59] J. Ebert *Ethanol Producer Magazine* 2008
- [60] Montane, D.; Salvado, J.; Torras, C.; Farriol, X. *Biomass Bioenergy* 2002, 22, 295.
- [61] Kottke, R. H. *Kirk-Othmer Encyclopedia of Chemical Technology*, 4th ed.; Kroschwitz, J. I., Howe-Grant, M., Eds.; John Wiley & Sons: New York, 1998; Vol. Supplement
- [62] Antal, M. J.; Leesomboon, T.; Mok, W. S.; Richards, G. N. *Carbohydr. Res.* 1991, 217, 71.
- [63] Zeitsch, K. J. *The Chemistry and Technology of Furfural and its Many By-Products*; Elsevier: London, 2000.
- [64] Zeitsch, K. J. *International Patent* WO 00/47569, 2000.
- [65] Dias, A. S.; Pillinger, M.; Valente, A. A. *J. Catal.* 2005, 229, 414.
- [66] Dias, A. S.; Pillinger, M.; Valente, A. A. *Appl. Catal. A* 2005, 285, 126.
- [67] Moreau, C.; Durand, R.; Peyron, D.; Duhamet, J.; Rivalier, P. *Ind. Crop. Prod.* 1998, 7, 95.
- [68] Huber, G.W.; Dumesic, J.A. *Catal. Today* 2006, 111, 119-132.

-
- [69] Roman-Leshkov, Y.; Barrett, C.J.; Liu, Z.Y.; Dumesic, J.A. *Nature* 2007, 447, 982-985.
- [70] Kelly, G.J.; Jackson, S.D. Aldol Condensation of Aldehydes and Ketones over Solid Base Catalysts. *Catalysis in Application*, Jackson, S.D.; Hargreaves, J.S.J.; Lennon, D. Royal Society of Chemistry (Great Britain).
- [71] Serrano-Ruiz, J.C.; Braden, D.J.; West, R.M.; Dumesic, J.A. *App. Catal. B* 2010, 100, 184-189.
- [72] Kunkes, E.L.; Gürbüz, E.I.; Dumesic, J.A. *J. Catal.* 2009, 266, 236-249.
- [73] Huber, G.W.; Chheda, J.N.; Barrett, C.J.; Dumesic, J.A. *Science* 2005, 308, 1446-1449.
- [74] West, R.M.; Kunkes, E.L.; Simonetti, D.A.; Dumesic, J.A. *Catal. Today* 2009, 147, 115-125.
- [75] Barrett, C.J.; Chheda, J.N.; Huber, G.W.; Dumesic, J.A. *Appl. Catal. B* 2006, 66, 111-118.
- [76] Seo, G.; Chon, H. *J. Catal.* 1981, 67, 424-429.
- [77] Rao, R.; Dandekar, A.; Baker, R.T.K.; Vannice, M.A. *J. Catal.* 1997, 171, 406-419.
- [78] Zheng, H.Y.; Zhu, Y.L.; Teng, B.T.; Bai, Z.Q.; Zhang, C.H.; Xiang, H.W.; Li, Y.W. *J. Mol. Catal. A* 2006, 246, 18-23.
- [79] Nagaraja, B.M.; Padmasri, A.H.; David Raju, B.; Rama Rao, K.S. *J. Mol. Catal. A* 2007, 265, 90-97.
- [80] Reddy, B.M.; Reddy, G.K.; Rao, K.N.; Khan, A.; Ganesh, I. *J. Mol. Catal. A* 2007, 265, 276-282.
- [81] Huang, W.; Li, H.; Zhu, B.; Feng, Y.; Wang, S.; Zhang, S. *Ultrason. Sonochem.* 2007, 14, 67-74.
- [82] Sitthisa, S.; Sooknoi, T.; Ma, Y.; Balbuena, P.B.; Resasco, D.E. *J. Catal.* 2011, 277, 1-13.
- [83] Claus, P. *Top. Catal.* 1998, 5, 51-62.

-
- [84] Claus, P. *Top. Catal.* 1998, 5, 51-62.
- [85] Li, H.; Luo, H.; Zhuang, L.; Dai, W.; Qiao, M. J. *Mol. Catal. A.* 2003, 203, 267-275.
- [86] Liaw, B.; Chiang, S.; Chen, S.; Chen, Y. *Appl. Catal. A* 2008, 346, 179-188.
- [87] Kijeński, J.; Winiarek, P.; Paryjczak, T.; Lewicki, A.; Mikolajska, A. *Appl. Catal. A* 2002, 233, 171-182.
- [88] Sitthisa, S.; Resasco, D.E. *Catal. Lett.* 2011, 141, 784-791.
- [89] Sitthisa, S.; Pham, T.; Prasomsri, T.; Sooknoi, T.; Mallinson, R.G.; Resasco, D.E. *J. Catal.* 2011, 280, 17-27.
- [90] Seo, G.; Chon, H. *J. Catal.* 1981, 67, 424-429.
- [91] Bradley, M.K.; Robinson, J.; Woodruff, D.P. *Surf. Sci.* 2010, 604, 920-925.
- [92] Singh, H.; Prasad, M.; Srivastava, R.D. *J. Chem. Technol. Biotechnol.* 1980, 30, 293-296.
- [93] Srivastava, R.D.; Guha, A.K. *J. Catal.* 1985, 91, 254-262.
- [94] Jung, K. J.; Gaset, A.; Molinier, J. *Biomass* 1988, 16, 63-76
- [95] Moshkin, P.A.; Preobrazhenskaya, E.A.; Berezina, B.B.; Markovich, V.E.; Kudrina, E.G.; Papsueve, V.P.; Sokolina, E.A. *Khimiya Oeterotsiklicheskih Soedinenii* 1966, 2, 3-7.
- [96] Coca, J.; Morrondo, E.S.; Sastre, H. *J. Chem. Technol. Biotechnol.* 1982, 32, 904-908
- [97] Coca, J.; Morrondo, E.S.; Parra, J.B.; Sastre, H. *React. Kinet. Catal. Lett.* 1982, 20, 3-4.
- [98] Sitthisa, S.; Resasco, D.E. *Catal. Lett.* 2011, 141, 784-791.

-
- [99] Sitthisa, S.; Pham, T.; Prasomsri, T.; Sooknoi, T.; Mallinson, R.G.; Resasco, D.E. *J. Catal.* 2011, 280, 17-27.
- [100] Srivastava, R.D.; Guha, A.K. *J. Catal.* 1985, 91, 254-262.
- [101] Jung, K. J.; Gaset, A.; Molinier, J. *Biomass* 1988, 16, 63-76.
- [102] Zhang, W.; Zhu, Y.; Niu, S.; Li, Y. *J. Mol. Catal A: Chem* (2011) In press.
- [103] Singh, H.; Prasad, M.; Srivastava, R.D. *J. Chem. Technol. Biotechnol.* 1980, 30, 293-296.
- [104] Coca, J.; Morrondo, E.S.; Sastre, H. *J. Chem. Technol. Biotechnol.* 1982, 32, 904-908
- [105] M. Mavrikakis, M. A. Barteau, *J. Mol. Catal. A:Chem.* 131 (1998) 135.

CHAPTER 2

Experimental Setup

2.1 Catalyst preparation

Three different monometallic catalysts were prepared by incipient wetness impregnation (IWI) of the support (SiO_2 , Hisil 210) with an aqueous solution of the respective metal precursor ($\text{Cu}(\text{NO}_3)_2$, $\text{Pd}(\text{NO}_3)_2$ or $\text{Ni}(\text{NO}_3)_2$), obtained from Fluka (>99% purity). To prepare the three catalysts, 10% wt. Cu/SiO_2 , 1% wt. Pd/SiO_2 and 5% wt. Ni/SiO_2 , metal salt aqueous solutions with the appropriate concentrations were added to the silica support, keeping a liquid/solid ratio of 1 cc/g. The bimetallic catalysts including $\text{Pd-Cu}/\text{SiO}_2$, $\text{Pd-Fe}/\text{SiO}_2$, and $\text{Ni-Fe}/\text{SiO}_2$ with varying metal loadings were prepared by incipient wetness co-impregnation with aqueous solutions of the corresponding metal precursors. After impregnation, the catalysts were dried overnight at room temperature and placed in an oven at 120°C for 12 h. The oven-dried catalysts were finally calcined for 4 h at 400°C , following a linear heating ramp of $10^\circ\text{C}/\text{min}$, under a flow of pure air at 100 ml/min.

2.2 Catalyst characterization

2.2.1 Temperature programmed reduction (TPR)

The reducibility of the calcined CATALYST samples was determined by temperature programmed reduction (TPR). In these measurements, 20-50 mg of a sample was placed in a quartz reactor and heated at 30°C/min up to 500°C under a He flow of 20 ml/min, and held at this temperature for 1 h. The reactor was then cooled down to 0°C and the sample exposed to a stream of 5% H₂/Ar at a flow rate of 20 ml/min. Subsequently, the sample was heated up to 800°C at a heating rate of 5°C/min. The variation in hydrogen uptake was monitored on a TCD detector as a function of temperature. The molar H₂ uptake per gram of sample was quantified from the peak area in the TPR profiles and calibrated with a CuO standard.

2.2.2 Carbon monoxide chemisorption

The fraction of Pd exposed (CO/Pd) was estimated from dynamic CO chemisorption, measured in a pulse system equipped with Thermal Conductivity Detector (TCD). Before

chemisorption, all catalysts were reduced in-situ under pure H₂ flow by heating up to 200° C with a heating rate of 10° C/min, held for 1 h, purged with He for 30 min, and cooled to room temperature. Multiple pulses of 5% CO/He mixture were sent over the catalyst from a 100 μL sample loop until a constant CO peak area was observed. The exposed metal fraction (CO/Pd) was calculated from the moles of adsorbed CO per total moles of Pd impregnated onto the catalyst support.

2.2.3 DRIFT of adsorbed CO

DRIFTS experiments were carried out in a Perkin Elmer Spectrum 100 FTIR spectrometer equipped with an MCT detector and a high temperature, low pressure chamber (HVC-DRP) fitted with KBr windows (Harrick Scientific Products, Inc). In each measurement, ~50 mg of catalyst was loaded to the DRIFTS chamber and reduced under 30 ml/min H₂ flow at a heating rate of 10°C/min to 250° C. Reduction was conducted for 1 h, then the sample was flushed with He for 30 min before cooling down to room temperature. A flow of 5% CO in He was passed through the chamber for 30 min at room temperature. Then, the chamber

was flushed with He for 20 min before collecting and averaging 256 scans at 4 cm⁻¹ resolution.

2.2.4 DRIFT of adsorbed furfural on copper catalyst

DRIFT spectra of adsorbed furfural were recorded in a high temperature DRIFT cell (HVC, Harrick) with CaF₂ windows. The Cu sample powder (100 mg) was loaded in the sample cup of the cell, reduced in situ at 500°C for 1 h under a flow of H₂ (30 ml/min), and then purged with He (30ml/min) for 30 min. Finally, the sample was cooled down to room temperature, and the background spectrum recorded. A He carrier gas (30ml/min) saturated at 0°C with furfural vapor was passed by the cell for approximately 30 min. The sample was then purged under He flow at room temperature for another 30 min. The DRIFT spectra were recorded at a resolution of 4 cm⁻¹ and accumulating 256 scans.

2.2.5 X-ray powder diffraction

X-ray powder diffraction patterns (XRD) for all the samples were collected on a D8 Series II X-ray Diffractometer (BRUKER AXS), using Cu K α radiation

generated at 40 kV and 35 mA. The samples were reduced ex situ under pure H₂ (100 ml/min) at 450°C for 1 h prior to the measurements. The scans covered the 2 θ range from 30° to 60°.

2.2.6 Transmission electron microscopy

Morphology and size of the metal clusters were characterized by transmission electron microscopy (TEM, JEOL model JEM-2100 LaB6). Before TEM analysis, the samples were reduced ex situ in pure H₂ (100 ml/min) at 450°C for 1 h. The reduced samples were then mixed with 2-propanol, sonicated, deposited onto the TEM (Cu) grids, and dried.

2.2.7 BET surface area

The BET surface area (S_g) was measured by conventional N₂ physisorption on a Micromeritics ASAP 2010 unit, after evacuation at 350°C for 3 h.

2.3 Catalytic activity testing

The catalytic activity testing was conducted in a 1/4" tubular quartz reactor. The pelletized catalyst (size range: 250-425 μm) was placed at the center of the reactor tube between two layers of glass beads and quartz wool. The catalyst was pre-reduced in H_2 flow (60 ml/min, Airgas, 99.99%) for 1 h at the temperature selected according to the TPR experiments (i.e., 250, 350, and 450°C for 1%Pd/SiO₂, 10%Cu/SiO₂ and 5%Ni/SiO₂, respectively). After reduction, the catalyst was cooled down to the selected reaction temperature (210-290°C) under the same H_2 flow. Prior to the reaction, furfural (Sigma Aldrich, 99.5%) was purified by vacuum distillation to remove residues and any oligomers formed during storage. The purified liquid was kept under He atmosphere until its use in the reaction test. A 0.5 ml/h or 0.006 mol/h flow of liquid furfural (provided by Sigma Aldrich, 99.5%) was fed continuously from a syringe pump (Cole Palmer) and vaporized into a gas stream of 60 ml/min H_2 . The reaction products were analyzed online on a gas chromatograph (Agilent model 6890) using a HP-5 capillary column and a FID detector. The carbon balance was checked in every run and it was found to be

higher than 95% in every case. The product yield and selectivity were calculated and defined as follows:

$$\text{Yield (\%)} = \frac{\text{mol of the product produced}}{\text{mol of furfural fed}} \times 100$$

$$\text{Selectivity (\%)} = \frac{\text{mol of the product produced}}{\text{mol of furfural consumed}} \times 100$$

CHAPTER 3

Comparative Study of the Furfural Conversion over Cu, Pd and Ni Monometallic Catalysts

3.1 Introduction

Furfural is one of the numerous oxygenated compounds commonly found in bio-oil [1-12]. Due to their high reactivity, these compounds need to be catalytically deoxygenated to improve bio-oil storage stability, boiling point range, and water solubility [13]. Dumesic et al. [14,15] have proposed that aldol condensation of furfural with small ketones is a promising approach to produce higher alkanes (C₈-C₁₅) for diesel fuel production. They have obtained high yields of condensation products by direct condensation of furfural with acetone in the presence of basic catalysts [15]. Selective hydrodeoxygenation may be an alternative route to increase the stability of furfural and convert it to compounds which may have value as gasoline components. For instance 2-methyl furan, could be a suitable option to be used as an octane booster (RON=131). Hydrodeoxygenation under relatively mild conditions can be performed over metal

catalysts [16,17]. Within this context, the goal of this contribution is to compare the conversion of furfural over different silica-supported monometallic catalysts. Copper, palladium and nickel catalysts have been selected to study their activity, selectivity, and possible reaction pathways for the deoxygenation of furfural. The study of the behavior of different metals may be useful in designing catalytic strategies towards the production of fuel components with specific characteristics (e.g. vapor pressure, octane number, etc.)

3.2 Catalyst characterization

The BET surface areas from N₂ physisorption measurement are 129 m²/g, 115m²/g, and 126 m²/g for 1%Pd/SiO₂, 10%Cu/SiO₂ and 5%Ni/SiO₂, respectively. The metals loading after synthesis was estimated from the H₂ consumption experiment and found to be 1.2 wt%, 10.3 wt% and 5.9 wt% for 1%Pd/SiO₂, 10%Cu/SiO₂ and 5%Ni/SiO₂, respectively. The TPR profiles of the 1%Pd/SiO₂, 10%Cu/SiO₂ and 5%Ni/SiO₂ catalysts are shown in Figure 3.1. For Pd/SiO₂, the TPR profile mainly exhibits one peak centered on 94°C, which has been previously ascribed to the

reduction of Pd(II) to Pd(0) [18,19]. The reduction profile of Cu/SiO₂ was previously reported [20] and showed two overlapping peaks at 335°C and 246°C. According to previous studies, these peaks originate from the reduction of respectively more highly and more poorly dispersed Cu oxide species on silica, [21]. Finally, the Ni catalyst shows the main reduction peak at 354°C with smaller peaks at lower and higher temperature (330 and 393°C, respectively), as previously seen [22,23]. The main peak has been attributed to the reduction of NiO to Ni metal [24]. The small peak at higher temperatures could be due to the reduction of small NiO particles or possibly nickel hydrosilicate species, resulting from strong metal-support interactions [25].

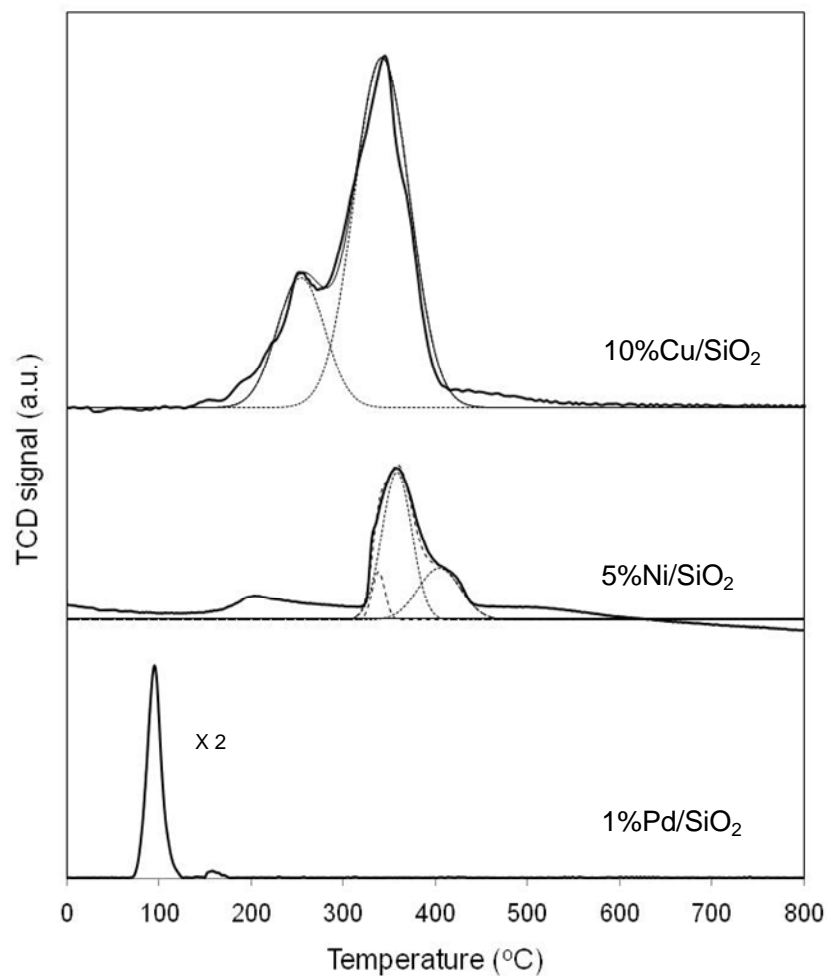


Figure 3.1 Temperature programmed reduction profiles (TPR) of 1%Pd/SiO₂, 5%Ni/SiO₂ and 10%Cu/SiO₂ catalysts.

3.3 Conversion of furfural over Cu/SiO₂

Table 3.1 summarizes the conversion and product distribution from the reaction of furfural over the Cu/SiO₂ catalyst.

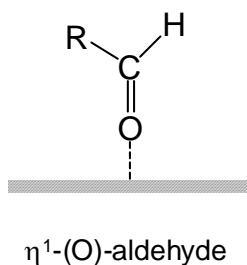
Table 3.1 Conversion and yield of products from the reaction of furfural over 10%Cu/SiO₂ catalyst

Temp. (°C)	W/F g _{.cat} /(mol/h))	Conv. (%)	Yield (%)	
			FOL	MF
230	10.4	24	24	0.2
	20.7	53	53	0.5
	41.3	69	68	1.5
270	3.5	15	14	0.2
	10.4	46	45	1.2
	20.7	66	63	2.9
	41.3	77	71	6.0
290	3.5	20	19	0.3
	10.4	48	46	1.7
	20.7	64	60	4.3
	41.3	71	63	8.2

Reaction conditions: H₂/Feed ratio = 25, H₂ pressure = 1 atm, TOS = 15 min

These results clearly show that the reaction of furfural mainly produces its corresponding alcohol, with only small amounts of 2-methyl furan (MF), formed as a by-product via C-O hydrogenolysis. A relatively higher yield of 2-methyl furan can be obtained at the highest reaction temperature studied (290°C). These results are in agreement with previous reports of furfural conversion over Cu-based catalysts, which show that furfuryl alcohol is the main

product [26-29]. As we have recently shown [20], the conversion of furfural on Cu catalyst involves the interaction of the surface preferentially with the carbonyl group, rather than the furanic ring. Furfural tends to adsorb through carbonyl O in a $\eta^1(\text{O})$ -aldehyde configuration, as previously proposed for all Group IB metals, according to HREELS and DFT evidence [30].



As shown in Table 3.1, only furfuryl alcohol and 2-methylfuran were observed in the reaction of furfural over Cu/SiO₂. No products from hydrogenation of the furanyl ring were obtained at any temperature or at any W/F. This result is in good agreement with the conclusion that the adsorption of the furan ring is not favored on the Cu surface.

A molecule that has shown similar behavior on Cu(111) is crotonaldehyde, which contains a carbonyl group and a C=C bond. As demonstrated by Boronat et al. [31] crotonaldehyde is bonded to the surface through the O of the carbonyl group, while the C=C bond remains undistorted and far from the surface. Likewise, several studies have shown that Cu catalysts are always more selective in the hydrogenation of the C=O bond in conversion of aldehydes containing C=O and C=C bonds than other metal catalysts [32,33]. It can be concluded that the Cu surface exerts a selective attraction to the O end of the carbonyl, but repulsion on the rest of the molecule.

3.4 Conversion of furfural over Pd/SiO₂

A very different behavior from that of Cu is observed for Pd. As shown in Table 3.2, the product distribution from the reaction of furfural over Pd/SiO₂ at different W/F and temperatures is clearly different from that on Cu. The main product is furan, which derives from the decarbonylation of furfural [34]. In contrast to Cu, Pd only produces small amounts of furfuryl alcohol, which indicates that on Pd decarbonylation is more favorable than hydrogenation. Another significant difference is the appearance of tetrahydrofuran (THF) and tetrahydro furfuryl alcohol (HFOL) at high W/F. These hydrogenated ring products were not observed in the case of Cu catalyst and clearly indicate that the interaction with the furan ring is favored on Pd.

Table 3.2 Conversion and yield of products from the reaction of furfural over 1%Pd/SiO₂ catalyst. **Reaction conditions:** H₂/Feed ratio = 25, H₂ pressure = 1 atm, TOS = 15 min

Temp. (°C)	W/F g _{.cat} /(mol/h)	Conv. (%)	Yield (%)			
			Furan	THF	FOL	HFOL
210	2.4	15	10	2	3	0.0
	4.8	27	17	5	5	1.1
	9.6	40	22	8	8	3.0
230	2.4	27	20	3	4	0.0
	4.8	46	30	7	7	2.0
	9.6	69	42	14	10	3.5
250	2.4	40	33	3	4	0.0
	4.8	63	46	8	7	1.5
	9.6	85	59	14	9	2.7

To interpret the observed results we need to elucidate which intermediate leading to decarbonylation is favored on the Pd surface. One can refer to the work of Barteau et al. [35,36], who made extensive studies of the interaction of aldehydes on metal single crystals. They showed that on Pd surfaces, aldehydes tend to form η^2 (C,O) surface intermediates, in which both C and O atoms of the carbonyl group interact with the metal. In the presence of hydrogen, this intermediate can be hydrogenated to alcohol. However, when the temperature is high enough, the η^2 (C,O) aldehyde may further convert into a more stable acyl surface species, in which the C atom of the carbonyl is strongly attached to the surface. This acyl species may in fact be a precursor for the decarbonylation reaction, producing hydrocarbon fragments and CO.



In the case of furfural conversion, this path results in furan, which is the main product. Interestingly, as shown in Figure 3.2, the selectivity to decarbonylation significantly increases as a function of temperature, which is consistent with an enhanced conversion of η^2 (C,O) into acyl species on the surface as temperature increases.

The formation of hydrogenated furan ring compounds, THF and HFOL, on Pd as opposed to Cu is also an important aspect to discuss. As opposed to Cu, Pd can readily adsorb the furan ring due to a strong interaction between the metal and the π bonds in the molecule. A rehybridization of the carbon bonds from sp^2 -to- sp^3 has been proposed to occur on Pd, which may account for the strong interaction [37].

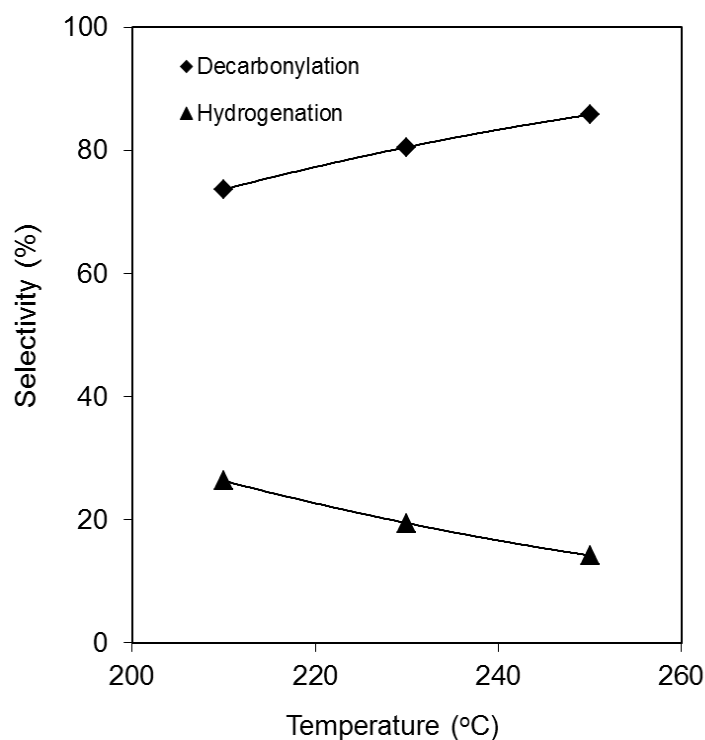


Figure 3.2 Selectivity of products from decarbonylation (Furan+THF) and hydrogenation (FOL+HFOL) reactions at difference temperatures. W/F = 9.6 g.cat.mol⁻¹.h, H₂/Feed ratio = 25, H₂ pressure = 1atm, TOS = 15 min

3.5 Conversion of furfural over Ni/SiO₂

A third different pattern of furfural conversion is observed on Ni, which exhibits unique characteristics with respect to Cu and Pd. Table 3.3 summarizes the product distribution over Ni/SiO₂ at different temperatures and W/F. While furan is the main product, and similar to Pd, Ni is active for decarbonylation, various other products

are observed. At high W/F, in addition to furfuryl alcohol, tetrahydro furfuryl alcohol and 2-methyl furan are observed, but most interestingly, butanal, butanol, and butane were observed in significant amounts. These products were not observed on Cu or Pd and can derive from the ring opening of furan. The C-O bond cleavage results in butanal, which can be further hydrogenated to butanol. At elevated temperature, butanol can be dehydrated to butene, which is rapidly hydrogenated to butane.

Table 3.3 Conversion and yield of products from the reaction of furfural over 5%Ni/SiO₂ catalyst. **Reaction conditions:** H₂/Feed ratio = 25, H₂ pressure = 1 atm, TOS = 15 min, FOL: furfuryl alcohol, HFOL: tetra hydrofurfuryl alcohol, BAL:butanal, BOL: butanol

Temp. (°C)	W/F g _{.cat.} .mol ⁻¹ .h	Conv. (%)	Yield (%)						
			Furan	FOL	HFOL	MF	BAL	BOL	Butane
210	2.4	26	11	10	1	0	3	0	1
	4.8	41	16	16	2	1	3	1	2
	9.6	84	32	31	5	2	5	3	5
230	2.4	37	16	10	1	1	5	1	3
	4.8	72	31	18	3	2	9	2	7
	9.6	100	45	19	5	4	6	9	12
250	2.4	51	23	7	1	1	9	1	8
	4.8	100	50	3	3	5	7	11	22
	9.6	100	50	0	3	5	4	14	24

The reaction selectivity as a function of temperature at constant W/F is shown in Fig. 3.3, in which we have lumped the products arising from each principal reaction path. That is, decarbonylation includes furan, hydrogenation includes FOL and HFOL, and ring opening includes butanal, butanol, and butane. It is clear that while hydrogenation dominates at low temperatures, decarbonylation and ring opening become dominant at high temperatures.

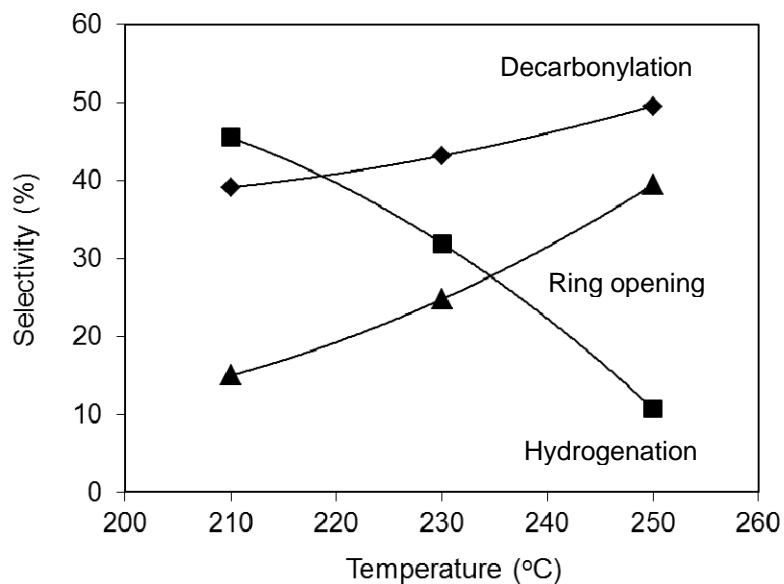


Figure 3.3 Selectivity of products from decarbonylation (Furan), and hydrogenation (FOL+HFOL) and ring opening (BAL+BOL+Butane) reactions at difference temperatures. W/F = 4.8 g.cat.mol⁻¹.h, H₂/Feed ratio = 25, H₂ pressure = 1atm, TOS = 15 min

One can speculate about the intermediates that lead to the furan ring opening and why this reaction is only observed on Ni. We note that, in principle, it is possible that the ring opening products can derive either from furan or THF, or both (see Figure 3.4). However, THF was not observed among the products on Ni catalyst, which might be due to either a very fast ring opening of THF, or that THF is not formed on Ni. In order to decide which of the two possibilities is correct, a reaction study was conducted at 250°C, using either furan or THF at the same W/F (9.6 g_{.cat.}.mol⁻¹. h). This comparative study showed that the highest yield of ring opening products was obtained with furan (32% and 8% yield for feeding furan and THF, respectively). That is, while THF resulted in some ring opening, it was much lower than that obtained with furan. Therefore, it is unlikely that the first possibility is correct. We can then conclude that on Ni, THF is not significantly formed and the ring opening path occurs preferentially via furan.

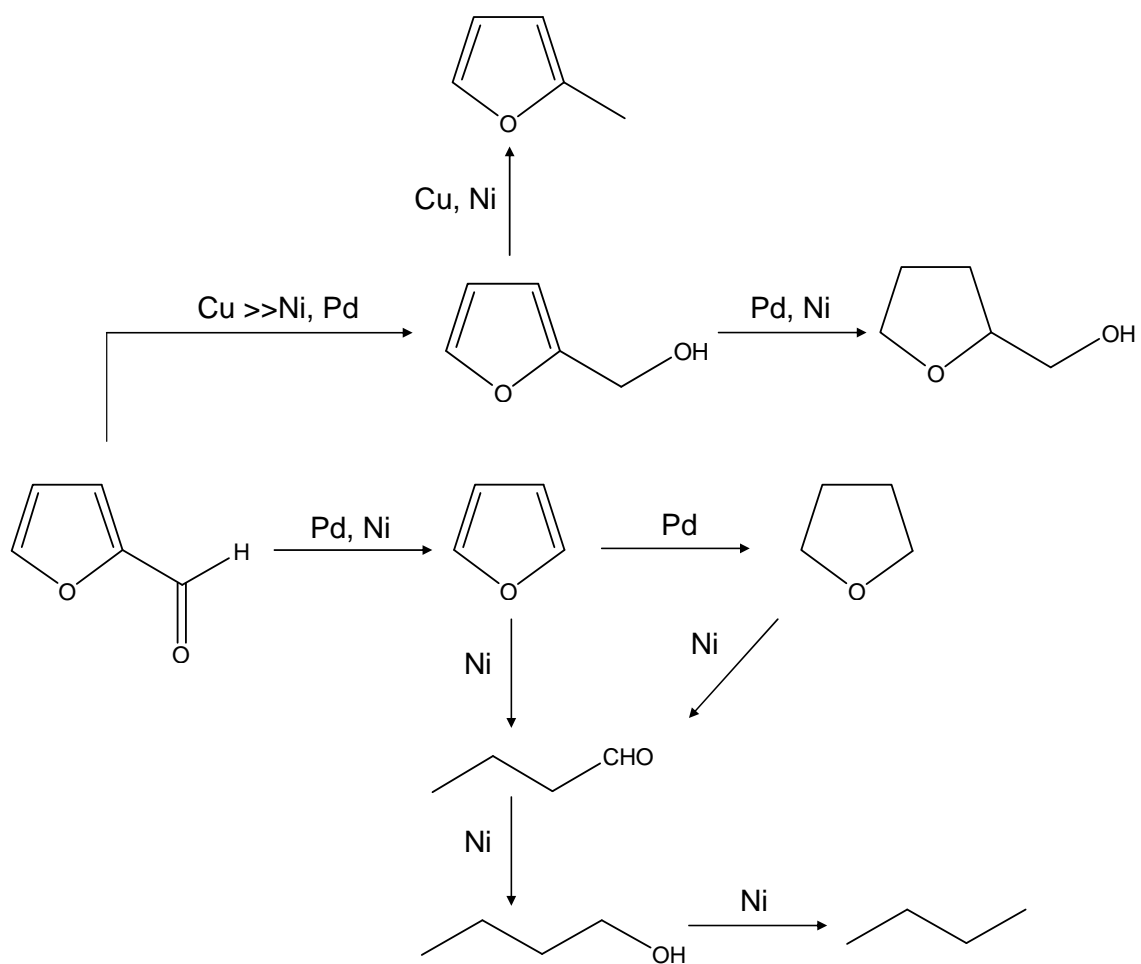


Figure 3.4 Possible reaction pathways for furfural conversion over Cu, Pd and Ni catalysts

It is interesting to note that while the aromaticity of furan makes it more stable than THF, the activity for ring opening is much higher with furan than with THF. That is, one expects that the delocalization of the π electrons makes the C-O bonds in furan stronger than in THF. Therefore, the reason for the higher reactivity of furan compared to THF should be ascribed to the stronger interaction of the ring with the metal surface. In fact, Bradley et al. [37] have shown that the relatively strong adsorption of furan on Group VIII metals is due to the interaction of the π bonds with the d orbitals of the metal, which in turn weakens the C-O bond. In contrast, this type of interaction with the metal does not happen with THF. Thus, the difference in the reactivity for ring opening observed between the two molecules can be ascribed to the role played by the presence of the aromatic ring.

3.6 Comparative analysis of the furfural conversion on Cu, Pd and Ni catalysts

A comparison of the overall furfural conversion at 230°C over the three different metal catalysts is made in Table 3.4. Large changes in turnover frequencies (TOF) were observed. The TOF were calculated from initial rates of reaction, measured at low conversions (<3 %) at 230°C, and the average metal particle size, as determined from TEM (Cu = 3.2 nm, Ni = 15.0 nm, Pd = 10.14 nm). The resulting TOFs at 230°C were Cu (1.3 s⁻¹), Ni (76.5 s⁻¹), and Pd (265.8 s⁻¹), which is the typical trend observed in hydrogenation catalysts, and usually explained in terms of the degree of d-orbital filling. That is, Cu is always much less active than Pd and Ni, which have partially filled d-orbitals.

Table 3.4 Selectivity of products from the reaction of furfural over 10%Cu/SiO₂, 1%Pd/SiO₂ and 5%Ni/SiO₂ catalysts. **Reaction conditions**, Temp = 230°C, H₂/Feed ratio = 25, H₂ pressure = 1atm, TOS = 5 min

Catalysts	10%Cu/SiO₂	1%Pd/SiO₂	5%Ni/SiO₂
Temp. (°C)	230	230	230
TOF (s ⁻¹)	1.3	265.8	76.5
W/F (g _{.cat.} .mol ⁻¹ .h)	41.3	9.6	4.8
Conversion (%)	69	69	72
Hydrogenation (%)			
FOL	98	14	25
MF	2	-	3
HFOL	-	5	4
Decarbonylation (%)			
Furan	-	60	43
THF	-	20	-
Ring opening (%)			
BAL	-	-	12
BOL	-	-	3
Butane	-	-	10

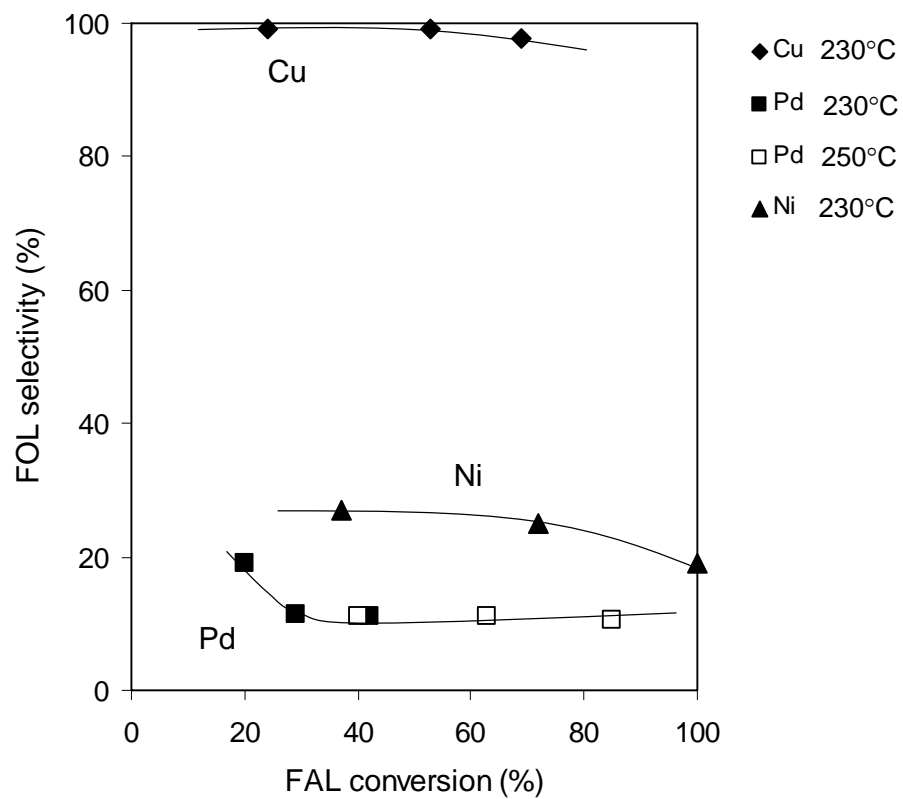


Figure 3.5 Selectivity of products from hydrogenation (FOL) over 1%Pd/SiO₂ Ni/SiO₂ and 10%Cu/SiO₂ at different conversions. H₂/Feed ratio = 25, H₂ pressure = 1atm, TOS = 15 min

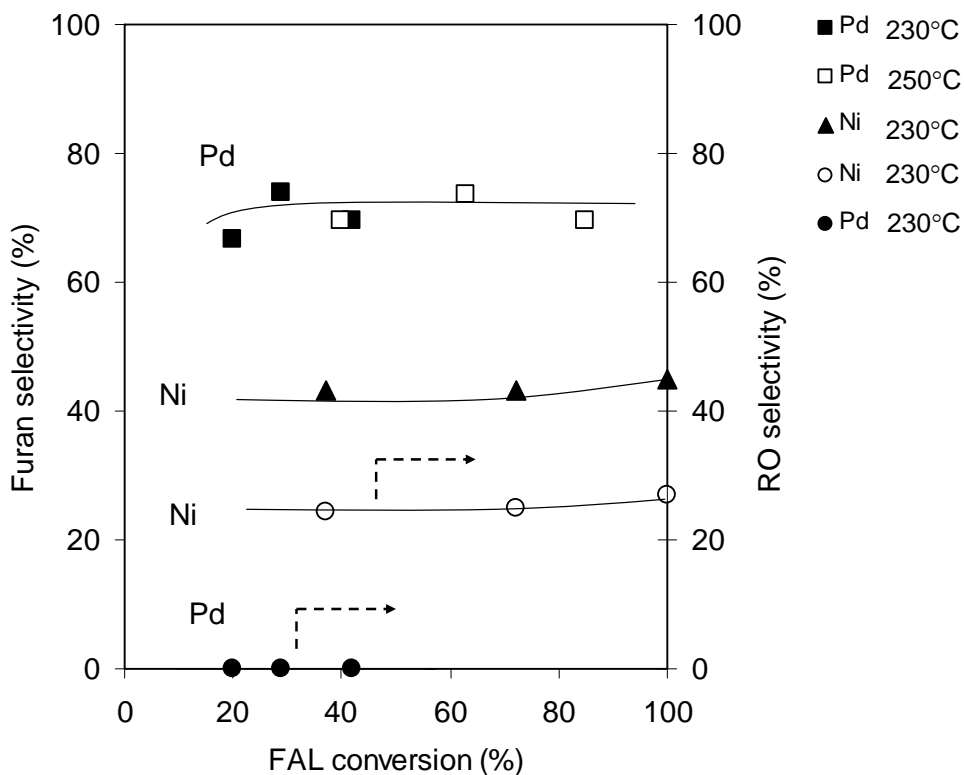


Figure 3.6 Selectivity of products from decarbonylation (Furan), and ring opening (BAL+BOL+Butane) reactions (RO) over 1%Pd/SiO₂ and 5%Ni/SiO₂ at different conversions. H₂/Feed ratio = 25, H₂ pressure = 1atm, TOS = 15 min

However, the most interesting variations are in the distribution of products obtained over the three different metals. An interesting comparison is made in Table 3.4 for the three metals at the same temperature (230°C) and about the same total conversion (~70%). It must be noted that the changes in selectivity due to changes in conversion or

in temperature are minor compared to the drastic changes in selectivity observed from one metal to another. This comparison is clearly shown in Figures 3.5 and 3.6.

First, regarding hydrogenation at the C=O bond, the three metals are all active in the conversion of furfural into the corresponding alcohol (FOL). However, extremely high selectivity (> 98%) towards furfuryl alcohol can be obtained over the Cu catalyst. The formation of only the η^1 -aldehyde intermediate of furfural on Cu surface [30] seems to be responsible for the high selectivity towards alcohol formation. In contrast, the most likely intermediate on Pd and Ni surfaces is the η^2 -aldehyde [38], which can react further with hydrogen to form either the corresponding alcohol or decompose to the acyl intermediate that results in the formation of furan. Therefore, the selectivity towards alcohol gets reduced for the case of Ni and Pd catalysts.

Second, regarding the selectivity towards furan, one can see that this is much higher on Pd than on Ni (i.e., 60% vs. 43%). Here again, the lower selectivity on Ni can be ascribed to further reaction on this metal to subsequent products obtained from the ring opening reaction, which only occurs on Ni, most probably due to a

strong interaction with the furan ring, which weakens the C-O bond enough to open the ring. In fact, recent studies have shown that ring opening of furfural can even be achieved at low temperatures by Ni-based catalysts in aqueous-phase [39].

Third, interesting differences are seen regarding the reaction of the furan ring. No hydrogenation of the ring happened on Cu but significant amounts were obtained on Pd. In addition, both hydrogenated and ring opening products were obtained from Ni. To explain this trend it would be interesting to compare the adsorption energies of the furan ring on the three different metal surfaces. To our knowledge there is no published theoretical or experimental study that includes adsorption data for furan on Cu, Ni and Pd surfaces calculated or measured under the same conditions. However, it is possible to evaluate the trends observed with the closely-related thiophene molecule, C_4H_4S to draw conclusions about our molecule of interest, furan, C_4H_4O . Coincidentally, Orita and Itoh [40] have conducted DFT calculations of the adsorption of thiophene on Ni(100), Cu(100) and Pd(100) surfaces. They report that the highest heat of adsorption of thiophene is on Ni, followed closely by Pd, and much farther by Cu

(i.e., -2.8, -2.2, and -0.47 eV for Ni(100), Pd(100) and Cu(100) surfaces, respectively). From this trend, one could expect that the strength of interaction of the furan ring with the three metals would also follow the trend Ni>Pd>>Cu. Therefore, the differences in product distribution can then be interpreted as follows. The ring/metal interaction on Ni is so strong that it promotes the weakening of the C-O bond leading to ring opening. On Pd the interaction is weaker, but still significant as to allow for ring hydrogenation. Finally, on Cu the interaction with the ring is so weak that no ring-conversion products are observed. Figure 3.4 summarizes the possible reaction pathways for conversion of furfural and indicates which paths are favored over Cu, Pd, or Ni.

3.7 Conclusion

In summary, the very different distributions of products observed on silica-supported Cu, Pd, and Ni catalysts can be explained in terms of the extent of molecular interactions with the metal surface as follows:

Cu mainly produces furfuryl alcohol via hydrogenation of the carbonyl group. This behavior is explained in terms

of the preferred adsorption mode on Cu, $\eta^1(\text{O})$ -aldehyde, since the interaction of Cu with C=C bond is very weak. No products involving the activation of the furan ring are observed.

Pd yields decarbonylation products due to the favorable formation of acyl surface species. It also generates products of ring hydrogenation and they are the result of a strong interaction of Pd with the ring.

While Ni has a product distribution similar to that of Pd, furan is not as abundant because it can further react with hydrogen forming ring opening products, due to the interaction of the ring with the surface that is even stronger than on Pd.

References

-
- [1] He R, Ye XP, English BC, Satrio JA (2009) *Bioresour Technol* 100:5305.
 - [2] Adam J, Blazso M, Meszaros E, Stocker M, Nilsen MH, A. Bouzgac, Hustada JE, Grønli M, Øyed G (2005) *Fuel* 84:1494.
 - [3] Baijun L, Lianhai L, Bingchun W, Tianxi C, Iwatani K (1998) *Appl Catal A* 171:117.
 - [4] Lohitharn N, Shanks BH (2009) *Catal Commun* 11:96

-
- [5] Nagaraja BM, Padmasri AH, Seetharamulu P, Hari Prasad Reddy K, David Raju B, Rama Rao KS (2007) *J Mol Catal A* 278:29.
- [6] Murthy MS, Rajamani K (1974) *Chem Eng Sci* 29:601.
- [7] Zheng HY, Zhu YL, Huang L, Zeng ZY, Wan HJ, Li YW (2008) *Catal Commun* 9:342.
- [8] Barrett CJ, Chheda JN, Huber GW, Dumesic JA (2006) *Appl Catal* 66:111.
- [9] Wu J, Shen Y, Liu C, Wang H, Geng C, Zhang Z (2005) *Catal Commun* 6:633.
- [10] Li H, Luo H, Zhuang L, Dai W, Qiao M (2003) *J Mol Catal A* 203:267.
- [11] Nski JK, Winiarek P, Paryjczak T, Lewicki A, Mikołajska A (2002) *Appl Catal A* 233:171.
- [12] Nagaraja BM, Padmasri AH, Raju BD, Rama Rao KS (2007) *J Mol Catal A* 265:90.
- [13] Resasco DE, Crossley S (2009) *AIChE J* 55:1082.
- [14] Chheda JN, Dumesic JA (2007) *Catal Today* 123:59.
- [15] West RM, Kunkes EL, Simonetti DA, Dumesic JA (2009) *Catal Today* 147:115.
- [16] Fisk CA, Morgan T, Ji Y, Crocker M, Crofcheck C, Lewis SA (2009) *Appl Catal A* 358:150.
- [17] Mercader FM, Groeneveld MJ, Kersten SRA, Way NWJ, Schaverien CJ, Hogendoorn JA (2010) *Appl Catal B* 96:57.
- [18] Barama S, Batiot CD, Capron M, Richard EB, Mohammedi OB (2009) *Catal Today* 141:385.
- [19] Gusovius AF, Watling TC, Prins R (2008) *Appl Catal A Gen* 343:16.

-
- [20] Sitthisa S, Sooknoi T, Ma Y, Balbuena PB, Resasco DE (2010) *J Catal* 277:1.
- [21] Aguila G, Gracia F, Araya P (1986) *App Catal A Gen* 101:162.
- [22] Colombo Y, Gazzarini F, Lanzavecchia G (1967) *Mater Sci Eng* 2:125
- [23] Szekely J, Lin CI, Sohn HY (1973) *Chem Eng Sci* 28:1975.
- [24] Ermakova MA, Ermakov DY (2002) *Catal Today* 77:225.
- [25] Montes M, Penneman de Bosscheyde Ch, Hodnett BK, Delannay F, Grange P, Delmon B (1984) *Appl Catal* 12:309.
- [26] Rao R, Dandekar A, Baker RTK, Vannice MA (1997) *J Catal* 171:406.
- [27] Wu J, Shen Y, Liu C, Wang H, Geng C, Zhang Z (2005) *Catal Comm* 9:633.
- [28] Nagaraja BM, Padmasri AH, Raju BD, Rao KSR (2007) *J Mol Catal A:Chem* 265:90.
- [29] Nagaraja BM, Kumar VS, Shasikala V, Padmasri AH, Sreedhar B, Raju BD, Rao KSR (2003) *Catal Comm* 4:287.
- [30] Avery NR (1983) *Surf Sci* 125:771.
- [31] Boronat M, May M, Illas F (2008) *Surf Sci* 602:3284.
- [32] Chambers A, Jackson SD, Stirling D, Webb G (1997) *J Catal* 168:301.
- [33] Saadi A, Rassoul Z, Bettahar MM (2000) *J Mol Catal A Chem* 164:205.
- [34] Srivastava RD, Guha AK, (1985) *J Catal* 91:254
- [35] Shekhar R, Plank RV, Vohs JM, Barteau MA (1997) *J Phys Chem B* 101:7939.
- [36] Davis JL, Barteau MA (1989) *J Am Chem Soc* 111:1782.

-
- [37] Bradley MK, Robinson J, Woodruff DP, (2010) Surf Sci 604:920.
- [38] Mavrikakis M, Barteau MA (1998) J Mol Catal A 131:135.
- [39] Xinghua Z, Tiejun W, Longlong M, Chuangzhi W (2010) Fuel 89:2697.
- [40] Orita H, Itoh N (2004) Surf Sci 550:177.

CHAPTER 4

Kinetics and Mechanism of Hydrogenation of Furfural on Copper Catalyst

4.1 Introduction

This chapter focuses on the detailed study of furfural conversion on Cu catalyst. As shown in chapter 3, Cu is highly selective for hydrogenation of furfural to furfuryl alcohol, with methyl furan only appearing at temperatures $>200^{\circ}\text{C}$. However, the exact reaction pathway by which the carbonyl group of aldehyde functional group gets hydrogenated is not fully understood. For example, it has been proposed that the first step is the formation of a C-H bond, yielding an alkoxy intermediate, which is then followed by the addition of the second H atom to this intermediate, forming an adsorbed alcohol [1]. Alternatively, it is also possible that the first step might involve the addition of H to the O atom, thus forming a hydroxylalkyl intermediate, which subsequently would yield the adsorbed alcohol [2,3]. In this chapter, we examine both mechanisms for the case of furfural on Cu surfaces, which has not been previously investigated. We

have investigated the kinetics and reaction pathways of furfural hydrogenation over a silica-supported Cu catalyst. These studies have been complemented with DFT calculations of adsorbed furfural on Cu(111) and Cu(110) planes, as well as DRIFTS analysis of adsorbed furfural species conducted on unsupported Cu metal powder, to avoid adsorption on the support that masks the signal from the metal. DFT calculations and DRIFTS have helped us identify the type of adsorbed species on the Cu surface and explore the reaction pathways involved in the conversion of furfural. It is important to note that the supplemented DFT results reported were taken from Yuguang Ma, Perla B. Balbuena [4]. Understanding the chemistry of the aldehyde functional group on Cu surfaces may have a broader impact on the study of other deoxygenation reactions involved in the refining of biomass-derived oils.

4.2 Cu/SiO₂ Catalyst characterization

A typical TEM image of the Cu/SiO₂ catalyst is presented in Figure 4.1. It can be seen that the metallic copper clusters are well dispersed on the silica support, with an average particle size of ~3 nm. Estimated Cu

dispersion (based on TEM Cu cluster size), Cu content, and BET total surface area of the catalyst are reported in Table 4.1. The maximum rate of H₂ consumption was observed at about 350°C. Therefore, complete reduction of Cu can be expected after a pre-reduction treatment conducted in pure H₂ at 350°C for 1 h.

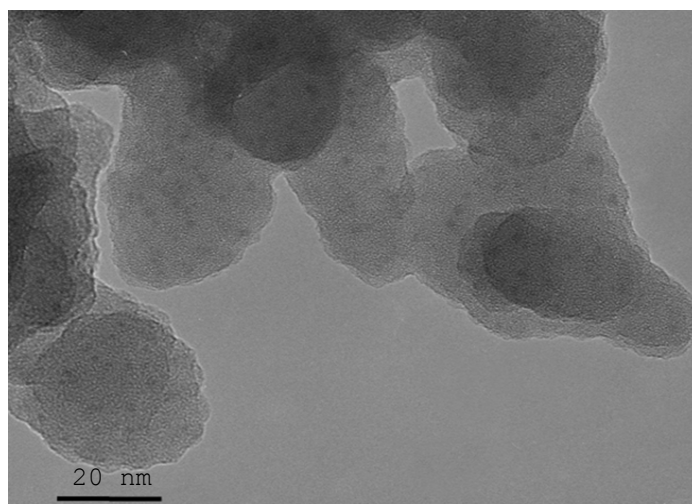


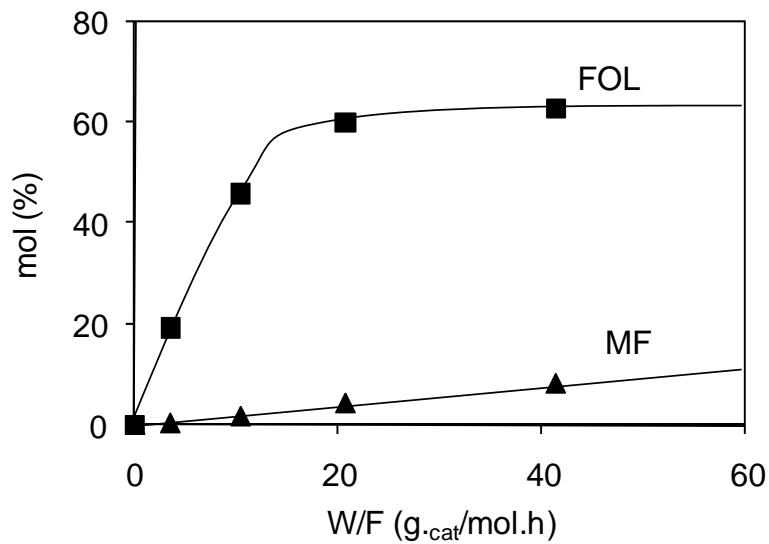
Figure 4.1 TEM micrograph of the 10% Cu/SiO₂ catalysts, showing ~3-4 nm Cu clusters dispersed on the silica support particles (~ 50 nm)

Table 4.1 Properties of the 10 wt% Cu/SiO₂ catalyst

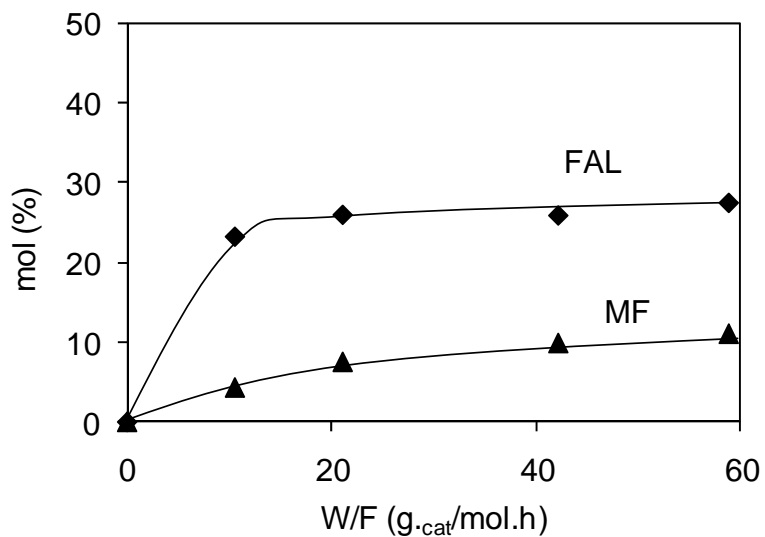
Cu average particle diameter	3.2 ± 0.2nm
Cu dispersion from TEM	40 ± 2.5%
BET surface area	110 ± 10 m ² /g
Catalyst particle size	250-425 μm
Cu metal content	10.3 wt%

4.3 Furfural reaction over Cu/SiO₂ catalyst

No deactivation was observed in any of the catalytic activity runs during 4 h of steady state conversion. However, to compare the runs under identical conditions, a fresh catalyst was used in each separate experiment. As previously shown in chapter 3 (Table 3.1), the reaction of furfural (FAL) on Cu/SiO₂ gives mainly furfuryl alcohol (FOL), with 2-methylfuran (MF) as a minor product, which is significant only above 230°C.



(a)

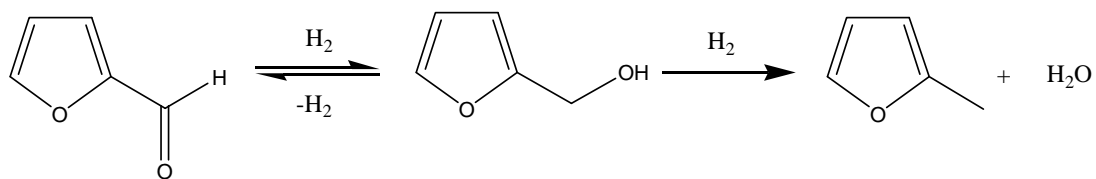


(b)

Figure 4.2 Yield of products from the reaction of (a) furfural (FAL) and (b) furfuryl alcohol (FOL) over 10 wt%Cu/SiO₂. Temp=290°C, H₂/feed ratio = 25, H₂ Pressure = 1 atm, TOS = 15 min.

As shown in Figure 4.2, 2-methylfuran is clearly a secondary product of the aldehyde (i.e. zero derivative at

low W/F in Figure 4.2a), but a primary product of the conversion of the alcohol (i.e., non-zero derivative at low W/F in Figure 4.2b). Therefore, it is apparent that furfural is first converted into furfuryl alcohol, and the deoxygenation only occurs from the alcohol. As shown in Figure 4.2a, at high W/F, the yield of furfuryl alcohol reaches a plateau as the aldehyde/alcohol equilibrium conversion is approached. Similarly, a plateau in furfural formation is reached at high W/F when the feed is pure furfuryl alcohol (Figure 4.2b). However, no decarbonylation product was observed at any temperature of the range in this investigation. In summary, from this simple analysis the reaction pathway can be described as follows:



4.4 Kinetics of furfural conversion on Cu/SiO₂

From the reaction pathway proposed above, a rate expression based on the conventional Langmuir-Hinshelwood kinetic model was derived, with the following assumptions [5,6].

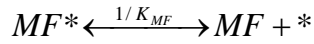
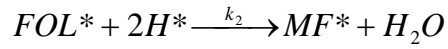
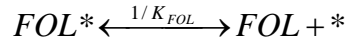
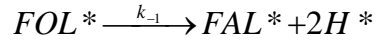
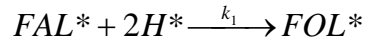
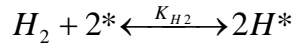
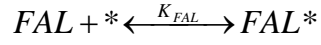
(i) molecular adsorption of furfuraldehyde (FAL),
furfuryl alcohol (FOL), and 2-methyl furan (MF),

(ii) dissociative adsorption of hydrogen,

(iii) all adsorption sites are equivalent and
independent of coverage, and

(iv) surface reaction is the rate-determining step.

Accordingly, the elementary steps for furfural conversion can be described by the following equations, in which * represents an active site.



Since in excess of hydrogen, the partial pressure of hydrogen can be considered constant during the entire reaction period, the rate expressions become:

$$r_{FAL} = -k_1\theta_{FAL} + k_{-1}\theta_{FOL}$$

$$r_{FOL} = k_1\theta_{FAL} - k_{-1}\theta_{FOL} - k_2\theta_{FOL}$$

$$r_{MF} = k_2\theta_{FOL}$$

where, θ_{FAL} is the fractional coverage of furfuraldehyde, θ_{FOL} the fractional coverage of furfuryl alcohol, and θ_{MF} the fractional coverage of 2-methyl furan.

$$\theta_{FAL} = K_{FAL} P_{FAL} \theta_V$$

$$\theta_{FOL} = K_{FOL} P_{FOL} \theta_V$$

$$\theta_{MF} = K_{MF} P_{MF} \theta_V$$

$$\theta_H = K_{H_2}^{1/2} P_{H_2}^{1/2} \theta_V$$

Using the conventional LH kinetics derivation, the rate expressions become:

$$r_{FAL} = -k_1 K_{FAL} P_{FAL} \theta_V + \frac{k_1}{K} K_{FOL} P_{FOL} \theta_V$$

$$r_{FOL} = k_1 K_{FAL} P_{FAL} - \left[\frac{k_1}{K} K_{FOL} P_{FOL} \theta_V + k_2 K_{FOL} P_{FOL} \theta_V \right]$$

$$r_{2-MF} = k_2 K_{FOL} P_{FOL} \theta_V$$

$$\theta_V = \frac{1}{1 + K_{FAL} P_{FAL} + K_{FOL} P_{FOL} + K_{MF} P_{MF} + K_{H_2}^{1/2} P_{H_2}^{1/2}}$$

The results of the fitting of the experimental concentrations of furfural, furfuryl alcohol and 2-methyl furan as a function of space time (W/F) with the kinetic model derived from these equations are shown in Figures 4.3, 4.4 and 4.5 for the feeds of furfural, furfuryl alcohol, and an equimolar mixture of furfural and furfuryl alcohol, respectively. A very satisfactory agreement between the kinetic model and the experimental data was obtained over the entire range of W/F and temperatures. Only a slight discrepancy has been observed in the prediction of 2-methyl furan, which seems to be slightly higher than the experimental measurement.

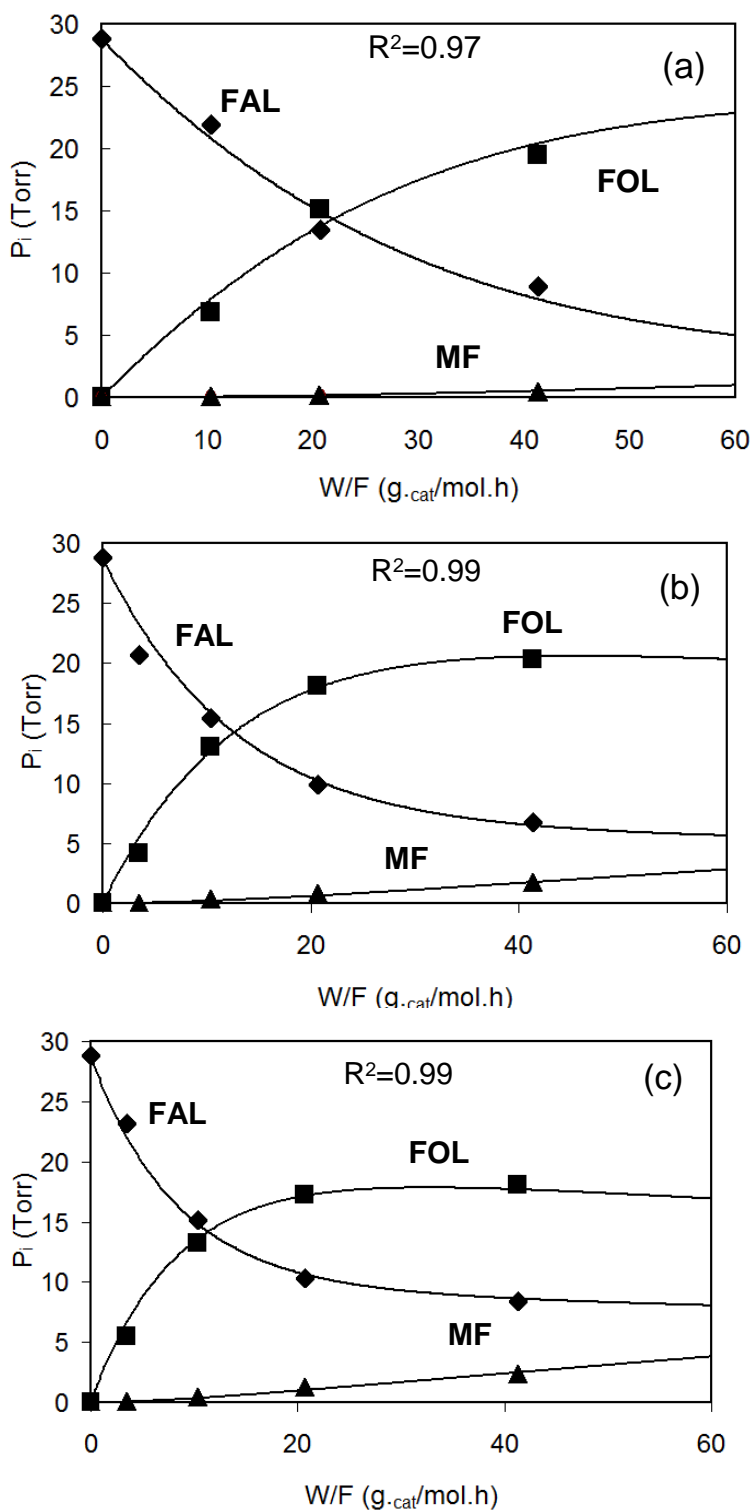


Figure 4.3 Partial pressures of the reactant and products from the reaction of furfural on the 10 %Cu/SiO₂ catalyst at (a) 230°C, (b) 270°C and (c) 290°C. The points are experimental data and the lines are calculated from the kinetics model.

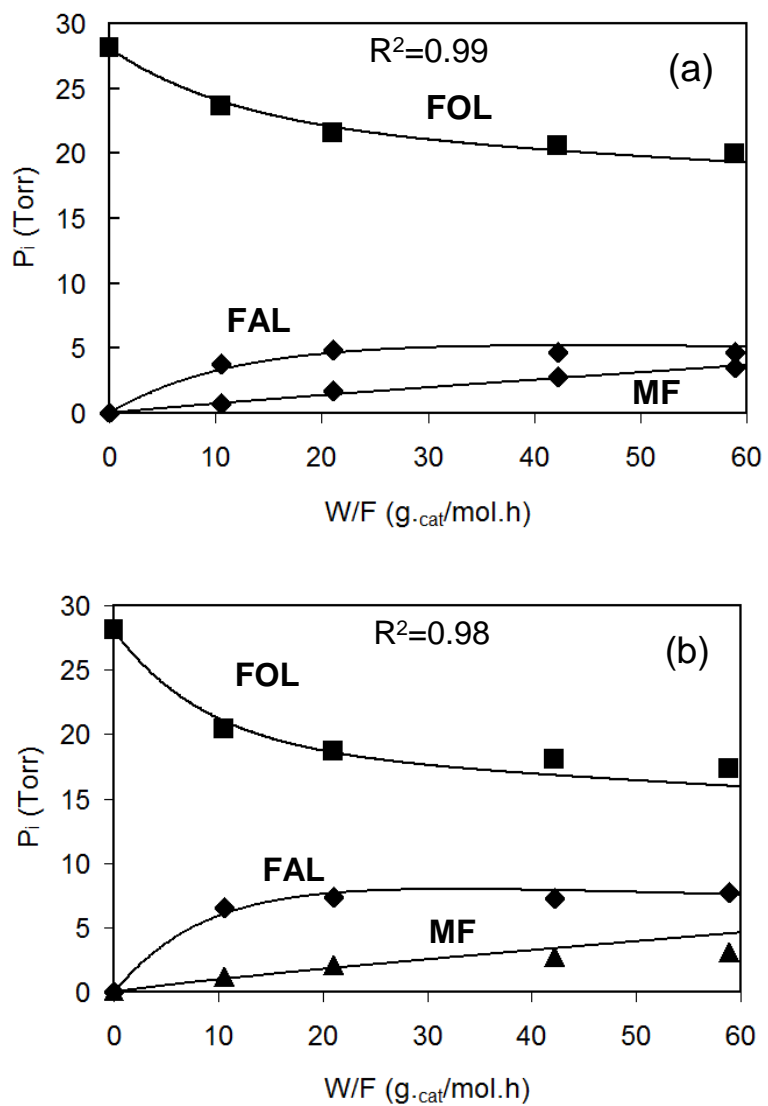


Figure 4.4 Partial pressures of the reactant and products from the reaction of furfuryl alcohol on the 10 wt%Cu/SiO₂ catalyst at (a) 270°C and (b) 290°C. The points are experimental data and the lines are calculated from the kinetics model.

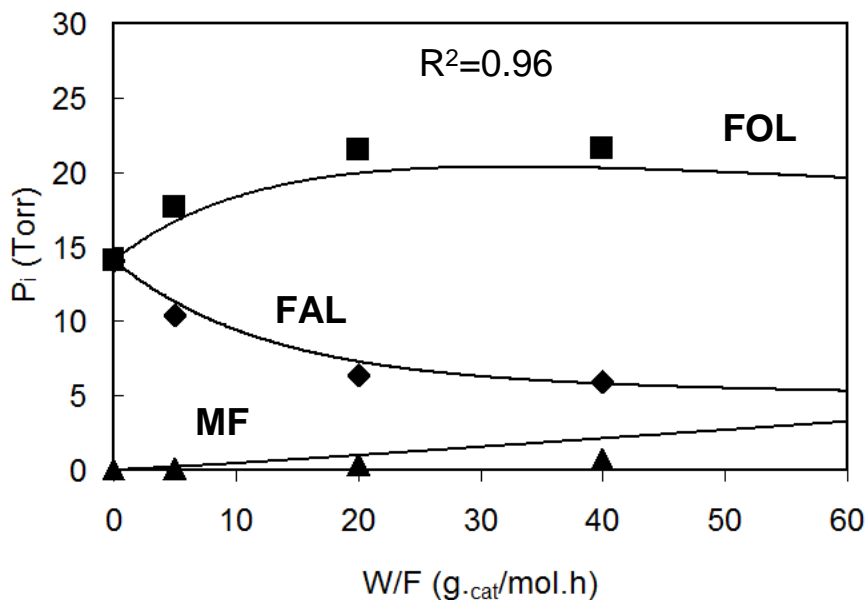


Figure 4.5 Partial pressures of the reactant and products from the reaction of a mixture of 50 mol% furfural and 50 mol% of furfuryl alcohol on the 10 wt%Cu/SiO₂ catalyst at 270°C. The points are experimental data and the lines are calculated from the kinetics model.

The equilibrium (K_{eq}) and kinetic (k_i) constants obtained from the fitting at three different temperatures are shown in Table 4.2.

Table 4.2 Kinetic and thermodynamic parameters obtained from fitting the experimental data with the kinetic model at various temperatures

Temp (°C)	Equilibrium	Rate constant			Adsorption constant (Torr ⁻¹)				
	constant	(mmol/g.cat.h)			K _{FAL}	K _{FOL}	K _{MF}	K _{H2}	K _W
	(K _{eq})	k ₁	k ₂						
230	4.56	3.00	0.10	0.29	0.18	0.083	11.9x10 ⁻⁵	0.25	
270	2.98	5.93	0.24	0.12	0.11	0.063	4.2x10 ⁻⁵	0.10	
290	2.01	8.05	0.34	0.08	0.09	0.056	2.7x10 ⁻⁵	0.07	

ΔS_{ads} (cal.mol ⁻¹ .K ⁻¹)					S_g (cal.mol ⁻¹ .K ⁻¹)				
FAL	FOL	MF	H ₂	H ₂ O	FAL	FOL	MF	H ₂	H ₂ O
-13.8	-4.0	-1.0	-32.9	-14.2	-	-	-	34.1	47.4

As expected, since K_{eq} represents the equilibrium constant for the exothermic furfural hydrogenation reaction it decreases with temperature. The corresponding heat of reaction (ΔH), calculated by substituting the equilibrium constants in the Van't Hoff equation was 11.9 kcal/mol. All the kinetic rate constants (k_i) increase with temperature and the Arrhenius plots (see Figure 4.6a) yield straight lines, from which true activation energies are readily obtained. The corresponding values were of 11.8 kcal/mol and 12.4 kcal/mol for the hydrogenation of furfuraldehyde (E_1) and the hydrodeoxygenation of furfuryl alcohol (E_2), respectively. These values are also in line with those reported for the same reactions conducted over a copper chromite catalyst [7], and as shown below, agree well with those predicted from DFT calculations.

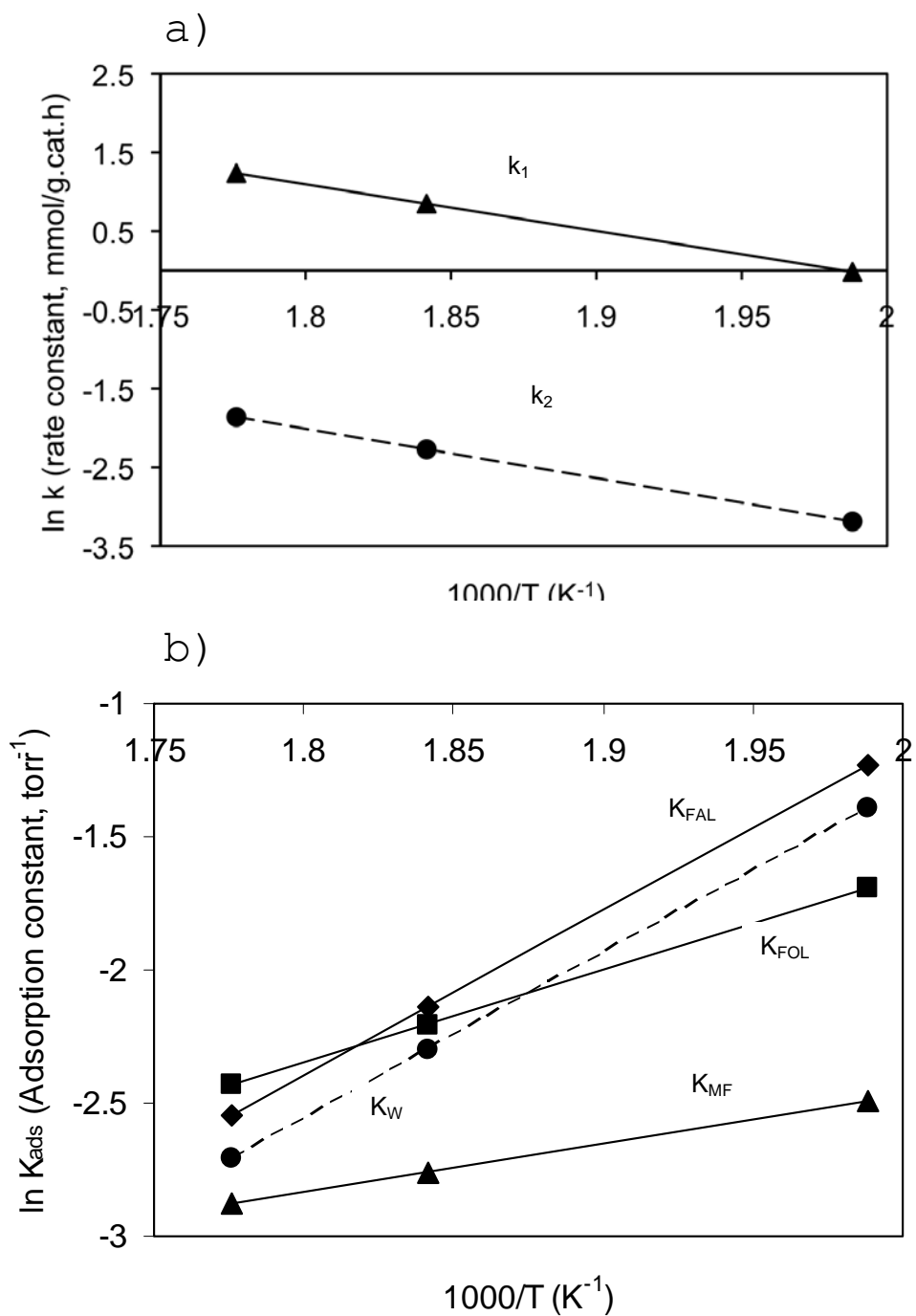


Figure 4.6 Rate constants, k_i , a) and adsorption equilibrium constants, K_{ads} , b) as a function of inverse temperature.

The equilibrium adsorption constants (K_i) can be readily derived from the fittings. The K_i values shown in Table 4.2 decrease with increasing temperature, as expected. Accordingly, the $\ln K_i$ Vs. $1/T$ plots (Figure 4.6b) can be used to estimate the heats of adsorption for all the species involved, according to the Van't Hoff equation. In line with previous reports [6], the values of K_{H_2} are relatively small in comparison with the other K_i on Cu catalyst. From these plots, the heat of adsorption of hydrogen on Cu/SiO₂ was determined to be 13.9 kcal/mol, which is in excellent agreement with those reported in the literature [5,6]. The heat of adsorption of furfural (12.3 kcal/mol) is shown to be higher than that of furfuryl alcohol (6.9 kcal/mol). In agreement with these estimates, Riox and Vannice [6], reported that the heat of adsorption of carbonyl-containing molecules on copper (aldehyde/ketone) is significantly higher than that of molecules containing the C-OH group (alcohol). More interestingly, the kinetically-derived heat of adsorption of 2-methylfuran (3.7 kcal/mol) on Cu is dramatically lower than that of furfural, and even close to a heat of physisorption. As discussed below, the DFT calculations clearly show that the strongest interaction of furfural with the Cu surface is via the carbonyl oxygen. However,

the furan ring is not strongly bound to the surface, but rather it exerts a repulsion that increases with the surface density of Cu atoms. This behavior contrasts with that of other metals such as Pd or Pt, which can strongly bind the furan ring [8,9].

The validity of the kinetic model and fitting parameters was tested with additional reactions runs, in which mixtures of furfural, furfuryl alcohol, and 2-methyl furan, were fed in different proportions. Without changing any of the fitting parameters obtained in the original fitting, the experimental yields obtained with the mixtures were compared with the values predicted from the model. As shown in Figure 4.7, excellent agreement between the predicted values and the experimental data was obtained in each of the additional runs.

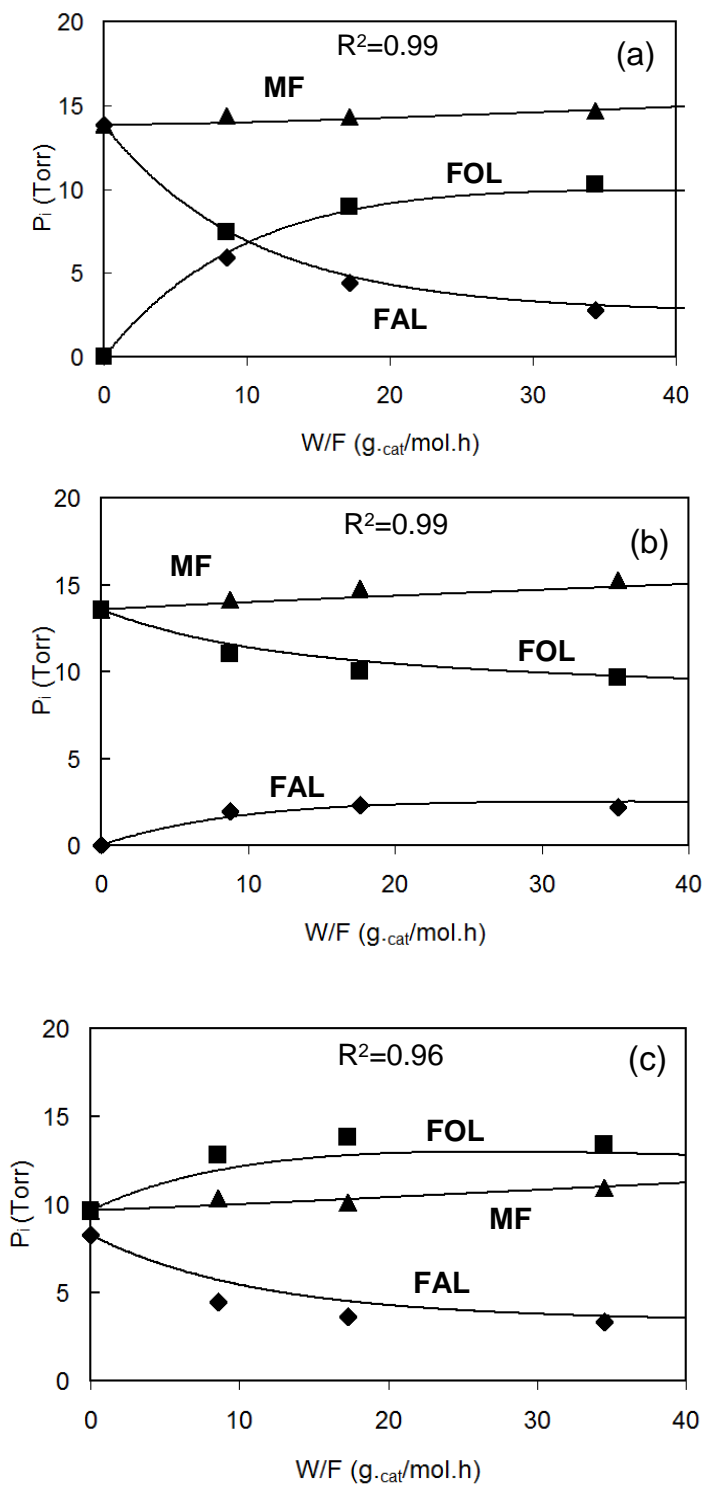


Figure 4.7 Partial pressures of the reactant and products from the reaction of the following mixtures a). 50% FAL - 50% MF b). 50% FOL - 50% MF c). 30% FAL - 35% FOL - 35% MF

The kinetic model and all the associated parameters were also valid for predicting the reaction of furfuraldehyde in the presence of water (at a H₂O/FAL ratio of 20 mol/mol). To account for the effect of water coverage (θ_w) a new term was included in the denominator of the kinetics model. By only fitting the new term in the kinetic model, K_w , but without modifying any of the other parameters obtained previously, the fitting was entirely in agreement with the experimental results, as shown in Figure 4.8. To test the robustness of the model, we allow the rest of the kinetic parameters to vary simultaneously with the variation of the water terms. Regardless of the initial conditions chosen for the fitting, the results were the same (within 0.1%); with only the new water term parameter changing with respect to the case of the water-free runs. This result indicates that water competes with the other species for adsorption sites without changing the equilibrium of the other species. That is, the original kinetic model and all the associated parameters were valid for predicting the reaction of FAL in the presence of water. The resulting equilibrium adsorption constant of water (K_w) varied from 0.249 to 0.067 as the temperature varied from 230 to 290°C. The linear plot of $\ln K_w$ Vs $1/T$ in Figure 6b was used to obtain a heat of

adsorption of 12.4 kcal/mol for water on the Cu surface of Cu/SiO₂. As the heat of adsorption of water is relatively high, the competitive adsorption of water with furfural molecule on the Cu surface can be expected to lower the conversion, as seen in Figure 4.9. However, in agreement with the rate expression, the effect of water was less pronounced at high temperature, despite the high concentration of water in the vapor phase.

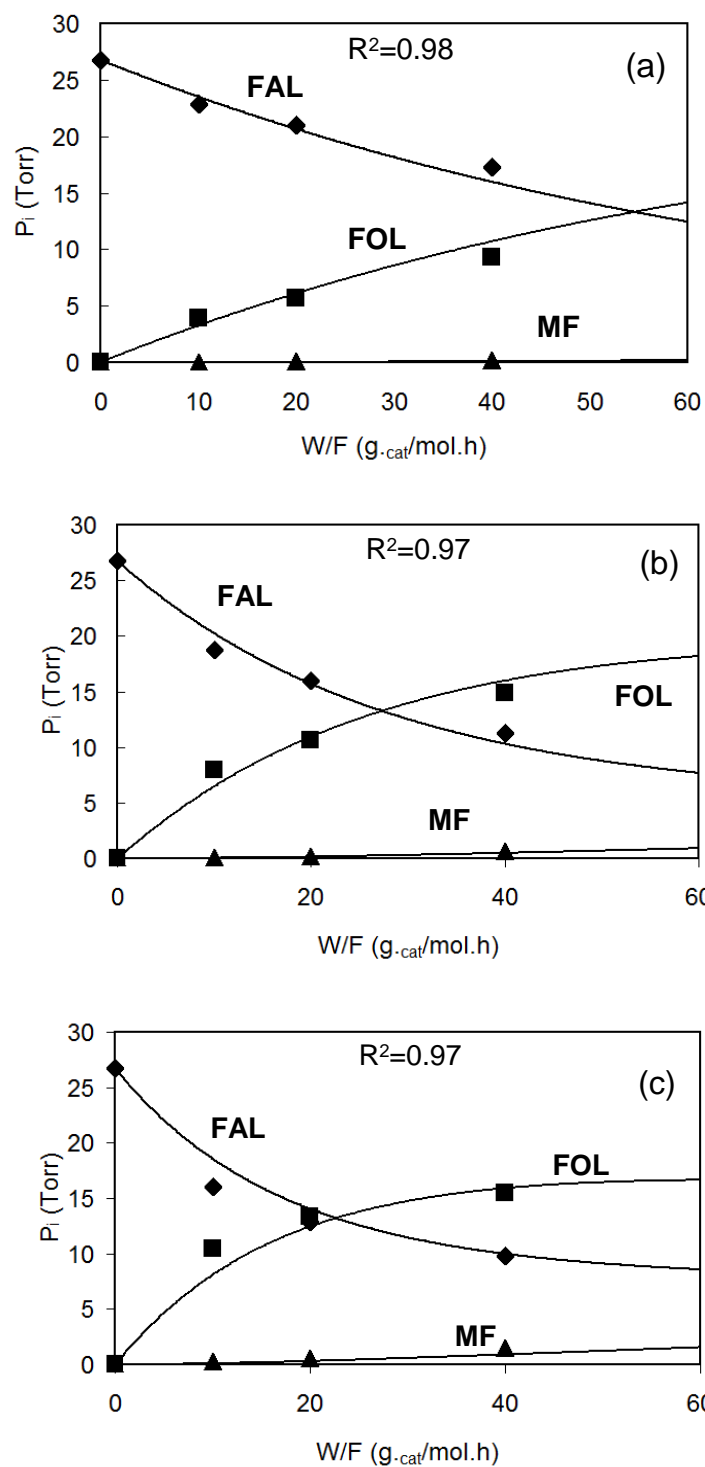


Figure 4.8 Partial pressures of the reactant and products from the reaction of furfural in the presence of water at (a) 230°C (b) 270°C and (c) 290°C . Feed mole composition-furfural:water, 1:20. The points are experimental data and the lines are calculated from the kinetics model.

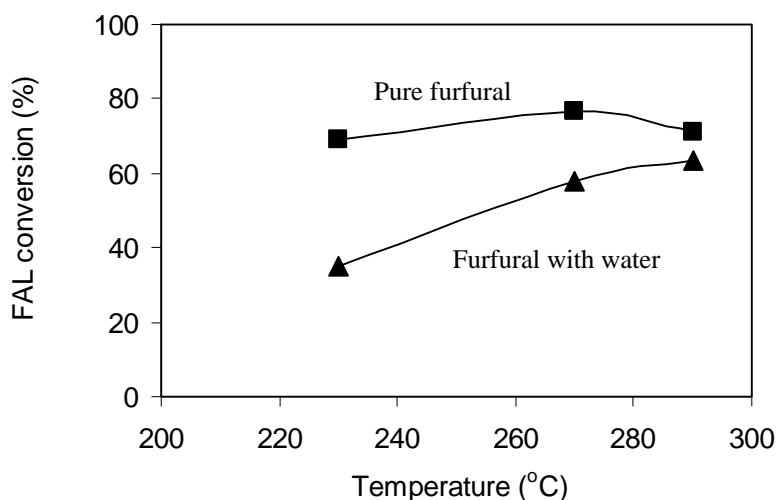


Figure 4.9 Conversion of furfural over 10 wt%Cu/SiO₂. Temp=290°C, H₂/feed ratio = 25, H₂ Pressure = 1 atm, TOS = 15 min.

Vannice [10] has recommended a set of criteria to validate the thermodynamic parameters extracted from kinetic fittings. The ΔS_{ads} must be negative and it must be in absolute value smaller than the standard entropy in the vapor phase. The calculated ΔS_{ads} values for all species, as derived from the fittings are summarized in Table 4.2. The calculated entropy change for adsorption of each one of the species obtained from the intercept in the Van't Hoff plot is negative and comply with the criteria $0 < -\Delta S_{\text{ads}} < S_{\text{g}}$ [10,11]. The ΔS_{ads} value for water ($-14.2 \text{ cal mol}^{-1} \text{ K}^{-1}$) and for hydrogen ($-32.9 \text{ cal mol}^{-1} \text{ K}^{-1}$) adsorption were

lower than the value of the absolute gas-phase entropy [12]. The values for gas-phase entropy (S_g) for FAL, FOL and MF were not available for comparison, but reported values for similar compounds (e.g. isopropanol, acetone) range between 65 and 75 cal mol⁻¹ K⁻¹[6], significantly higher than the ΔS_{ads} values obtained from the fittings. The ΔS_{ads} value of -32.4 cal.mol⁻¹.K⁻¹ for H₂ on Cu, which is close to the S_g value of -34.1 cal.mol⁻¹.K⁻¹ [12], is higher than that for H₂ on Pd (-28.9 cal.mol⁻¹.K⁻¹) [13], and this indicates that the H atoms are weakly adsorbed and should be quite mobile on the Cu surface.

4.5 DRIFT spectra of furfural adsorbed on Cu

Barteau and co-workers have extensively investigated the nature of surface species during the adsorption of aldehydes on different metals [14-17]. They have shown that, depending on the type of metal surface and reaction conditions, aldehydes tend to form surface intermediates, in which either only the carbonyl O is adsorbed atop a metal atom, i.e. $\eta^1(O)$, or both C and O interact with the surface, i.e. $\eta^2(C,O)$. For example, they have shown that while the $\eta^2(C,O)$ state is preferred on clean Pd surfaces,

the $\eta^1(0)$ state is preferred when oxygen is preadsorbed [15,16].

In this work, we have conducted DRIFT spectroscopy to elucidate the nature of the most abundant surface aldehydes on Cu. On a high surface-area supported catalyst, such as Cu/SiO₂, furfural mainly adsorbs on the surface of silica [18], as seen by the decrease in the intensity of the silanol group band (-Si-OH, 3,740 cm⁻¹) [19] and the increase of a broad band at 3,450 cm⁻¹ due to the interaction of silanol with furfural (Figure 4.10a). The silanol group band can be recovered by increasing the temperature to 400°C (Figure 4.10b). Therefore, due to the strong interaction between furfural and silica, the adsorption of furfural on Cu cannot be clearly observed. Therefore, to eliminate the effect of the support, pure copper metal was used.

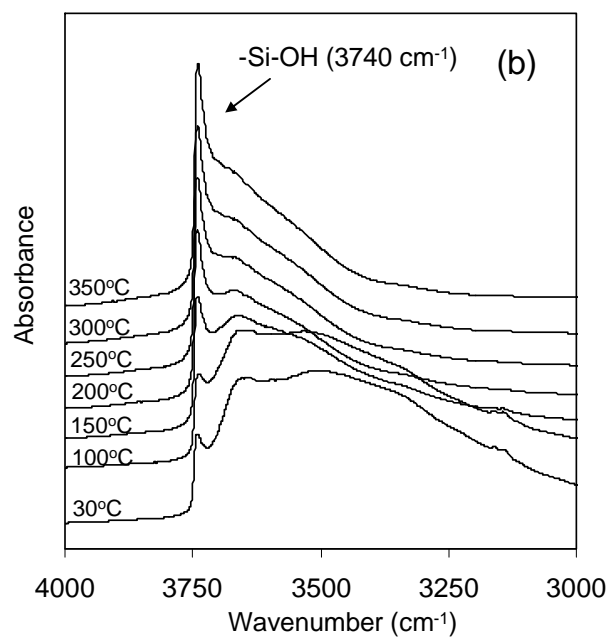
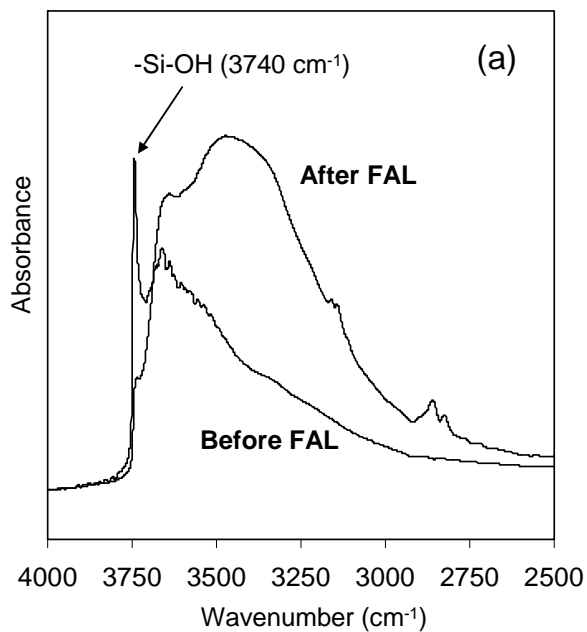


Figure 4.10 DRIFT spectra of 10 Cu/SiO_2 at 30°C recorded before and after adsorption of furfural(a); and at increasing temperatures following adsorption (b).

Gas phase furfural shows the C=O stretching vibration mode at $1,720\text{ cm}^{-1}$ along with the C-H stretching band of the aldehydic hydrogen at $2,700\text{ cm}^{-1}$ and $2,800\text{ cm}^{-1}$. As shown in Figure 4.11, the C=O stretching band in the adsorbed furfural species appears at around $1,670\text{ cm}^{-1}$, downshifted from the wavenumber observed for gas-phase furfural. This lower frequency indicates a weakening of the C=O bond as a result of the interaction with the surface [20,21], but only through an interaction with the carbonyl O, that is, $\eta^1(\text{O})$. Formation of a bi-coordinated $\eta^2(\text{C},\text{O})$ surface species would result in a much larger downshift, i.e., below wavenumbers of $1,450\text{ cm}^{-1}$ [22].

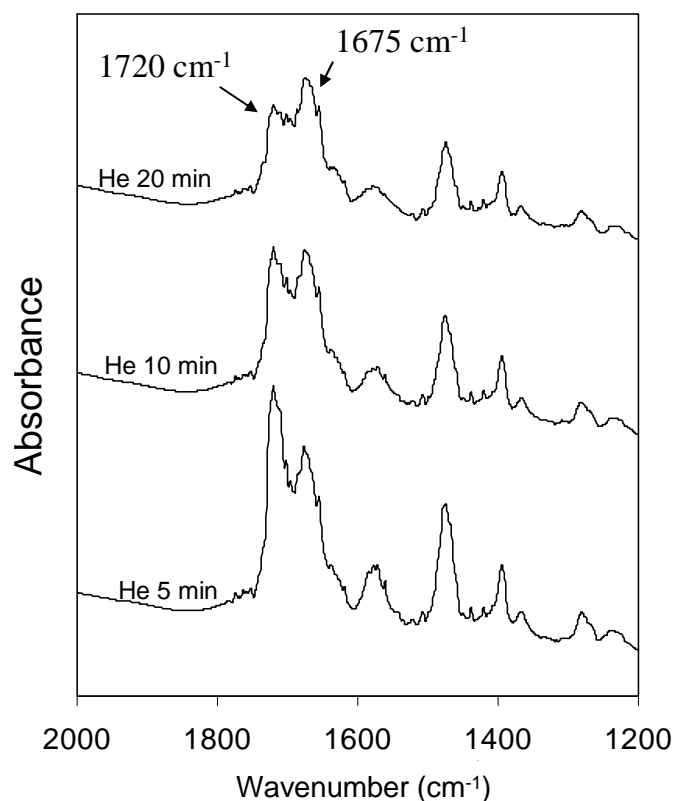


Figure 4.11 DRIFT spectra of furfural adsorbed on pure Cu metal powder at 30°C after pretreatment in H₂ at 350°C for 1 h.

4.6 DFT calculations of furfural on Cu surfaces

Density Functional Theory (DFT) calculations have been made to investigate geometries of the possible furfural on the surface of Cu(111). Fifteen geometries investigated by the DFT calculation were compared (see Appendix A). The results show that none of the parallel-ring configuration are stable on Cu(111). The perpendicular-ring mode shows stronger surface adsorption

than the parallel-ring one. The optimized geometries of the perpendicular-ring mode show that the carbonyl oxygen is closer to the Cu(111) surface compared to the furanyl ring oxygen, suggesting that the interaction the interaction between the carbonyl oxygen and the Cu(111) surface is the main contributor to the adsorption. The most stable configuration of furfural on Cu(111) surface is shown in Figure 4.12.

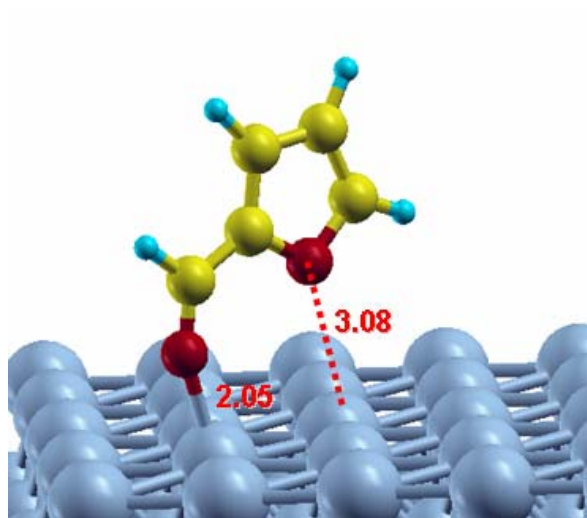


Figure 4.12 The most stable configuration of furfural on Cu(111) [4]

4.7 Discussion

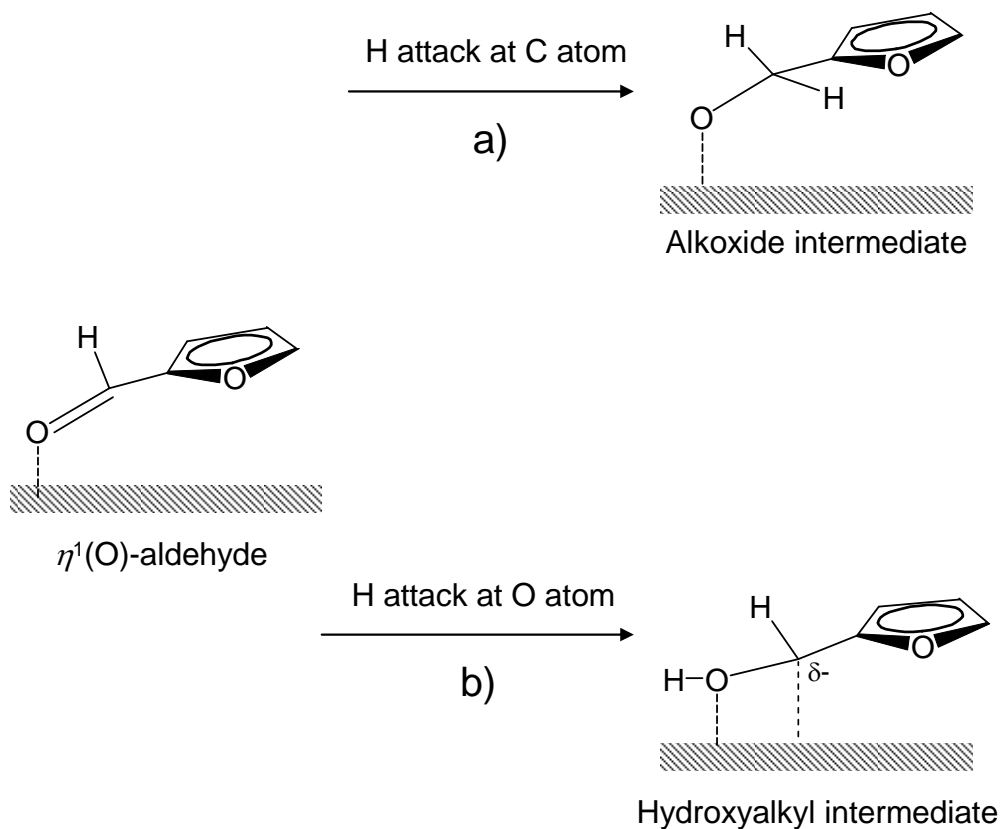
The hydrogenation of furfural on Cu yields furfuryl alcohol at high selectivity. Combined experimental and theoretical studies indicate that the molecularly adsorbed furfural interacts with the Cu surface via the lone pair of oxygen to produce $\eta^1(\text{O})$ -aldehyde species. This intermediate then becomes a precursor for the hydrogenation reaction. While the di-sigma complex $\eta^2(\text{C-O})$ aldehyde could also be a precursor for hydrogenation [24], our DRIFTS results suggest that furfural adsorbs via the carbonyl O atom. Similarly, DFT calculations show that the carbonyl perpendicular mode (O on top) is preferred on both Cu(111) and (110). The calculated adsorption enthalpies are in reasonable agreement with the fitting values obtained from kinetics model. The interaction between C and Cu atoms surface is relatively weak. There is a tendency of the adsorbed aldehyde to shift the C atoms away from the surface, even when both the C and O atoms were placed close to the surface in the initial configuration. That is, the $\eta^2(\text{C-O})$ aldehyde, commonly observed on other metals (e.g. Pd, Pt) is not preferred on the Cu surface. The DFT calculations also give evidence for a repulsion of the furan ring from the Cu(111)

surface, presumably due to the overlap of the 3d band of the surface Cu atoms and the anti-bonding orbital of the aromatic furan ring. On the Cu(110), the furan ring comes closer to the surface because a lower density of Cu atoms is involved in the interaction with the aromatic ring.

It is interesting to contrast the molecular interactions occurring on Cu with those on noble metals. For example, as opposed to Cu, Pd is known to adsorb the furan ring rather strongly due to a sp^2 -to- sp^3 rehybridisation [8,9]. A similar comparison can be made with the interaction of a molecule such as crotonaldehyde, which contains a carbonyl and a C=C bond. Analogous to the behavior shown here for furfural, it has been shown that on the Cu(111) surface, crotonaldehyde is bonded to the surface through the carbonyl O atom, with the C=C bond remaining largely unaffected and away from the surface [23]. By contrast, on Pt(111) the adsorption includes both C=O and C=C groups, with formation of $\eta^2(C,O)$ and $di-\sigma_{CC}$, respectively [24].

To analyze the hydrogenation reaction pathway on Cu, one can start with the $\eta^1(O)$ species. Two possibilities for the first attack by a H atom to the carbonyl group have been considered in the present contribution. The

corresponding surface intermediates adsorbed on the surface are shown below:



Based on the DFT calculations (see Appendix A), a first H attack to the O atom of the carbonyl that results in the formation of an hydroxyalkyl species (mechanism b) would have a lower energy barrier than a first H attack to the C atom of the carbonyl, which would lead to the formation of an alkoxy intermediate (mechanism a). The

difference in stability between the two intermediates can be ascribed to the stabilization role played by the aromatic furan ring. The addition of the first H atom to the O atom produces an unpaired electron on the C atom, which can be delocalized by the furan ring, which favors the formation of the hydroxylalkyl intermediate.

A similar concept can be applied to explain the higher stability of the hydroxyalkyl intermediate compared to the alkoxy intermediate in the hydrogenation of unsaturated aldehydes on Pt(111) [1-3]. In that case, the conjugation with the C=C bond would be expected to lower the energy barrier for the H attack at the O atom.

4.8 Conclusion

The conversion of furfural on Cu/SiO₂ yields mainly furfuryl alcohol from hydrogenation of the carbonyl, with only small amounts of 2-methylfuran, obtained from a subsequent cleavage of the C-O bond in furfuryl alcohol. A kinetic model for furfural conversion has been developed based on a Langmuir-Hinshelwood model. The results from the fitting show a good agreement with experimental data obtained independently and the model shows to be valid

when different mixtures are used as a feed, including the addition of water. Water is found to suppress furfural conversion, particularly at low temperatures. The physical parameters obtained from the fitting (heats of adsorption and activation energies) are in line with values previously reported in the literature. The rate constant for hydrogenation of furfural (k_1) is significantly higher than that for hydrodeoxygenation of furfuryl alcohol (k_2) to produce 2-methylfuran. The heat of adsorption (ΔH_{ads}) for furfuraldehyde (12.3 kcal/mol) is similar to that of adsorption of water (12.4 kcal/mol), but higher than those for furfuryl alcohol (6.9 kcal/mol) and 2-methylfuran (3.7 kcal/mol). Moreover, the heat of adsorption of furfuraldehyde is in agreement with the adsorption energy predicted by the DFT calculations using a Cu(110) surface (7.3 kcal/mol).

The DRIFTS and DFT results demonstrate that the adsorption of furfural takes place preferentially in a $\eta^1(\text{O})$ -aldehyde (perpendicular) binding mode. Two possible mechanisms for furfural hydrogenation have been compared, based on the order of the first H atom attack to the carbonyl group, resulting in two possible surface intermediates adsorbed on the Cu surface. The activation

energy barrier for the first H addition to the O carbonyl group to form adsorbed hydroxyalkyl intermediates was found to be lower than when the first addition of H is to the carbonyl C forming an alkoxy intermediate (i.e., 7.6 kcal/mol compared to 10.8 kcal/mol). These results suggest that the presence of the aromatic furan ring helps stabilizing the hydroxylalkyl intermediate, lowering the energy barrier for this path.

References

-
- [1] G.M.R. van Druten, V. Ponec, *Appl. Catal. A: General* 191 (2000) 163
 - [2] N.V. Pavlenko, A.I. Tripol'skii, G.I. Golodets, *Kinet. Katal.* 30 (1989) 1192
 - [3] R. Alcala, J. Greeley, M. Mavrikakis, J.A. Dumesic, *J. Chem. Phys.* 116 (2002) 8973
 - [4] S. Sitthisa, T. Sooknoi, Y. Ma, P.B. Balbuena, D.E. Resasco, *J. Catal.* 277 (2011) 1.
 - [5] M.A. Natal Santiago, M.A. Sanchez-Castillo, R.D. Cortright, J.A. Dumesic, *J. Catal.* 193 (2000) 16
 - [6] R.M. Rioux, M.V. Vannice, *J. Catal.* 216 (2003) 362
 - [7] R. Rao, A. Dandekar, R.T.K. Baker, M.A. Vannice, *J. Catal.* 171 (1997) 406
 - [8] M.K. Bradley, J. Robinson, D.P. Woodruff, *Surf. Sci.* 604 (2010) 920

-
- [9] M.J. Knight, F. Allegretti, E.A. Kroger, M. Polcik, C.L.A. Lamont, D.P. Woodruff, *Surf. Sci.* 602 (2008) 2524
- [10] M. A. Vannice, in "Kinetics of Catalytic Reactions," Springer (2005)
- [11] M.A. Vannice, S.H. Hyun, B. Kalpakci, W.C. Liauh, J. *Catal.* 56 (1979) 358
- [12] R.C. Weast, in "Handbook of Chemistry and Physics" CRC press (1975)
- [13] B. Wang, D.W. Goodman, G.F. Froment, *J. Catal.* 253 (2008) 229
- [14] R. Shekhar, M. A. Barteau, R. V. Plank, J. M. Vohs, *J. Phys. Chem. B* 101 (1997) 7939
- [15] J.L. Davis, M.A. Barteau, *J. Am. Chem. Soc.* 111 (1989)1782
- [16] J.L. Davis, M.A. Barteau, *Surf. Sci.* 268 (1992) 11.
- [17] M. Mavrikakis, M. A. Barteau *J. Mol. Catal. A: Chemical* 131 (1998) 135
- [18] J. Fujiki, H.J. Fan, H.H. Hattori, K. Tajima, Y.S. Tsai, E. Furuya, *Sep. Purif. Technol.* 60 (2008) 223
- [19] J.N. Kondo, E. Yoda, H. Ishikawa, F. Wakabayashi, K. Domen, *J. Catal.* 191 (2000) 275
- [20] N.R. Avery, *Surf. Sci.* 125(1983) 771
- [21] L.E. Murillo, and J.G. Chen, *Surf. Sci.* 602 (2008) 919
- [22] J.L. Davis and M.A. Barteau, *Surf. Sci.* 235 (1990) 235
- [23] M. Boronat, M. May, F. Illas, *Surf. Sci.* 602 (2008) 3284
- [24] F. Delbecq, P. Sautet, *J. Cata.* 211 (2002) 398

CHAPTER 5

Conversion of Aldehydes on Pd/SiO₂ and Bimetallic Pd-Cu/SiO₂ Catalysts

5.1 Introduction

In this chapter, we have investigated the hydrogenation, decarbonylation, and etherification of aldehydes on Pd and Pd-Cu catalysts. To predict the aldehyde adsorbed species that can be formed on both Pd and Pd-Cu surfaces, DFT calculations were performed. In particular, we compare here the reactivity of two different aldehydes, furfural and 2-methyl-pentanal (Experimental result of 2-methyl-pentanal from Trung Pham [1]), which not only exhibit interesting differences in their chemical behavior, but represent aldehydes that are of importance in the upgrading of renewable fuels. Furfural is produced both during pyrolysis of cellulose and in the dehydration of sugars [2,3]. 2-Methyl-pentanal is formed upon aldol condensation and hydrogenation of propanal, which also can be obtained from glycerol, a biodiesel by-product.

5.2 Catalyst characterization

5.2.1 Temperature Programmed Reduction (TPR)

The TPR profiles of the monometallic Pd/SiO₂ and Cu/SiO₂ and the bimetallic Pd-Cu/SiO₂ catalysts are compared in Figure 5.1. As previously observed, supported Pd can be more easily reduced than Cu. In fact, while Pd/SiO₂ exhibits mainly one peak at 97°C [4,5], Cu/SiO₂ shows mainly two peaks at 250°C and 325°C [6]. The formation of an alloy in bimetallic Cu-Pd catalyst can be made evident by the appearance of an additional broad peak located between the reduction temperature of Pd and Cu [7]. It is also seen that the intensity of this peak increases with Cu content, while that in the position of unalloyed Pd diminishes. From the TPR results, it can be concluded that on the 0.5 Pd : 0.5 Cu (% by weight) most of the Pd is forming an alloy with Cu, since the reduction peak corresponding to free-Pd has practically disappeared, in good agreement with previous TPR studies combined with X-ray absorption spectroscopy [8]. It is also worth noting that the presence of Pd increases the reducibility of Cu, leading to a shift toward lower temperatures.

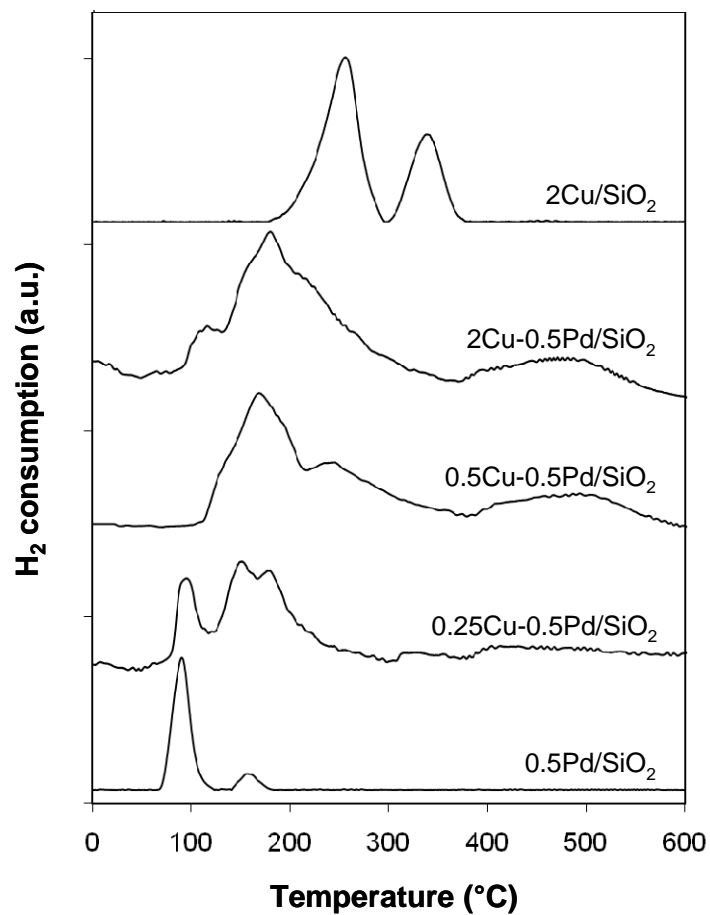


Figure 5.1 Temperature programmed reduction profiles (TPR) of Pd and Pd-Cu catalysts.

5.2.2 DRIFTS of adsorbed CO

DRIFT spectra of adsorbed CO on the Pd monometallic and Pd-Cu bimetallic catalysts are shown in Figure 5.2. On the pure Pd catalyst, the two characteristic bands at about 1,967 and 2,083 cm^{-1} are clearly seen, the former is typically associated to bridge and multiply bonded CO species, the latter to linearly adsorbed CO [9]. In line with previous reports [10-12] the bridge and multiply bonded CO species are greatly reduced, when even a small amount of the Group Ib metal is incorporated in the catalyst, typically explained in terms of the dilution of Pd ensembles [13,14]. In addition, as the Cu loading was increased, a new band was observed to grow at around 2,118 cm^{-1} . This band has previously been assigned to CO weakly adsorbed on either Cu sites or bimetallic Pd-Cu sites [15]. The 35 cm^{-1} shift to higher wavenumbers relative to that of CO linearly adsorbed on pure Pd surfaces may be due to a perturbation of the electronic structure of Pd caused by the presence of Cu. As discussed below, the XPS results show that the addition of Cu results in a slight increase in the electron binding energy of Pd 3d_{5/2}, which might indicate an electron transfer to Cu. In fact, a decreased electron density would cause a lower extent of

π -backdonation into anti-bonding orbitals of CO, which would explain the increased vibrational frequency. However, while Pd-Cu catalysts have been extensively investigated the extent and exact nature of electronic interactions are still a matter of discussion [16,17]. Recent theoretical studies [18,19] aiming at explaining the effects of electronic interactions in alloys on the adsorption phenomena indicate that, even without considering an electron transfer, alloying Cu to Pd causes a change in the position of the d-band center of Pd relative to the Fermi level. For example, Lopez and Norskov have observed that the Pd d-band center for Cu₃Pd(111) is shifted about 0.43 eV compared to the position of that for Pd(111), (i.e., -2.23 vs -1.80 eV). This shift away from the Fermi level causes a lower extent of π -backdonation from Pd to CO, resulting in a weakening of CO adsorption on PdCu alloy surfaces, as observed experimentally. Therefore, regardless of the exact nature of the Pd-Cu interaction, the net effect of Cu addition is a decreased extent of backdonation and a weaker adsorption strength.

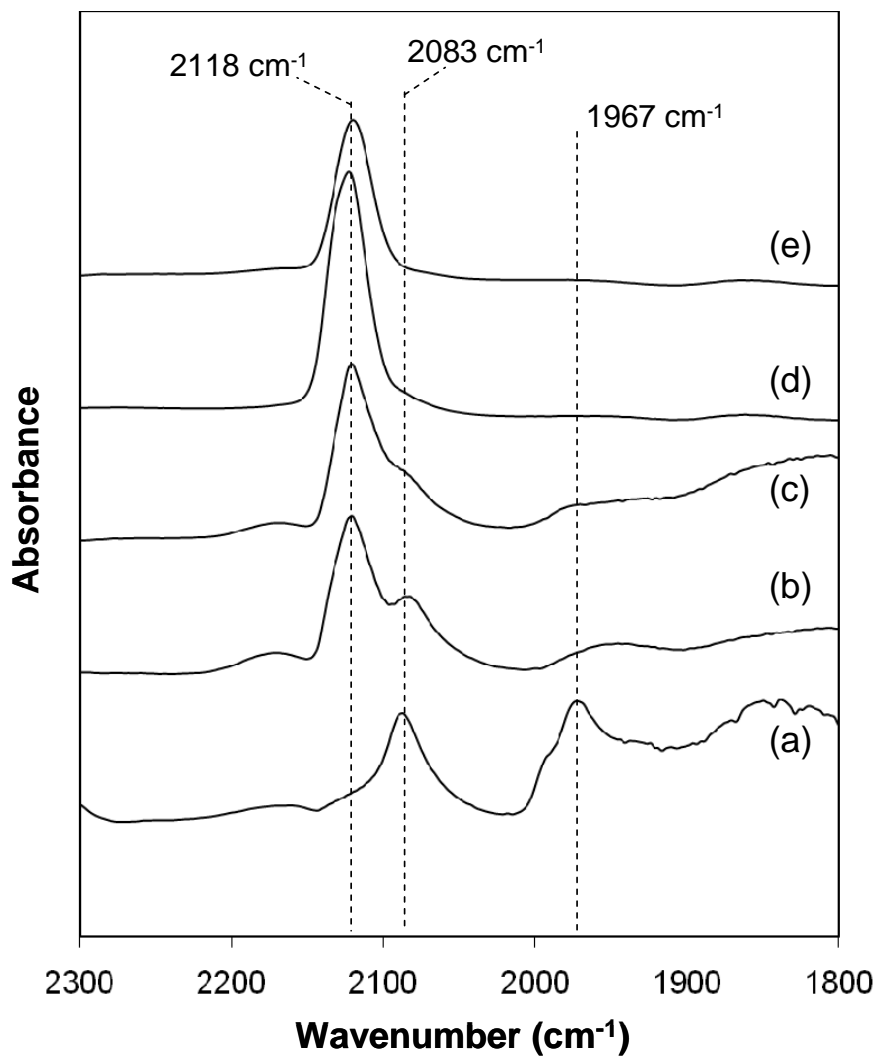


Figure 5.2 Infrared spectra of CO adsorbed on (a) 0.5Pd/SiO₂, (b) 0.25Cu-0.5Pd/SiO₂, (c) 0.5Cu-0.5Pd/SiO₂, (d) 2Cu-0.5Pd/SiO₂ and (e) 0.5Cu/SiO₂.

5.2.3 CO Chemisorption

Table 5.1 summarizes the CO/Pd chemisorption data obtained on the Pd-Cu catalysts of varying Cu loading. The results show that the CO uptake is significantly reduced with the addition of Cu on Pd/SiO₂. It is clear that a significant fraction of the surface is covered by PdCu, which has a weaker interaction with CO compared to pure Pd, as discussed above. These CO chemisorption results are also consistent with TPD-HREEL studies by Jeroro *et al.* [20], which show that the addition of Cu to Pd(111) resulted in a slight decrease in the area of the CO desorption peak as well as a small shift in the desorption temperature from 470 K to 465 K.

Table 5.1 Characteristics of the catalysts investigated.

Catalysts	Pd (%wt)	Cu (%wt)	CO/Pd ratio
5Pd	5	0	0.079
5Pd-0.25Cu	5	0.25	0.024
5Pd-2.5Cu	5	2.5	0.017

5.2.4 X-Ray Photoelectron Spectroscopy (XPS)

The XPS spectra for the reduced Pd and Pd-Cu catalysts are shown in Figure 5.3. While the catalysts were reduced ex-situ and then transferred into the UHV chamber, it is clear that they remained reduced during the transfer since the observed binding energy for Pd $3d_{5/2}$ in the monometallic catalyst was 335.4 eV, in good agreement with those reported in the literature [21]. It is observed that the overall intensity of the Pd peaks decreased with the addition of Cu, indicating a lower degree of exposed Pd in the bimetallic catalyst. In addition, there is a broadening of the peaks, which indicate changes in binding energy of a fraction of the Pd. The XPS bands of PdCu catalysts were deconvoluted by imposing two restrictions to the fit, the Pd $3d_{5/2}$ -to- $3d_{3/2}$ ratios were kept fixed at the value given by the relative multiplicity $(2j+1)$ and the energy separation between the two 3d peaks was kept the same for each Pd species proposed in the fit. Ruling out oxidation, this new peak may be attributed to electronic interactions between Pd and Cu, as discussed above. This result is consistent with XPS studies of bulk PdCu alloys obtained from Martensson *et al.* [22] which

also show an increase (< 1 eV) in binding energy for Pd $3d_{5/2}$ upon the addition of Cu compared to pure Pd.

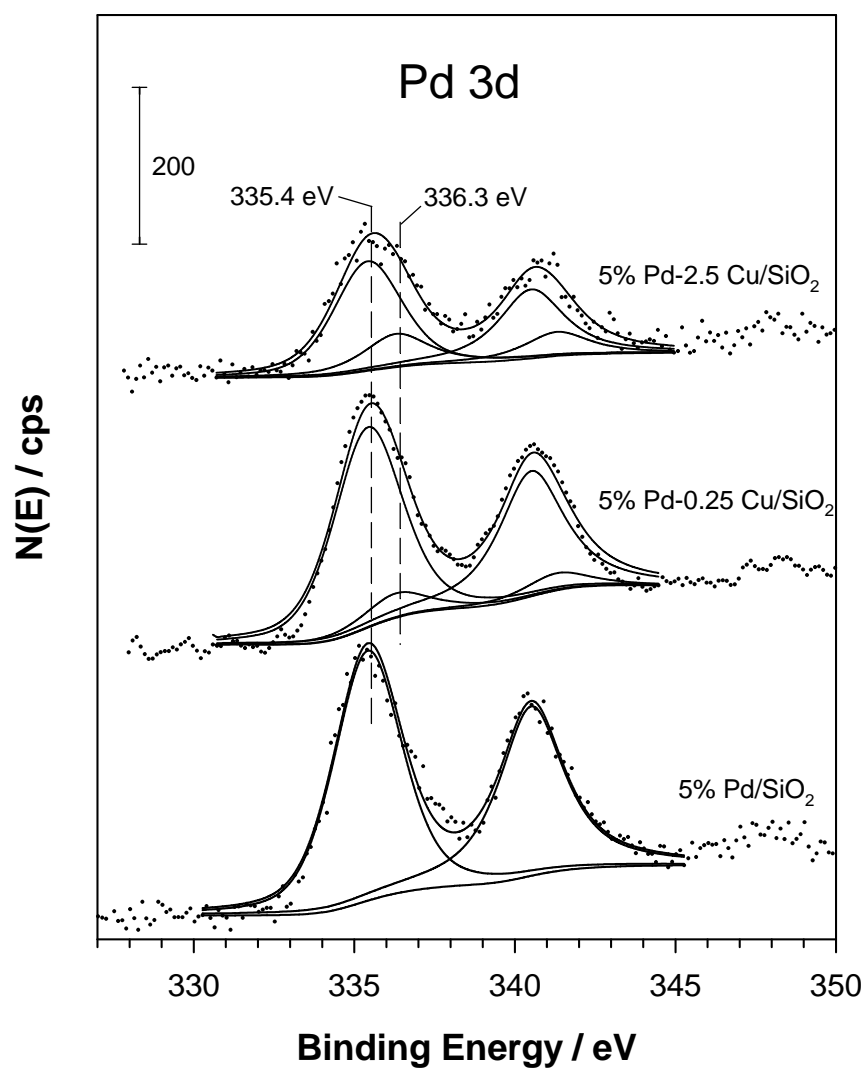


Figure 5.3 X-Ray Photoelectron Spectroscopy (XPS) of Pd_{3d} for different loadings of Cu in Pd/SiO₂ catalysts.

5.3 Reaction of aldehydes on monometallic Pd/SiO₂

The total conversion of furfural together with its product distribution is shown in Figure 5.4 as a function of W/F.

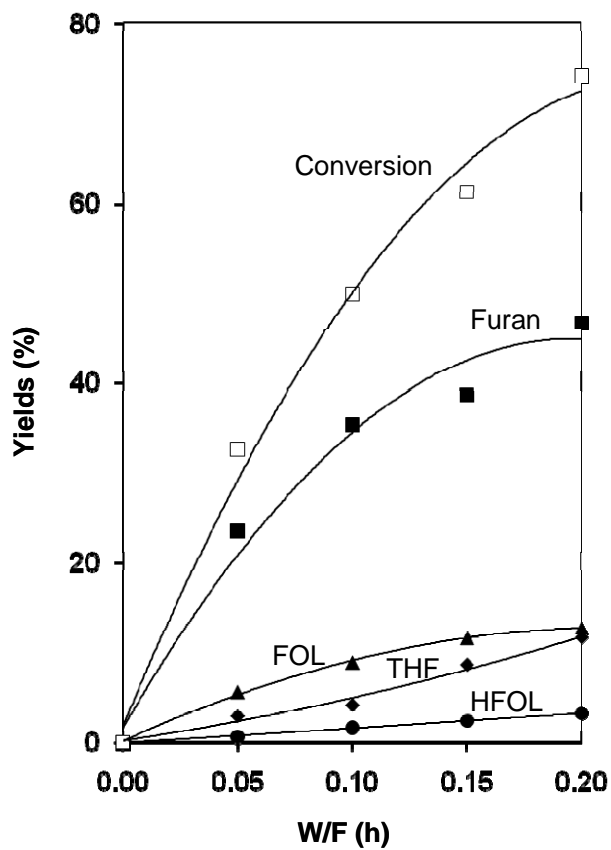
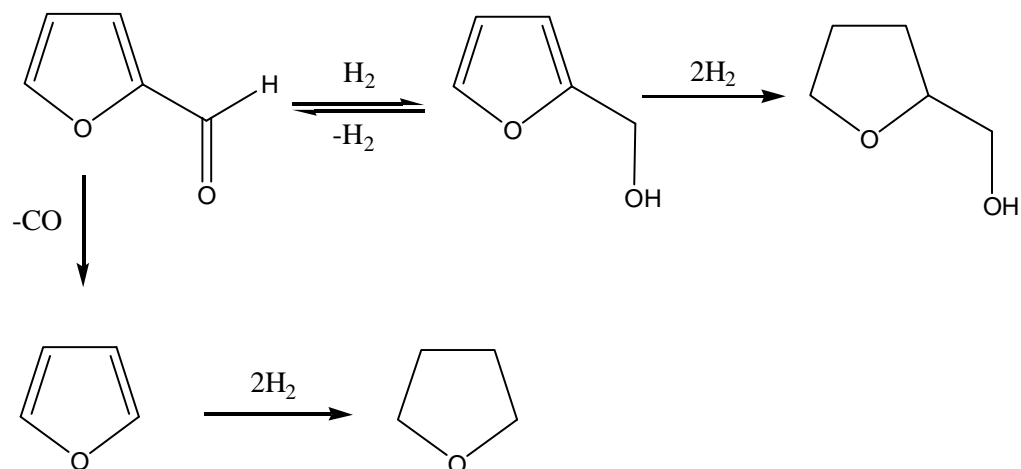


Figure 5.4 Conversion and product distribution from furfural over 0.5%Pd/SiO₂ as a function of W/F. Temp = 230°C, H₂/Feed ratio = 25, H₂ pressure = 1atm, TOS = 15 min.

It is clear that the main reaction product at every W/F is furan, while furfuryl alcohol is observed from the lowest W/F as a minor product. In contrast, tetrahydrofuran (THF) and tetrahydro furfuryl alcohol (HFOL), formed as secondary products, are observed mostly at high W/F. In summary, furfural conversion on Pd can be described as two parallel routes: (i) decarbonylation to furan that subsequently hydrogenates to THF, and (ii) hydrogenation to furfuryl alcohol that subsequently hydrogenates to HFOL (Scheme 1).



Scheme 1

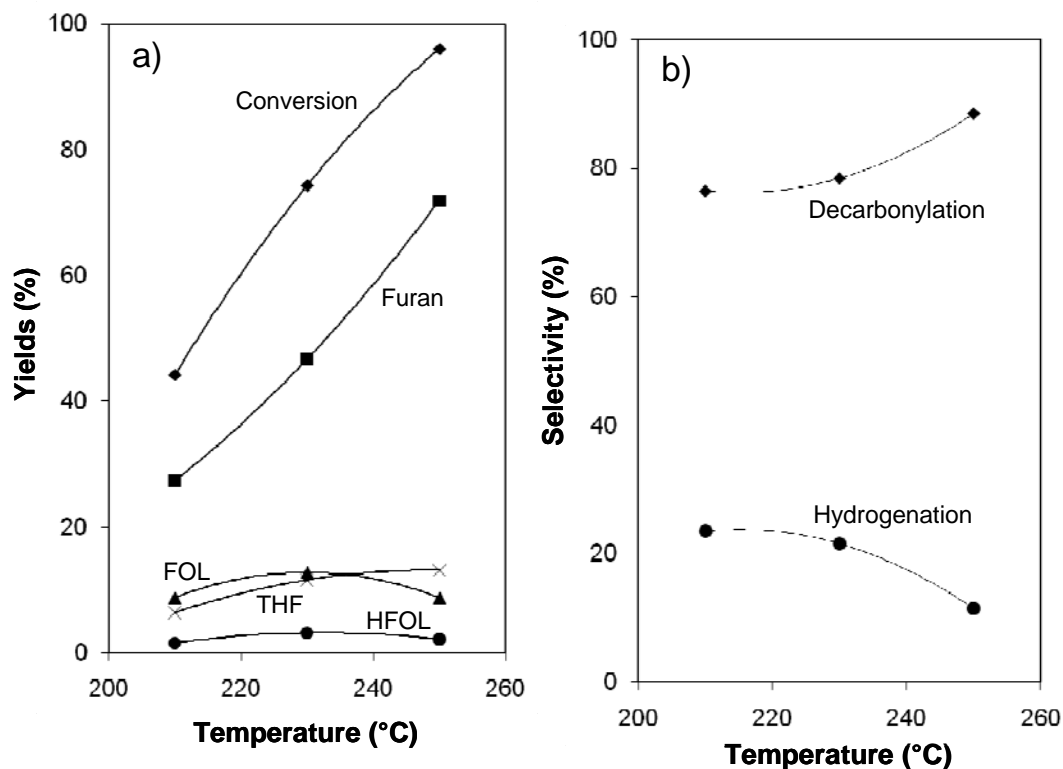


Figure 5.5 (a) Yield and (b) selectivity of products from furfural conversion over 0.5%Pd/SiO₂ catalyst as a function of reaction temperature. W/F = 0.2 h, H₂/Feed ratio = 25, H₂ pressure = 1atm, TOS = 15 min

As shown in Figure 5.5, decarbonylation has a rather high activation energy and the yield of furan significantly increases at higher temperatures, while furfuryl alcohol is seen to increase with temperature and then to decrease, since as previously shown [23], the

equilibrium conversion to furfuryl alcohol quickly decreases with temperature.

When the same 0.5%Pd/SiO₂ catalyst used for the reaction of furfural was tested for the reaction of methyl-pentanal almost no conversion was observed even at very high W/F, indicating a much lower reactivity of 2-methyl-pentanal on Pd compared to furfural. Therefore, to study the 2-methyl-pentanal conversion a higher-loading (5%Pd) catalyst was employed and the reaction was conducted at higher W/F. The total conversion of 2-methyl-pentanal and the corresponding product distribution are shown in Figure 5.6 as a function of W/F.

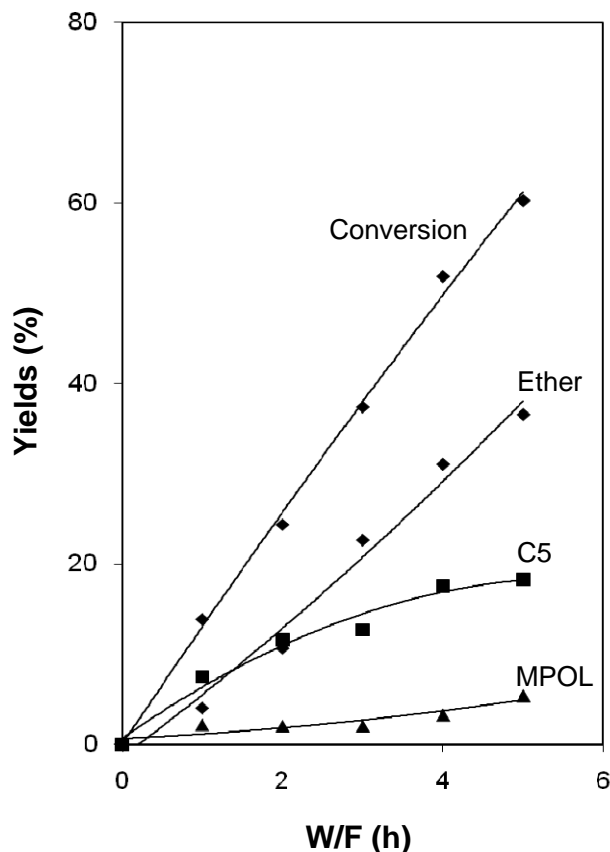


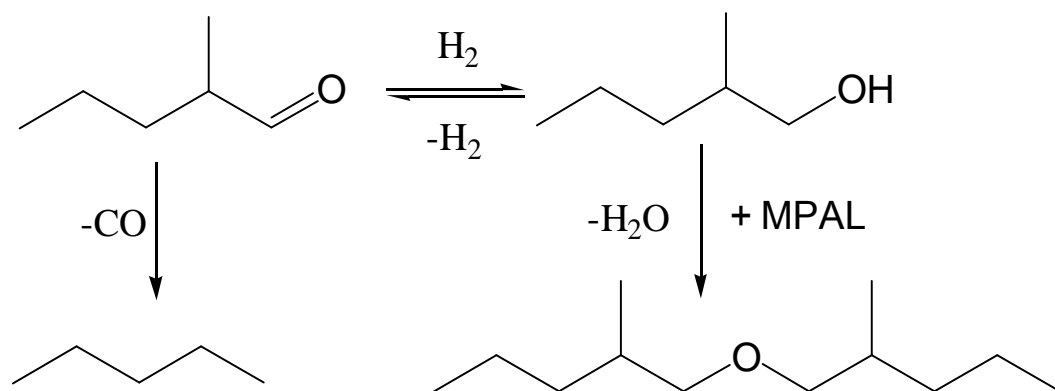
Figure 5.6 Conversion and product distribution from 2-methyl-pentanal over 5%Pd/SiO₂ catalyst. Temp = 125°C, H₂/Feed ratio = 12, H₂ pressure = 1atm, TOS = 15 min. (Trung Pham [1])

Upon increasing W/F from 1 to 5 h, the 2-methyl-pentanal conversion increases from 15 to 60%. While the activity level was much lower than that of furfural, the evolution of primary products was somewhat similar. That is, the main primary products were n-pentane (C5) and 2-methyl-pentanol (MPOL) that derive from direct decarbonylation and hydrogenation, respectively. An important difference with respect to furfural became

apparent at higher W/F. It was observed that, as the conversion increased, an etherification product di-(methylpentyl) ether (DMPE) became dominant while the yields of C5 and 2-methyl-pentanol reached plateau. This behavior is clearly different from that observed with furfural, but has been observed before. In fact, the previous study with 2-methyl-pentanal [24] showed that using a high-metal-loading Pd catalyst (16% Pd/SiO₂) and low reaction temperatures (125°C), formation of ethers is remarkably high.

Since in the present study we have used higher reaction temperature (210-250°C) and lower Pd loading (0.5% Pd/SiO₂) with furfural compared to those with 2-methyl-pentanal, we conducted additional experiments to make the comparison more analogous. Furfural has a rather high boiling point (161.5°C), therefore, to conduct the reaction low reaction temperatures (100°C) a liquid-phase reactor was used. Also, to make a closer comparison to our previous study, a high-Pd-loading (5wt%) catalyst was used. However, even under these conditions, no ether formation was detected. We conclude that the nature of the furfural molecule inhibits the etherification reaction.

In fact, in the case of methyl-pentanal (MPAL) reaction, we have previously shown that MPAL reacts with MPOI forming a hemiacetal intermediate on the surface that readily converts to DMPE [24]. That is, the overall reaction pathways for 2-methyl-pentanal on Pd catalyst can be summarized as shown in the Scheme 2.



Scheme 2

5.4 Reactions of aldehydes on bimetallic Pd-Cu/SiO₂

The effect of incorporating Cu to the catalysts has been studied for the same two reactions, furfural and 2-methyl-pentanal, described above. The results show that the total activity for FAL is decreased when the Cu metal was incorporated (Figure 5.7a). This effect was also found when using 2-methyl-pentanal as a feed (Figure 5.8a). Based on the TPR analysis, one can conclude that the addition of Cu leads to the formation of bimetallic Pd-Cu alloys. Similarly, the frequency shifts in DRIFT of adsorbed CO indicate that the addition of Cu results in a weaker binding of CO to the surface than on pure Pd. This weakening can be ascribed to a lower extent of electron back donation from the metal to π^* of the CO molecule. While CO interacts with the surface through its C end and the aldehyde involves both C and O, it is reasonable to speculate that the electron back donation from the metal to the carbonyl π^* orbital should be weaker on the Pd-Cu alloy than on pure Pd. A lower heat of adsorption of the aldehyde on the bimetallic catalyst, not only would cause a lower conversion, but as discussed below, a change in product distribution.

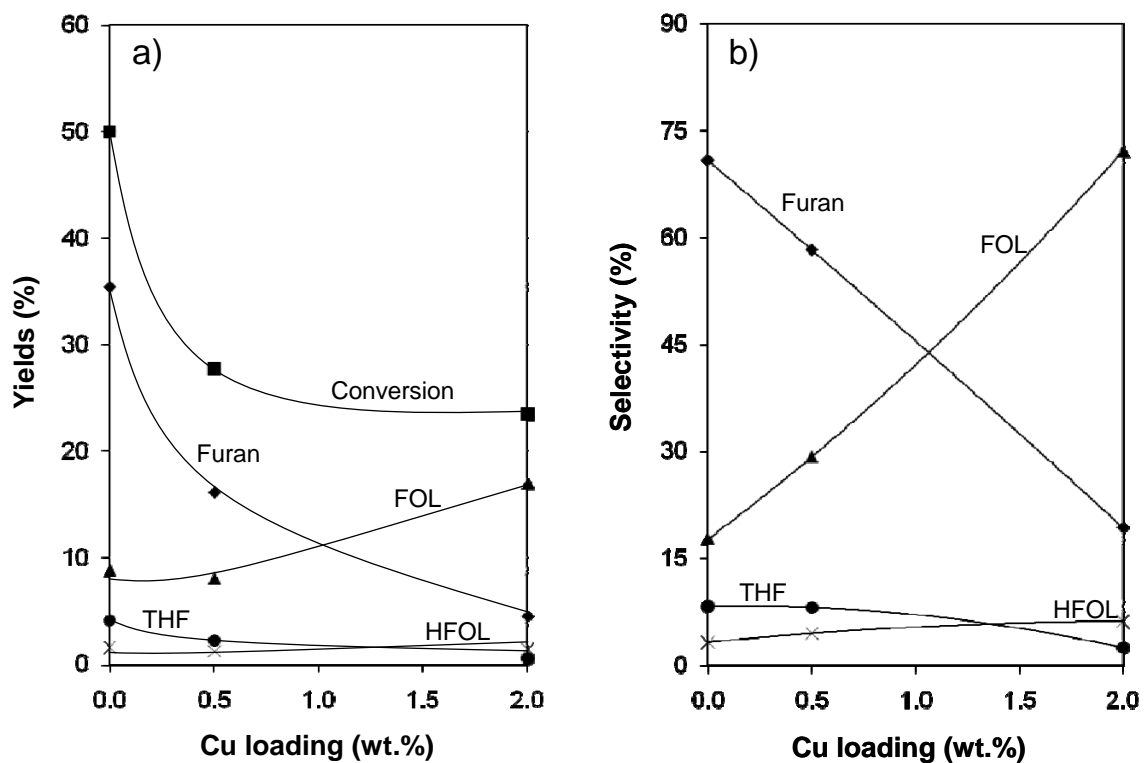


Figure 5.7 (a) Yield and (b) selectivity of products from the reaction of furfural on Pd/SiO₂ as a function of Cu loading. W/F = 0.1 h, Temp = 230°C, H₂/Feed ratio = 25, H₂ pressure = 1 atm, TOS = 15 min

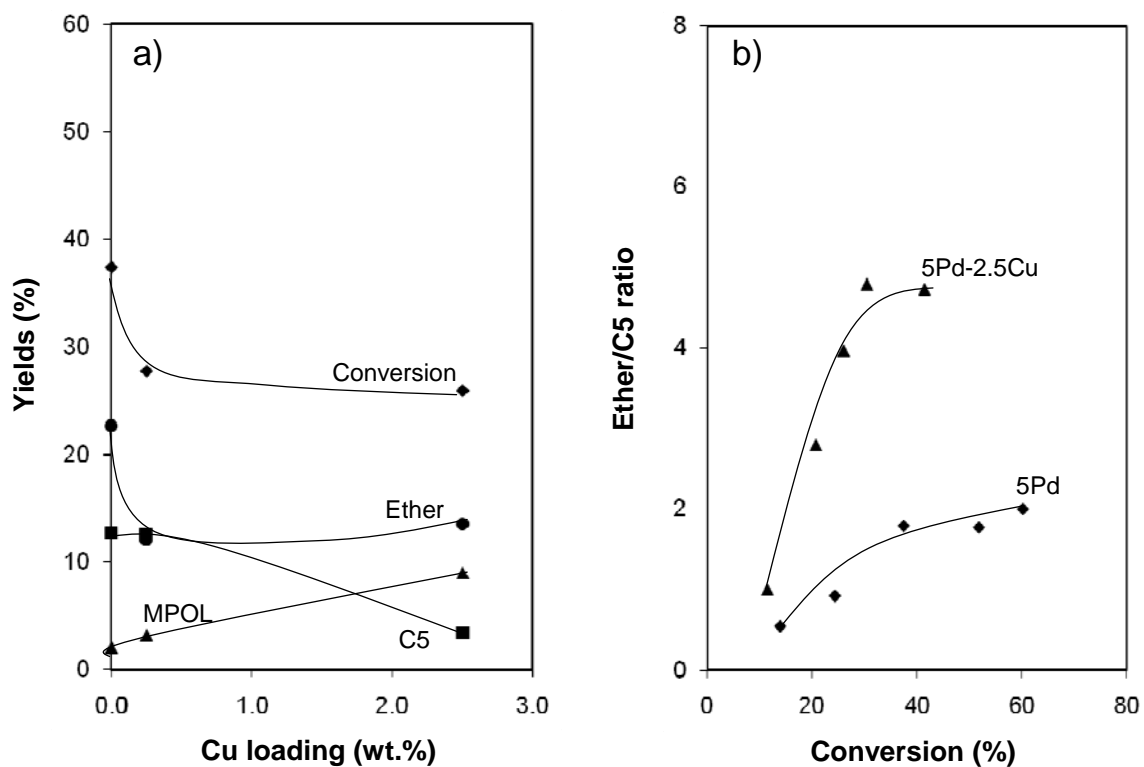


Figure 5.8 (a) Yield of products from the reaction of 2-methyl-pentanal on Pd/SiO₂ as a function of Cu loading. W/F = 3 h, Temp = 125°C, H₂/Feed ratio = 12, H₂ pressure = 1 atm, TOS = 15 min (b) Ether/C5 ratio as a function of conversion for Pd/SiO₂ and Pd-Cu/SiO₂ catalysts (Trung Pham et. al. [1]).

In fact, in both cases, with FAL and MPAL feeds, the yield of the decarbonylation products, furan and pentane, respectively, was greatly reduced, while the yield of hydrogenated products (FOL and MPOL) significantly increased as a function of Cu loading (Figure 5.7a and 5.8a). As shown in Figure 5.9, no significant hydrogenation activity was observed for Cu alone under these conditions.

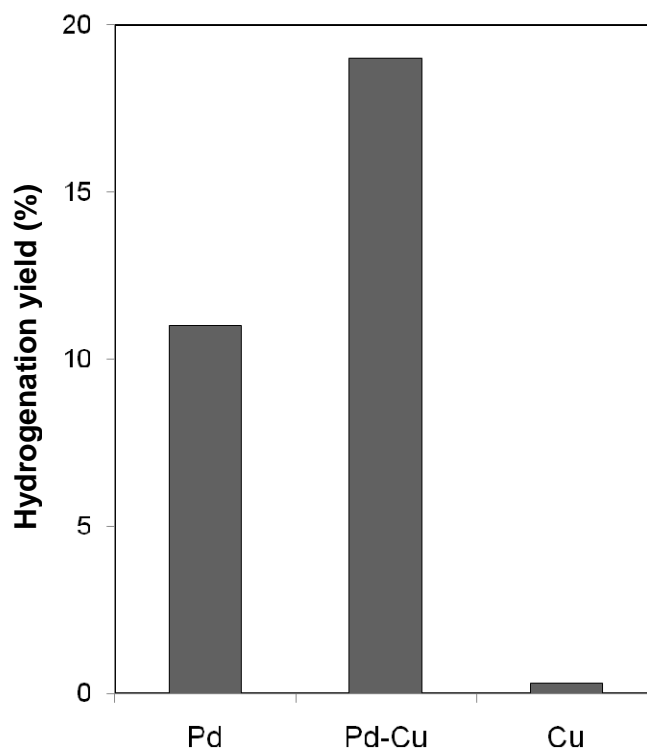


Figure 5.9 Yield of hydrogenation products on 0.5Pd/SiO₂, 0.5Pd-0.5Cu/SiO₂ and 0.5Cu/SiO₂ catalysts. W/F = 0.2 h, Temp = 250°C, H₂/Feed ratio = 25, H₂ pressure = 1atm, TOS = 15 min.

5.5 DFT calculations of 2-methylpentanal (MPAL) and furfural (FAL) adsorption on Pd(111) and PdCu(111) slabs (calculation results from Teerawit Prasomsri [1])

DFT calculations were performed to compare the adsorption energetic for MPAL and FAL on both Pd(111) and PdCu(111) slabs. Calculating the adsorption of such large molecules is complicated because the system exhibits numerous possibilities. We have selected the ones that we believe are most relevant for catalysis. To minimize the effect of adsorbate-adsorbate intermolecular interactions, we have chosen a low-coverage surface (1/16 ML) by setting a relatively large unit cell (4×4).

The optimized structures of MPAL in the gas phase and on the various surfaces are illustrated in Figure 5.10. The corresponding adsorption energies (E_{ads}) and bond lengths are summarized in Table 5.2. The calculations show that on Pd(111) the adsorption of the MPAL molecule occurs via the carbonyl group, interacting with the surface in a η^2 -(C,O) configuration, in which both C and O atoms of the carbonyl group are linked to the metal surface, while the aliphatic hydrocarbon part remains away from the surface. This theoretical result is consistent with the HREELS results obtained from Shekhar et al. [25],

which have shown that the η^2 -(C,O) aldehyde is the dominant species observed on clean Pd surfaces, with some η^1 species only appearing at low temperatures. As summarized in Table 5.2, the adsorption energy for MPAL on Pd(111) is 27.0 kJ/mol. Also, it is worth noting that the C=O bond, d_1 , in the adsorbed state is 0.06 Å longer than that in the gas phase, which may be ascribed to the interaction of the carbonyl π bond with Pd(111) surface (i.e. electron backdonation). In contrast, the lengths for the other bonds d_2 , d_3 , d_4 , d_5 , and d_6 remain unchanged, indicating a low extent of interaction.

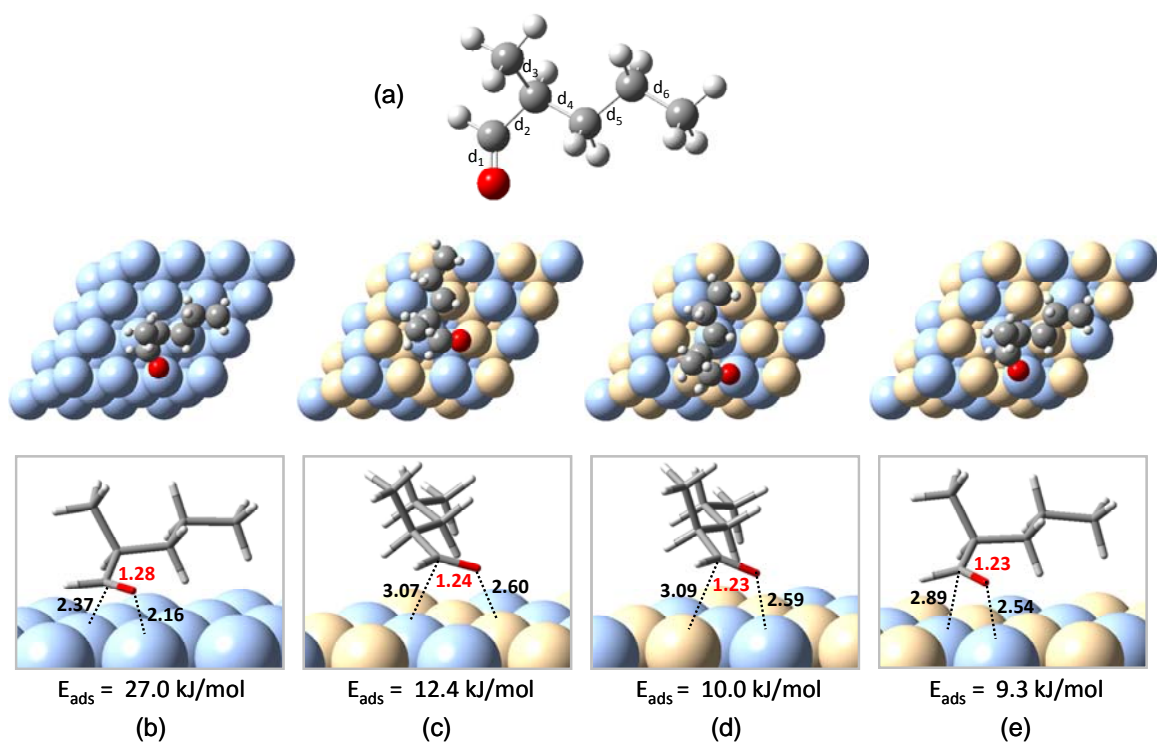


Figure 5.10 DFT optimized structures of 2-methylpentanal (MPAL) in gas phase (a), and its adsorption on Pd(111) (b) and PdCu(111) (c-e) slabs. The corresponding bond lengths are given in Table 5.2 (Calculation result from Teerawit Prasomsri).

Table 5.2 Adsorption energies (kJ/mol) and optimized bond lengths (Å) of 2-methylpentanal on Pd(111) and PdCu(111) slabs (see Figure 5.10).

Model	MPAL	MPAL/Pd(111)	MPAL/PdCu(111)		
	(a)	(b)	(c)	(d)	(e)
E_{ads}	-	27.0	12.4	10.0	9.3
d_1	1.22	1.28	1.24	1.23	1.23
d_2	1.52	1.52	1.51	1.51	1.51
d_3	1.54	1.54	1.54	1.54	1.54
d_4	1.53	1.53	1.53	1.53	1.53
d_5	1.53	1.53	1.53	1.53	1.53
d_6	1.53	1.53	1.53	1.53	1.53

A similar calculation was conducted for furfural (FAL). The optimized structures of FAL in the gas phase and adsorbed on the different surfaces are illustrated in Figure 5.11. The corresponding adsorption energies (E_{ads}) and bond lengths are summarized in Table 5.3.

On Pd(111), the presence of the aromatic ring in FAL plays a crucial role in promoting a flat adsorption on the surface. This results in a twofold increase in heat of adsorption of FAL (55.4 kJ/mol, Figure 5.11b) compared to MPAL (27.0 kJ/mol, Figure 5.10b). This result is consistent with DFT calculations of furan adsorption on Pd(111) made by Bradley et al. [26], who showed that preferred adsorption is with the ring essentially parallel to the surface. As opposed to Pd, our recent DFT calculations of FAL on Cu(111) surface [23] have shown a strong repulsion between the furan ring and the Cu(111) surface, due to the overlap of the 3d band of the surface Cu atoms and the aromatic furan ring. As a result, the adsorption of FAL on Cu(111) is weak and can only occur in the η^1 (O)-aldehyde configuration, via the carbonyl O atom.

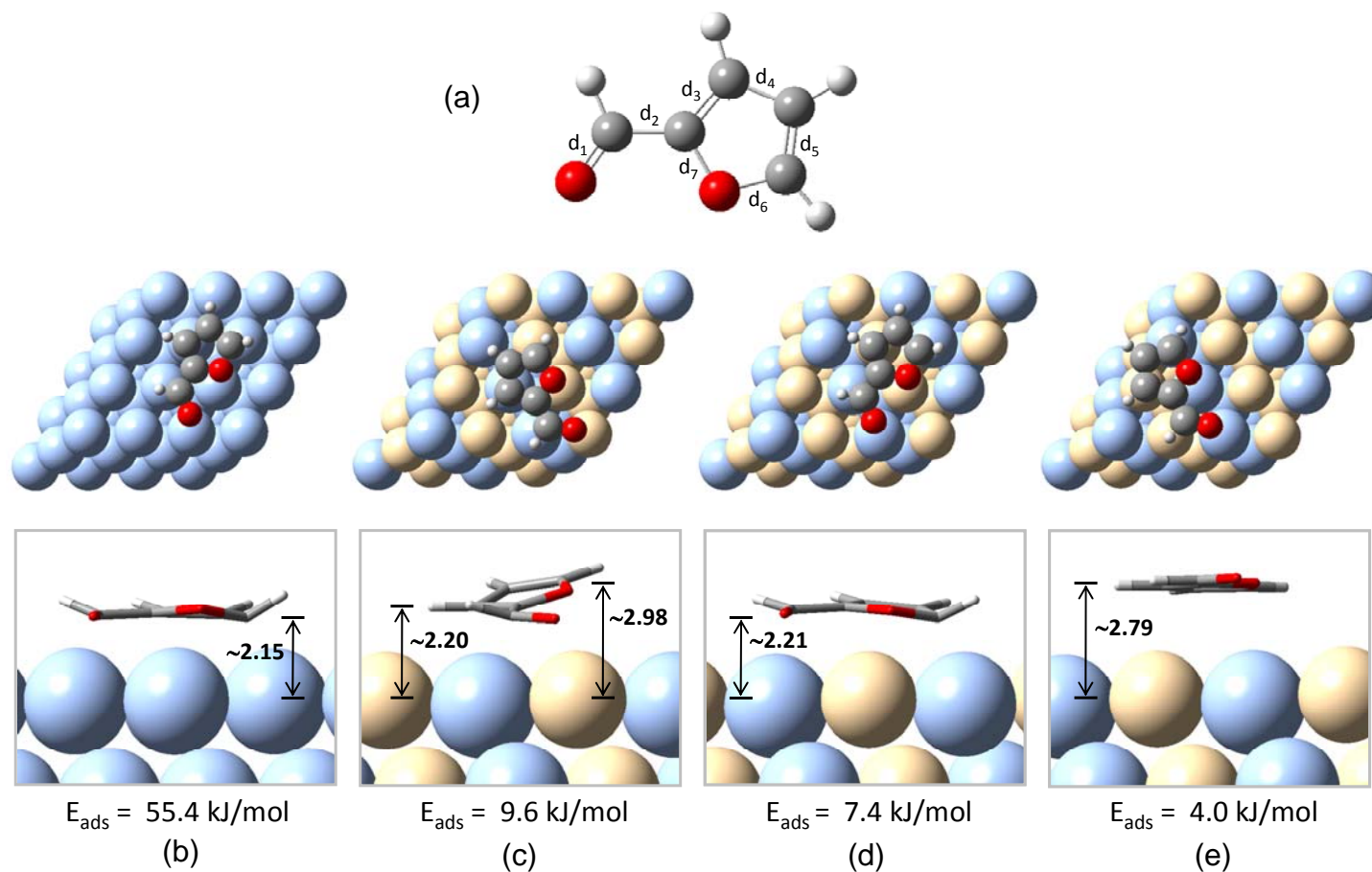


Figure 5.11 DFT optimized structures of furfural (FAL) in gas phase (a), and its adsorption on Pd(111) (b) and PdCu(111) (c-e) slabs. The corresponding bond lengths are given in Table 5.3.

Table 5.3 Adsorption energies (kJ/mol) and optimized bond lengths (Å) of furfural on Pd(111) and PdCu(111) slabs (see Figure 5.11).

Model	FAL	FAL/Pd(111)	FAL/PdCu(111)		
	(a)	(b)	(c)	(d)	(e)
E_{ads}	-	55.4	9.6	7.4	4.0
d_1	1.23	1.31	1.30	1.28	1.23
d_2	1.46	1.47	1.47	1.45	1.46
d_3	1.39	1.44	1.42	1.41	1.39
d_4	1.43	1.44	1.44	1.42	1.43
d_5	1.38	1.45	1.37	1.44	1.38
d_6	1.37	1.40	1.39	1.40	1.37
d_7	1.39	1.40	1.39	1.40	1.39

A similar comparison of the DFT results can be made for MPAL and FAL over the PdCu(111) surface. It is clearly seen that the presence of Cu significantly reduces the interaction of both aldehydes with the metal surface. Relative to those on the pure Pd, the heats of adsorption on the bimetallic surface are significantly reduced. That is, the adsorption strength of MPAL drops from 27.0 kJ/mol on Pd(111) to 12.4 kJ/mol on PdCu(111). Moreover, the heat of adsorption of FAL changes from 55.4 kJ/mol on Pd(111) to 9.6 kJ/mol on PdCu(111), a dramatic reduction in the strength of interaction related to the effect of the aromatic ring.

Another aspect important to discuss is the significant changes in strength of interaction observed with respect to the place in which the molecule is adsorbed on PdCu(111). For instance, in the case of MPAL, the η^2 -(C-O) aldehyde adsorption with the C atom on top of Pd and the O atom on Cu (see Figure 5.10c.) results in a higher adsorption energy (12.4 kJ/mol) than the other configurations (i.e. C/Cu-O/Pd or C/Pd-O/Pd). The preferential adsorption mode results in the higher elongation of the carbonyl bond, d_1 . Again, as in the case of pure Pd, the lengths of the other bonds (d_3 , d_4 , d_5 , and

d_6) remain unmodified upon adsorption. In addition, the distances between C or O and the surface are significantly longer $\sim 0.4-0.7$ Å than those on Pd(111). This difference is in agreement with the trends in adsorption energy and the length of the C=O bond. A weaker interaction results in longer adsorbate-surface distances and shorter/stronger carbonyl bonds.

The case of FAL is somewhat different due to the important role played by the furanic ring in the interaction with the surface. As mentioned above, on the pure Pd the presence of the ring greatly enhances the interaction. However, when Cu atoms are added, the stability of the adsorbed FAL is dramatically decreased. In the FAL adsorbed on Pd(111) all bonds are elongated, particularly the C=O and C=C bonds. To investigate this interaction, various FAL/PdCu(111) configurations were simulated.

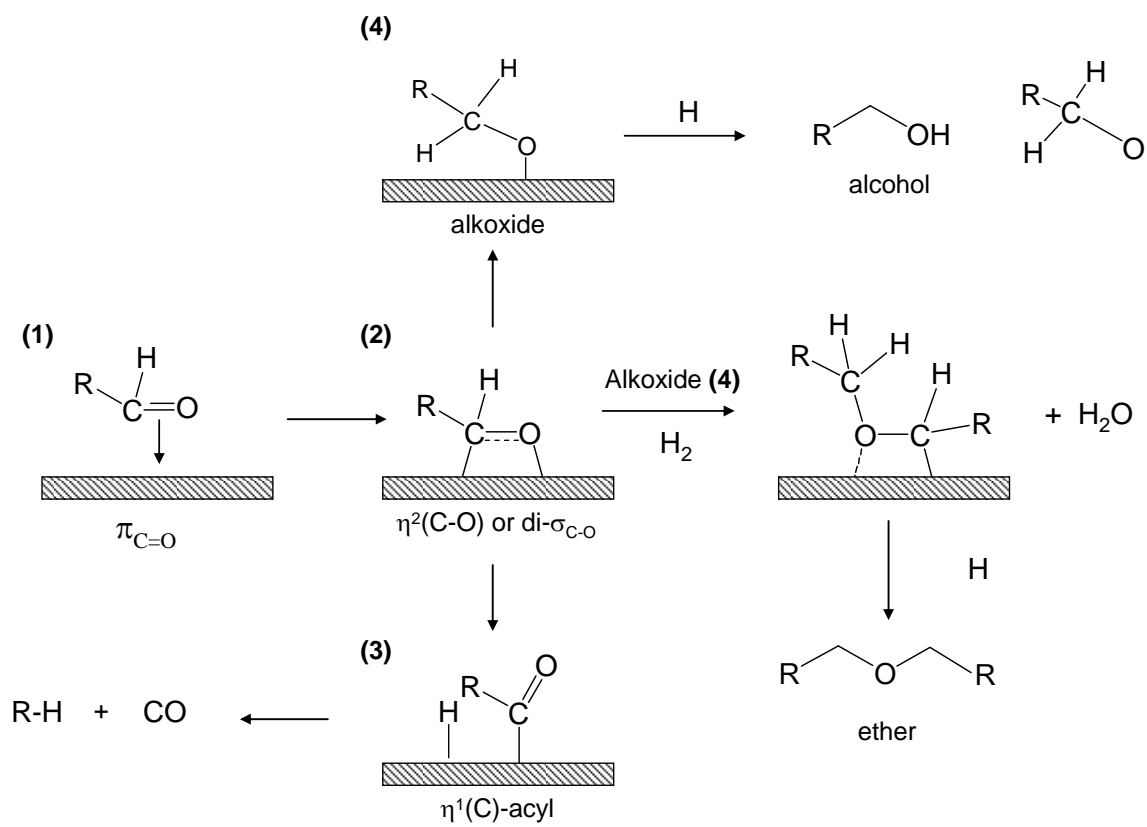
It is interesting to see the different calculated energies and bond lengths as the molecule is placed on different places on the alloy surface. That is, while the heat of adsorption is much lower than on pure Pd, it is not as low when the O atoms in FAL are placed over Cu atom and the furanic ring over Pd atoms. By contrast, the

adsorption energy is even lower when the ring is placed over Cu atoms. As shown on the side view of Fig 11d, the molecule even bends away from the Cu atom due to the apparent repulsion.

5.6 Discussion

5.6.1 Reaction of aldehydes on Pd/SiO₂

The reaction pathways for furfuraldehyde and 2-methyl-pentanal conversion on Pd and PdCu surfaces have been investigated on silica-supported catalysts. To discuss the observed product distributions and their strong dependence on the catalyst formulation and type of aldehyde used as a feed, we should consider the following possible reaction paths (Scheme 3).



Scheme 3

The starting interaction of the carbonyl compounds **(1)** with the Pd surface appears to involve a side-on complex ($\pi_{C=O}$) [27]. In the case of Pd, as discussed above, a rather extensive electron back-donation into the carbonyl group can occur. This interaction readily weakens the C=O, helping stabilizing a di-sigma complex ($di-\sigma_{C-O}$) **(2)**, also known as $\eta^2-(C-O)$ aldehyde. The formation of this species upon adsorption of saturated aldehydes, (i.e. formaldehyde, acetaldehyde, and propionaldehyde) on Pd, Pt, Rh and Ru metal surfaces has been confirmed using high resolution electron energy loss spectroscopy (HREELS) [27-31]. Moreover, the $\eta^2-(C-O)$ aldehyde **(2)** has been found to be a precursor for aldehyde hydrogenation over a Pd catalyst [25]. In contrast, on Cu catalysts the $\eta^1-(O)$ aldehyde is known to be the main precursor for aldehyde hydrogenation [23,32]. In our present study, formation of alcohols via hydrogenation of either furfural or 2-methyl-pentanal was also observed as a minor reaction path. On the other hand, decarbonylation products (furan and pentane from FAL and MPAL, respectively) were dominant over Pd/SiO₂ even at the lowest W/F values.

The HREELS experiments of acetaldehyde adsorbed on clean Pt(111) [30] show that, at low temperatures, an η^2 -(C-O) surface species was formed, but it was readily decomposed above 330K, producing an acetyl intermediate (η^1 (C)-acyl, **(3)**) that was stable up to 440K. Consequently, it is conceivable that a similar acyl intermediate may be readily formed on Pd under our reaction conditions. In fact, as shown in Figure 5.5, the decarbonylation product, furan, increases as a function of temperature.

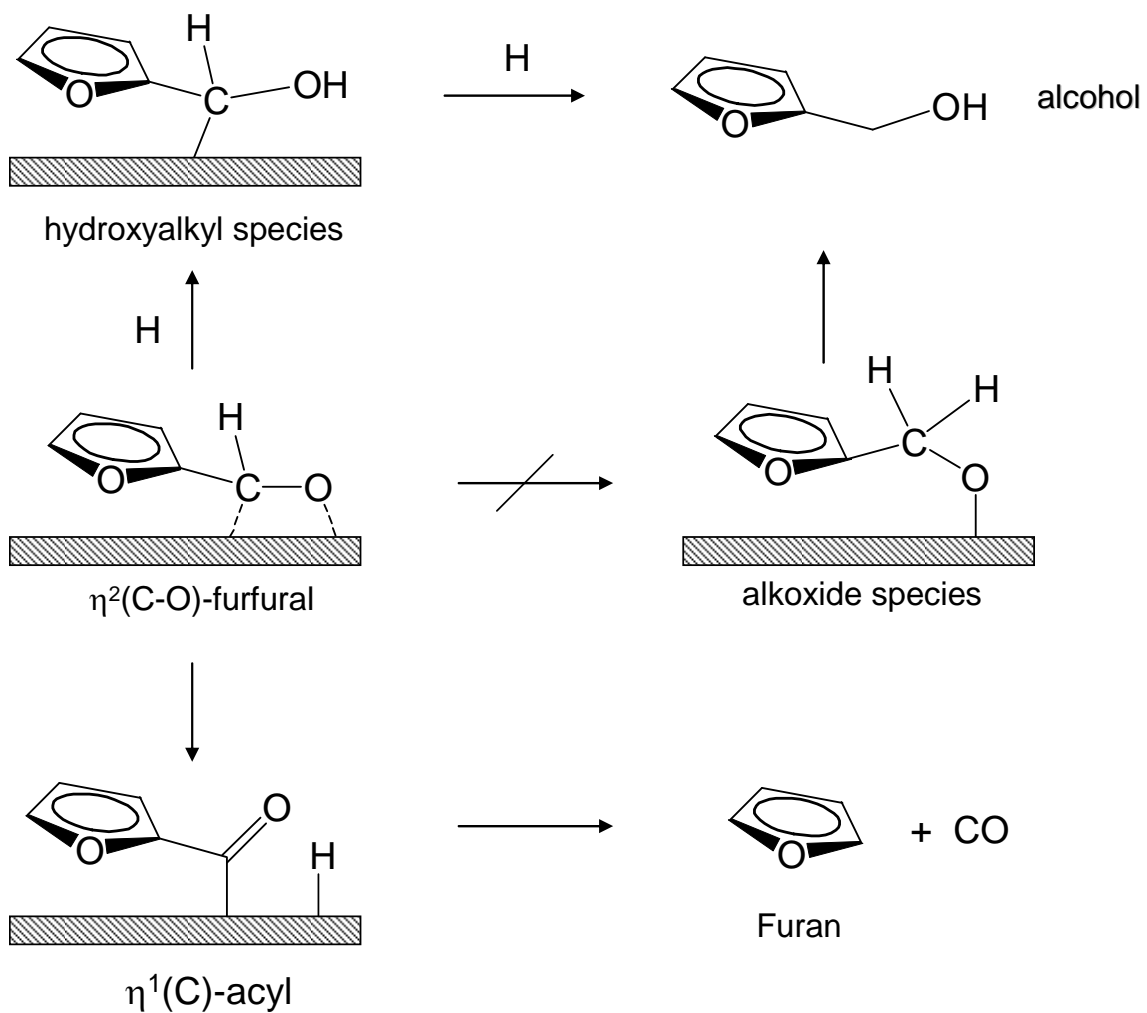
In the presence of hydrogen, together with formation of the acyl intermediate that leads to decarbonylation, the η^2 -(C-O) aldehyde **(2)** can be hydrogenated to the alkoxide complex **(4)** [33-37], which is the intermediate for the hydrogenated products (alcohol), i.e., MPOL produced from MPAL.

Formation of alkoxide intermediates from saturated aldehydes has been typically thought to occur via H attack to the carbonyl C of the η^2 -(C-O) aldehyde [38]. In contrast, in the case of furfural, our recent mechanistic studies on Cu catalysts have shown that the first H attack may take place at the carbonyl O [23], which results in the formation of a hydroxyalkyl surface species. Our DFT

calculations showed that this intermediate results in a somewhat lower energy barrier than the one involving the formation of the alkoxide intermediate. We have ascribed the higher stability of the hydroxyalkyl species to the stabilization role played by the conjugation with the aromatic furan ring [23]. Thus, in this case, it is more likely that the hydroxyalkyl species is the dominant intermediate in furfural hydrogenation. Therefore, a mechanism for furfural conversion over Pd catalysts can be proposed, as shown in scheme 4.

In contrast to furfural, methyl pentanal does not have a conjugated system and therefore formation of a hydroxyalkyl species would not be favorable. In this case, the reaction would most probably go via an alkoxide species (**4**) in Scheme 3, which would favor formation of the ether, as observed experimentally (see Figure 5.6), particularly at high contact times. As previously proposed [27,39], the η^2 -(C-O) intermediate is readily stabilized on Pd at low temperatures and reacts with the alkoxide to form the ether, a bimolecular reaction that is facilitated on large Pd ensembles, i.e., maximum ether yield is obtained at low reaction temperatures on high-loading, large-particle Pd catalysts. With furfural, even under

these optimum etherification conditions, no ether was observed.



Scheme 4

5.6.2 Effect of Cu loading on Pd/SiO₂

While TPR analysis gives evidence for the formation of a Pd-Cu bimetallic phase XPS shows both a decrease in the relative intensity of Pd and the appearance of a high-binding energy state. At the same time, the shift of the linear C≡O stretching vibration band to a higher wavenumber observed by DRIFTS of adsorbed CO upon Cu incorporation in the bimetallic Pd-Cu catalyst indicates a weaker interaction of CO with the metal surface. These results indicate a high concentration of PdCu alloy at the Pd surface and a chemical modification compared to unalloyed Pd. The higher vibrational frequency of adsorbed CO reflects a lower extent of electron back donation from the metal to π^* of the CO molecule [40]. An analogous modification occurs during the interaction with the aldehydes as the η^2 -(C-O) configuration. A more efficient transfer of electrons into the antibonding states of the molecule's π system enhances the strength of interaction with the metal, while it weakens the C-O bond. That is, the formation of the di-sigma surface aldehyde species η^2 -(C-O) should be disfavored on the Pd-Cu compared to pure Pd. This is in agreement with the observed decrease in the

conversion of FAL and MPAL as a function of Cu loading as seen in Figure 5.7a and 5.8a, respectively.

In agreement with this conjecture, the DFT calculations show that the η^2 -(C-O) aldehyde is more stable on the surface of the pure Pd(111) as the adsorption energy is relatively higher than that on the bimetallic PdCu(111). The long distance between both C and O atoms of η^2 -(C-O) and the metal surface indicates a very weak interaction between aldehyde and the Pd atoms in the presence of Cu. However, the O atom of η^2 -(C-O) aldehyde is still linked to the Cu atom, while the C atom remains away from the surface suggesting that the interaction between the carbonyl O and the Cu atom is the main contributor to the adsorption. In fact, the η^2 -(C-O) aldehyde becomes more like an η^1 -(O) aldehyde on the bimetallic PdCu(111) surface in which an aldehyde is bonded to the surface through the oxygen lone pair orbital, acting as a Lewis base [27]. It is important to point out that, on pure Cu surfaces, aldehydes adsorb exclusively in the η^1 -(O) configuration, but they adsorb in both η^1 and η^2 configurations on Group VIII metals, at a ratio that depends on the metal [41]. For example, the higher η^2/η^1 ratio observed on Ru compared to Pt has been ascribed to the higher extent of electron

back-donation, resulting from the higher position of the Fermi level in Ru compared to Pt. Moreover, while $\eta^2\text{-(C-O)}$ is dominant on clean Ru surfaces and even more so when electron-donating K is co-adsorbed, $\eta^1\text{-(O)}$ is dominant on oxygen-covered Ru surfaces [42], which illustrates the importance of electronic effects in the adsorption of aldehydes, as also proposed by others [43,44].

In the case of the Pd-Cu alloys, as the stability of the di-sigma $\eta^2\text{-(C-O)}$ species is decreased, we may expect that the interaction with the electronegative atom (i.e. carbonyl oxygen) forming the intermediate which is similar to the $\eta^1\text{(O)}$ aldehyde will be favored. At the same time, a longer distance of the carbonyl C with the metal surface would make the formation of acyl intermediates less favorable since the C-metal bond need to be developed during the acyl formation. This would explain the drastic decrease in decarbonylation for both aldehydes, i.e. the yields of furan and pentane were greatly reduced as a function of Cu loading (Figure 5.7a and b) in the conversion of FAL and MPAL, respectively. In contrast, this $\eta^1\text{(O)}$ likes aldehyde can still undergo hydrogenation resulting in not only the selectivity but also the yield towards hydrogenated product (FOL and MPOL, respectively)

was observed to increase at higher Cu contents. Finally, in the case of MPAL, as the formation of acyl species is suppressed, hydrogenation of the adsorbed aldehyde forming the alkoxide intermediate leading to an increase in the ether selectivity may be favored, thus explaining the higher ether/C5 ratio for Pd-Cu catalyst (Figure 5.8b).

5.7 Conclusion

From the comparative study of the different reactions that furfural and methyl-pentanal undergo on Pd and Pd-Cu catalysts we draw the following conclusions:

- a) On pure Pd, decarbonylation is the dominant reaction for both types of aldehydes, even at low W/F. This behavior is due to the preferential formation of an acyl intermediate at higher temperatures, which can readily decompose into CO and hydrocarbons. This proposed trend explains the high decarbonylation / hydrogenation ratios obtained for both aldehydes on Pd.
- b) In the case of 2-methyl-pentanal, when large Pd ensembles are available, and the temperature is low enough, the reaction of the η^2 -(C-O) aldehyde with an

adjacent alkoxide becomes important to ether formation. This is not the case for furfural, for which hydrogenation may occur via a hydroxyalkyl intermediate, which is more stable than the alkoxide. As a result, there is no etherification with furfural.

c) Incorporation of Cu onto Pd/SiO₂ catalyst results in the formation of Pd-Cu alloys, which may exhibit an electronic structure different from that of pure Pd. This electronic perturbation results in a lower extent of electron back-donation to the π^* system of the aldehydes. As a result, the formation of the side-on η^2 -(C-O) aldehyde species is unstable on Pd-Cu relative to Pd alone, which results in the formation of acyl species is less favored. Therefore, a decrease in the decarbonylation rate, but an increase in the hydrogenation rate for both aldehydes was observed.

References

- [1] S. Sitthisa T. Pham, T. Prasomsri, T. Sooknoi, R.G. Mallinson, D.E. Resasco, *J. Catal.* 280 (2011) 17.
- [2] J. Piskorza, D. Radlein, D.S. Scott, *J. Anal. Appl. Pyrol.* 9 (1986) 121.
- [3] J.N. Chheda, Y. Román-Leshkov and J.A. Dumesic, *Green Chem.* 9 (2007) 342.
- [4] S. Barama, C.D. Batiot, M. Capron, E.B. Richard, O.B. Mohammedi, *Catal. Today* 141 (2009) 385.
- [5] A.F. Gusovius, T.C. Watling, R. Prins, *Appl. Catal. A:Gen.* 188 (1999) 187.
- [6] G. Aguila, F. Gracia, P. Araya, *Appl. Catal. A:Gen.* 343 (2008) 16.
- [7] D. Gasparovicova, M. Kralik, M. Hronec, Z. Vallusova, H. Vinek, B. Corain, *J. Mol. Catal. A:Chem.* 264 (2007) 93.
- [8] M. Fernandez-Garcia , G.L. Haller, *J. de Phys. IV*, 7 (1997) 895.
- [9] M. Primet, V. Mathieu, W. M. H. Sachtler, *J. Catal.* 44 (1976) 324.
- [10] F. Skoda, M.P. Astier, G.M. Pajonk, M. Primet, *Catal. Lett.* 29 (1994) 159.
- [11] S.S. Ashour, J.E. Bailie, C.H. Rochester, J. Thomson, G.J. Hutchings, *J. Mol. Catal. A:Chem.* 123 (1997) 65.
- [12] F.B. Noronha, M. Schmal, M. Primet, R. Frety, *Appl. Catal.* 78 (1991) 125.
- [13] M. Fernandez-Garcia, J.A. Anderson, G.L. Haller, *J. Phys. Chem.* 100 (1996) 16247.
- [14] V. Ponec, *Appl. Catal. A:Gen.* 222 (2001) 31.

-
- [15] A.B. Hungria, A. Iglesias-Juez, A. Martinez-Arias, M. Fernandez-Garcia, J.A. Anderson, J.C. Conesa, J. Soria, *J. Catal.* 206 (2002) 281.
- [16] E. Jerero, M.P. Hyman, J.M. Vohs, *Phys. Chem. Chem. Phys.* 11 (2009) 10457.
- [17] H.L. Tierney, A. E. Baber, E.C. H. Sykes, *J. Phys. Chem. C*, 113 (2009) 7246.
- [18] N. Lopez, J.K. Norskov, *Surf. Sci.* 477 (2001) 59.
- [19] S. Sakong, C. Mosch, A. Gross, *Phys. Chem. Chem. Phys.* 9 (2007) 2216.
- [20] E. Jerero, M.P. Hyman, J.M. Vohs, *Phys. Chem. Chem. Phys.* 11 (2009) 10457.
- [21] B.L. Gustafson, P.S. Wehner, *Appl. Surf. Sci.* 52 (1991) 261.
- [22] N. Martensson, R. Nyholm, H. Calen, J. Hedman, *Phys. Rev. B* 24 (1981) 1725.
- [23] S. Sitthisa, T. Sooknoi, Y. Ma, P.B. Balbuena, D.E. Resasco, *J. Catal.* 277 (2011) 1.
- [24] T. Pham, S.P. Crossley, T. Sooknoi, L.L. Lobban, D.E. Resasco, R.G. Mallinson, *Appl. Catal. A: Gen.* 379 (2010) 135
- [25] R. Shekhar, R.V. Plank, J.M. Vohs, M.A. Barteau, *J. Phys. Chem. B* 101 (1997) 7939.
- [26] M.K. Bradley, J. Robinson, D.P. Woodruff, *Surf. Sci.* 604 (2010) 920.
- [27] M. Mavrikakis, M. A. Barteau, *J. Mol. Catal. A:Chem.* 131 (1998) 135.
- [28] J.L. Davis, M.A. Barteau, *J. Amer. Chem. Soc.* 111 (1989) 1782.
- [29] J.L. Davis, M.A. Barteau, *Surf. Sci.* 235 (1990) 235.

-
- [30] M.A. Henderson, Y. Zhou, J.M. White, J. Amer. Chem. Soc. 111(1989) 1185.
- [31] R.J. Madix, T. Yamada, S.W. Johnson, Appl. Surf. Sci. 19 (1984) 13.
- [32] B.A. Sexton, A.E. Hughes, N.R. Avery, Surf. Sci. 155 (1985) 366.
- [33] J.B. Benziger, R.J. Madix, J. Catal. 65 (1980) 49.
- [34] P.H. McBreen, W. Erley, H. Ibach, Surf. Sci. 133 (1983) 469.
- [35] J. Hrbek, R.A. Depaola, F.M. Hoffmann, J. Chem. Phys. 81 (1984) 2818.
- [36] J.E. Demuth, H. Ibach, Chem. Phys. Lett. 60 (1976) 395.
- [37] S.R. Bare, J.A. Stroscio, W. Ho, Surf. Sci. 150 (1985) 399.
- [38] R. Alcalá, J. Greeley, M. Mavrikakis, J.A. Dumesic, J. Chem. Phys. 116 (2002) 8973.
- [39] G.M.R. van Druten, V. Poncic, Appl. Catal. A:Gen. 191 (2000) 163.
- [40] G. Blyholder, J. Phys. Chem. 68 (1964) 2772.
- [41] N.R. Avery, W.H. Weinberg, A.B. Anton and B.H. Toby, Phys. Rev. Lett. 51 (1983) 682.
- [42] A.B. Anton, N.R. Avery, B.H. Toby, W.H. Weinberg, J. Am. Chem. Soc. 108 (1986) 684.
- [43] H. Steininger, H. Ibach, S. Lehwald, Surf. Sci. 117 (1982) 685.
- [44] J.F. Paul, P. Sautet, J. Phys. Chem. 98 (1994) 10906.

CHAPTER 6

Conversion of Furfural on Bimetallic Pd-Fe Catalysts

6.1 Introduction

From the point of view of fuel production neither hydrogenation nor decarbonylation is desirable. While the former does not remove O, the latter loses C in the process. Hydrogenolysis to 2-methylfuran (via C1-O1 hydrogenolysis) would be the most desirable product, since not only has intrinsically good fuel properties (high octane number, RON=131, low water solubility, 7 g/L [1]), but also can be considered an archetypical product of the desired reaction paths in bio-oil upgrading, i.e., removing O while keeping a high C yield [2,3].

The study in chapter 5 showed that bimetallic Pd-Cu catalysts can greatly alter the furfural reaction paths. The results showed that adding Cu to Pd and forming bimetallic Pd-Cu alloys greatly suppresses the production of furan from furfural. However, only furfuryl alcohol, rather than 2-methylfuran was observed [4]. Alternatively,

one could use an alloying metal like Fe that has a stronger affinity for oxygen to enhance the selectivity towards C-O hydrogenolysis forming 2-methylfuran as a final product. In this chapter, we have compared the behavior of Pd-Fe with that of Pd catalysts for the conversion of furfural.

6.2 Conversion of furfural over Pd/SiO₂ and Pd-Fe/SiO₂ catalysts

As shown in Figure 6.1, the main product from the reaction of furfural on 1%Pd/SiO₂ at 250°C is furan (~ 60 % yield at W/F = 0.1 h) which is derived from decarbonylation while hydrogenation of furfural to furfuryl alcohol was observed as a minor reaction (~ 10 % yield at W/F = 0.1 h). Pd catalyst also catalyzed aromatic furan ring saturation as tetrahydrofuran and tetrahydro furfuryl alcohol was observed from furan and furfuryl alcohol, respectively at high W/F. In addition, there is no formation of 2-methylfuran which could be derived from C-O bond scission of furfuryl alcohol.

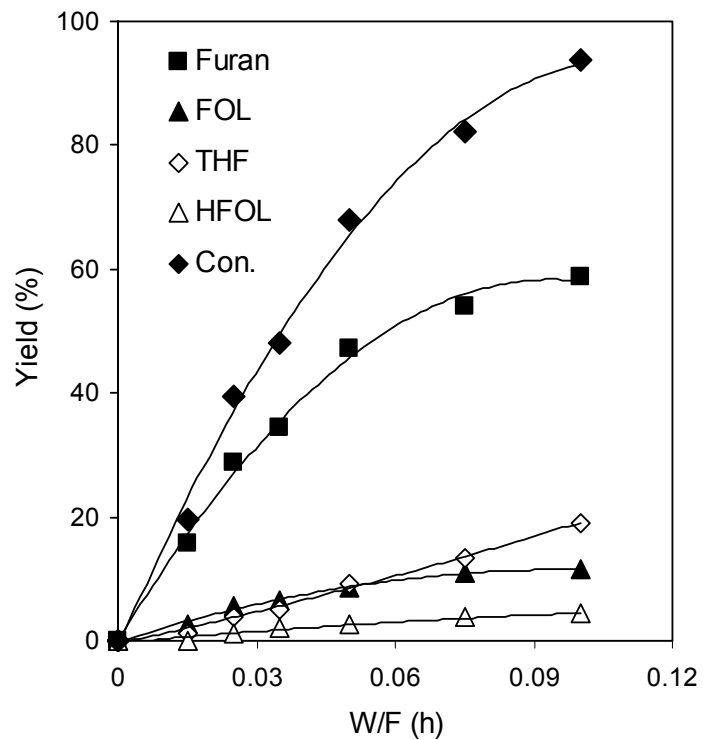


Figure 6.1 Product distribution from the reaction of furfural over a monometallic 1%Pd/SiO₂ catalyst, at 250°C, H₂/Feed ratio = 25, pressure = 1atm.

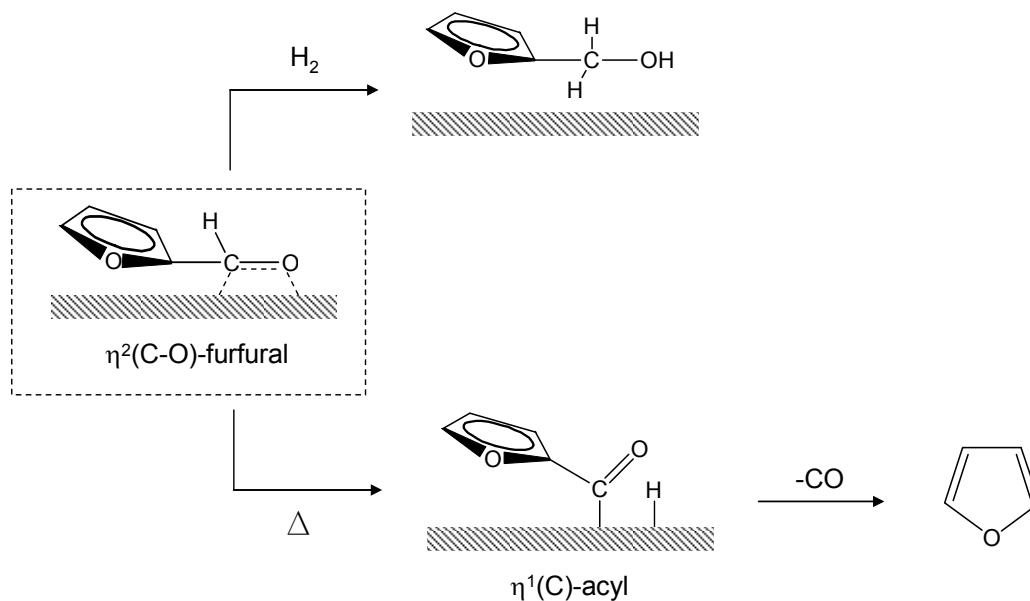


Figure 6.2 Possible surface species on the Pd surface during conversion of furfural

It is clearly seen that monometallic Pd exhibited very high selectivity toward furan. This reaction also produced carbon monoxide as a co-product. The production of furan from furfural proceeds first through C-H bond cleavage of the aldehydic hydrogen, followed by C-C bond breaking produced furan and CO. This step occurs after the molecular adsorption of furfural as η^2 -aldehyde configuration (see Figure 6.2).

The molecular adsorption of furfural as η^2 -aldehyde configuration also undergoes C=O hydrogenation to produce

furfuryl alcohol. However, the lower selectivity of furfuryl alcohol compared to furan on monometallic Pd catalyst can be ascribed to the emergence of decomposition of η^2 -furfural to an acyl intermediate at high reaction temperature [5,6]. The results reported here suggest that monometallic Pd promotes much more C-C scission reactions of furfural compared to C-O scission reactions since we can observe a relatively high yield of furan and no formation of 2-methylfuran which could be a product derived from C-O hydrogenolysis of furfuryl alcohol.

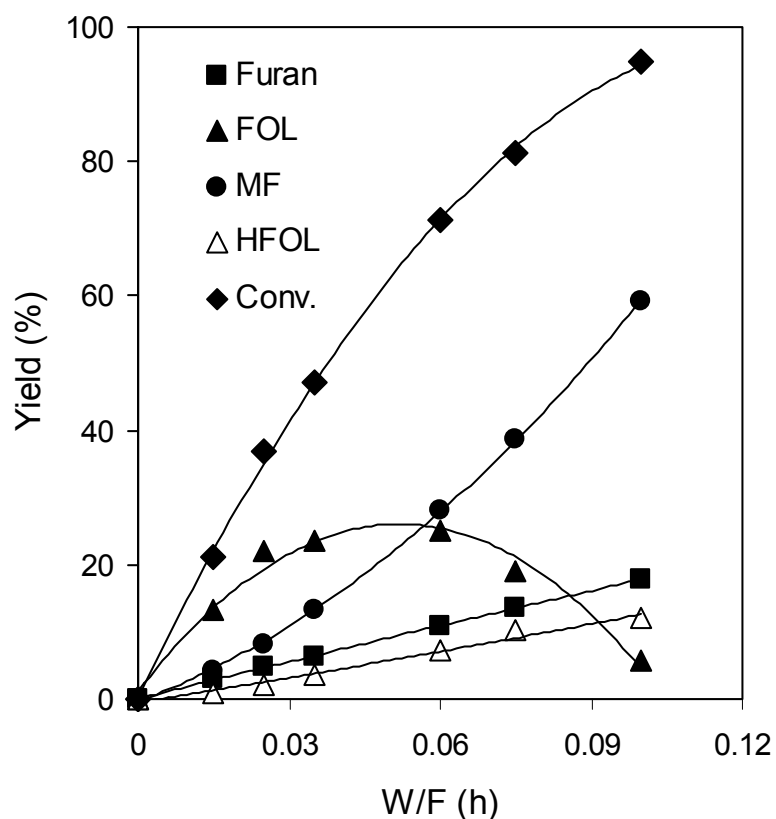


Figure 6.3 Product distribution from the reaction of furfural over a bimetallic 1%Pd-0.5%Fe/SiO₂ catalyst, at 250°C, H₂/Feed ratio = 25, pressure = 1atm.

Interesting differences in product distribution are observed when the Pd catalyst was incorporated with Fe. As shown in Figure 6.3, a remarkable change in product selectivity is observed over 1%Pd-0.5%Fe/SiO₂ catalyst. It is clear that the main products from the reaction of furfural over 1%Pd-0.5%Fe/SiO₂ catalyst are furfuryl alcohol and 2-methylfuran which is not observed over

1%Pd/SiO₂. It appears that 2-methylfuran is a secondary product from the reaction of furfural and it is derived from the C-O hydrogenolysis of furfuryl alcohol. The yield of furfuryl alcohol is dominant at low W/F and increases with increasing W/F to the maximum value then decreases, while the 2-methyl furan yield is relatively low at the beginning and keeps increasing with W/F. In addition, a higher yield of 2-methylfuran was observed when using furfuryl alcohol as a feed rather than that on furfural (see entry 2 vs. 6 in Table 6.1).

Table 6.1 Conversion and yield of products from the reaction of furfural and furfuryl alcohol over 1%Pd/SiO₂ and 1%Pd-0.5%Fe/SiO₂ catalysts

Entry	Catalysts	Feed	Conv. (%)	Yield (%)				
				Furan	THF	FOL	MF	HFOL
1	Pd/SiO ₂	FAL	82.1	54	13.4	11	0	3.8
2	Pd-Fe/SiO ₂	FAL	81.4	13.5	0.0	19.0	38.6	10.2
3	Pd/SiO ₂ +Fe/SiO ₂	FAL	80.3	53	11.9	10.6	0.1	4.8
4	Fe/SiO ₂	FAL	0.0	0.0	0.0	0.0	0.0	0.0
5	Pd/SiO ₂	FOL	19.2	2.0	2.8	-	0.7	13.7
6	Pd-Fe/SiO ₂	FOL	92.7	2.8	0.4	-	83.3	6.2
7	Pd/SiO ₂ +Fe/SiO ₂	FOL	19.6	1.6	2.0	-	1	15.1
8	Fe/SiO ₂	FOL	0.0	0.0	0.0	-	0.0	0.0

A comparison of product distributions at the furfural conversion level ~80% over 1%Pd/SiO₂ and 1%Pd-0.5%Fe/SiO₂ catalysts is shown in Table 6.1 (entry 1 vs. 2). The yield of furan derived from decarbonylation was dramatically decreased from 54% on Pd/SiO₂ to 13.5% on Pd-Fe/SiO₂. Furthermore, as opposed to the case of monometallic Pd catalyst that no formation of 2-methylfuran was observed, the 1%Pd-0.5%Fe/SiO₂ catalyst produced 2-methylfuran in significant amounts, particularly at high W/F. To show that the enhance rate in production of 2-methyl furan on Pd-Fe bimetallic catalyst is due to a direct interaction between Pd and Fe, a physical mixture of monometallic 1%Pd/SiO₂ and 1%Fe/SiO₂ (entry 3) was tested and the result are compared in Table 6.1. The results show that the product distributions and furfural conversions from 1%Pd/SiO₂ and a physical mixture with 1%Fe/SiO₂ are almost the same. That is, furan from decarbonylation of furfural is the main product and the production of 2-methylfuran is not observed. In contrast, 2-methylfuran is the main product on bimetallic 1%Pd-0.5%Fe/SiO₂ catalyst. It should be noted that under the present conditions, the monometallic Fe/SiO₂ exhibited no activity for the reaction of furfural and furfuryl alcohol (entry 4 and 8).

It is clear that the presence of Fe on bimetallic catalyst has both a promoting and a suppressing effect on a product yield and selectivity. The yield of furfuryl alcohol from hydrogenation of furfural and 2-methylfuran from hydrogenolysis of furfuryl alcohol are promoted while the yield of furan from decarbonylation is suppressed. It is speculated that the presence of Fe on bimetallic Pd-Fe catalyst may suppress the formation of acyl species which is the precursor for decarbonylation of furfural. The oxophilic nature of Fe may in fact make the stronger interaction of the O atom of C=O group with the Pd-Fe alloy surface. As a result, it is possible that breaking aldehydic C-H bond to form an acyl intermediate in which the O atom of C=O stays far away from the surface would require a higher energy barrier and this will greatly hinder the formation of an acyl intermediate needed for decarbonylation [7]. In contrast, a stronger interaction of the C=O group with Pd-Fe alloy surface would make the reduction of carbonyl group more favorable.

The similar behavior was also observed when having furfuryl alcohol as feed over Pd/SiO₂ and bimetallic Pd-Fe/SiO₂ catalysts. The most important result on Pd-Fe bimetallic catalyst is the formation of 2-methylfuran

which can be derived from the C-O hydrogenolysis of furfuryl alcohol. As shown in Table 6.1 (entry 5), when feeding furfuryl alcohol there is no significant amount of 2-methylfuran formed on Pd/SiO₂ (yield < 1%). It is also interesting to note that the major product from furfuryl alcohol on 1%Pd/SiO₂ is a saturation of furanyl ring to tetrahydro furfuryl alcohol. In contrast, more than 83% of furfuryl alcohol is converted to 2-methylfuran with 1%Pd-0.5%Fe/SiO₂ catalyst. The results from this work have demonstrated that bimetallic Pd-Fe catalyst is very selective toward C-O bonds cleavage reactions instead of C-C bonds which mainly occur on monometallic Pd catalyst.

6.3 Adsorption of furfural and furfuryl alcohol on Pd(111) and PdFe(111) surfaces (calculation results from Wei An)

The DFT calculations were conducted to interpret the changes observed in the product distribution between monometallic Pd to Pd-Fe bimetallic catalysts. We calculated the adsorption of furfural, furfuryl alcohol on Pd (111) and PdFe(111) surfaces. The optimized structures of furfural and furfuryl alcohol in gas phase are shown in Figure 6.4 and the adsorbed structures on Pd and Pd-Fe are shown in Figure 6.5 and 6.6, respectively. The adsorption configurations under the conditions of low coverage of adsorbates showed that all favors a “planar” adsorption configuration. However, the detailed geometry in terms of bond length change is distinctive on Pd (111) and PdFe(111) surface. In Table 6.2, it can be seen that both C1-O1 and C1-C2 bond lengths of furfural and furfuryl alcohol are increased on Pd (111) surface, compared to those in gas-phase. In addition, the C1-O1 bond length of furfural is increased more on PdFe(111) surface than that on Pd (111) surface. The longer C1-O1 bond length of adsorbed furfural as η^2 -aldehyde configuration indicates that the overall stronger interaction of the carbonyl group with the Pd-Fe alloy surface. As a result, it is

possible that the presence of Fe will greatly promote the hydrogenation of carbonyl group forming furfuryl alcohol but hinder the formation of an acyl intermediate needed for decarbonylation.

As shown in Figure 6.5, the optimized geometries of furfuryl alcohol show that the furanyl ring is closer to the Pd(111) surface compared to the hydroxyl group, suggesting that the interaction between the furanyl ring and Pd(111) surface is the main contributor to the adsorption. This is consistent with the experimental results that we only observed the product from hydrogenation of the furanyl ring (i.e. tetrahydrofurfuryl alcohol, HFOL) when feeding furfuryl alcohol with monometallic Pd catalyst. In contrast with Pd(111), the adsorption of furfuryl alcohol on the PdFe(111) surface is largely due to the interaction with O of C-OH bond where furan ring is repelled from the surface as shown in Figure 6.6. It is clearly seen from DFT calculation results that the presence of Fe significantly increases the interaction of the hydroxyl group with the metal surface. As a result, we may expect that the hydrogenolysis of C1-O1 bond will be favored, thus explaining the formation of 2-methylfuran experimentally observed on the Pd-Fe catalyst.

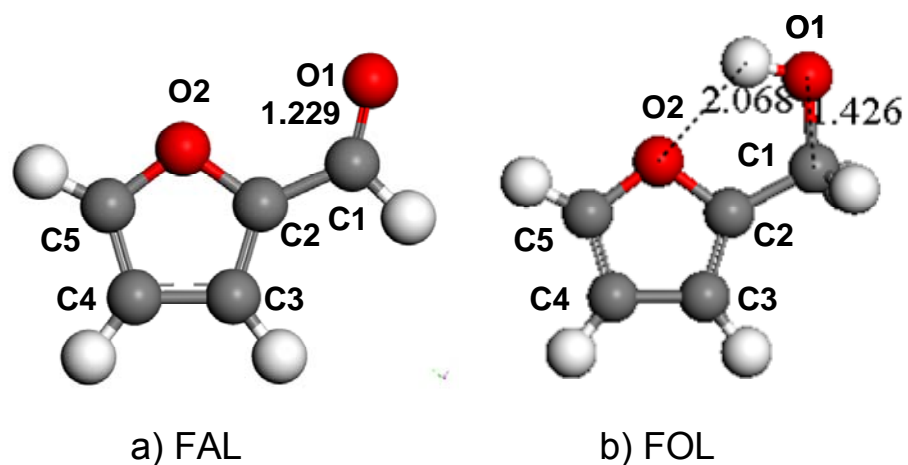


Figure 6.4 Optimized structures of gas phase a) furfural and b) furfuryl alcohol

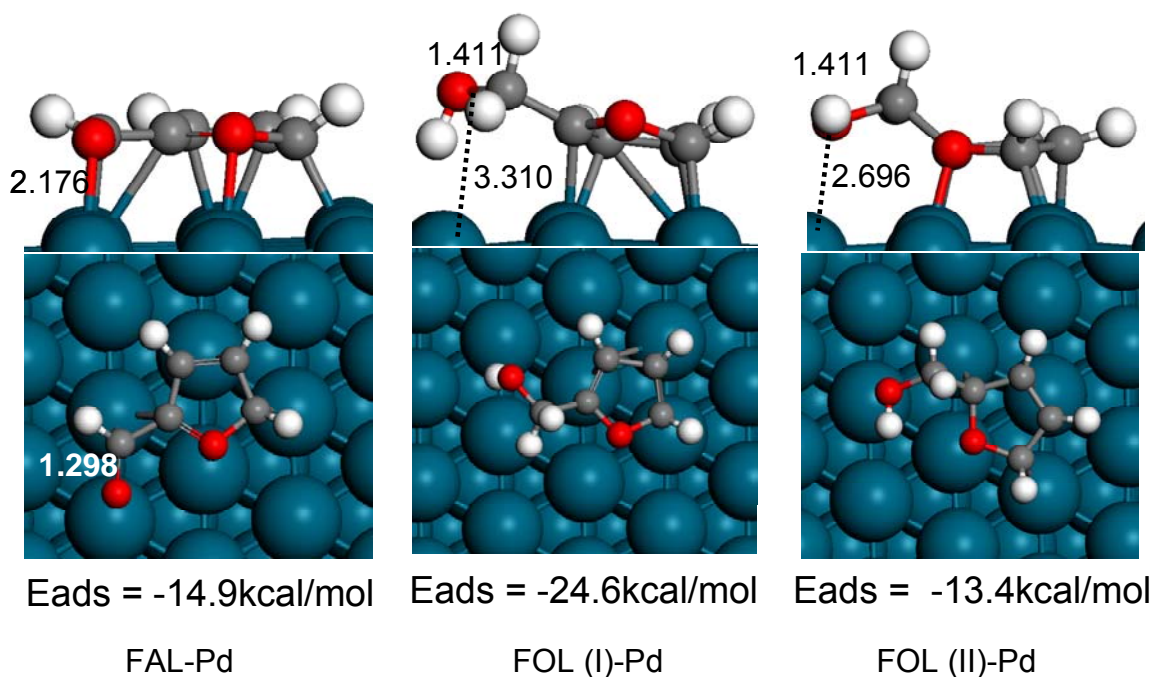


Figure 6.5 Optimized structures of furfural and furfuryl alcohol on Pd(111) surface

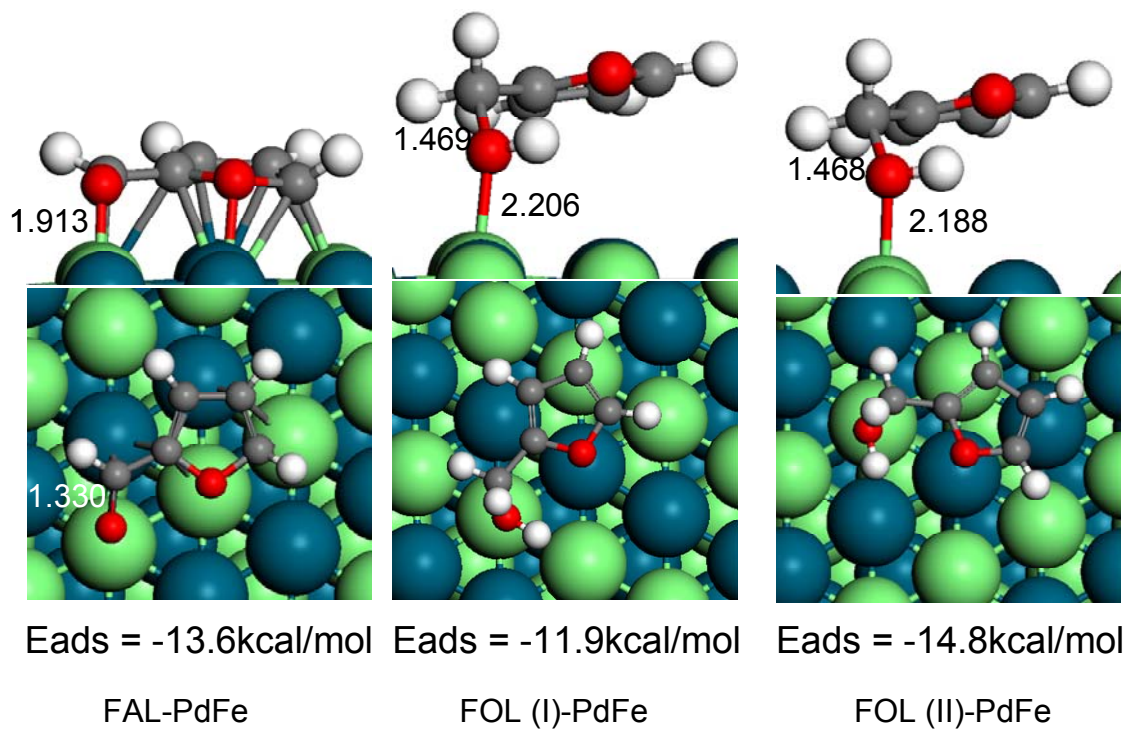


Figure 6.6 Optimized structures of furfural and furfuryl alcohol on PdFe(111) surface

Table 6.2 Comparison of bond lengths (Å) of furfural/furfuryl alcohol in gas-phase and adsorbed on Pd (111) and PdFe (111) surfaces. See Figure 6.4, 6.5 and 6.6 for adsorption configurations and for the assignment of each C, O, and H atom. Adsorption energies (E_{ads}) in Kcal/mol are included.

d (Å)	Furfural			Furfuryl alcohol		
	Gas phase	Pd (111)	PdFe(111)	Gas phase	Pd (111)	PdFe(111)
C1-O1	1.229	1.298	1.330	1.426	1.433/1.411	1.468/1.469
C1-C2	1.448	1.448	1.429	1.501	1.522/1.509	1.478/1.478
C2-C3	1.382	1.428	1.427	1.367	1.452/1.417	1.372/1.371
C3-C4	1.419	1.426	1.417	1.434	1.425/1.456	1.433/1.432
C4-C5	1.373	1.443	1.445	1.363	1.450/1.472	1.366/1.367
C5-O2	1.359	1.447	1.453	1.378	1.444/1.427	1.370/1.369
C2-O2	1.378	1.380	1.387	1.376	1.454/1.380	1.379/1.379
E_{ads} (kcal/mol)	–	-14.9	-13.6	–	-13.4/-24.6	-14.8/-11.9

6.4 Mechanism of hydrogenolysis of furfuryl alcohol on Pd-Fe/SiO₂ catalyst

Pd-Fe/SiO₂ catalyst was found to be very selective for the C-O hydrogenolysis reaction of furfuryl alcohol forming 2-methylfuran. The DFT calculations suggest that the oxophilic nature of Fe makes a very strong interaction of the hydroxyl group with the metal surface resulting in the weakening of the C1-O2 bond. However, the exact reaction mechanism by which the hydroxyl group of furfuryl alcohol gets removed is not fully understood. The optimized structures of furfuryl alcohol on PdFe(111) surface show that only the oxygen atom of hydroxyl group is bonded to the surface (see Figure 6.7). Since the carbon atom is repelled from the surface, we may expect that C-H bond scission on an α -carbon must occur prior to the C-O hydrogenolysis forming 2-methylfuran as shown in Figure 6.7 (mechanism I). In addition to mechanism I, the direct hydrogenolysis of C-O bond may happen since the interaction of the hydroxyl group is very strong (mechanism II).

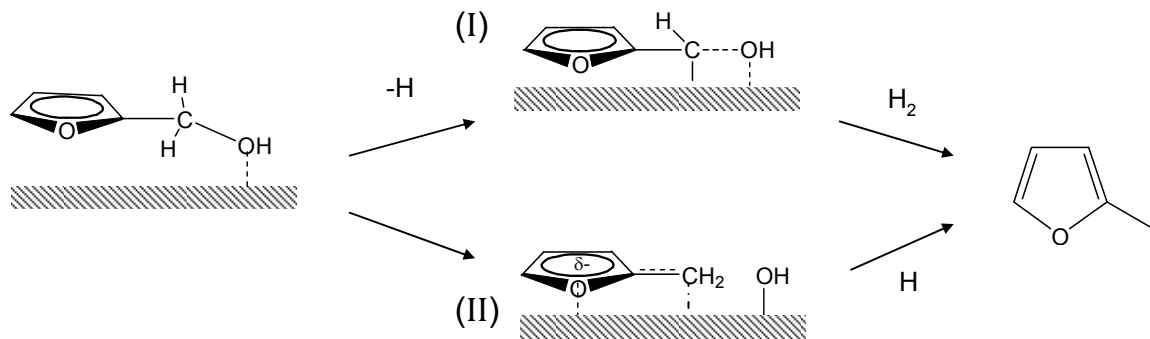


Figure 6.7 Proposed reaction mechanisms for the conversion of furfuryl alcohol on Pd-Fe catalyst.

To investigate whether the C-H scission is required prior to the C-O hydrogenolysis for the reaction of furfuryl alcohol to 2-methylfuran, isotopic labeling experiments have been conducted. The experiment consists in pulsing 5 μL of furfuryl alcohol to the 30 mg of PdFe catalyst bed at 250°C under a gaseous stream of D_2 using a mass spectrometer as a detector. Before discussing the observed distribution of D in the 2-methylfuran product from the feed of furfuryl alcohol with D_2 it is important to ponder what distribution one should expect on the basis of the possible reactions mechanisms. In the case of mechanism I, if a C-H bond scission on an α -carbon is a pre-requisite for the C-O bond cleavage, then 2-methylfuran should contain 2 deuterium atoms. In

contrast, if the C-O bond breaks without a prior deuteration of the ring, the replacement of the OH group by a D will leave the 2-methylfuran product with only one deuterium. As shown in Figure 6.8, none of the 2-methylfuran molecule with two deuterium atoms ($m/z = 84$) is detected, suggesting the mechanism I, in which the C-H bond scission is required before the C-O bond cleavage is unlikely. On the other hand, the product shows a large fraction of 2-methylfuran with one deuterium atom ($m/z = 83$). This result can be explained by the mechanism II that involves the direct cleavage of the C-O bond, without participation of a C-Metal bond formation. In addition to $m/z = 83$, there are significant peaks at $m/z = 82$ and 81 . These correspond to the two major fragments with the loss of one atom of hydrogen ($m/z = 82$) or deuterium ($m/z = 83$) from a singly deuterated 2-methylfuran ($m/z = 83$).

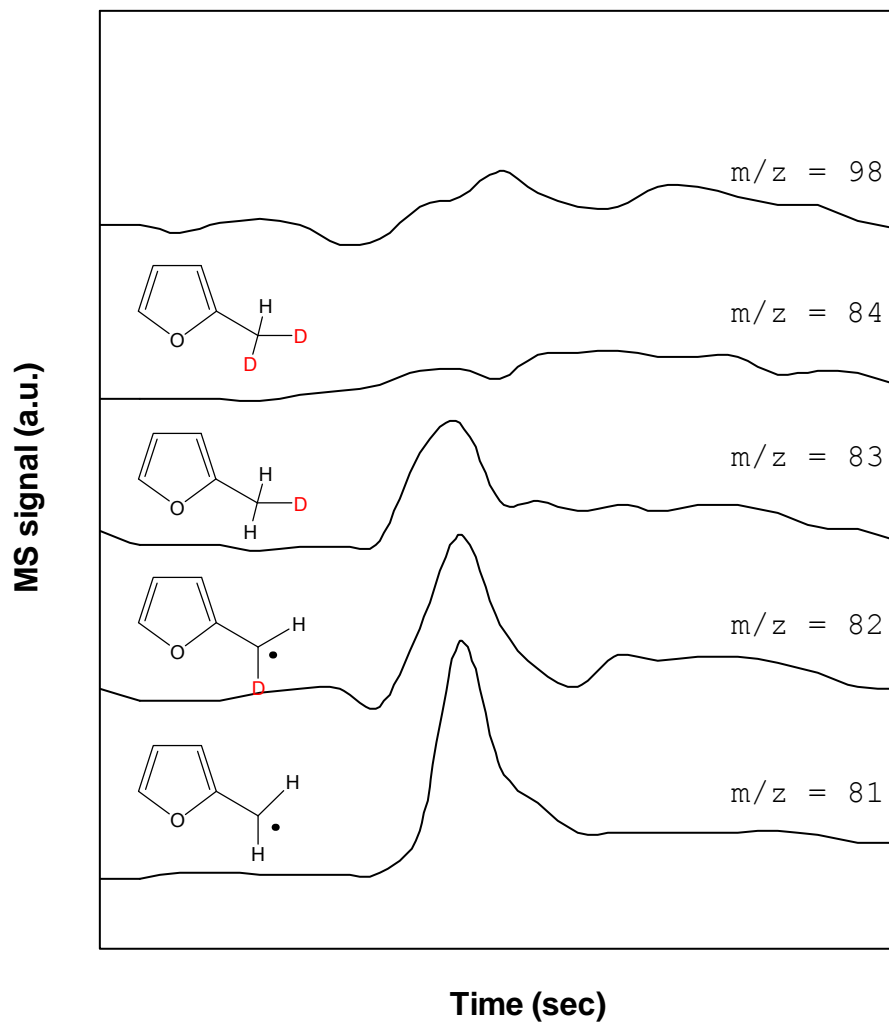


Figure 6.8 MS spectrum after the reaction of furfuryl alcohol with D₂ on Pd-Fe/SiO₂ catalyst.

6.5 Effect of supports on the 2-methylfuran selectivity

The conversion of furfural over Pd-Fe bimetallic catalyst has been studied over SiO_2 , $\alpha\text{-Al}_2\text{O}_3$ and $\gamma\text{-Al}_2\text{O}_3$ supports (Figure 6.9). Among the Pd-Fe supported catalysts, Pd-Fe/ SiO_2 showed the highest selectivity toward the formation of 2-methylfuran. By contrast, 2-methylfuran is not produced to a great extent on Pd-Fe/ $\alpha\text{-Al}_2\text{O}_3$ and Pd-Fe/ $\gamma\text{-Al}_2\text{O}_3$ (selectivity < 10%) at any level of overall furfural conversion. This result suggests that the formation of 2-methylfuran is affected by the support. Since the production of 2-methylfuran from a physical mixture of Pd/ SiO_2 and Fe/ SiO_2 is very small due to there is no interaction between Pd and Fe, one could expect that the formation of Pd-Fe bimetallic alloy which is required for the C-O hydrogenolysis may not be present in both alumina supports. To verify this hypothesis, XPS and XRD technique were employed to characterize the surface of Pd-Fe catalysts on difference supports (experimental results from Tanate Danuthai).

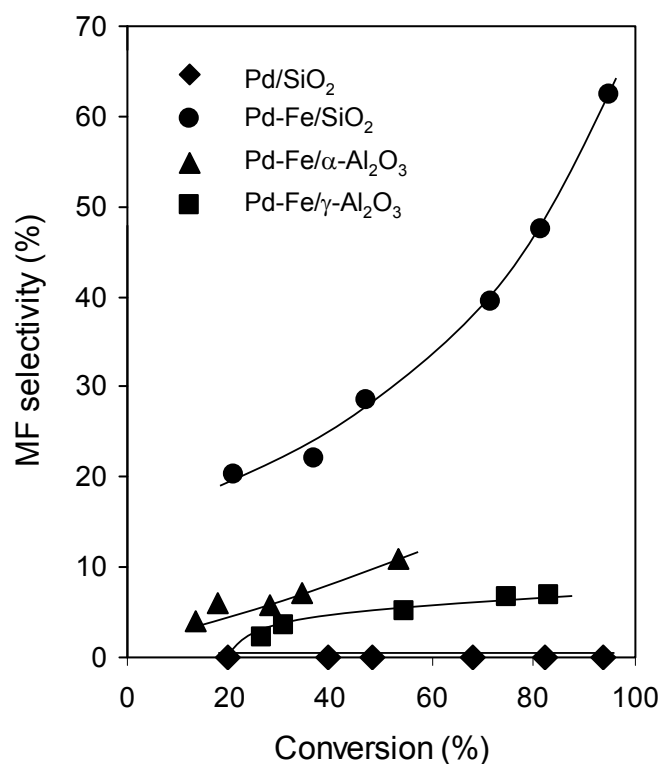


Figure 6.9 2-Methyfuram selectivity as a function of furfural conversion over supported Pd-Fe catalysts at 250°C, H₂/Feed ratio = 25, pressure = 1atm.

The XPS spectra of the in-situ reduced Pd and Pd-Fe catalysts are shown in Figure 6.10. In line with those reported in the literature [8,9], the observed binding energy of Pd/SiO₂ catalyst located at 335.4 eV can be assigned to Pd 3d_{5/2} in the metallic palladium. It is clear that the addition of Fe on Pd/SiO₂ catalyst shifted the Pd 3d_{5/2} peak to 335.8 eV, indicating the changes in the

electronic structure of Pd-Fe/SiO₂ catalyst. The shift in binding energy may attributed to the Pd-Fe alloying metal, which is consistent with the XPS studies of the Pd-Fe/C samples obtained by Tang et al. [10]. On the other hand, the Pd 3d_{5/2} bands of Pd-Fe/γ-Al₂O₃ and Pd-Fe/α-Al₂O₃ catalysts appear at the same binding energy as Pd/SiO₂. This indicates that the addition of Fe on both Pd supported on alumina samples does not affect the electronic structure and energy level of Pd atom. In the other word, there is no Pd-Fe alloy formation when either γ-Al₂O₃ or α-Al₂O₃ is used as support.

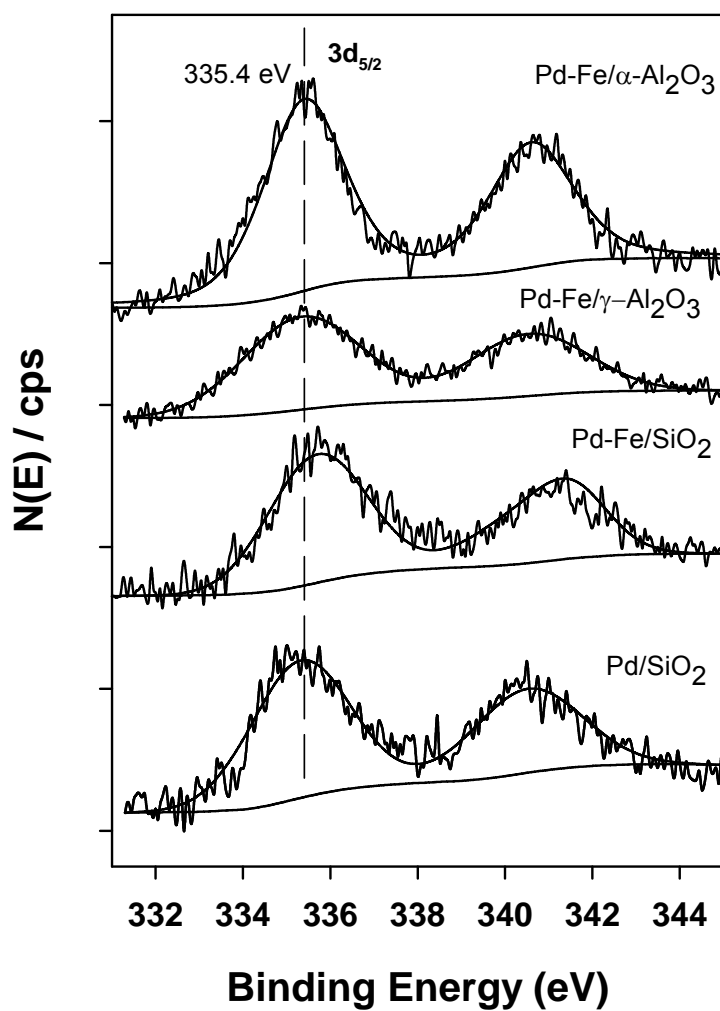


Figure 6.10 X-ray photoelectron spectroscopy (XPS) of Pd_{3d} for Pd and Pd-Fe catalysts with different supports

The XRD patterns of Pd and bimetallic Pd-Fe samples after reduction at 523 K are shown in Figure 6.11. It is observed that Pd/SiO₂ sample exhibited four diffraction peaks at the 2θ values of 39.91°, 45.60°, 67.15°, and

80.57°, which are the characteristic peaks for Pd (1 1 1), (2 0 0), (2 2 0), and (3 1 1) of the FCC crystalline structure of Pd metal, respectively. The four characteristic diffraction peaks of Pd disappeared from the XRD pattern of the Pd-Fe/SiO₂ sample, but a new diffraction peak was observed at 34.38°. The XRD pattern of Pd-Fe/SiO₂ was refined using metallic forms of both metals (i.e. Pd and Fe) and Pd-Fe metal alloy as models. According to the XRD pattern refinement exercise of Pd-Fe/SiO₂, it gives a clear evidence of Pd-Fe alloy presented on the Pd-Fe/SiO₂ sample. The new diffraction peak corresponds to the Pd-Fe alloy formed on the sample, which is line with the XPS results discussed above. For Pd-Fe/ γ -Al₂O₃ and Pd-Fe/ α -Al₂O₃ catalysts, it is quite difficult to differentiate the characteristic peaks of metals due to the relatively higher crystalline of alumina supports and low metal loading. Hence, the refinement exercises with same fundamental parameters and models were applied for both Pd-Fe/ γ -Al₂O₃ and Pd-Fe/ α -Al₂O₃ catalysts. It was found that Pd-Fe metal alloy does not exist in the Pd-Fe/ γ -Al₂O₃ and Pd-Fe/ α -Al₂O₃ catalysts. The only Pd and Fe metals were observed. This fact indicates that the addition of Fe can

enter the Pd lattice, forming the Pd-Fe alloy when SiO₂ support is used.

It is clear from the detailed XPS and XRD characterization that there is only formation of Pd-Fe alloy when silica support is used. As a result, very small amount of 2-methylfuran is produced over alumina supports.

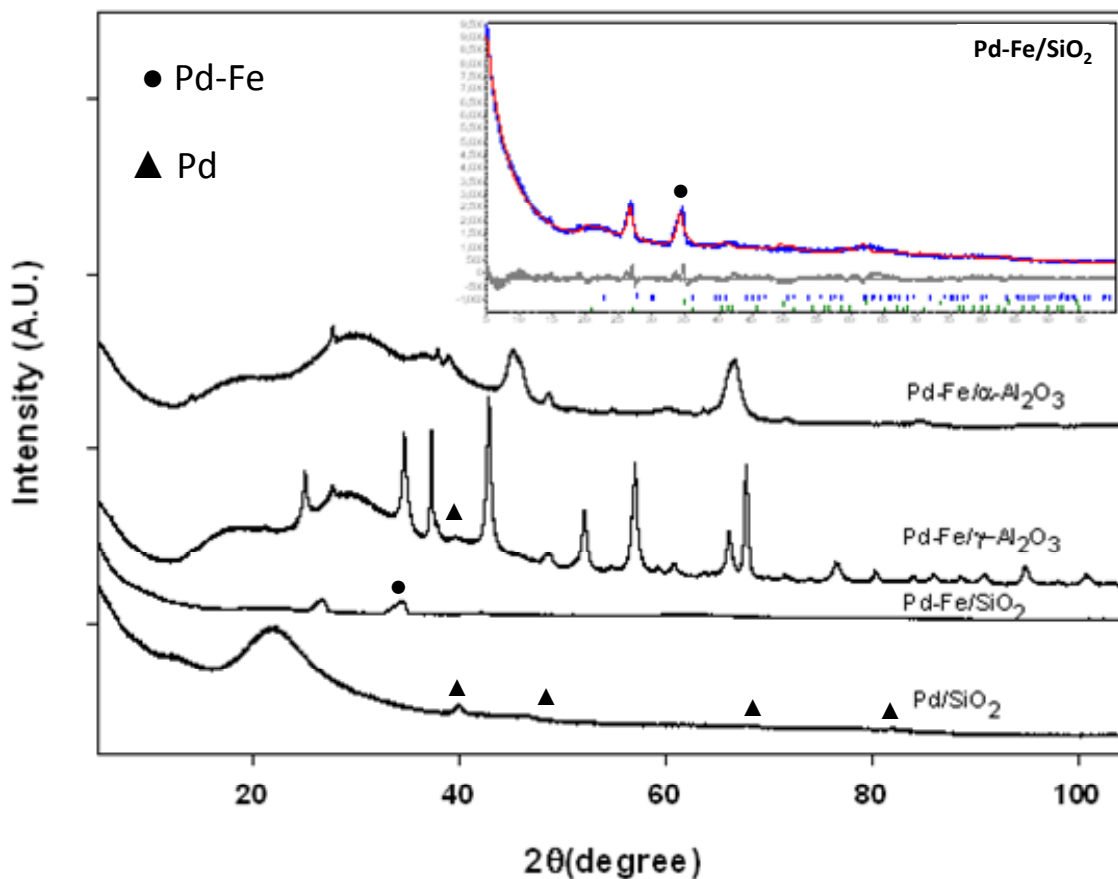


Figure 6.11 XRD patterns of Pd and Pd-Fe catalysts with different supports

6.6 Conclusion

The conversion of furfural on pure Pd/SiO₂ catalyst yield primarily decarbonylation products due to the favorable formation of acyl species, which can readily decompose in to furan and CO. By contrast, on Pd-Fe bimetallic catalysts, the yield of furfuryl alcohol and 2-methylfuran greatly increases while the yield of furan decreases. The presence of Pd-Fe alloy greatly promotes the hydrogenation of carbonyl group forming furfuryl alcohol and the C-O bond hydrogenolysis of furfuryl alcohol to 2-methyl furan but hinder the formation of an acyl intermediate needed for decarbonylation to furan. Detailed XPS and XRD characterization indicate that no formation of Pd-Fe alloy on alumina supports resulting in a very small production of 2-methylfuran.

References

-
- [1] Y. Roman-Leshkov, C.J. Barrett, Z.Y. Liu, J.A. Dumesic, *Nature Letters* 447 (2007) 982.
 - [2] S. Sitthisa, T. Sooknoi, Y. Ma, P.B. Balbuena, D.E. Resasco, *J. Catal.* 277 (2011) 1.
 - [3] S. Sitthisa, Wei An, D.E. Resasco, *J. Catal.* 284 (2011) 90.

-
- [4] S. Sitthisa T. Pham, T. Prasomsri, T. Sooknoi, R.G. Mallinson, D.E. Resasco, *J. Catal.* 280 (2011) 17.
- [5] S. H. Pand, J. W. Medlin, *ACS Catal.* 1 (2011) 1272
- [6] J. W. Medlin, *ACS Catal.* 1 (2011) 1248.
- [7] M. Mavrikakis, M. A. Barteau, *J. Mol. Catal. A: Chem.* 131 (1998) 135.
- [8] B. L. Gustafson, P.S. Wehner, *Appl. Surf. Sci.* 52 (1991) 261.
- [9] J. Tarabay, W. Al-Maksoud, F. Jaber, C. Pinel, S. Prakash, L. Djakovitch, *Appl. Catal. A* 388 (2010) 124.
- [10] Y. Tang, S. Cao, Y. Chen, T. Lu, Y. Zhou, L. Lu, J. Bao, *Appl. Surf. Sci.* 256 (2010) 4196.

CHAPTER 7

Conversion of Furfural on Bimetallic Ni-Fe Catalysts

7.1 Introduction

Bimetallic alloys appear as promising candidates for the selective removal of oxygen from the carbonyl group of furfural under relatively mild operating conditions. We have recently shown that different bimetallic catalysts exhibit very different product distributions depending on the type and relative stability of the surface species that they are able to form. For example, we recently showed that while furfural preferentially yields furan via decarbonylation on pure Pd catalyst, the selectivity shifts to hydrogenation to furfuryl alcohol when Cu is alloyed with Pd due to the formation of the side-on $\eta^2(\text{C}-\text{O})$ -aldehyde species is less stable on Pd-Cu than on pure Pd, which in turn makes the formation of the acyl intermediates less likely. Alternatively, one could use an alloying metal like Fe that has a stronger affinity for oxygen to enhance the interaction with the oxygenated group. In fact, in a recent study, we have shown that Pd-

Fe catalysts have a much higher selectivity towards C-O hydrogenolysis of furfural than Pd catalysts, which preferentially catalyzes decarbonylation. Pd-Cu bimetallic catalysts are highly selective for hydrogenation of furfural to furfuryl alcohol. Moreover, the addition of Fe to Pd and forming Pd-Fe alloys greatly suppresses the production of furan from furfural. In the chapter, we have investigated the conversion of furfural over Ni-Fe bimetallic catalysts. The effect of adding Fe on the catalytic properties of silica-supported Ni is investigated. Samples with different Ni/Fe ratios were prepared and characterized by XRD, TEM, TPR and BET techniques to evaluate the structural changes and the extent of alloy formation. Structure-activity relationships were investigated by combining the results of catalytic activity measurements with characterization and theoretical DFT (Density Functional Theory) calculations.

7.2 Catalyst characterization

The XRD patterns of monometallic (Ni/SiO₂ and Fe/SiO₂) and bimetallic (various Ni-Fe/SiO₂) samples, pretreated in H₂ at 450°C for 1 h, are shown in Figure 7.1. No diffraction peaks due to the SiO₂ support were observed. In agreement with previous observations [1], the Ni(111) and Fe(110) peaks for the monometallic samples were observed at $2\theta = 44.41^\circ$ and 44.64° , respectively. The bimetallic Ni-Fe/SiO₂ samples exhibited a single peak in this region, and this gradually shifted from the position of pure Ni (44.41°) to smaller angles as the Fe content increased. This shift gives clear evidence for the formation of Ni-Fe solid solution alloys with fcc structure. The absence of any intensity near 44.64° suggests that no unalloyed Fe is present in significant amounts (i.e., detectable by XRD). The lattice constants of Ni and Ni-Fe alloys were estimated from the position of the XRD peaks assuming a cubic symmetry for the crystal structure as shown in Table 7.1. The lattice constant of Ni is 3.530 Å, which is close to the value obtained from DFT calculation (3.522 Å). Increasingly larger lattice constants (3.542–3.584 Å) were obtained for the Ni-Fe bimetallic samples, in agreement with the DFT calculations and previous reports [2].

The average particle sizes for Ni and Ni-Fe alloy particles were estimated from the XRD peak broadening, using the Scherrer equation. The values estimated by this method are in the range 10-12 nm for the monometallic Ni and Ni-Fe bimetallic samples. These results agree with those estimated from TEM (see Figure 7.2) in the sense that there are no significant size differences between monometallic Ni and Ni-Fe bimetallic particles. By contrast, the monometallic Fe sample has much larger particles than those of Ni or Ni-Fe samples, as shown by both XRD ($d=19.1$ nm) and TEM (23.4 nm). This difference also supports the conclusion that the bimetallic samples do not contain significant amounts of unalloyed Fe, which would tend to form larger particles.

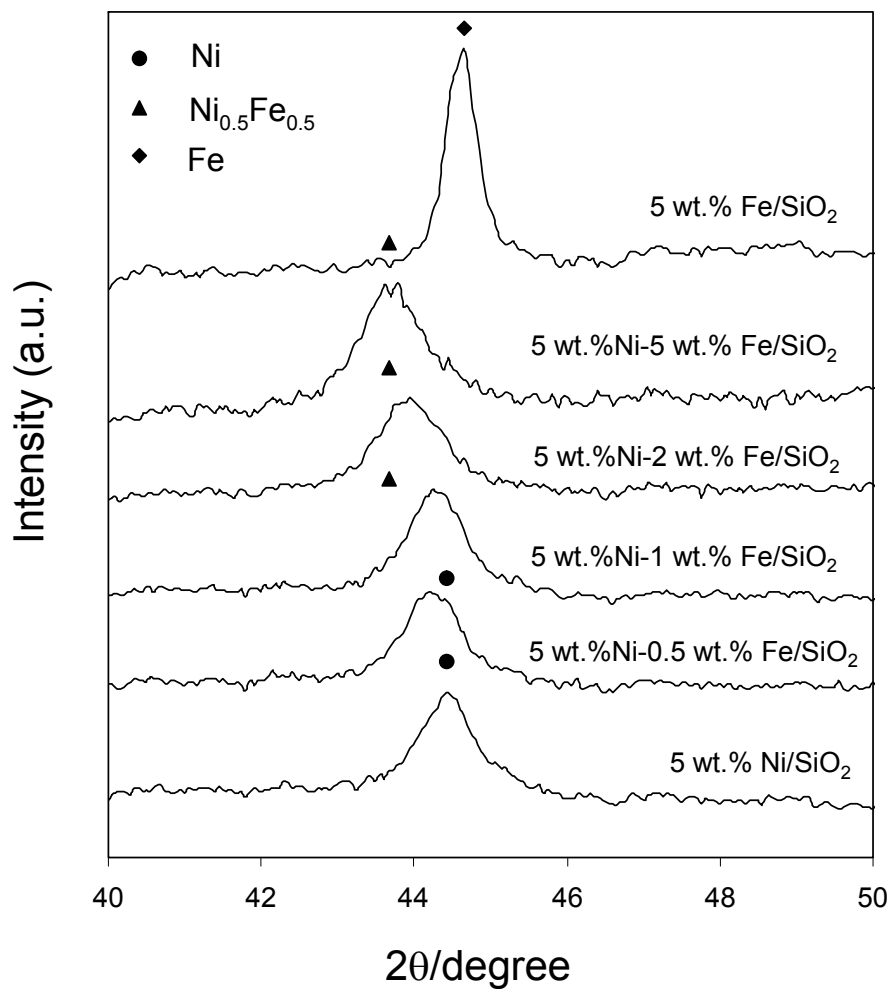


Figure 7.1 XRD patterns of monometallic Ni, Fe and bimetallic Ni-Fe catalysts reduced at 450°C for 1h.

Table 7.1 Physical properties of catalysts

Catalysts	Metals loading (mmol.g _{cat} ⁻¹)		H ₂ consumption from TPR (mmol.g _{cat} ⁻¹)	diameter (nm)		lattice constant (Å)			BET (m ² /g)
	Ni	Fe		TEM	XRD	XRD	DFT	Std.	
5Ni	0.85	0.00	1.01	16.8	11.2	3.530	3.522	3.524	126
5Ni-0.5Fe	0.85	0.09	1.16	16.9	11.9	3.542	-	-	130
5Ni-1Fe	0.85	0.18	1.27	16.7	11.9	3.534	-	-	118
5Ni-2Fe	0.85	0.36	1.48	17.1	10.0	3.567	-	-	130
5Ni-5Fe	0.85	0.90	2.20	15.7	10.0	3.584	3.553*	3.587*	115
5Fe	0.00	0.90	-	23.4	19.1	2.868	-	2.866	128

* Ni_{0.5}Fe_{0.5}

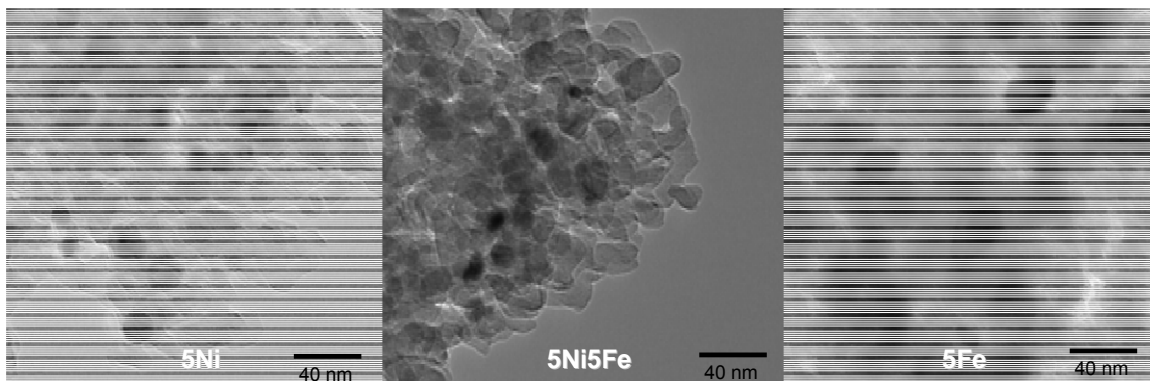


Figure 7.2 TEM images of 5%Ni/SiO₂, 5%Ni-5%Fe/SiO₂, and 5%Fe/SiO₂ catalysts after H₂ pretreatment at 450°C for 1 h.

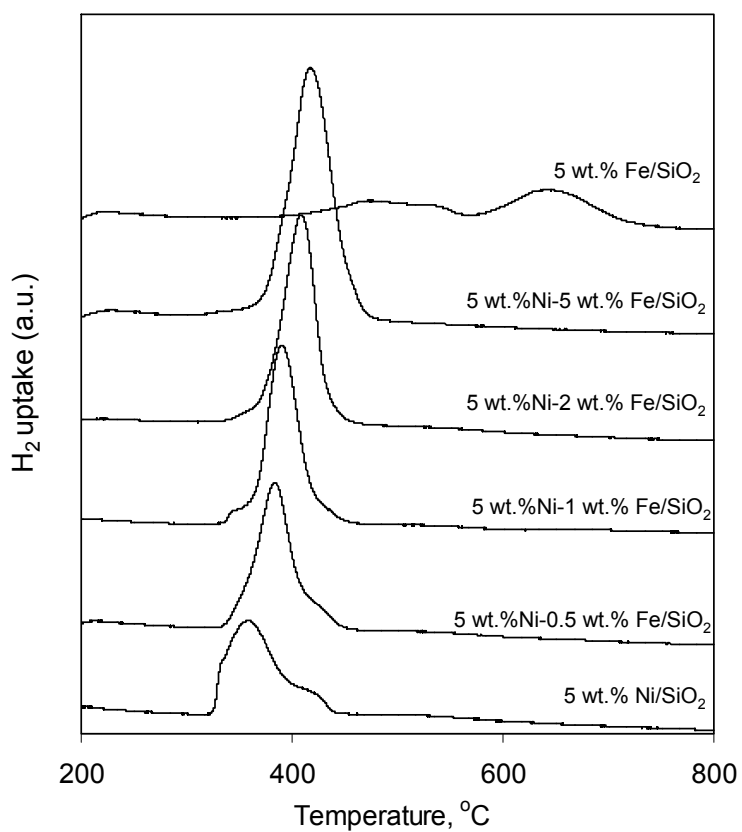


Figure 7.3 Temperature programmed reduction (TPR) of monometallic Ni, Fe and bimetallic Ni-Fe catalysts.

The high extent of alloy formation is further demonstrated by TPR. As shown in Figure 7.3, the reduction profile for the monometallic Ni catalyst displays a main reduction peak at 365°C with shoulder peaks at lower and higher temperatures (336 and 425°C, respectively). According to previous studies [3,4], the first peak is the result of an endothermic phase transition occurring simultaneously with a partial reduction of the NiO. The main peak is attributed to the reduction of NiO to Ni metal [5]. The third peak at higher temperatures could be due to the reduction of small nickel oxide crystallites strongly attached to the support, even forming Ni silicate species (nickel hydroxysilicates, antigorite, or montmorillonite) [6]. The reducibility pattern of unalloyed Fe is very different from that of Ni. As seen in Figure 7.3, the broad hydrogen consumption peaks for the reduction of Fe/SiO₂ appeared shifted to much higher temperatures from those of Ni. Similar behavior has been reported for monometallic Fe catalysts in previous studies [7]. The first broad peak ranging from 410 to 570°C has been ascribed to the reduction of α -Fe₂O₃ into α -Fe₃O₄. The second broad peak ranging from 590 to 730°C with the maximum at 650°C is typically attributed to the reduction of iron oxides to α -Fe. In sharp contrast to the

monometallic Fe sample, the TPR profiles of the Ni-Fe samples do not show any consumption on the high temperature range, which is typical of unalloyed Fe. Instead, as shown in Figure 7.3, the addition of Fe only causes a gradual shift to higher reduction temperatures relative to that of pure Ni, in agreement with previous studies [8,9].

In addition to the consistent trend in peak position, the H₂ uptake linearly increased with increasing Fe loading in the bimetallic catalysts (see Table 7.1). Since the Ni loading was kept constant at 0.85mmol/g, this proportional increase in H₂ uptake with Fe loading clearly demonstrates the reduction of Fe. The unalloyed Fe is not able to reduce by itself below 500°C, as previously reported [10]. Therefore, the almost complete reduction of Fe observed in the bimetallic catalysts demonstrates a close interaction with Ni, consistent with the formation of an alloy.

7.3 Conversion of furfural over monometallic Ni catalyst

The product distribution obtained over the Ni/SiO₂ catalyst at 210°C is shown in Figure 7.4. The most abundant products at this temperature are furfuryl alcohol (FOL, yield = 31 % at 0.1 h⁻¹) and furan (yield = 32 % at 0.1 h⁻¹), which as shown in scheme 1, derive from the hydrogenation and decarbonylation reactions, respectively. The next abundant products are those lumped together as C₄ products (yield = 14 % at 0.1 h⁻¹), which include butanal, butanol and butane. The C₄ products derive from the ring opening reaction via C-O hydrogenolysis of the furan ring (i.e. C2-O2, see Fig. 11a for the assignment of each C, O, and H atom), a typical reaction characteristic of Ni catalysts [11]. Interestingly, no C₅ products were observed, indicating that the C₄ products mostly derive from furan, rather than from furfural or furfuryl alcohol.

Finally, 2-methylfuran (2MF) produced as a secondary product by the C-O hydrogenolysis of furfuryl alcohol (i.e. C1-O1) is only observed in measurable amounts at high W/F (yield <2% at 0.1h⁻¹). Similarly, tetrahydrofurfuryl alcohol (HFOL), resulting from hydrogenation of the furanyl ring of furfuryl alcohol, is

only observed in significant amounts at high W/F (yield = 5 % at 0.1 h^{-1}).

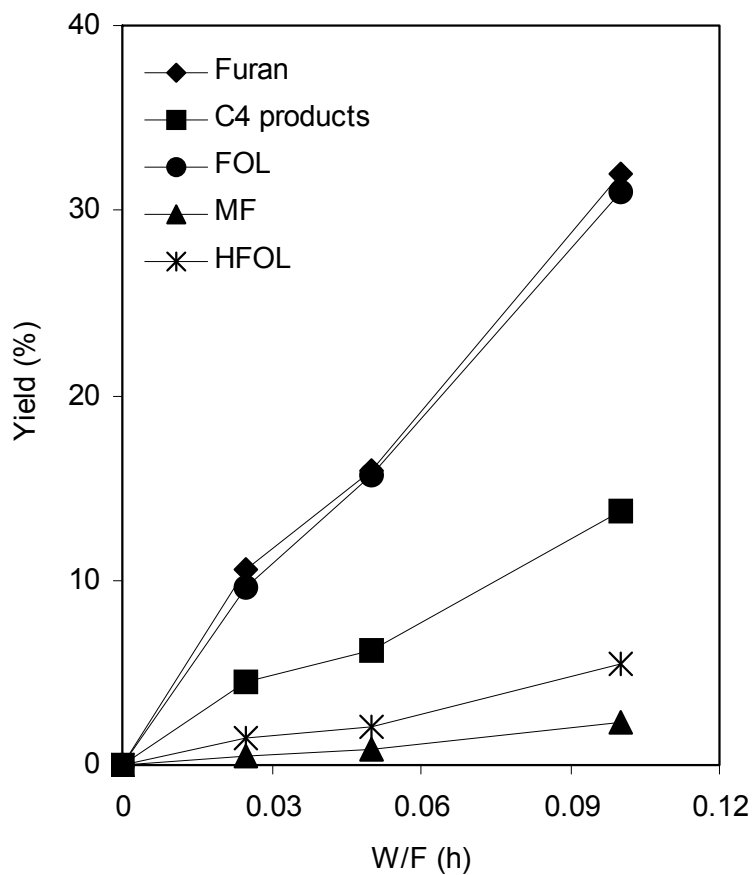
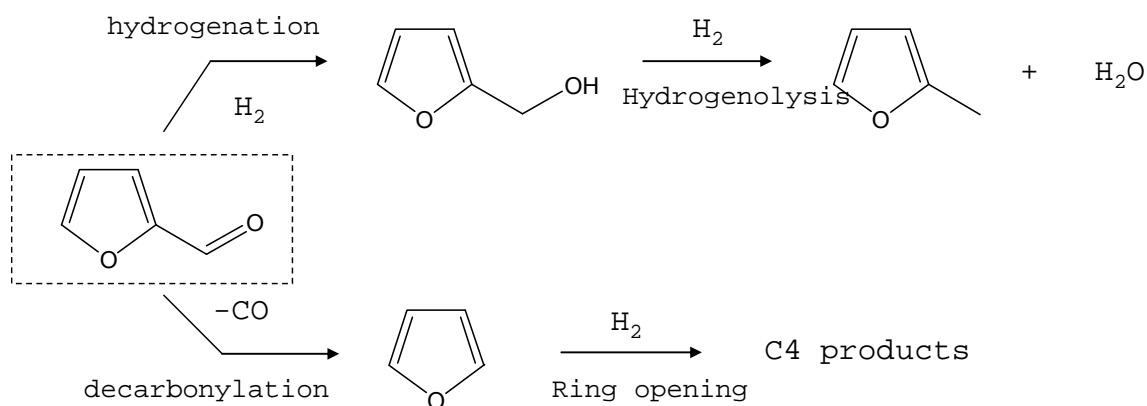


Figure 7.4 Product distribution from the reaction of furfural over a monometallic 5 wt.%Ni/SiO₂ catalyst, at 210°C, H₂/Feed ratio = 25, pressure = 1atm.



Scheme 1 Reaction pathways for furfural conversion.

As shown in Figure 7.5, a remarkable change in product distribution is observed as the reaction temperature increases. While the yields of furan and its secondary ring-opening C₄ products increase with temperature, furfuryl alcohol rapidly decreases, becoming insignificant near 250°C. It is clear that decarbonylation and hydrogenation are two parallel routes not strongly dependent on conversion but strongly depend on reaction temperature and type of metals [12].

Finally, it is important to note that on the monometallic Ni catalyst, the increase in yield of 2-methylfuran with temperature is much less pronounced than that of the other products, reaching only ~ 12% at 250 °C.

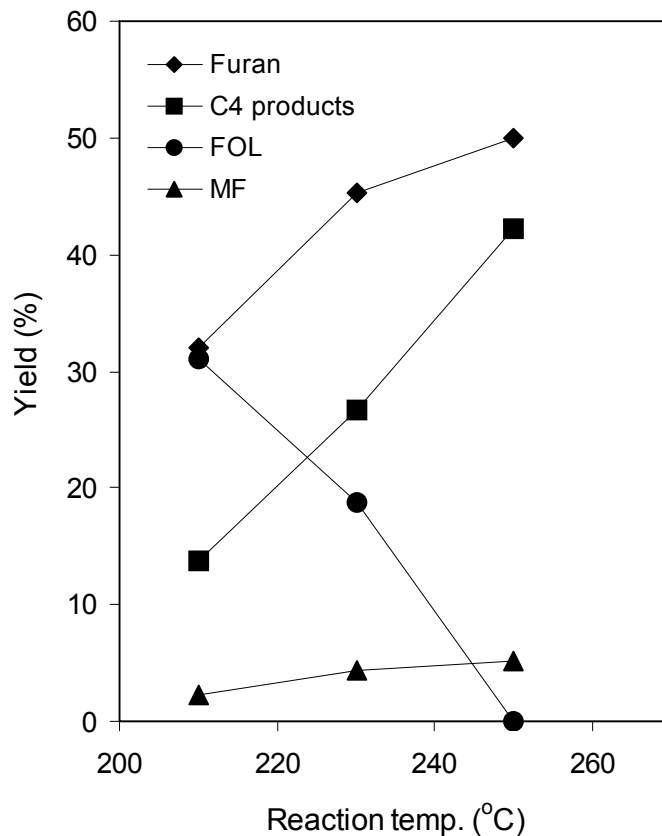


Figure 7.5 Yield of products from the reaction of furfural over a monometallic 5 wt.%Ni/SiO₂ catalyst as a function of temperature. Reaction conditions: W/F = 0.1 h, H₂/Feed ratio = 25, pressure = 1atm.

7.4 Conversion of furfural over Ni-Fe bimetallic catalysts

A comparison of the conversion levels and product distributions obtained at 250°C over monometallic 5wt.%Ni/SiO₂ and bimetallic 5wt.%Ni-2wt.%Fe/SiO₂ catalysts at various space times (W/F) is shown in Table 7.2. The first difference observed is in the level of conversion obtained over the two catalysts under the same reaction conditions. For example, at the same temperature and at W/F= 0.025 h, the overall furfural conversion on the bimetallic catalyst (i.e., 28.2%) was about half of that obtained on the monometallic Ni catalyst (i.e., 50.9%).

Table 7.2 Conversion and yield of products from the reaction of furfural over 5wt.%Ni/SiO₂ and 5wt.%Ni-2wt.%Fe/SiO₂ catalysts

Catalysts	5wt.%Ni/SiO ₂	5wt.%Ni-2wt.%Fe/SiO ₂		
W/F (h)	0.025	0.025	0.05	0.1
Conversion (%)	50.9	28.2	51.1	96.3
Furan	23.1	3.8	5.9	12.1
FOL	7.2	5.0	6.4	9.5
MF	1.4	5.0	16.8	39.1
C ₄ Products	18.1	12.4	19.9	27.6
POL	-	1.0	2.1	7.9

Reaction condition: Temp. = 250°C, H₂/Feed ratio = 25, pressure = 1atm.

In addition, interesting differences in product distribution are observed when comparing the two catalysts. Specifically, comparing them at the same level of conversion (~50%), a clear enhancement in the yield of 2-methylfuran is observed over the bimetallic catalyst. At the same time, the yield of furan greatly decreases on this catalyst. Furthermore, as opposed to the case of monometallic Ni catalyst that did not make any C₅ products, the Ni-Fe catalyst produced pentanol (POL) in significant amounts, particularly at high W/F.

It appears that pentanol is formed in a secondary ring-opening reaction of the furanyl ring of 2-

methylfuran, which is not significantly formed over the monometallic Ni catalyst. It is also interesting to note that the yield of C₄ products also increased by the addition of Fe, even though the yield of furan was drastically reduced. Since methane was not observed in the products, the C₄ products do not result from the C₅ products. Therefore, it can be concluded that the addition of Fe not only promotes the ring opening reaction of 2-methylfuran, but also of furan.

The effect of Fe loading in the bimetallic catalysts on product distribution is summarized in Figure 7.6. It is clear that the addition of Fe on bimetallic catalysts has both a promoting and a suppressing effect on product yield and selectivity. That is, the yield of 2-methylfuran first increases with increasing Fe content to a maximum value at 2%Fe but then decreases, while the selectivity towards 2-methylfuran keeps increasing at all Fe contents. In contrast, the yield and selectivity of furan and C₄ products continuously decrease with Fe loading. It should be noted that, under the present conditions, the monometallic Fe/SiO₂ exhibited no activity for furfural conversion.

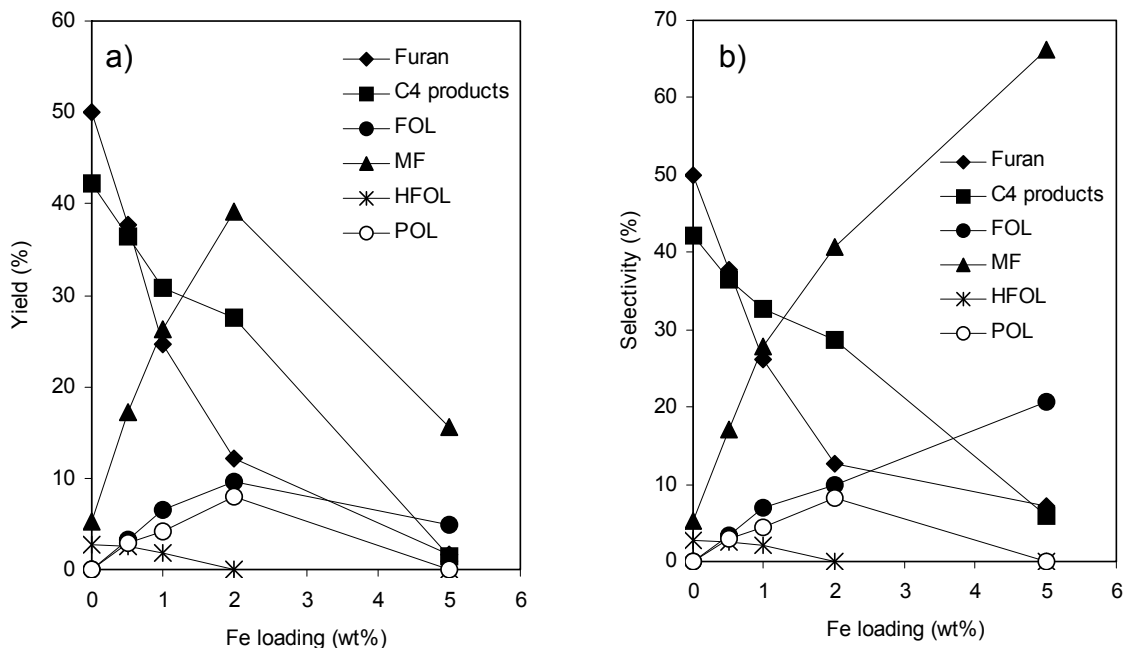


Figure 7.6 a) Yield and b) selectivity of products from the reaction of furfural over bimetallic Ni-Fe catalysts as a function of Fe loading. Reaction conditions: Temp. = 250°C, W/F = 0.1 h, H₂/Feed ratio = 25, pressure = 1atm.

To show that the enhanced rate in production of 2-methylfuran at low Fe loadings catalysts is due to a direct interaction between Fe and Ni, a physical mixture of monometallic 5wt.%Ni/SiO₂ and 5wt.%Fe/SiO₂ was tested and the results are compared in Figure 7.7. They confirm that the product distribution and conversion level are almost the same as those of pure 5wt.%Ni/SiO₂. That is, furan and its related C₄ products are dominant and the production of 2-methylfuran is very small. By contrast, on

the bimetallic 5wt.%Ni-5wt.%Fe/SiO₂ catalyst, 2-methylfuran is the main product. Therefore, it is clear that the change in products selectivity of Ni catalyst observed in our experiments is due to the formation of Ni-Fe bimetallic alloys, which have been undoubtedly identified by physicochemical techniques.

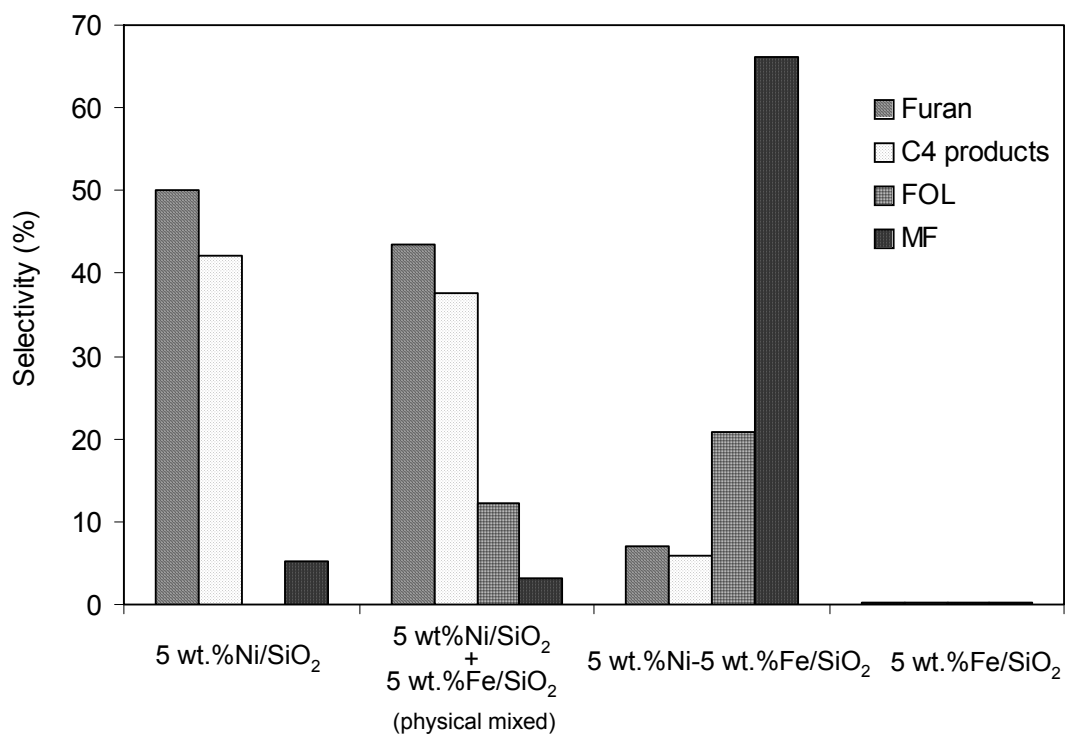


Figure 7.7 Product distributions from furfural conversion over various types of catalysts. Reaction conditions: Temp. = 250°C, W/F = 0.1 h, H₂/Feed ratio = 25, pressure = 1atm

The effect of reaction temperature on product distribution over the bimetallic catalyst can be analyzed in Figure 7.8. The results, show that while furfuryl alcohol and 2-methylfuran are the main products at low temperatures (210°), the yield of 2-methylfuran significantly increases as a function of temperature and it becomes the main product at high temperatures (250°C). In addition to 2-methylfuran, the ring-opening products from furan and 2-methylfuran also increased with temperature. In contrast to 5wt.%Ni/SiO₂ catalyst in which furan was the main product at 250°C, less than 10% yield of furan was observed on the bimetallic 5 wt.%Ni-2wt.%Fe/SiO₂ catalyst at the same temperature. Again, this result indicates that the presence of Ni-Fe alloys suppresses the decarbonylation activity while it promotes C1-O1 hydrogenolysis reactions, for both the cleavage of the carbonyl group and the opening of the ring. The fact that hydrogenation to furfuryl alcohol was dominant at low temperatures while C1-O1 hydrogenolysis dominated at high temperatures is due to the higher activation of the latter.

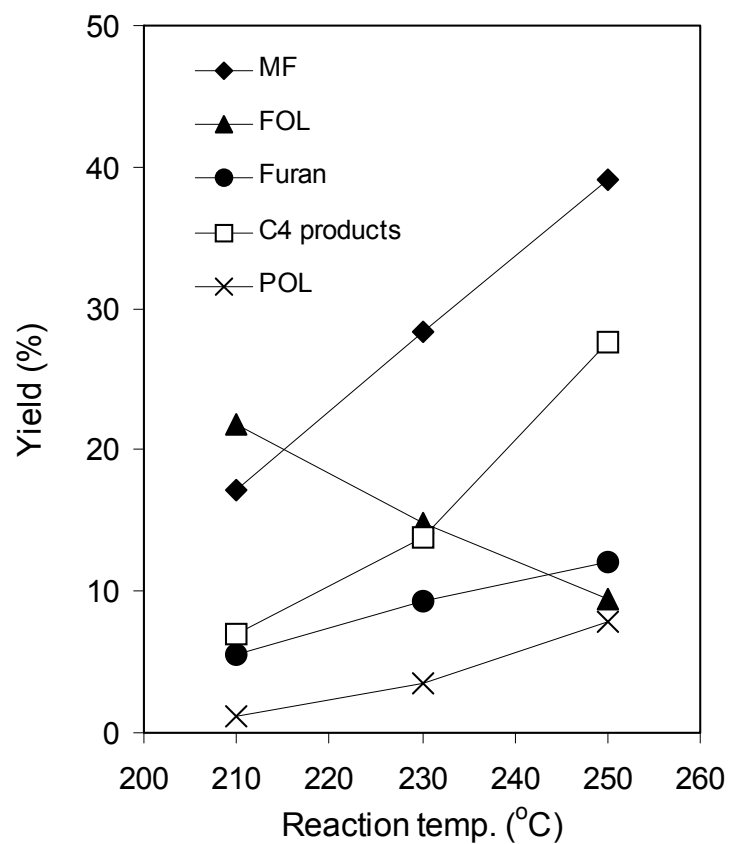


Figure 7.8 Product distribution as a function of temperature from the reaction of furfural over 5 wt.%Ni-2 wt.%Fe/SiO₂. Reaction conditions: Temp. = 250°C, W/F = 0.1 h, H₂/Feed ratio = 25, pressure = 1atm.

7.5 Conversion of furfuryl alcohol (FOL) over Ni-Fe bimetallic catalysts

To further investigate the reaction pathways of oxygenates over the Ni-Fe bimetallic catalysts and shed more light on the results obtained with furfural, we conducted reaction measurements using additional oxygenated molecules on the same catalyst series. We first chose to study the conversion of furfuryl alcohol under the same reaction conditions as those used with furfural to determine whether the hydrogenation of the carbonyl group makes hydrogenolysis easier. If that is the case, C1-O1 hydrogenolysis could occur as a secondary reaction with the alcohol acting as an intermediate (see Scheme 1).

Having furfuryl alcohol as the feed, the main primary products on pure Ni are furan and 2-methylfuran (see Figure 7.9(a)). As the Fe loading increases, the yield of furan decreased while 2-methylfuran increased, as with the furfural feed. The yield of pentanol (POL), which derives from C2-O2 hydrogenolysis of 2-methylfuran also increased significantly when Fe was incorporated.

While similar distribution of products are obtained with furfuryl alcohol and furfural feeds, the most important difference is the high activity for 2-methylfuran formation from furfuryl alcohol compared to that from furfural, as shown in Figure 7.9(b) as a function of Fe loading in the Ni-Fe bimetallic catalysts. A significantly higher yield of 2-methylfuran is obtained from furfuryl alcohol than from furfural in every one of the catalysts, but the difference becomes more pronounced as the Fe/Ni ratio increases.

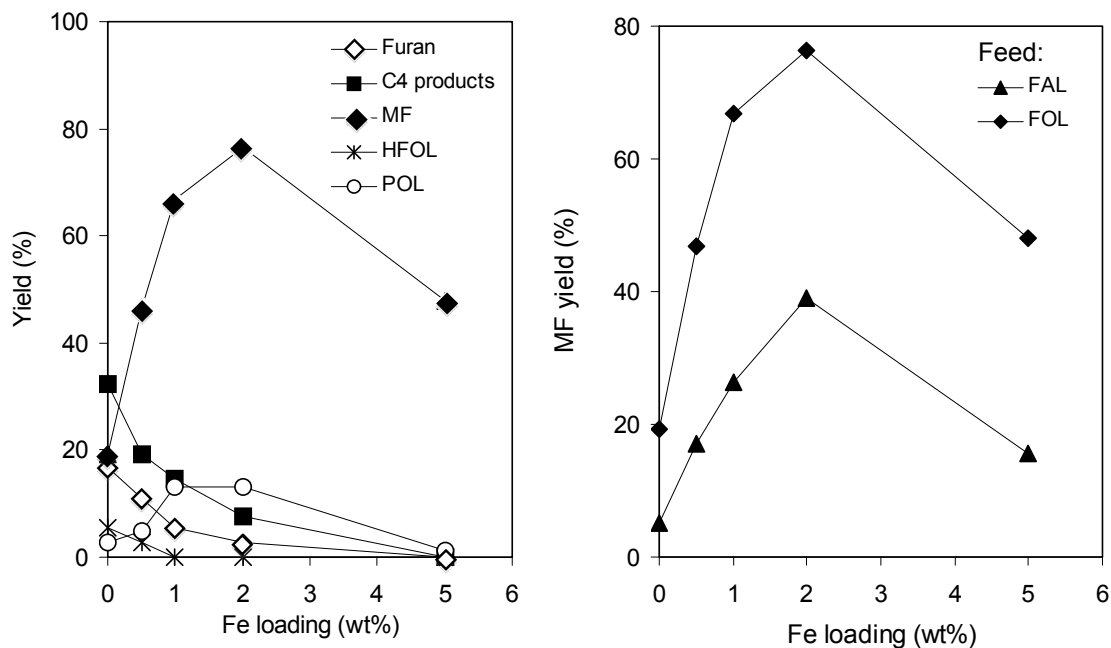


Figure 7.9 Yield of products from the reaction of furfuryl alcohol over Ni-Fe bimetallic catalysts as a function of Fe loading. Reaction conditions: Temp. = 250°C, W/F = 0.1 h, H₂/Feed ratio = 25, pressure = 1atm.

7.6 Conversion of tetrahydrofurfuryl alcohol (HFOL) over Ni-Fe bimetallic catalysts

It is important to determine whether the much faster deoxygenation observed with the alcohol compared to that with the aldehyde is due to enhanced C1-O1 hydrogenolysis reaction or a combination of partial hydrogenation/dehydration. One could speculate that instead of the direct activation of the C-O bond via a di-sigma intermediate mentioned above, a partial hydrogenation of the furanyl ring, followed by dehydration of the alcohol, may operate on these catalysts leading to 2-methylfuran. Therefore, to eliminate this possibility we measured the conversion of tetrahydrofurfuryl alcohol (HFOL) over the same 5wt.%Ni-2wt.%Fe/SiO₂ catalyst, under the same reaction conditions as those used with furfuryl alcohol and furfural. Contrary to the reaction with furfural and particularly with furfuryl alcohol for which a high yield of 2-methylfuran was observed (~40%), with the fully saturated tetrahydrofurfuryl alcohol the yield of 2-methyltetrahydrofuran was very low (~1.5%) and 2-methylfuran was not observed. The much lower reactivity of tetrahydrofurfuryl alcohol demonstrates that dehydration is not an important reaction path on these catalysts. By

contrast, the strong interaction of the furanyl ring with the metal surface seems to play an important role in the C-O hydrogenolysis reaction. In fact, it is generally known that furan has a strong interaction with the surface of Group VIII metals due to the interaction of the p bonds of the ring with the d orbitals of the metal [13, 14].

7.7 Conversion of benzyl alcohol (BZOL) over Ni-Fe bimetallic catalysts

To investigate whether the presence of an aromatic ring in the molecule plays a similar role in reactivity as that of the furanyl ring in the conversion of the oxygenated group, we investigated the conversion of benzyl alcohol over the same catalysts series as that used for the furanyl compounds. To determine to what extent the relative decarbonylation/hydrogenolysis reaction rates can be modified by the addition of Fe we evaluated the formation of benzene and toluene as direct products of decarbonylation and hydrogenolysis, respectively. The major difference with the products from furfural and furfuryl alcohol was the lack of ring opening products,

which indicate that the aromatic ring remains unperturbed during the reaction.

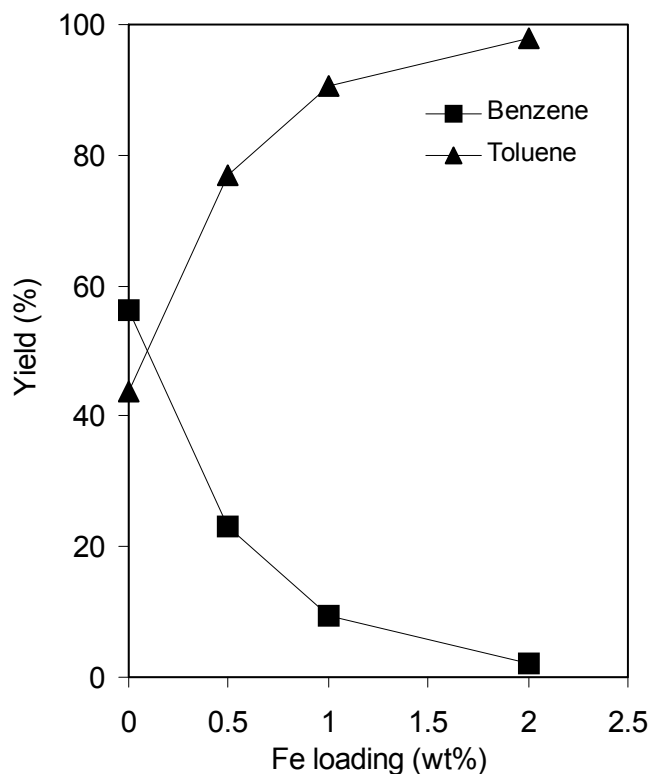


Figure 7.10 Yield of products from the reaction of benzyl alcohol over Ni-Fe bimetallic catalysts as a function of Fe loading. Reaction conditions: Temp. = 250°C, W/F = 0.1 h, H₂/Feed ratio = 25, pressure = 1atm.

The most important similarity was the enhancement of hydrogenolysis and reduction in decarbonylation activity as the Fe/Ni ratio increased. Figure 7.10 clearly shows that as the Fe content increases in the bimetallic catalysts the product distribution drastically changes

from almost 60 % benzene on pure Ni to almost 100% toluene on the 5wt.%Ni-2wt.%Fe/SiO₂ catalyst.

7.8 Adsorption of furfural on Ni(111) and NiFe(111) surfaces (calculation results from Wei An)

Density Functional Theory (DFT) calculations have been made to investigate geometries and relative stabilities of the possible furfural species adsorbed on the surface of pure Ni(111) and a bimetallic NiFe(111) alloy. These calculations have helped us to interpret the changes observed in product selectivities from monometallic Ni to Ni-Fe bimetallic catalysts and to elucidate possible reaction pathways.

First, the optimized structures of furfural in the gas phase and adsorbed on the Ni(111) and NiFe(111) surfaces in an upright and planar configuration are illustrated in Figures 7.11 and 7.12 respectively. The corresponding adsorption energies (E_{ads}) and bond lengths of a planar configuration are summarized in Table 7.3. It can be seen that under the conditions investigated (i.e., low furfural coverage), an upright configuration on both Ni(111) and NiFe(111) surfaces in which only the carbonyl

O sitting on the metal surface is less favored compared to a planar adsorption configuration, indicates by their adsorption energies are relatively lower than that from a planar adsorption configuration (i.e. -8.9 vs. -15.6 kcal/mol on Ni(111) for upright and planar configurations, respectively).

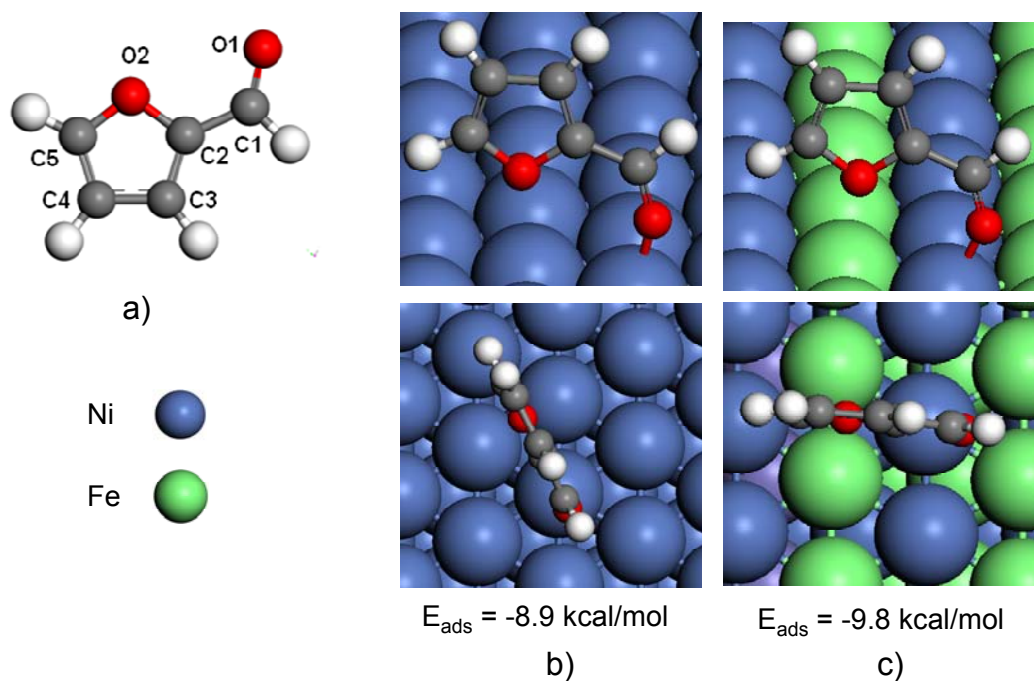


Figure 7.11 Optimized furfural structures of a) gas-phase b) adsorbed on Ni (111) and c) adsorbed NiFe(111) surfaces with a upright configuration

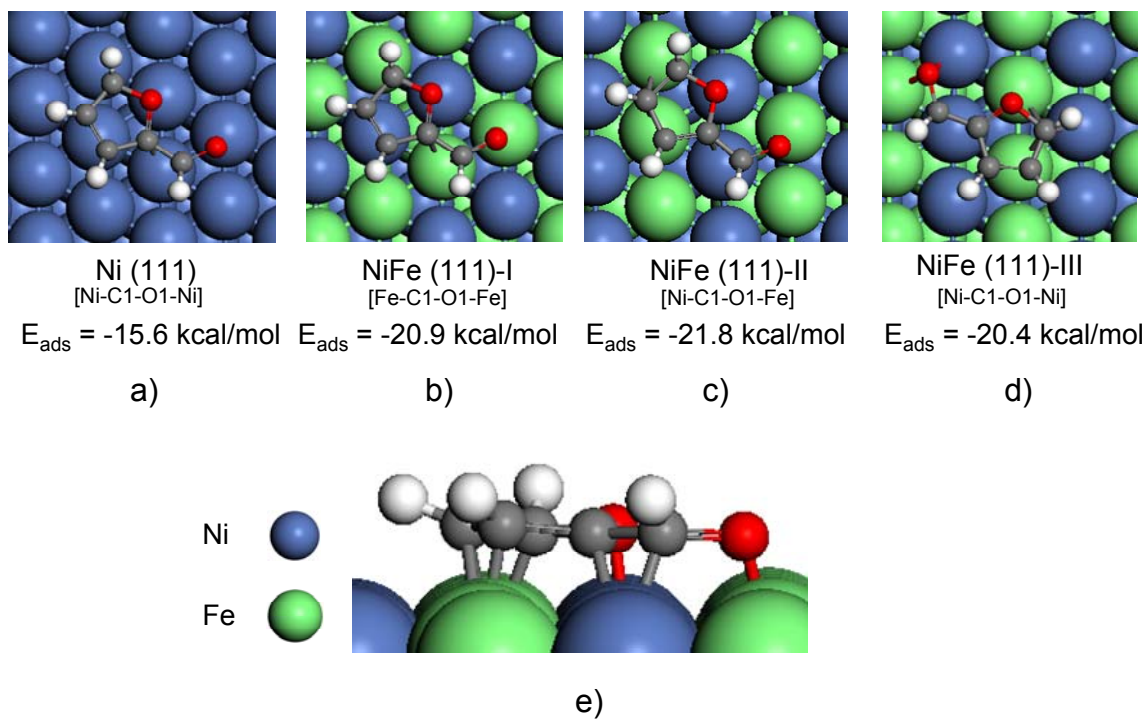


Figure 7.12 Optimized structures of furfural adsorbed on a) Ni (111) surface and NiFe(111) surface b), c), d), and side view e) with a planar configuration

The optimized geometries of planar configuration show that the carbonyl group (C=O) adsorbed on a bridge site and the furanyl ring plane sitting parallel to the surface across two 3-fold hollow sites on.

Table 7.3 Comparison of bond lengths of furfural in gas-phase and adsorbed on Ni (111) and NiFe (111) surfaces. See Figure 1 (a)-(e) for adsorption configurations and (f) for the assignment of C, O, and H atoms. Adsorption energies (E_{ads}) also included.

Bond length d(Å)	Gas-phase	Ni (111)	NiFe(111)-I	NiFe(111)-II	NiFe(111)-III
C1-H1	1.120	1.103	1.101	1.100	1.102
C1-O1	1.229	1.319	1.340	1.347	1.349
C1-C2	1.448	1.439	1.425	1.440	1.446
C2-C3	1.382	1.440	1.438	1.444	1.448
C3-C4	1.419	1.429	1.448	1.443	1.420
C4-C5	1.373	1.450	1.455	1.449	1.452
C5-O2	1.359	1.465	1.456	1.459	1.476
C2-O2	1.378	1.408	1.389	1.403	1.428
E_{ads} (kcal/mol)	0.00	-15.6	-20.9	-21.8	-20.4

As shown in Table 7.3 for more stable planar configurations, the bond lengths for the C-C bonds in the furanyl ring increase on both surfaces, suggesting a slight enlargement of the ring, resulting from the interaction with the surface. In addition, a more significant increase in bond length upon adsorption is observed for the C-O bond of the carbonyl group. It is well known that aldehydes on Group VIII metals adsorb in an η^2 -(C,O) configuration with both C and O atoms linked to the metal surface [17]. Therefore, an increased C-O bond length is expected on the adsorbed furfural species on Ni. On the other hand, of greater interest is the small but consistent increase in C-O bond length observed on the Ni-Fe bimetallic surfaces compared to the pure Ni surface. This difference not only shows that the presence of Fe does not inhibit the formation of the η^2 -(C,O) configuration, but rather it enhances the interaction with the carbonyl group. We recently described an opposite behavior working with the Pd-Cu bimetallic system in chapter 5. In that case, experimental and theoretical data gave evidence to the inhibition of the formation of η^2 -(C,O) when Cu was added to Pd. Addition of Cu generates a strong repulsion to the C atom that favors the formation

of η^1 -(O) over the η^2 -(C,O) species. Previously we had also shown in chapter 4 that a similar repulsion occurs between the monometallic Cu(111) surface and the furanyl ring, due to the overlap of the 3d band of the surface Cu atoms and the aromatic furan ring. As a result, the adsorption of furfural on Cu(111) is weak and can only occur in the η^1 (O)-aldehyde configuration, via the carbonyl O atom

This is not the case with the addition of Fe to Ni, which causes a significant increase in the resulting furfural adsorption energy (i.e. 15.6 kcal/mol on Ni to 20.4-21.8 kcal/mol on NiFe). Some variations in energy are observed depending on the position of the molecule on the NiFe(111) surface. Adsorption with the C atom on top of Ni and the O atom on Fe showed the highest energy (NiFe(111)-II) indicating a strong interaction between the carbonyl O atom and Fe on the surface. This result is consistent with those of acrolein adsorption on Pt and PtFe surfaces [15]. It was concluded that acrolein adsorbs in a parallel configuration on Pt(111) surface with both double bonds interacting with the surface. When Fe atoms are present in the surface, adsorption geometries including O-Fe interactions become much more stable.

Figure 7.13 shows calculated projected-DOS for C1-O1 in the carbonyl group of the adsorbate and two metal atoms of the metal bridge site on which they are bound. For comparison with these electronic structures, the discrete (C1-O1)-2p states for gas-phase furfural and the PDOS for the clean metal surfaces are included in Figures 13 (f) and (e), respectively. In particular, it is observed that the π^* -states of carbonyl C1-O1, which are unoccupied in the gas-phase furfural and centered near 3 eV above the Fermi level, are downshifted below the Fermi level and significantly broadened in the adsorbed state. This shift reflects the electron-backdonation from the metal 3d-states to the anti-bonding π^* -states of the carbonyl, which is in line with the observed increases in C1-O1 bond length, as reported in Table 7.3. It is interesting to note the slight differences in the position of this peak below the Fermi level for the various adsorbate/metal species. In particular, for Ni and NiFe in the configuration I, it appears around 3.0 eV below the Fermi level, but it shifts to 3.3 and 3.7 eV for configurations II and III, respectively. These results indicate that certain configurations on the bimetallic surface may result in a greater extent of back-donation, which may further weaken the C-O bond.

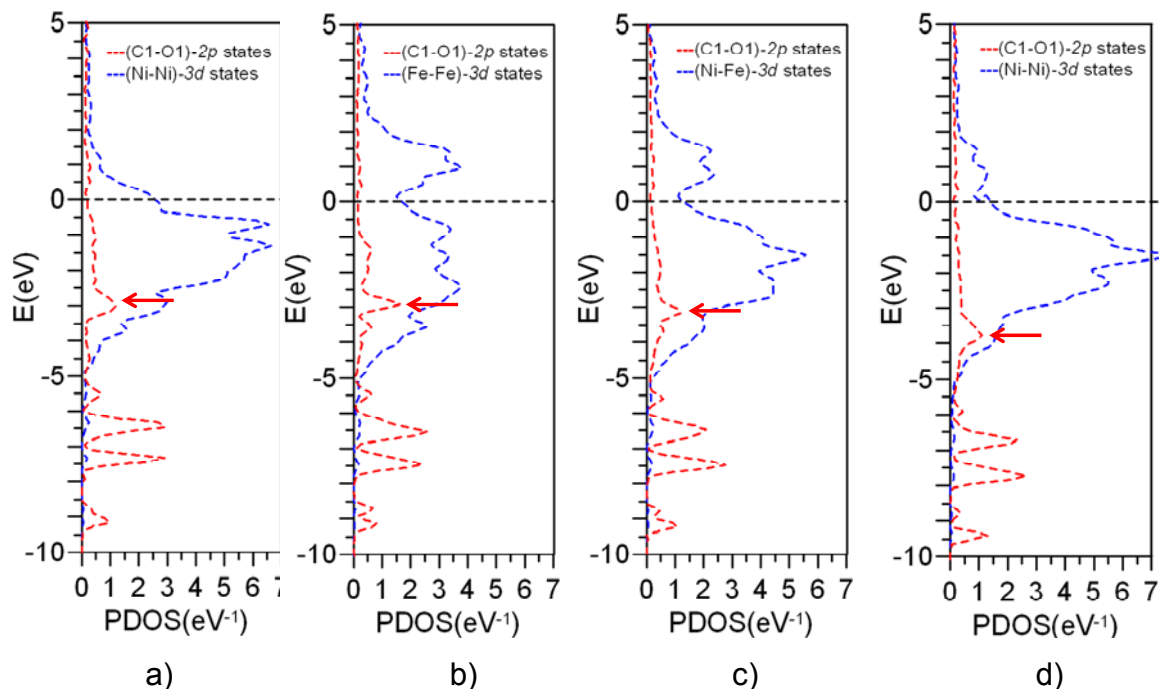


Figure 7.13 Calculated PDOS for furfural adsorbed on Ni(111) and NiFe(111) surface, corresponding to the adsorption configuration in Figure 7.12 (a)-(d), respectively. PDOS for clean surface (e) and gas-phase furfural (f) also included for comparison.

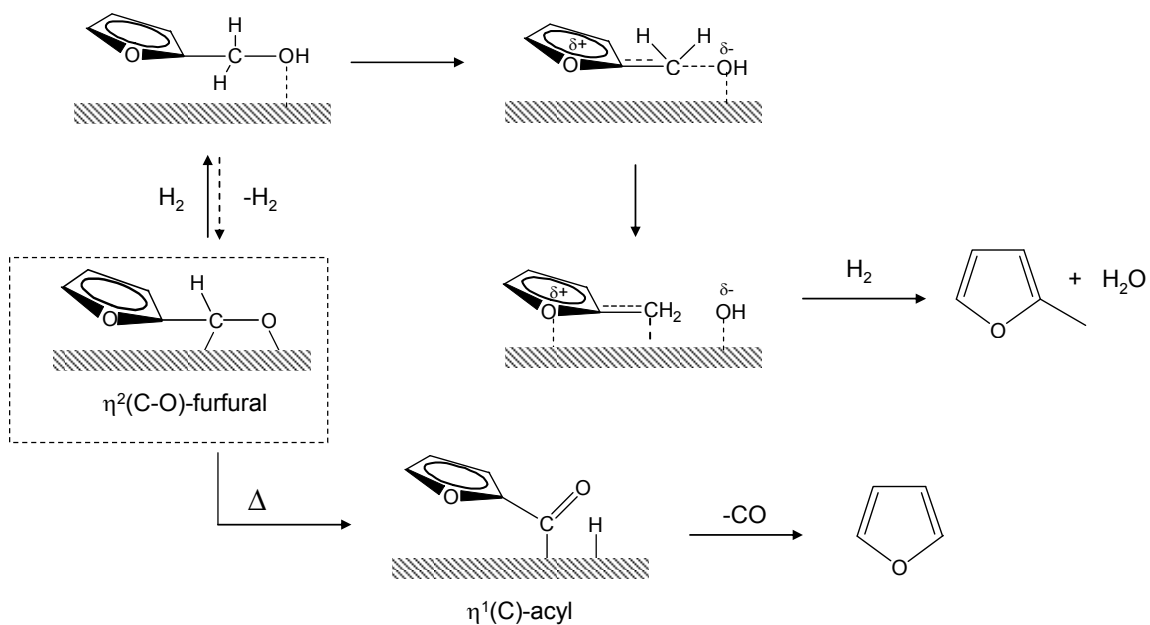
7.9 Discussion

The proposed reaction pathways for furfural conversion are summarized in scheme 1. Furfuryl alcohol and furan are primary products typically observed over Ni-based catalysts [16], and they can further convert to 2-methylfuran and ring-opening C₄ products, respectively. We have shown here that this product distribution can vary

significantly with reaction temperature and the presence of Fe in the bimetallic catalysts.

Our results show that on monometallic Ni catalyst, decarbonylation is favored over hydrogenation, particularly at high reaction temperatures. A behavior that is similar to that of Pd catalysts. This behavior can be explained in terms of the stability of the surface species at different temperatures. Spectroscopic results and DFT calculations show that, on group VIII metals, aldehydes tend to adsorb with the carbonyl group parallel to the surface (η^2 (C,O)-aldehyde) [17-19]. As summarized in scheme 2, this configuration favors the hydrogenation of the carbonyl group, yielding furfuryl alcohol, as experimentally observed at low temperature. However, at high temperature η^2 (C,O)-furfural tends to decompose into a more stable acyl species, in which the C atom of the carbonyl remains strongly attached to the surface. This acyl species may in fact be a precursor for the decarbonylation reaction, yielding furan and CO. As shown in Figure 7.5, the selectivity to decarbonylation significantly increases as a function of temperature, which is consistent with an activated conversion of η^2 (C,O)-furfural into the acyl species that increases

decarbonylation while reducing hydrogenation. This observation is in excellent agreement with the HREELS experiments of acetaldehyde adsorbed on clean Pt(111) [20] which shows that, at low temperatures, an $\eta^2(\text{C},\text{O})$ surface species was formed, but it was readily decomposed above 330K, producing an acetyl intermediate that was stable up to 440K.



Scheme 2 Possible species on the surface during conversion of furfural

In addition to the differences in interaction with the carbonyl group itself, different metals have a different extent of interaction with the furanyl ring. For example, while Cu exerts a repulsion on the ring [21], Group VIII metals tend to interact strongly with aromatic [22] and furanyl rings [23], as well as C=C double bonds [24]. In particular, on Ni surfaces the furanyl ring/metal interaction is so strong that C-O bond in the ring weakens and leads to a significant extent of ring opening (i.e. C2-O2 hydrogenolysis), a reaction that is also favored as temperature increases.

The selectivity to 2-methylfuran is an interesting case. Since, as shown above the C1-O1 hydrogenolysis occurs mainly after furfural has been hydrogenated to furfuryl alcohol and this product is not favored on pure Ni, particularly at the high temperatures required for C-O hydrogenolysis, very small amounts of 2-methylfuran are produced on monometallic Ni.

This situation is drastically altered when Fe is added to the Ni-based catalysts. First of all, decarbonylation is greatly suppressed on the bimetallic catalysts, which can be again explained in terms of the stability of the surface species. In this case, the DFT

calculations suggest that the oxophilic nature of Fe makes the di-bonded $\eta^2(\text{C},\text{O})$ -furfural more stable than on the pure Ni surface. The longer C1-O1 bond length of the adsorbed $\eta^2(\text{C},\text{O})$ -furfuryl alcohol indicates that the overall stronger interaction of the C=O group with the Ni-Fe alloy surface results in the weakening of the C1-O1 bond. As a result, it is reasonable to speculate that the formation of acyl intermediate would require a higher energy barrier, which explains the drastic reduction in the rate of decarbonylation observed on the bimetallic catalysts (see scheme 2).

The enhanced yield of C1-O1 hydrogenolysis products over Ni-Fe bimetallic catalysts from furfuryl alcohol and benzyl alcohol further support this concept. On the monometallic Ni catalysts, furan and benzene are the main products resulting from decarbonylation of furfuryl alcohol and benzyl alcohol, respectively. These products greatly decrease on the bimetallic catalysts, which mainly yield C1-O1 hydrogenolysis products due to the stabilization of the $\eta^2(\text{C},\text{O})$ intermediate compared to the acyl intermediate.

7.10 Conclusion

The conversion of furfural on pure Ni/SiO₂ catalysts yields primarily decarbonylation products due to the favorable formation of acyl species, which can readily decompose into furan and CO at high temperature. In addition, furan can further react to ring-opening products due to the strong interaction of the furan ring with Ni surfaces. In contrast, furfuryl alcohol is produced in significant low amounts, which in turn results in low formation of 2-methylfuran.

By adding Fe to the catalysts, Ni-Fe alloys are formed, as evidenced by TPR and XRD. The product selectivity is drastically shifted to 2-methylfuran while decarbonylation products and their derivatives are suppressed. This reduction in decarbonylation can be attributed to an increase of the stability of $\eta^2(\text{C},\text{O})$ -surface species. The increase in the interaction of the carbonyl O with surfaces through Fe-O interaction hinders the formation of acyl species which is responsible for decarbonylation. In addition, the C-O hydrogenolysis of the adsorbed furfuryl alcohol is improved by this interaction.

References

- [1] L. Wang, D. Li, M. Koike, S. Koso, Y. Nakagawa, Y. Xu, K. Tomishige, *Appl. Catal. A:Gen.* 392 (2011) 248.
- [2] T. Ishihara, K. Eguchi, H. Arai, *Appl. Catal.* 30 (1987) 225.
- [3] Y. Colombo, F. Gazzarini, G. Lanzavecchia, *Mater. Sci. Eng.* 2 (1967) 125.
- [4] J. Szekely, C.I. Lin, H.Y. Sohn, *Chem. Eng. Sci.* 28 (1973) 1975
- [5] M.A. Ermakova, D.Y. Ermakov, *Catal. Today* 77 (2002) 225.
- [6] B. Mile, D. Stirling, M.A. Zammitta, A. Lovell, and M. Webb, *J. Mol. Catal.* 62 (1990) 179.
- [7] H. Jung, W.J. Thomson, *J. Catal.* 128 (1991) 218.
- [8] T. Ishihara, K. Eguchi, H. Arai, *Appl. Catal.* 30 (1987) 225.
- [9] A.L. Kustov, A.M. Frey, K.E. Larsen, T. Johannessen, J.K. Norskov, C.H. Christensen, *Appl. Catal. A: General* 320, 98 (2007).
- [10] E.E. Unmuth, L.H. Schwartz, J.B. Butt, *J. Catal.* 61 (1980) 242.
- [11] Z. Xinghua, W. Tiejun, M. Longlong, W. Chuangzhi, *Fuel* 89 (2010) 2697.
- [12] R.D. Srivastava, A. K. Guha, *J. Catal.* 91 (1985) 254.
- [13] M.K. Bradley, J. Robinson, D.P. Woodruff, *Surf. Sci.* 604 (2010) 920.
- [14] C. J. Kliewer, C. Aliaga, M. Bieri, W. Huang, C-K. Tsung, J. B. Wood, K. Komvopoulos, and G. A. Somorjai, *J. Am. Chem. Soc.*, 132 (2010) 13088.

-
- [15] R. Hirschl, F. Delbecq, P. Sautet, J. Hafner, J. Catal. 217 (2003) 354.
- [16] R.M. Lukes, C.L. Wilson, J. Am. Chem. Soc. 73 (1951) 4790.
- [17] M. Mavrikakis, M. A. Barteau, J. Mol. Catal. A: Chem. 131 (1998) 135.
- [18] R. Shekhar, R.V. Plank, J. M. Vohs, M. A. Barteau, J. Phys. Chem B 101 (1997) 7939.
- [19] J. L. Davis, M. A. Barteau, J. Am. Chem. Soc. 111 (1989) 1782.
- [20] M.A. Henderson, Y. Zhou, J.M. White, J. Amer. Chem. Soc. 111(1989) 1185.
- [21] S. Sitthisa, T. Sooknoi, Y. Ma, P.B. Balbuena, D.E. Resasco, J. Catal. 277 (2011) 1.
- [22] C. Morin, D. Simon, and P. Sautet, J. Phys. Chem. B, 108 (2004) 12084.
- [23] S. Sitthisa T. Pham, T. Prasomsri, T. Sooknoi, R.G. Mallinson, D.E. Resasco, J. Catal. 280 (2011) 17.
- [24] F. Delbecq and P. Sautet, J. Catal. 211 (2002) 398.

CHAPTER 8

Conversion of Catechol on Bimetallic Ni-Fe Catalysts

8.1 Introduction

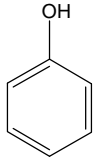
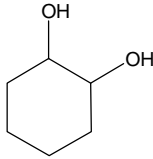
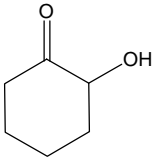
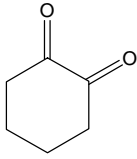
Phenolic compounds represent a significant fraction of the biomass pyrolysis bio-oil [1,2,3] and remain a challenge for upgrading. While building up the carbon chain is necessary for small oxygenates conversion, most phenolics are already in the gasoline range, but they require a deoxygenation process that should preserve the carbon number within the range of gasoline. High temperature (250–400°C) and high pressure (3–5 MPa) hydrotreating of bio-oil over sulfided CoMo or NiMo catalysts can effectively reduce the oxygen content of phenolics in the bio-oil [4]. However, this type of processing results in a significant loss of liquid yield, requires high hydrogen consumption, and produces a sulfur containing stream. Increasing attention has been paid to unsulfided metal catalysts such as Pt, Pd, or Ni [5], which can be used under milder conditions. However, catalytic reactions involving aromatic C-O bond cleavage

of phenolics occur with low selectivities, typical product mixtures include saturated cyclic hydrocarbons and cycloalkanols from hydrogenation of aromatic rings. This aromatic saturation wastes hydrogen and renders the reaction less useful for aromatic feedstocks [6,7]. In this regard, bimetallic alloy catalysts may be interesting systems because the typically strong interaction of aromatic rings with Group VIII metals can be significantly lowered. For example, we have recently shown in chapter 6 that while furfuryl alcohol preferentially yields tetrahydrofurfuryl alcohol via furanyl ring hydrogenation on pure Pd catalysts, the selectivity shifts to the C-O bond hydrogenolysis to 2-methylfuran when Fe is alloyed with Pd due to a weakening of the interaction of the aromatic ring with the surface. Alternatively, in chapter 7, we have shown that Ni-Fe catalysts have a much higher selectivity towards C-O hydrogenolysis of furfural and benzyl alcohol than Ni, which preferentially catalyzes decarbonylation. In this chapter, we have compared the behavior of Ni-Fe with that of Ni for the hydrodeoxygenation of catechol to phenol and we also exhibited the inside mechanism for this reaction on Ni-Fe catalyst.

8.2 Conversion of catechol over Ni/SiO₂ and Ni-Fe/SiO₂ catalysts

The initial tests of catalytic reactions of catechol with H₂ were carried over Ni and Ni-Fe bimetallic catalysts. The catalysts were well characterized by several techniques and the results are shown in chapter 7. The detailed XRD and TPR characterizations clearly indicate the formation of Ni-Fe alloy.

Table 8.1 Conversion and product distribution for the reaction of catechol over Ni/SiO₂ and Ni-Fe/SiO₂ catalysts

Catalysts	Conv. (%)	Selectivity (%)			
					
Ni/SiO ₂	39.0	43.2	26.8	22.4	7.6
Ni/SiO ₂	13.7*	46.8	23.8	18.1	10.6
Ni-Fe/SiO ₂	9.1	100	-	-	-

Reaction condition: Temp = 210°C, H₂ flow rate = 60 ml/min, Feed flow rate = 0.5 ml/h of 10 wt% of catechol in methanol, Catalyst weight = 0.015 g, *Catalyst weight = 0.005 g

As shown in Table 8.1, in the presence of H₂ at 210°C, the pure Ni catalyst exhibits a higher conversion and broader product distribution than the bimetallic Ni-Fe/SiO₂ catalyst, when tested under the same reaction conditions. With monometallic Ni catalyst, not only product from C-O hydrogenolysis of aromatic C-O bonds (phenol) but also a large fraction of products with saturated ring (1,2-cyclohexanediol, 2-hydroxy-cyclohexanone and 1,2-cyclohexadione) were observed. This indicates that monometallic Ni catalyst is not selective for C-O hydrogenolysis of aromatic C-O bonds as a mixture of products from competing hydrogenolysis of aromatic C-O bonds and hydrogenation of aromatic ring were observed. The hydrogenation of aromatic ring wastes hydrogen and renders the reaction less useful for the producing of aromatic feedstocks in which selective hydrogenolysis of the aromatic C-O bonds is required for the generation of fuels and chemical feedstocks from biomass [6,7].

Interestingly, Ni-Fe bimetallic catalyst only yields the product involving aromatic C-O bond cleavage to phenol and no detectable products from hydrogenation of aromatic ring were observed. This indicates that Ni-Fe catalyst is

very selective toward the product from hydrogenolysis aromatic C-O bonds.

8.3 Mechanistic studies of catechol conversion on bimetallic Ni-Fe catalyst

Several mechanisms have been proposed for hydrodeoxygenation (HDO) of phenolic compounds. It is generally assumed that the HDO reaction pathway involves the previous hydrogenation of the ring since the direct hydrogenolysis of the C(sp^2)-O bond, without breaking the aromaticity, appears energetically unfavorable due to this bond is stabilized by delocalization of the out-of-plane O lone pair orbital [8]. However, there is no definite proof that ring saturation is (or is not) directly involved in the HDO pathway, as a required step. To investigate whether partial saturation of the ring is required in the C-O hydrogenolysis reaction, we have conducted isotopic labeling experiments, a technique that has been used for a long time to investigate mechanistic aspects of hydrogenation reactions [9]. The technique consists in exposing the reactant, catechol, to the catalyst bed under a gaseous stream of D₂ in the vapor

phase. The product is collected by condensation after the reactor outlet and injected to a mass spectrometer.

Catechol was co-fed with D_2 instead of H_2 over the monometallic Ni and bimetallic Ni-Fe catalysts at $210^\circ C$. The parent ions in the range of values of m/z from 94 to 110 and 110 to 116 were used to determine the composition of the isotopic catechol and phenol, respectively. As shown in Figure 8.1a, the most abundant mass of catechol after the reaction with D_2 is $m/z = 110$ (d(0)-catechol) indicating a very low extent of H/D exchange in the catechol molecule over Ni-Fe catalyst. In contrast, the Ni catalysts exhibited a high degree of H/D exchange in the catechol (Figure 8.1b). This result indicates that pure Ni catalysts may not be suitable for investigating the reaction mechanism due to a very high extent of H/D exchange in the catechol molecule producing deuterated reactant.

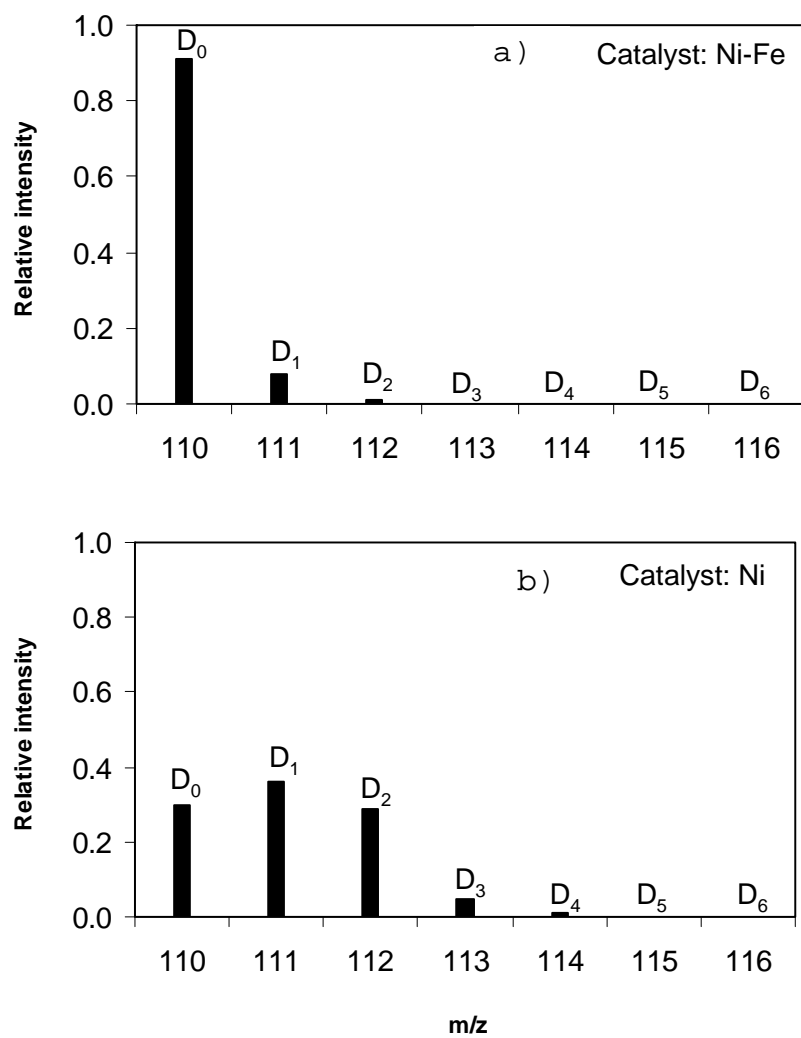
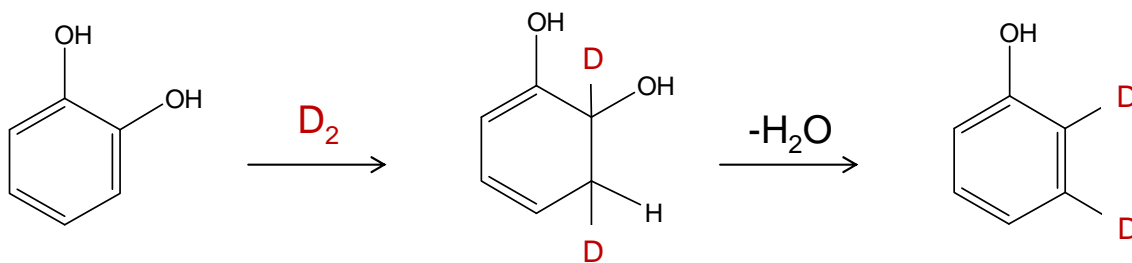


Figure 8.1 The m/z of catechol after the exchange on a) Ni-Fe and b) Ni catalysts

a. Partial hydrodeoxygenation of the phenyl ring followed by elimination of H₂O



b. Direct hydrogenolysis of the C(sp²)-O bond

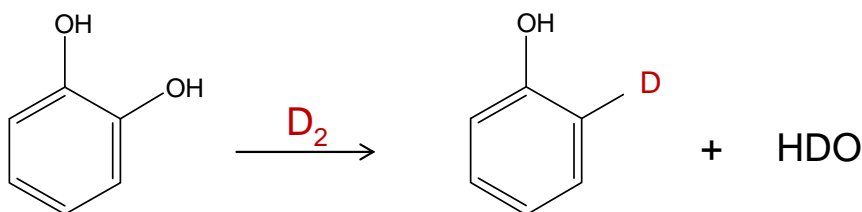
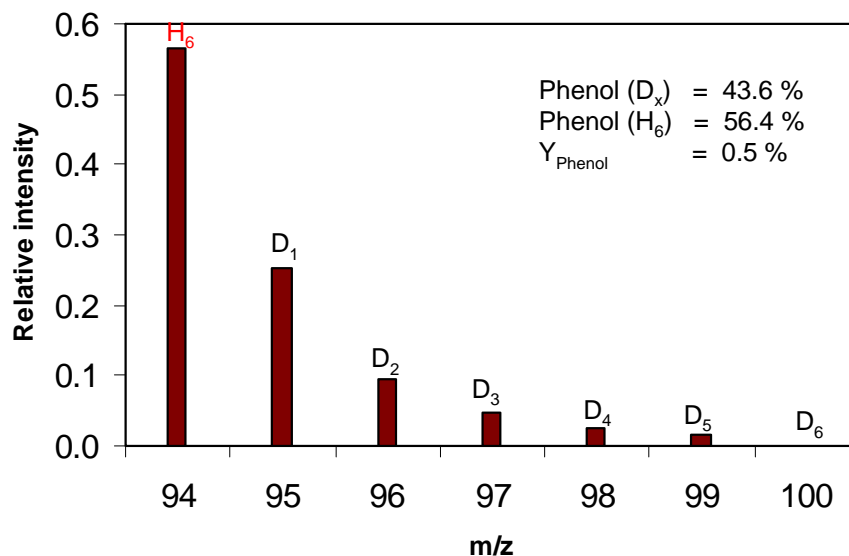


Figure 8.2 Proposed reaction pathways for conversion of catechol to phenol

Before discussing the observed distribution of D in the phenol product from the feed of catechol with D₂ it is important to ponder what distribution one should expect on the basis of the possible reactions mechanisms. For instance, if a partial saturation of the ring is a prerequisite for the C-O bond cleavage, then the phenol product should contain at least 2 deuterium atoms, i.e. D(2)-phenol (see Figures 8.2a). Contrarily, if the C-O bond breaks without a prior deuteration of the ring (see

Figure 8.2b), the replacement of the OH group by a D will leave the phenol product with only one deuterium (D1-phenol).



Reaction condition: Temp.= 210°C, Feed flow rate = 0.5 ml/h of 10 wt.% of catechol in methanol, Catalyst weight = 0.020g, P_{D₂} = 25.33 kPa

Figure 8.3 The m/z of phenol product after the reaction of catechol over Ni-Fe/SiO₂ catalyst.

Interestingly, none of these reaction pathways would predict a phenol product without deuterium in the molecule. However, as shown in Figure 8.3, a remarkable result is observed with the most abundant mass of phenol is m/z=94, which corresponds to undeuterated, D(0)-phenol. Unexpectedly, in the presence of D₂ in the gas phase the

product from deuterolysis of catechol to phenol is D(0)-phenol. However, there are some amounts of the D(x)-phenol products were observed which could be derived from the further H/D exchange of D(0)-phenol. To verify this hypothesis, phenol was co-fed with D₂ over the Ni-Fe catalyst at 210°C and the result shows a high degree of H/D exchange in phenol as more than 70% of D(0)-phenol was exchanged with deuterium to D(x)-phenol, x=1-6 (Figure 8.4). However, the results from this work have demonstrated that D(0)-phenol is the most abundant products from the reaction of catechol under deuterium atmosphere.

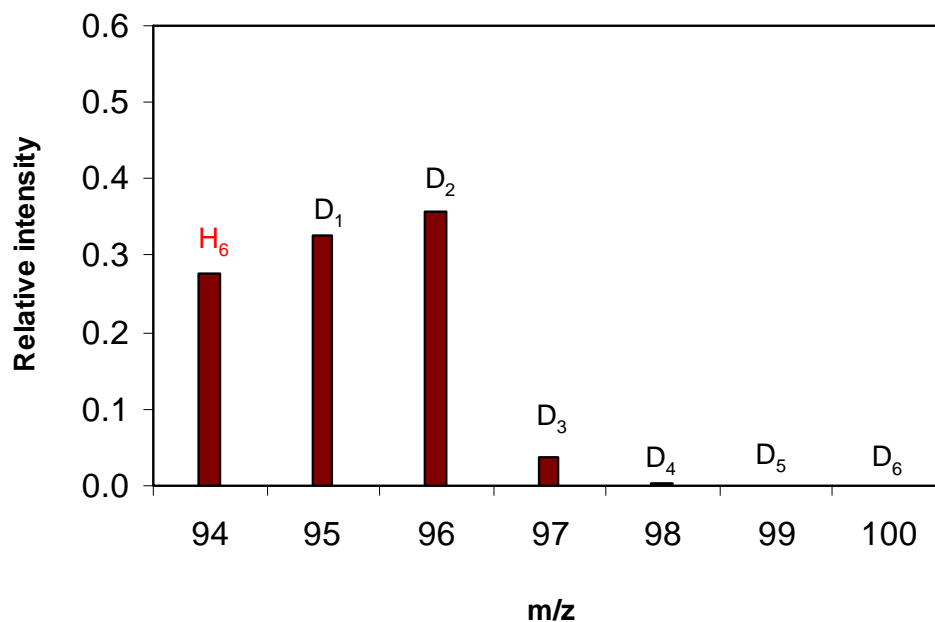


Figure 8.4 The m/z of phenol after the H/D exchange over Ni-Fe/SiO₂ catalyst.

The evidence from isotopic labeling experiments indicates that the new H attached to the phenol ring must be transferred from the OH group of catechol before the cleavage of C-O bond forming phenol. In this case, the OH group of catechol must necessarily be replaced by the H of the same OH group to form phenol since no additional H is being added. A proposed reaction pathway consistent with the observed results is shown in Figure 8.5.

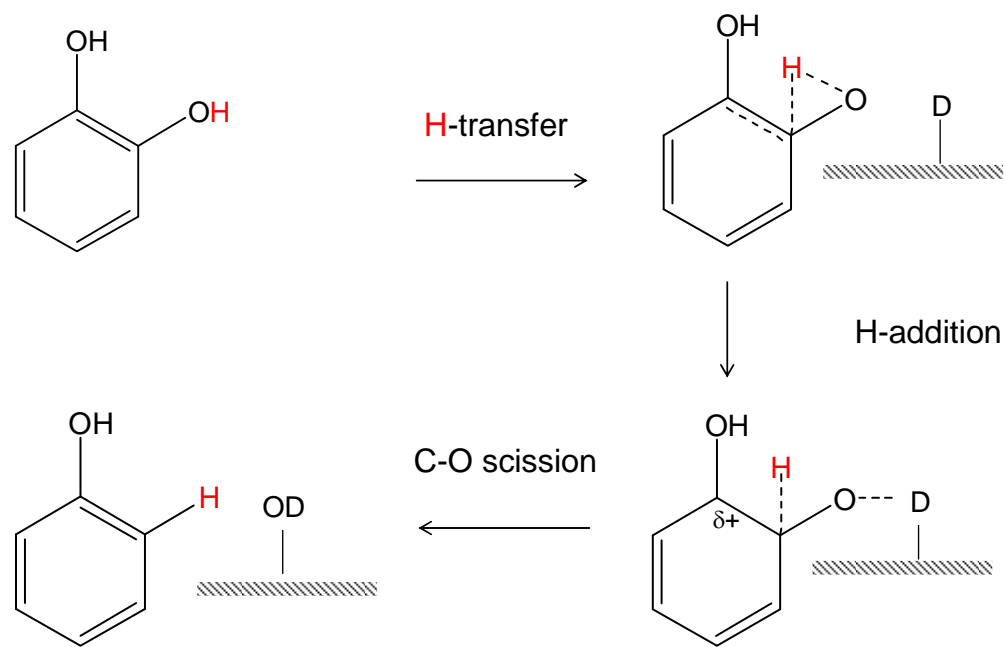


Figure 8.5 Proposed reaction pathways for conversion of catechol to phenol via internal H transfer without incorporation of external H (or D)

The adsorption of hydroxyl group of catechol on Ni-Fe surface appears to occur via donation of a lone pair electron from the oxygen to the metal surface. The initial adsorption in which the transfer of electron to Ni-Fe surface would make the H of hydroxyl group more electrons deficient. As a result, the charge of H at the hydroxyl group becomes more positive before transferring to the adjacent aromatic carbon by the O-H bond cleavage. The cleavage of the O-H bond of alcohols upon their adsorption on transition metal appears to be a general phenomenon, leading to the formation of stable alkoxide intermediates and adsorbed H on metal surfaces [10]. In addition, the intramolecular proton transfer from phenol OH to a carbon of an aromatic ring of phenolic compounds (i.e. 2-phenylphenol) has been previously observed from the photochemical deuterium exchange experiments [11,12,13,14]. In our case, intramolecular H transfer from the OH group to adjacent aromatic carbon proposed is analogous to a general mechanism for electrophilic aromatic substitution. In this case, the electron deficient H atom of hydroxyl group will act as an electrophile. For the first step of the reaction mechanism, the electron-rich aromatic ring of catechol attacks the electrophile H from the hydroxyl group forming

a sigma C-H bond to the adjacent carbon atom of benzene ring. Formation of this bond interrupts the cyclic system of π electron because the carbon that forms a bond to the H becomes sp^3 hybridized and no longer has an available p orbital. As discussed below in the theoretical analysis part, the adjacent carbon atom that acts as a receptor of the H atom from the OH group showed a sp^2 to sp^3 rehybridization which is reflected in the significantly longer C-C lengths (i.e. ~ 1.53 A) compared to the aromatic bond lengths (~ 1.4 A). Now only five carbon atoms of the ring are still sp^2 hybridization. This step leads to the formation of a positively-charged cyclohexadienyl cation, also known as an arenium ion. This carbocation is unstable, owing both to the positive charge on the molecule and to the temporary loss of aromaticity. However, the cyclohexadienyl cation is partially stabilized by resonance, which allows the positive charge to be distributed over three carbon atoms. In addition, the cyclohexadienyl cation is stabilized by the contribution of electron from the adjacent hydroxyl group. While the H atom from the OH group transferred onto the ring, the surface H atom also forms a bond with the O of the OH group. As a result, the C-O bond is broken and two electrons that bonded to this carbon to oxygen become a

part of π system. Now all six carbon atoms become sp^2 hybridization again and benzene derivative with six fully delocalized π electrons is formed.

8.4 Theoretical analysis of the proposed mechanism

(calculation results from wei An)

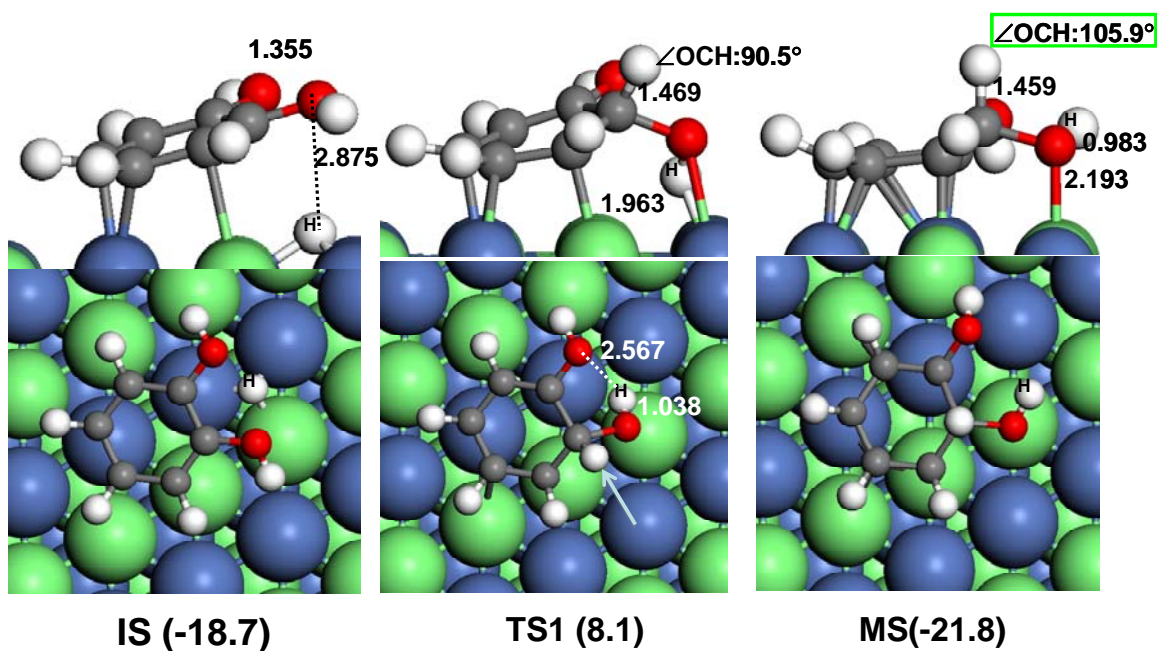


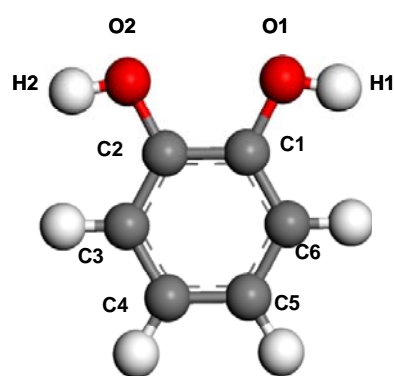
Figure 8.6 Calculated structures along minimum-energy pathway for H-transfer step of catechol on NiFe(111)

To investigate the energetics of the proposed reaction pathway, we conducted DFT calculations with the

Vienna ab initio simulation package (VASP). Specifically, we attempted to calculate the activation energy for the H-transfer step depicted in Figure 8.5 from the OH group onto the aromatic ring. To search for transition states for this process we used the nudged elastic band method. As shown in Figure 8.6, we selected as the initial state (IS) an optimized configuration of the catechol molecule adsorbed next to a H atom on the surface of a NiFe(111) stoichiometric alloy ($E = -18.7$ Kcal/mol). As a metastable state (MS), we used an optimized configuration of the molecule with the H atom from the OH group transferred onto the ring and the surface H atom forming a bond with the resulting O ($E = -21.8$ Kcal/mol). The search for a transition state (TS) resulted in the configuration shown as TS1 ($E = 8.1$ Kcal/mol) in Figure 8.6. The energy of this TS is relatively low and indicates that this reaction pathway is feasible. In this TS, the H from the OH now forms an angle of near 90° with the C-O bond and the distance with the C atom of the ring is close to that of a C-H chemical bond length. Moreover, as shown in Table 8.2, the TS has lost its initial aromaticity. The carbon atom that acts as a receptor of the H atom from the OH group has more of an sp^3 character than sp^2 , which is reflected in the significantly longer C1-C2 and C1-C6 bond

lengths (i.e. ~ 1.53 Å) compared to the aromatic bond lengths (~ 1.4 Å). As discussed before, converting the hybridization of C from sp^2 to sp^3 , i.e. breaking aromaticity, is indeed a required step. However, this step does not necessarily require external hydrogenation, but rather it can occur via an internal H-transfer.

Table 8.2 Bond lengths of catechol species on the surface. Adsorbed initial state (IS), transition state (TS1), and metastable (final) state



bond length (Å)	Gas	on NiFe (111) surface		
		IS	TS1	MS1
C1-O1	1.371	1.355	1.469	1.459
C2-O2	1.383	1.359	1.360	1.402
C1-C2	1.407	1.429	1.533	1.510
C2-C3	1.392	1.394	1.385	1.438
C3-C4	1.399	1.422	1.447	1.455
C4-C5	1.396	1.427	1.434	1.450
C5-C6	1.398	1.429	1.461	1.454
C6-C1	1.394	1.398	1.529	1.503

8.5 Conclusion

Monometallic Ni catalyst is not selective for C-O hydrogenolysis of aromatic C-O bonds as a mixture of products from competing hydrogenolysis of aromatic C-O bonds and hydrogenation of aromatic ring were observed. In contrast, Ni-Fe bimetallic catalyst only yields the product involving aromatic C-O bond cleavage to phenol and

no detectable products from hydrogenation of aromatic ring were observed. This indicates that Ni-Fe catalyst is very selective toward the product from hydrogenolysis aromatic C-O bonds. An isotopic labeling study combined with theoretical analysis of the hydrodeoxygenation of catechol on Ni-Fe catalysts give the evidence in favor of a reaction pathway that eliminates the need of a partial or temporary saturation of the aromatic ring, but involves an internal H transfer from the OH group of the catechol to the aromatic ring.

References

-
- [1] D. Mohan, C.U.P. Pittman Jr., P.H. Steele, *Energy Fuels* 20 (2006) 848.
- [2] G.W. Huber, S. Iborra, A. Corma, *Chem. Rev.* 106 (2006) 4044-4098.
- [3] J. Jae, G.A. Tompsett, Y.C. Lin, T.R. Carlson, J.C. Shen, T.Y. Zhang, B. Yang, C.E. Wyman, W.C. Conner, G.W. Huber, *Energy Environ. Sci.* 3 (2010) 358-365.
- [4] E. Furimsky, *Appl. Catal. A-General* 199 (2000) 147.
- [5] C. Zhao, Y. Kou, A. A. Lemonidou, X. Li and J. A. Lercher, *Angew. Chem. Int. Ed.* 48 (2009) 3987
- [6] J. Zakzeski, P. C. A. Bruijninx, A. L. Jongerius, B. M. Weckhuysen, *Chem. Rev.* 110 (2010) 3552.

-
- [7] A. L. Marshall, P. J. Alaimo, *Chem. Eur. J.* 16 (2010) 4970.
- [8] D. E. Resasco *J. Phys. Chem. Lett.* 2, 2294–2295 (2011)
- [9] R. J. Harpert and C. Kemball *J. Chem. Soc. Faraday Trans.*, 90 (1994) 659
- [10] M. Mavrikakis, M. A. Barteau, *J. Mol. Catal. A: Chem.* 131 (1998) 135.
- [11] M. Lukeman and P. Wan, *Chem. Commun.* (2001) 1004
- [12] M. Lukeman, P. Wan, *J. Am. Chem. Soc.* 124 (2002) 9458
- [13] N. B. Aein, P. Wan, *J. Photochem. Photobiol. A* 208 (2009) 42
- [14] M. K. Nayak and P. Wan, *Photochem. Photobiol. Sci.* 7 (2008) 1544

APPENDIX A

Adsorption and Hydrogenation of Furfural on Cu Surface

Yuguang Ma and Perla B. Balbuena

Department of Chemical Engineering and
Materials Science, Engineering Program, Texas A&M
University, College Station, TX, 77843

A.1 Density functional theory calculations

Spin-polarized periodic DFT calculations were performed using the Vienna *ab initio* simulation package (VASP) [1-5], in which the Kohn-Sham equations are solved by self-consistent algorithms. The valence electrons were described by plane wave basis sets with a cutoff energy of 300 eV and the core electrons were replaced by the projector augmented wave (PAW) pseudo-potentials [6,7] for improving the computational efficiency. The Brillouin zone was sampled with a 4×4×1 Monkhorst-Pack k-point mesh. The exchange-correlation functional was described within the generalized gradient approximation (GGA) proposed by Perdew, Burke and Ernzerhof (PBE) [8]. The Methfessel-Paxon method was employed to determine electron occupancies with a smearing width of 0.2 eV.

Both Cu(111) and Cu(110) slab models were constructed based on a 5×5 unit cell. The Cu(111) slab model consists of three metal layers and seven equivalent vacuum layers (>16 Å); the Cu(110) slab is also composed of three metal layers, with a ~18 Å vacuum gap in the direction perpendicular to the surface. The lattice constant of the face-centered cubic (fcc) Cu from our bulk calculation, 3.626 Å, was in good agreement with the experimental value of 3.610 Å [9]. The two uppermost layers of the slab were allowed to relax to their lowest energy configuration, while the atoms of the bottom layer were fixed to the bulk positions, keeping their optimized lattice constants. The slab model was relaxed until the forces were convergent to 0.01 eV/Å.

Surface adsorption takes place on the topmost layer of the slab. Three adsorption types for furfural molecules, named parallel-ring modes, perpendicular-ring modes, and single-site adsorption modes, were examined. All adsorbate atoms were allowed to relax to their optimized positions. The adsorption energy, E_{ads} , is given by the equation, $E_{ads} = E_{slab/ads} - E_{slab} - E_{gas}$, in which $E_{slab/ads}$ is the total energy of the slab with adsorbates, E_{slab} is the energy of the slab, and E_{gas} is the energy of the

adsorbates in gas phase. For the hydrogenation reactions, the minimum energy paths, transition states (TS) and energy barriers were determined by the nudged elastic band (NEB) method [10,11].

A.2 Adsorption of furfural on Cu(111)

Calculating the adsorption of furfural on Cu(111) is complex because of its numerous plausible adsorption modes, and it could be even more complicated if intermolecular interactions of furfural molecules are taken into account. In order to neglect intermolecular interactions of adsorbed molecules on the Cu(111) surface, we choose a low-coverage surface (1/25 ML) by setting a relatively large unit cell (5×5). The furfural contains two O atoms, one in the carbonyl and one in the aromatic ring. According to our DFT calculations, the distance between these two atoms, which are the possible adsorption points in the furfural molecule, is 2.809 Å (in the gas phase). This distance is comparable to the distance between the centers of two hollow sites or between one top and one hollow site (2.96 Å) on the Cu(111) surface, as shown in Figure A.1.

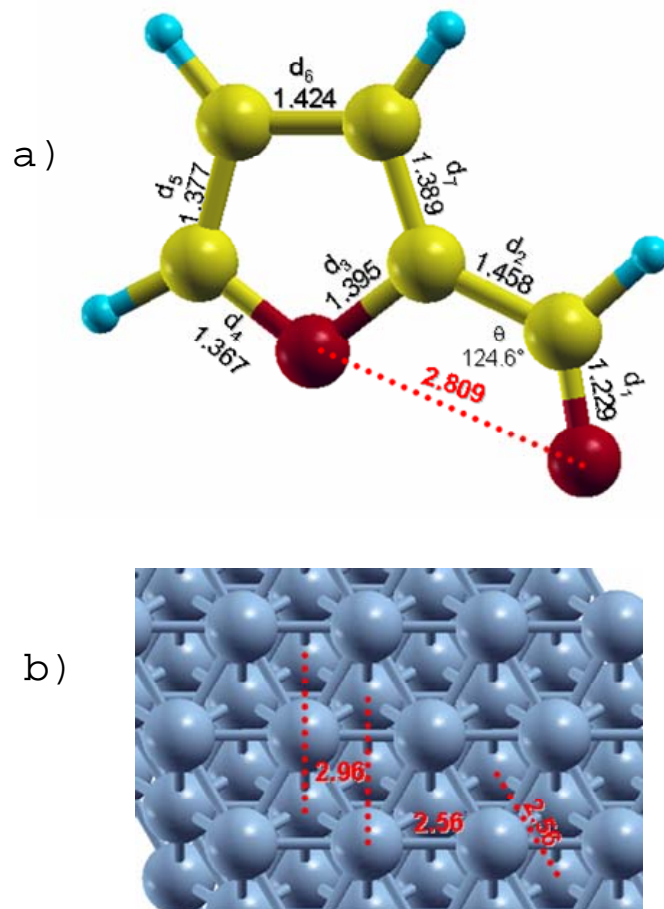


Figure A.1 a) DFT optimized geometry of furfural in gas phase. Red, yellow and light blue spheres represent oxygen, carbon and hydrogen atoms, respectively. b). DFT optimized geometry of Cu(111) slab. Cu atoms are denoted by blueish grey spheres. Bond angles, bond lengths and some important distances (Å) are labeled.

Accordingly, we suppose that the oxygen atoms are located on top and/or hollow sites. Plausible adsorption configurations of furfural are thus constructed and can be classified into three types: (a) parallel-ring adsorption: the furfural molecule is roughly parallel to the surface; (b) carbonyl adsorption: the C=O bond is involved into the interaction with the surface; and (c) perpendicular adsorption: the furfural molecule is approximately perpendicular to the Cu(111) surface. Fourteen initial geometries investigated by our DFT calculations are listed in Figures A.2, A.3 and A.4.

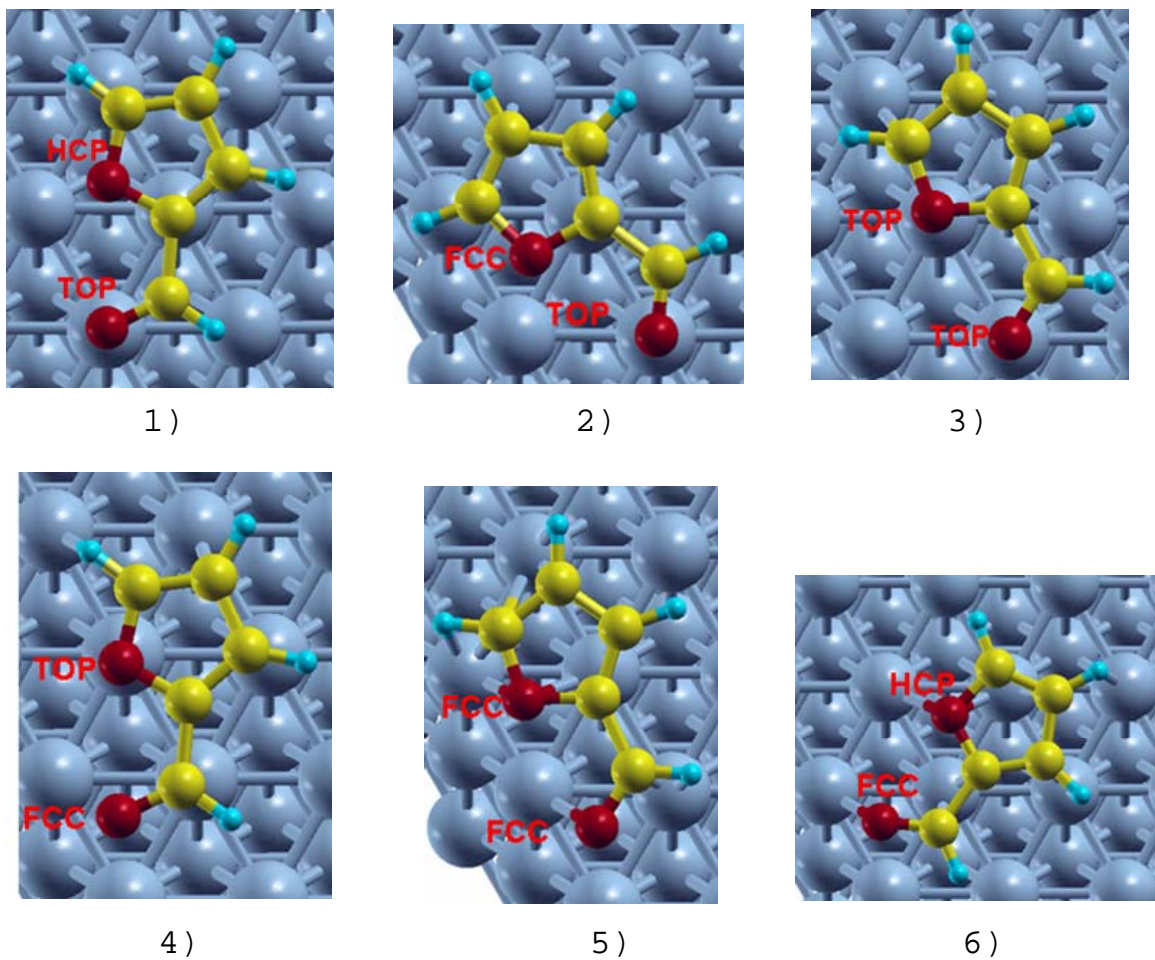


Figure A.2 Plausible adsorption configurations of furfural on Cu(111) in parallel modes.

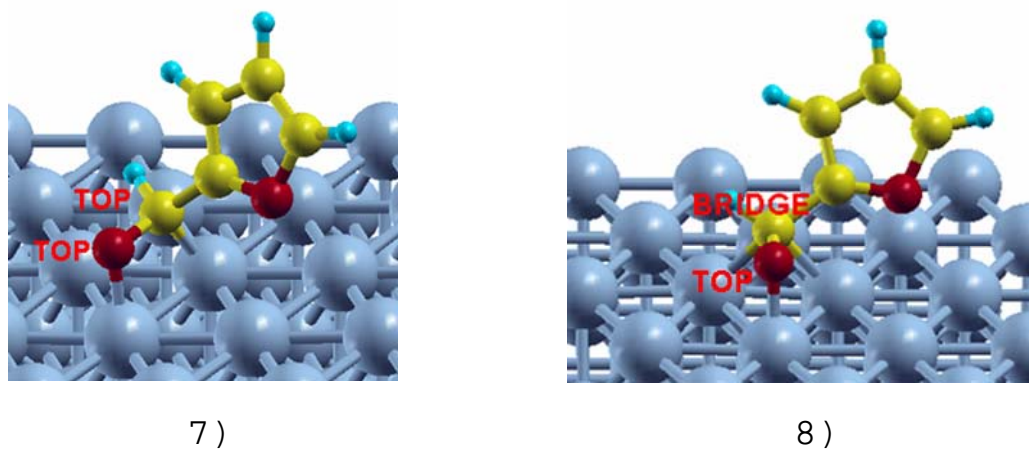
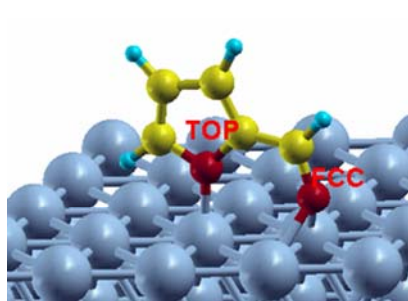
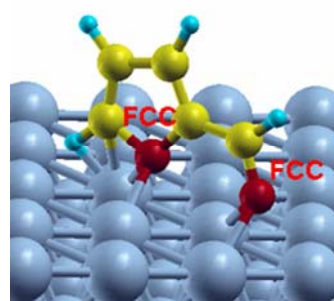


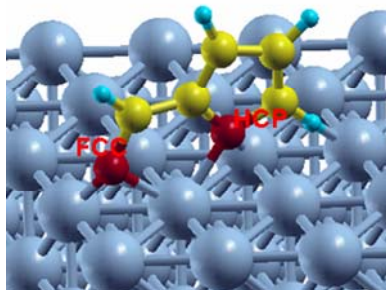
Figure A.3 Plausible adsorption configurations of furfural on Cu(111) in the parallel C=O modes.



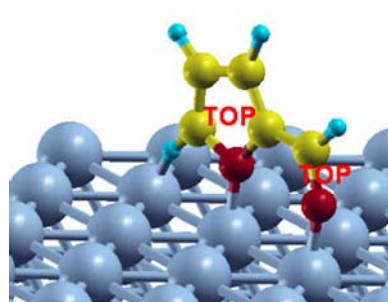
9)



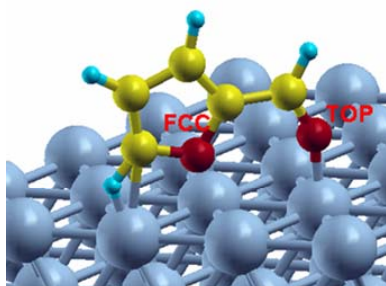
10)



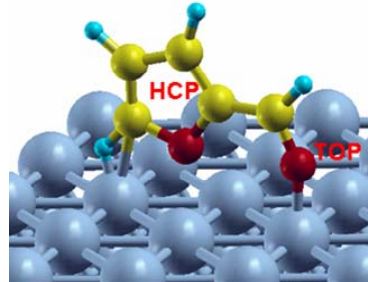
11)



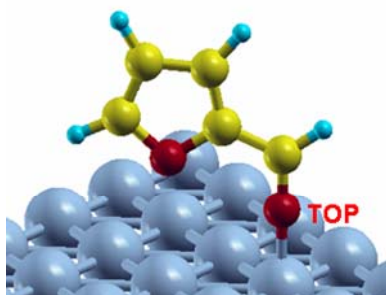
12)



13)



14)



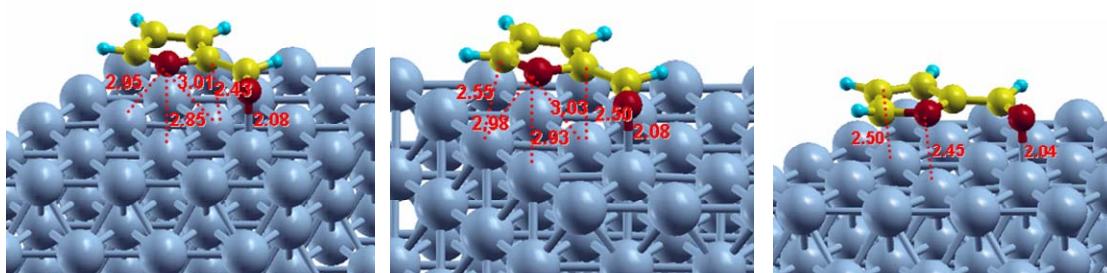
15)

Figure A.4 Plausible adsorption configurations of furfural on Cu(111) in perpendicular modes.

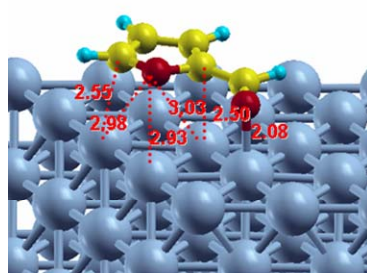
Table A.1 Calculated bond lengths (Å), bond angle (degree) and surface adsorption energy (eV), E_{ads} , for furfural adsorption on Cu(111).

Furfural Geometry	E_{ads}	d_1	d_2	d_3	d_4	d_5	d_6	d_7	θ
gas		1.229	1.458	1.395	1.367	1.377	1.424	1.389	124.6
1	0.36	1.280	1.439	1.397	1.396	1.402	1.416	1.412	125.0
2	0.33	1.280	1.438	1.396	1.382	1.396	1.419	1.409	124.8
3	0.50	1.294	1.432	1.400	1.408	1.413	1.417	1.415	122.9
4	0.06	1.259	1.441	1.389	1.370	1.380	1.417	1.395	126.3
5	0.41	1.288	1.449	1.401	1.377	1.386	1.435	1.407	121.5
6	0.50	1.299	1.438	1.395	1.401	1.409	1.407	1.411	126.9
7	-0.13	1.259	1.433	1.389	1.365	1.383	1.419	1.382	123.0
8	-0.15	1.257	1.433	1.391	1.366	1.383	1.425	1.383	123.7
9	0.06	1.263	1.425	1.394	1.368	1.379	1.422	1.393	124.6
10	0.12	1.253	1.436	1.388	1.363	1.381	1.422	1.394	124.1
11	0.03	1.255	1.433	1.392	1.366	1.375	1.424	1.396	123.9
12	-0.05	1.250	1.427	1.394	1.377	1.374	1.420	1.391	127.8
13	0.03	1.255	1.432	1.390	1.374	1.375	1.422	1.389	126.9
14	0.02	1.251	1.431	1.391	1.369	1.377	1.423	1.389	126.9
15	-0.17	1.251	1.429	1.392	1.370	1.379	1.424	1.389	128.1

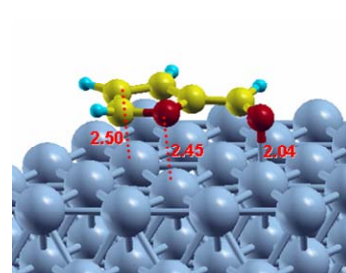
Our calculations show that none of the parallel-ring configurations (see Figure A.5 and structures 1 to 6 in Table A.1) are stable on Cu(111). The adsorption energies range from 1.38 to 11.53 kcal/mol. As shown in Figure A.5. The carbonyl oxygen atom is ~2.0-2.1 Å from the metal surface, indicating a strong interaction between the O and Cu atoms. Nevertheless, these adsorption modes destabilize the aromatic furan ring structure. Compared to the geometry in the gas phase (Figure A.1), the bond lengths d_4 , d_5 , and d_7 are elongated in the adsorption state, while d_6 is slightly shortened (Table A.1). In general, the weakened aromatic bonds raise the total energy of the adsorbed molecule, leading to a positive (endothermic) adsorption energy. Moreover, the bond length of C=O, d_1 , is 0.03-0.07Å longer in the parallel mode, mainly due to the interaction of O and the surface.



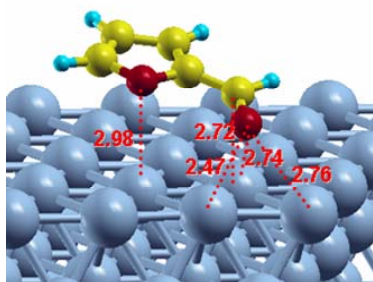
1)



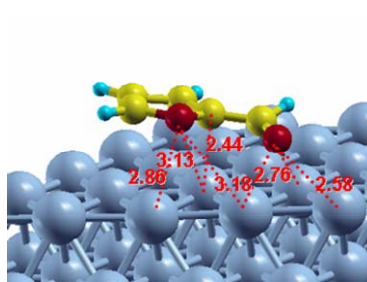
1)



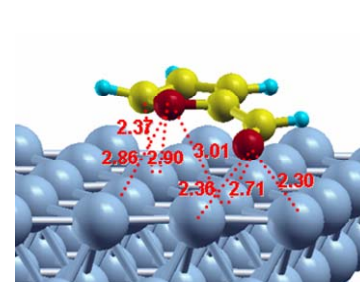
3)



4)



5)



6)

Figure A.5 Optimized geometries for plausible adsorption in parallel modes. The distances shown in the figure are in Å.

Our calculations reveal that the initial carbonyl configurations, in which both the C and O atoms interact with the surface are not stable on Cu(111). It is observed that the carbonyl C atom moves away from the Cu(111) surface after energy optimization. Consequently, the binding strength solely depends on the carbonyl O-Cu interaction. This adsorption mode (structures **7** and **8** in Figure A.6) is determined as the most stable. For the top-top and top-bridge geometries, the calculated adsorption energies are -2.99 to -3.46 kcal/mol, respectively. The top-bridge geometry, **8**, is slightly more stable than the top-top geometry.

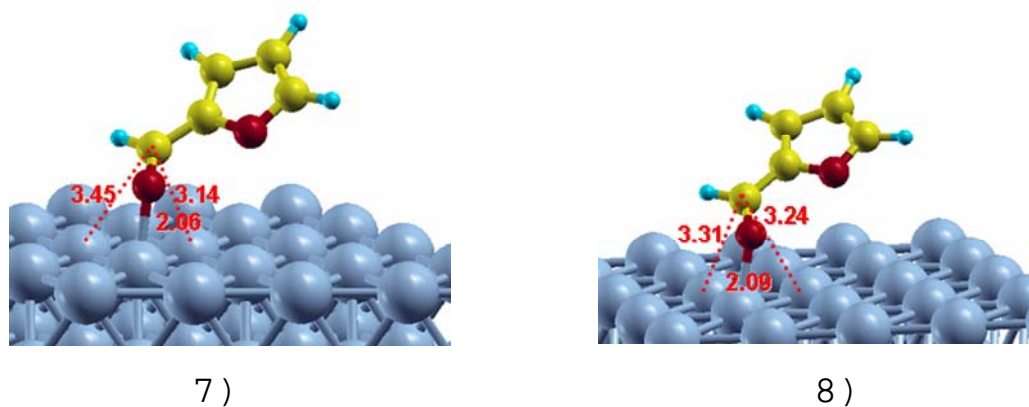
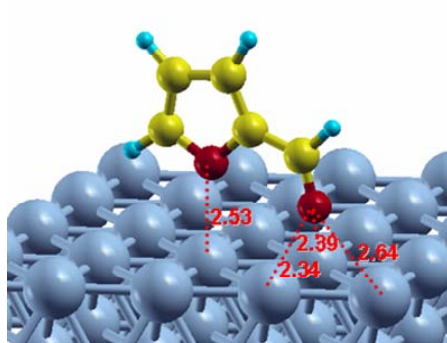


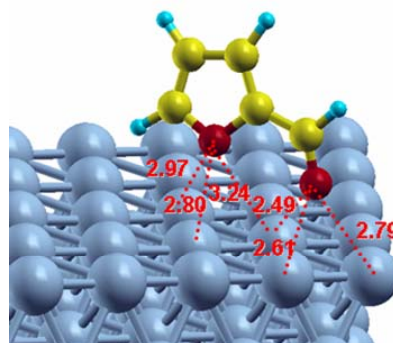
Figure A.6 Optimized geometries for plausible adsorption in the parallel C=O modes. The distances shown in the figure are in Å.

The perpendicular-ring mode (structures **9** to **15** in Table A.1 and Figure A.7) shows stronger surface adsorption than the parallel-ring one: The values of E_{ads} range from -3.92 to 2.77 kcal/mol. Only two configurations, **12** and **15**, possess negative adsorption energy. Two possible points for adsorption in the furfural molecule are the carbonyl oxygen atom and the ring oxygen atom. The optimized geometries show that the carbonyl O is closer to the Cu(111) surface compared to the ring O, suggesting that the interaction between the carbonyl O and the Cu(111) surface is the main contributor to the adsorption. In general, a short carbonyl O-surface distance results in strong surface adsorption. Since the 3d band of the surface Cu atoms partially overlaps the anti-bonding orbital of the aromatic ring, the ring O-Cu surface interaction may reduce the binding strength. This is confirmed by comparing the adsorption energy of two similar configurations (**12** and **15**): Configuration **15** has a stronger binding strength ($E_{ads} = -3.92$ kcal/mol) but a much longer ring O-surface distance (3.08 Å), corresponding to a weaker ring O-surface interaction. Moreover, the carbonyl O-surface distance in the perpendicular configurations is comparable to that in the parallel configurations. The stronger surface adsorption

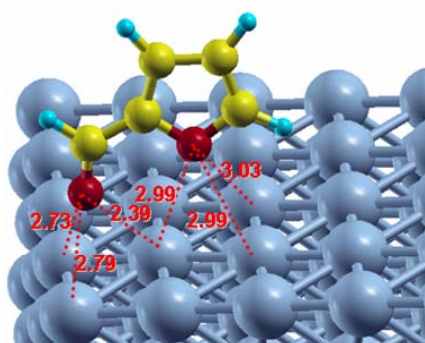
in the perpendicular-ring mode can be attributed to the approximately unchanged structure of the aromatic furan ring.



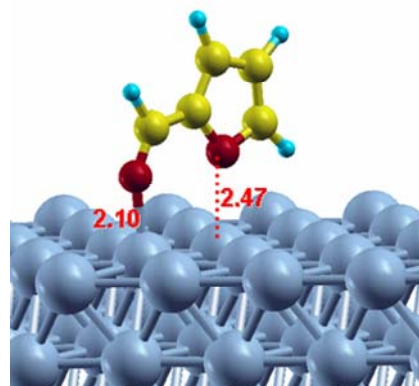
9)



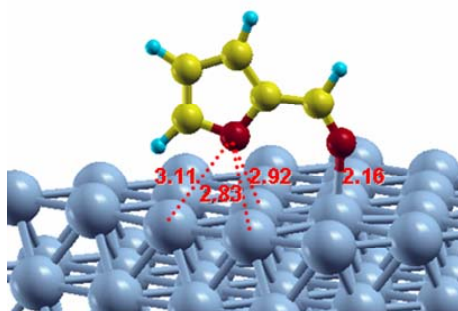
10)



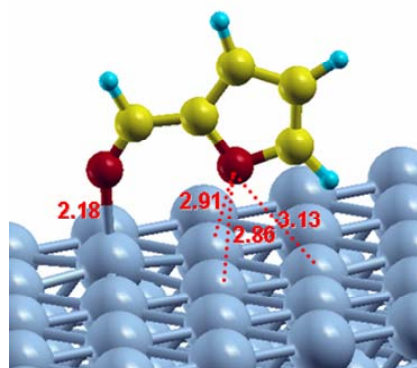
11)



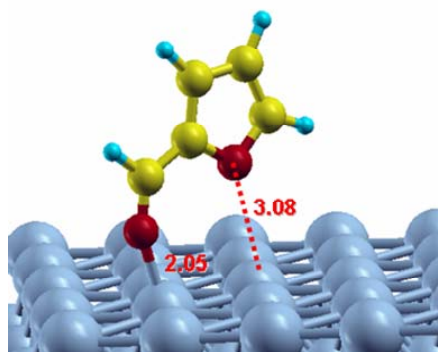
12)



13)



14)



15)

Figure A.7 Optimized geometries for plausible adsorption in the perpendicular modes. The distances shown in the figure are in Å.

A.3 Adsorption of furfural on Cu(110)

As shown in Figure A.8, the Cu(110) surface has higher rugosity and is not as close-packed than Cu(111). This configuration may lessen the repulsion of the furan ring when the carbonyl O approaches the surface. Consequently, more stable binding of furfural molecules is expected on Cu(110) than on Cu(111), on which interaction with the aromatic ring was found unfavorable.

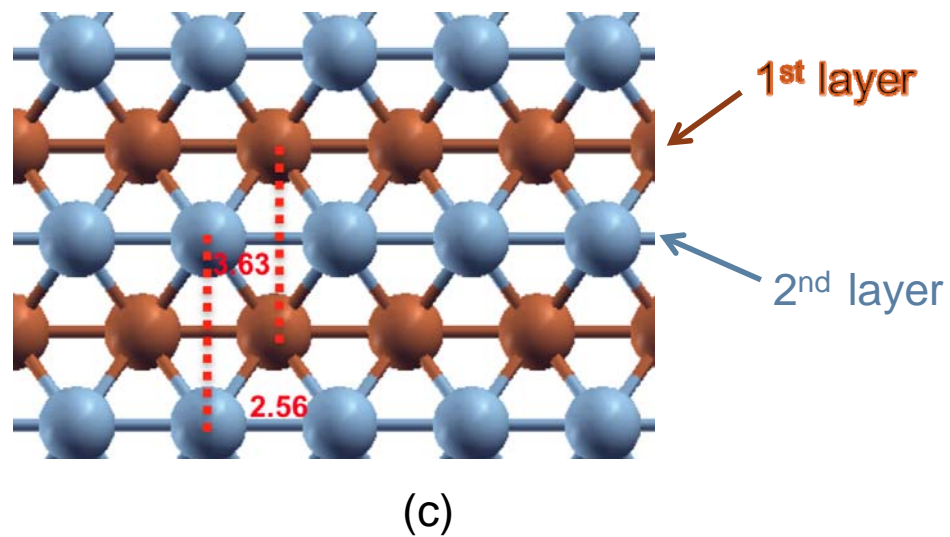


Figure A.8 DFT optimized surface layer geometry of Cu(110) slab. Cu atoms on top layer are denoted by bluish grey spheres, those in the second layer are denoted by brown spheres. Bond angles, bond lengths and some important distances (Å) are labeled.

Table A.2 Calculated bond lengths (Å), bond angles (degree) and surface adsorption energies (kcal/mol), E_{ads} , for furfural adsorption on Cu(110).

Geometry	E_{ads}	d_1	d_2	d_3	d_4	d_5	d_6	d_7	θ
gas		1.229	1.458	1.395	1.367	1.377	1.424	1.389	124.6
1	-2.77	1.283	1.420	1.410	1.428	1.413	1.406	1.410	123.9
2	-4.84	1.283	1.438	1.389	1.369	1.382	1.421	1.394	122.7
3	-7.38	1.249	1.438	1.392	1.366	1.379	1.422	1.392	125.6
4	-5.07	1.255	1.434	1.398	1.373	1.375	1.423	1.395	128.3
5	-5.07	1.259	1.436	1.392	1.366	1.380	1.418	1.398	126.4

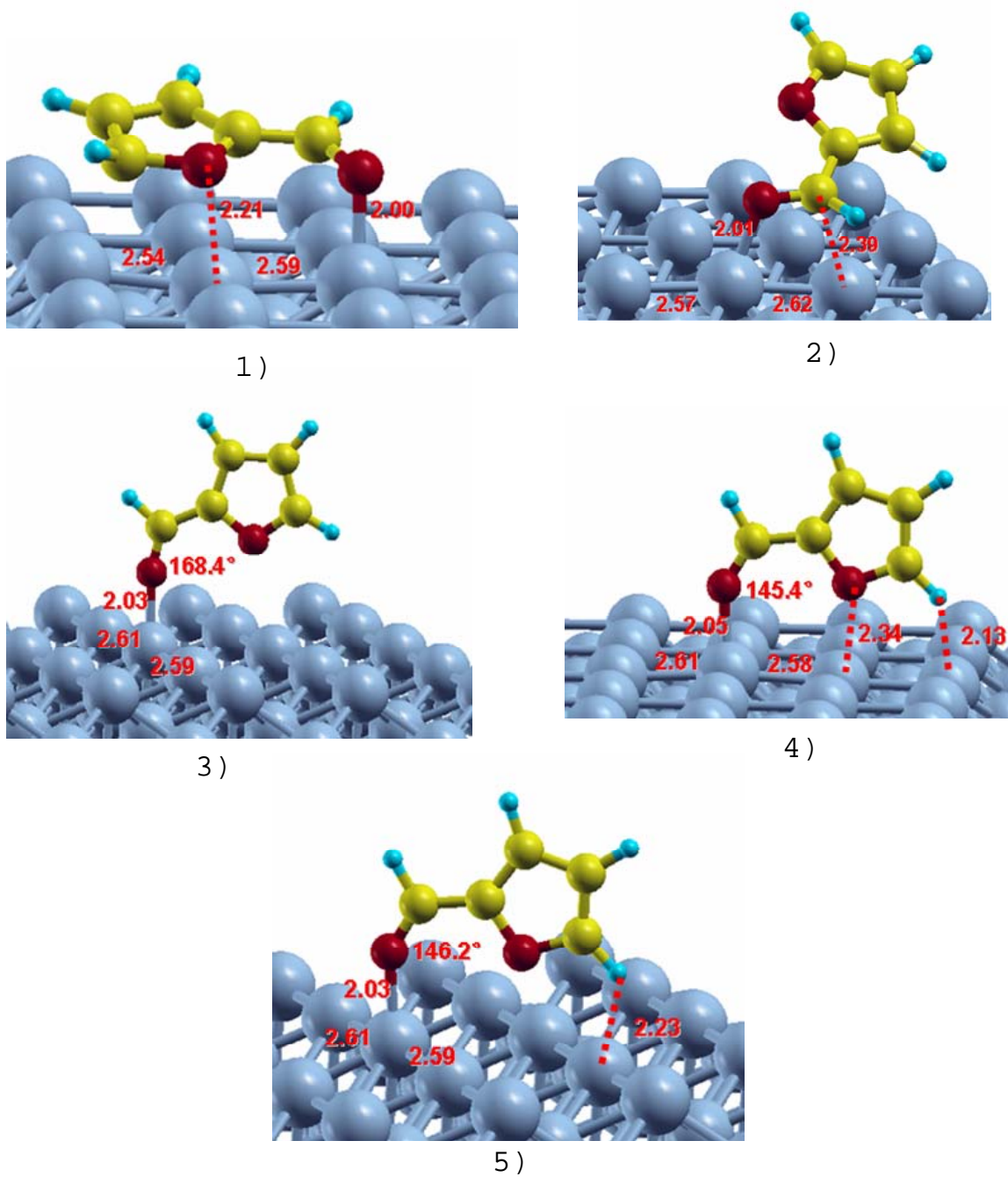


Figure A.9 Optimized geometries for adsorption configuration on Cu(110). The distances shown in the figure are in Å.

Analogous to the adsorption on Cu(111), the adsorption configurations can also be roughly divided into parallel, carbonyl and perpendicular modes. We select five typical geometries to examine their respective adsorption behavior on a low coverage Cu(110) surface (1/25ML), including one parallel configuration, one carbonyl adsorption configuration, and three perpendicular configurations.

The adsorption of furfural is stable for all five configurations. The calculated adsorption energy varies from -2.77 kcal/mol to -7.38 kcal/mol, which are stronger than those on the Cu(111) surface. The geometric parameters are summarized in Table A.2: a longer C=O bond (d_1) and a shorter C-C bond (d_2), primarily arising from the carbonyl O-surface interaction, are found in the adsorbed furfural molecule. In the parallel-ring configuration, the furan ring has the closest distance to the surface, corresponding to the weakest binding strength on Cu(110) ($E_{ads} = -2.77$ kcal/mol), in line with the repulsion effects seen in the case of Cu(111). The adsorption, however, is still stronger than the parallel-ring mode on Cu(111), because less Cu atoms are involved in the interaction with the aromatic ring on the (110)

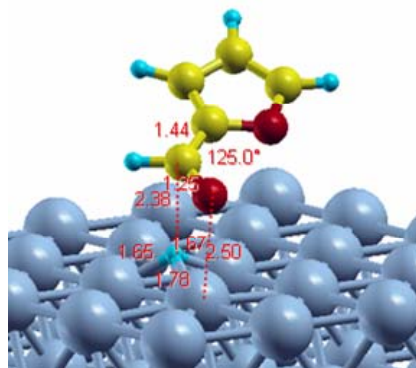
surface. The distortion of the ring structure is also observed and the general trend is similar to that on Cu(111), with elongated bond lengths d_3 , d_4 , d_5 , and d_7 , and a shortened bond length d_6 . Comparing with the carbonyl adsorption on Cu(110) and that on Cu(111), we notice significant difference between them: The carbonyl C atom shows a tendency to stay away from the Cu(111) surface; whereas it gets much closer to the Cu(110) surface. The C-Cu and O-Cu distances are 2.39 and 2.01 Å, respectively. The discrepancy can be attributed to the different structures of Cu(111) and Cu(110). The furfural molecule is inclined to keep a planar structure owing to the conjugation effect. Cu(110), as a sparse surface, is able to bind the carbonyl C atom and to keep the planar structure as well. The close-packed Cu(111) surface, however, cannot allow the carbonyl C adsorption and the planar furfural structure simultaneously. The calculated adsorption energy (-4.84 kcal/mol) indicates a little stronger binding strength on Cu(110). Among the perpendicular configurations, **3** is found to be the most stable one ($E_{ads} = -7.38$ kcal/mol), because of the relatively long distance of the ring atoms and the surface. In configurations **4** and **5** (not shown), the furan ring comes nearer to the (110) surface and the additional

adsorption sites weaken the binding strength due to the same reason described in the previous section.

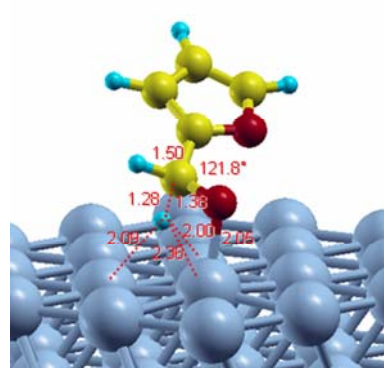
A.4 Hydrogenation of Furfural on Cu(111)

A mechanism for the hydrogenation of propanal and acetone has been proposed [12] in which hydrogenation of the carbonyl group first takes place on the C atom, leading to an alkoxy intermediate. In the following step, addition of a second hydrogen atom to the alkoxy intermediate yields an alcohol. An alternative mechanism is also possible [13,14] in which hydrogenation occurs in the first step at the carbonyl O atom with formation of a hydroxylalkyl intermediate, followed by addition of the second hydrogen atom to form furfuryl alcohol. In this work, first we examine both mechanisms on Cu (111) and aim at comparing their similarity and differences using configuration **8** (Table A.1).

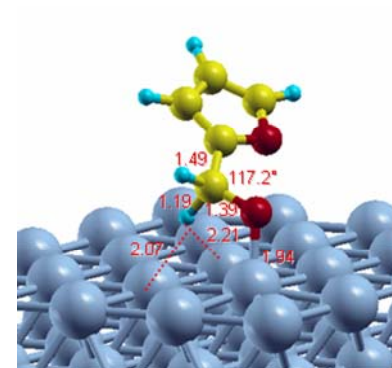
Mechanism (a)



Reactant

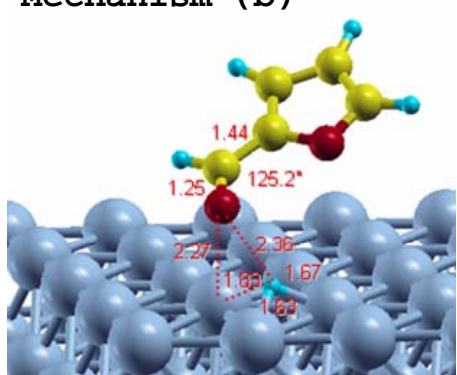


TS

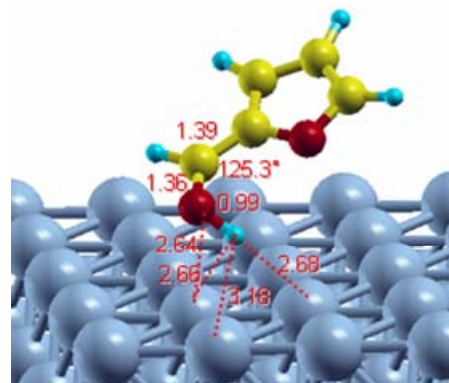


Intermediate

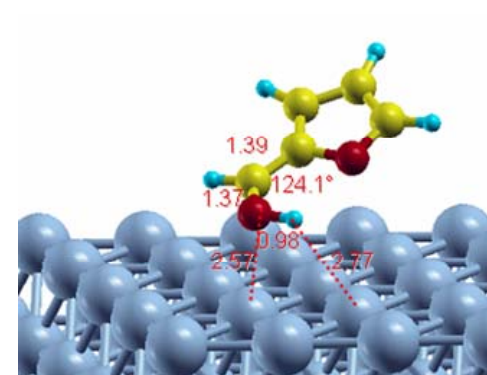
Mechanism (b)



Reactant



TS



Intermediate

Figure A.10 Optimized geometries of the adsorbed furfural molecules, transition states and intermediates Cu(111) via Mechanisms (a) and (b). The distances shown in the figure are in Å.

Dihydrogen dissociation yields adsorbed hydrogen atoms on the metal surface and the most stable adsorption site is determined as fcc hollow according to our calculations. We therefore suppose the hydrogen atoms are located on the fcc site initially. The detailed geometries of the adsorbed furfural molecules, their transition states and intermediates are given in Fig. 16 for mechanism (a) and (b). In Mechanism (a), a weak surface adsorption of furfural is observed: The distance between the surface and the carbonyl O is 2.50 Å. The adsorbed H atom located below the furfural molecule moves toward the carbonyl C atom in the process. The energy barrier of this step is 10.84 kcal/mol. The geometry of the transition state is similar to the alkoxy intermediate, suggesting an endothermic reaction. The bond length of C=O increases from 1.25 Å to 1.39 Å, indicating that the bond is significantly weakened and partially converted to a single bond. The alkoxy species is strongly adsorbed by the metal surface with a short Cu-O distance of 1.94 Å, as the unpaired electron on the O atom forms a bond with the Cu(111) surface.

Analogous to Mechanism (a), the formation of the hydroxylalkyl intermediate is also an endothermic reaction

in Mechanism (b), with a reaction energy of 7.38 kcal/mol. The surface species, however, moves apart from the Cu(111) surface during the process. This may be explained by the hydrogen addition to the carbonyl O atom reducing the surface-O interaction. Notably, the C-C bond decreases from 1.44 Å to 1.39 Å in the hydroxylalkyl intermediate, whereas the bond length increases in the alkoxy intermediate. The C-C bond in furfural is shorter than a normal C-C single bond due to the delocalization of π electrons. The conjugation effect ceases after the hydrogen atom addition to the carbonyl C in the alkoxy species, leading to a longer C-C bond. In the hydroxylalkyl species, the unpaired electron on the carbonyl carbon atom delocalizes to the aromatic ring and thus strengthens the C-C bond.

References

-
- [1] G. Kresse, J. Furthmüller, J. Phys. Rev. B 54 (1996) 11169
 - [2] G. Kresse, J. Hafner, J. Phys. Rev. B 49 (1994) 14251.
 - [3] G. Kresse, J. Hafner, J. Phys. Rev. B 48 (1993) 13115.
 - [4] G. Kresse, J. Hafner, J. Phys. Rev. B 47 (1993) 558.

-
- [5] G. Kresse, J. Furthmuller, *Comput. Mater. Sci.* 6 (1996)15.
- [6] G. Kresse, D. Joubert, *J. Phys. Rev. B* 59 (1999) 1758.
- [7] P. E. Bloechl, *J. Phys. Rev. B* 50 (1994) 17953.
- [8] J. P. Perdew, K. Burke,, M. Ernzerhof, *Phys. Rev. Letters* 77 (1996) 3865.
- [9] American Institute of Physics Handbook, 3rd ed.; McGraw-Hill: New York, 1972.
- [10] G. Mills, H. Jonsson, G.K. Schenter, *Surf. Sci.* 324 (1995) 305.
- [11] Jonsson, H.; Mills, G.; Jacobsen, K. W. *Nudged Elastic Band Method for Finding Minimum Energy Paths of Transitions*; World Scientific: Singapore, 1998.
- [12] G.M.R. van Druten, V. Ponc, *Appl. Catal. A: General* 191 (2000) 163
- [13] N.V. Pavlenko, A.I. Tripol'skii, G.I. Golodets, *Kinet. Katal.* 30 (1989) 1192
- [14] R. Alcala, J. Greeley, M. Mavrikakis, J.A. Dumesic, *J. Chem. Phys.* 116 (2002) 8973

APPENDIX B

DFT Calculation on Reaction Pathway on Pd(111) and PdFe(111) Surfaces (Calculation results from Wei An)

B.1 Density functional theory calculations

All DFT calculations were performed with the Vienna ab initio simulation package (VASP) [1,2]. A spin-polarized GGA PBE functional [3], all-electron plane-wave basis sets with an energy cutoff of 400 eV, and a projector augmented wave (PAW) method [4,5] were adopted. The Brillouin-zone of the $p(4\times 4)$ lateral supercell was sampled by $3\times 3\times 1$ k -points using the Monkhorst-Pack scheme [5]. First-order Methfessel-Paxton smearing [6] of 0.2 eV was employed in the integration to speed up the convergence. The conjugate gradient algorithm was used in the optimization. The convergence threshold was set 10^{-4} eV in total energy and 10^{-2} eV/Å in force on each atom. All reported energies were extrapolated to $k_B T = 0$ eV.

The Pd (111) surface was modeled by a three-layer slab with the bottom two layers fixed at their equilibrium bulk phase positions (calculated lattice constant = 3.952 Å), while the top layer was allowed to relax. The two

successive slabs were separated by a 10 Å vacuum region to ensure that the adsorbate (e.g., furfural, furfuryl alcohol, etc.) and the subsequent slab would not interact. The $p(4\times 4)$ supercell has a dimension of 11.178 Å \times 11.178 Å \times 14.563 Å to also ensure that the effect of adsorbate-adsorbate interactions is negligible.

The PdFe(111) alloy surface [i.e., Pd_{0.5}Fe_{0.5}(111), subscript is omitted thereafter for simplicity] was cleaved from optimized PdFe tetragonal unit cell (calculated lattice constant $a=b= 3.744$ Å $c=3.685$ Å) and was modeled in the same fashion as the pure Pd(111) surface. The calculated lattice constant is identical to those in a previous study employed CASTEP package [6]. The $p(4\times 4)$ supercell has a dimension of 10.050 Å \times 10.091 Å \times 14.114 Å. While it is not uncommon that surface reconstruction may occur on bimetallic clusters, the PdFe system is one in which surface segregation is less favored. For example, Ruban et al. [7] have shown that the surface segregation energies of PdFe alloys are unfavorable; positive energies of 0.3–0.7 eV suggest strong antisegregation. In addition, our calculations show that formation of "islands" of a single component on the same plane (i.e., Pd or Fe patches in the parallel

direction) is also thermodynamically unfavorable. The energy cost is 0.32 kcal/mol per surface atom for the formation of islands. Therefore, a uniform bulk alloy model is a good representation of the bimetallic clusters, experimentally verified by XRD. The adsorption energy (E_{ads}) in this work is defined as

$$E_{\text{ads}} = E(\text{adsorbate/slab}) - E_{\text{slab}} - E(\text{ads}),$$

where $E(\text{adsorbate/slab})$, E_{slab} , and $E(\text{ads})$ are the total energy of adsorbate/slab, clean surface, and gas-phase adsorbate molecules in one supercell.

B.2 Results and discussion

In our DFT calculations, we treated furfuryl alcohol as the reactant and explored furfural hydrogenolysis via the furfuryl alcohol route, i.e., C-OH bond scission followed by H-addition (mechanism (II) in Figure 6.6).

We first calculated the adsorption of furfural, furfuryl alcohol, methylfuran (i.e., hydrogenolysis product) and furan (i.e., decarbonylation product) on Pd (111) and PdFe(111) surface. The adsorption configurations resemble those in our previous study on Ni (111) and NiFe(111) surface [8], that is, under the conditions of low coverage of adsorbates, all favors a "planar" adsorption configuration (Figure B.1 and B.2). In particular, on PdFe(111) surface, it is observed that C1-O1 bond length is increased while C1-C2 bond length is decreased with respect to gas-phase furfural and furfuryl alcohol (Table B.1). And the binding strength of furfuryl alcohol on Pd (111) surface is largely due to the interaction with furan ring but on PdFe(111) surface, it is largely due to the interaction with O of C-OH bond where furan ring is repelled from the surface. As shown later on, this could give implication to the critical role

of Fe in promoting hydrogenolysis reaction while inhibiting decarbonylation reaction.

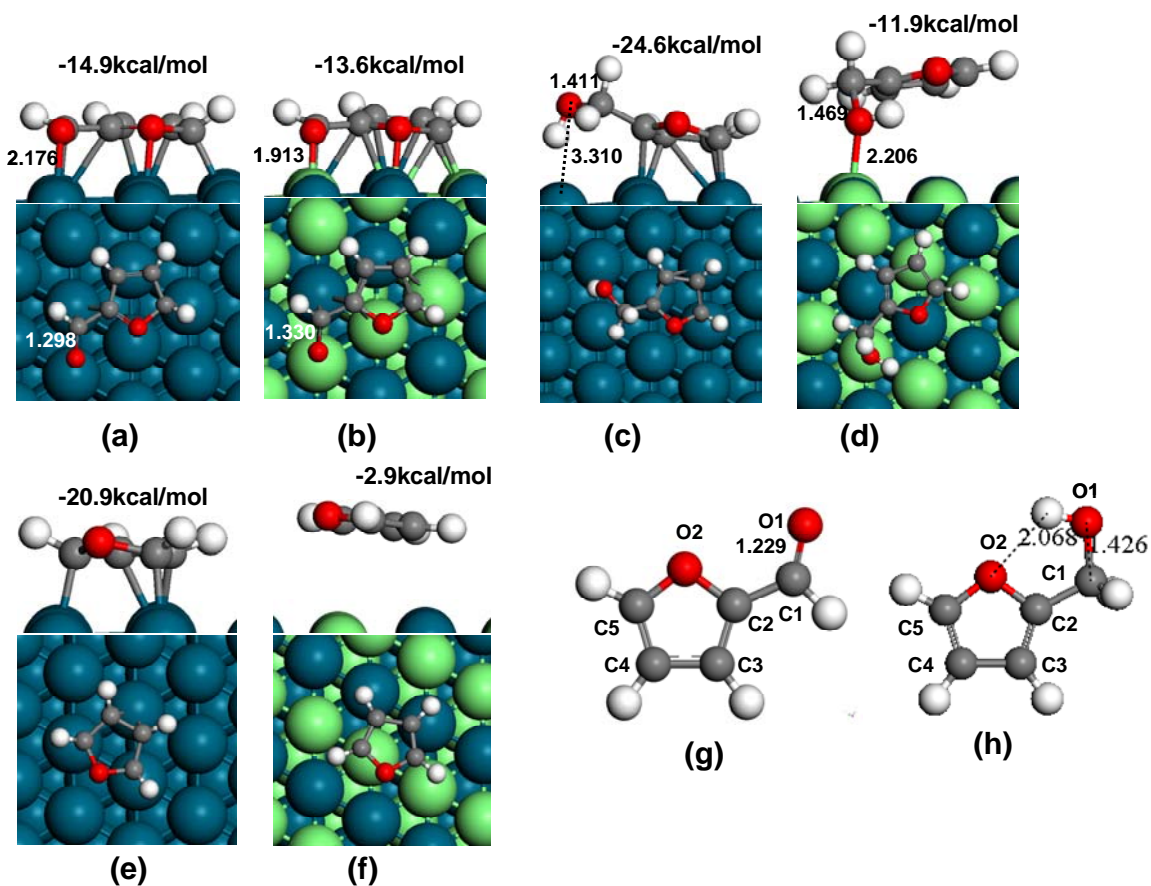
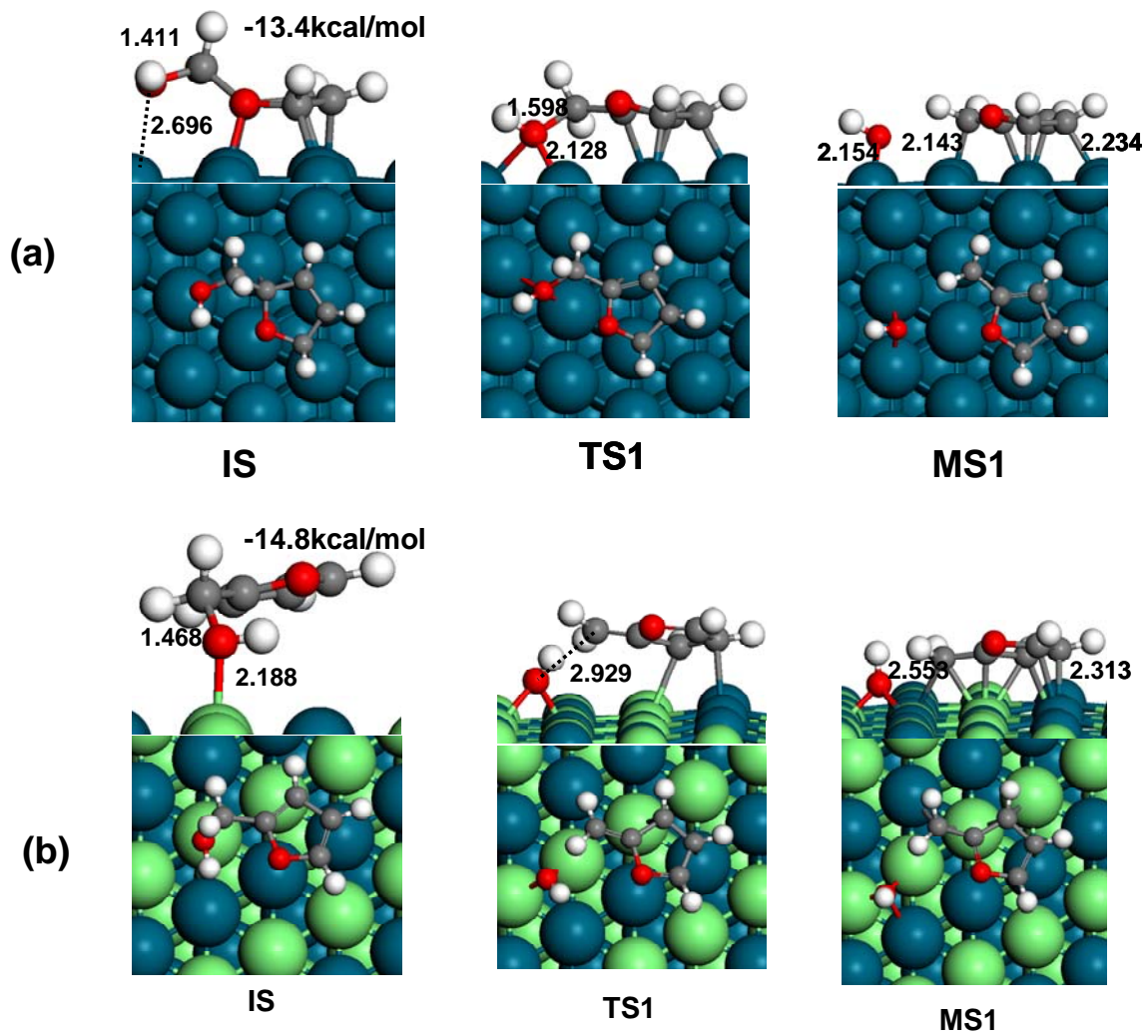


Figure B.1 Optimized adsorption structures of furfural, furfuryl alcohol, methylfuran, and furan on Pd (111) and PdFe(111) surface and corresponding adsorption energies. (a) FAL/Pd; (b) FAL/PdFe; (c) FOL/Pd; (d) FOL/PdFe; (e) Furan/Pd; (f) Furan/PdFe. Additional adsorption structures see IS and FS in Figure B.2. For comparison, optimized structures of gas-phase furfural and furfuryl alcohol are displayed in (g) and (h). Characteristic bond length and binding distance (in Å) as well as adsorption energy are labeled.

Table B.1 Comparison of characteristic bond lengths of furfural/furfuryl alcohol in gas-phase and adsorbed on Pd (111) and PdFe (111) surfaces. See Figure B.1 and B.2 for adsorption configurations and for the assignment of atoms. Adsorption energies (E_{ads}) are included.

$d(\text{\AA})$	Furfural			Furfuryl alcohol		
	Gas phase	Pd (111)	PdFe(111)	Gas phase	Pd (111)	PdFe(111)
C1-O1	1.229	1.298	1.330	1.426	1.433/1.411	1.468/1.469
C1-C2	1.448	1.448	1.429	1.501	1.522/1.509	1.478/1.478
E_{ads} (kcal/mol)	—	-14.9	-13.6	—	-13.4/-24.6	-14.8/-11.9

We then conducted TS search in elementary reaction of C-OH bond scission followed by H-addition. As shown in Figure B.2, an early TS was identified for C-OH bond scission reaction on Pd (111) surface but a late TS on PdFe(111) surface. The difference in activation energy barrier is significant, i.e., 36.0 vs 12.1 kcal/mol. In contrast, H-addition reaction has similar early TS on both Pd (111) and PdFe(111) surface, with activation barriers of 19.5 and 23.2 kcal/mol, respectively. Therefore, the rate determining step of hydrogenolysis reaction is C-OH bond scission on Pd (111) surface but H-addition on PdFe(111) surface (Figure B.3). Our DFT calculations support the experimental observations that no 2-methylfuran (i.e., hydrogenolysis product) was found on Pd catalyst but as primary product on PdFe catalyst.



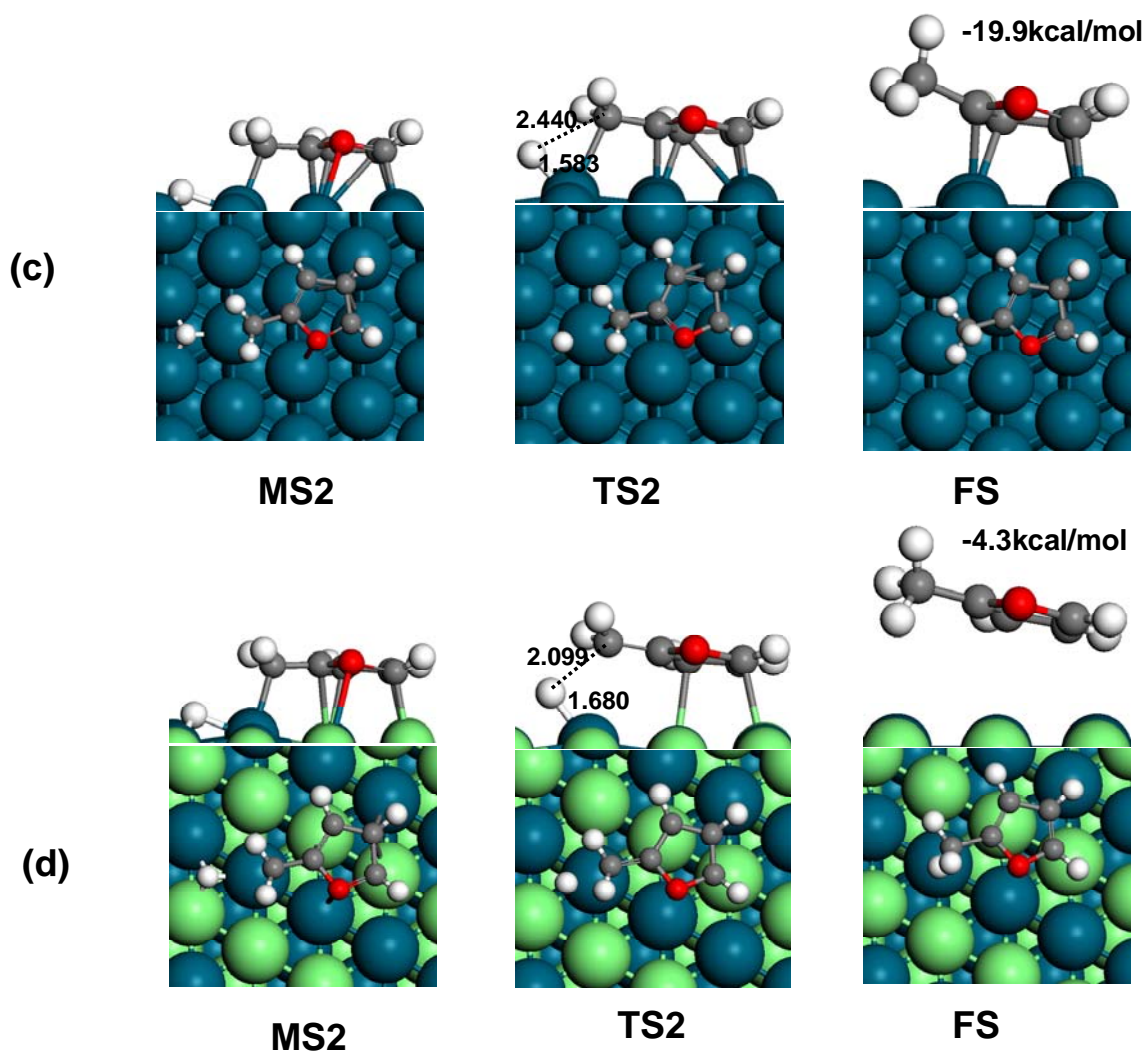


Figure B.2 Calculated structures along minimum-energy pathway for C-O bond scission (a and b) and H-addition (c and d) in furfural hydrogenolysis via furfuryl alcohol route on Pd (111) and PdFe(111) surface. IS: initial state; TS: transition state; MS:metastable state; FS: final state. Characteristic bond length and binding distance (in Å) as well as adsorption energy are labeled.

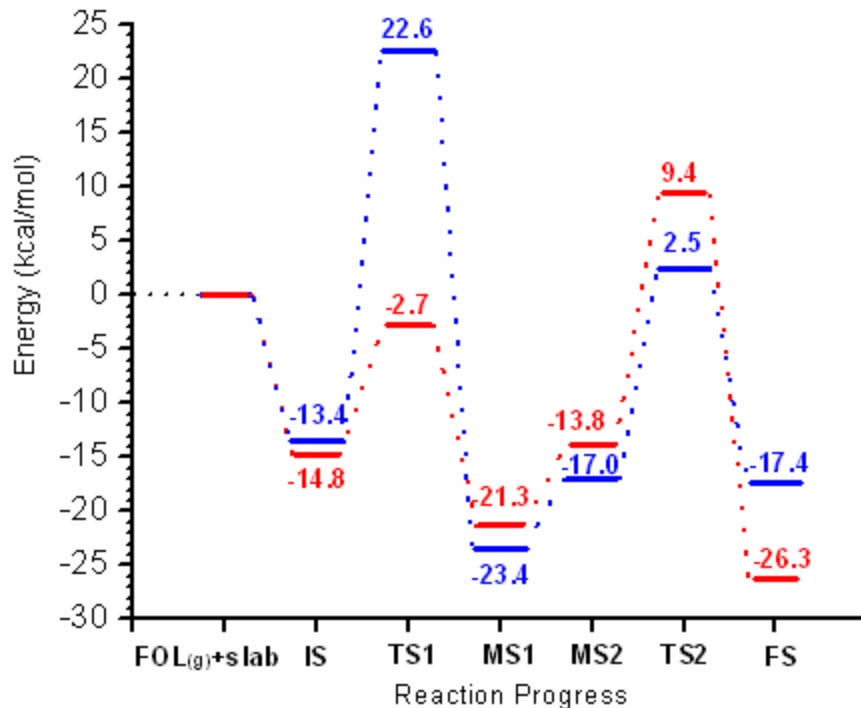


Figure B.3 Energy profile for furfural hydrogenolysis via furfuryl alcohol route on Pd (111) surface (blue, E_{a1}/E_{a2} = 36.0/19.5 kcal/mol) and PdFe(111) surface (red, E_{a1}/E_{a2} = 12.1/23.2 kcal/mol). The zero line represents the gas-phase furfuryl alcohol and a clean slab.

Figure B.4 shows calculated projected-DOS for (C1-O1) of furfuryl alcohol adsorbed on Pd(111) and PdFe(111) surface and one metal atom to which they are bound. It is observed that (C1-O1)-2p states are downshifted with respect to those of gas-phase furfuryl alcohol due to the electronic interactions with the metal surface. In particular, those on PdFe(111) surface are deeper below Fermi level than those on Pd(111) surface, indicating stronger electronic interactions of C1-O1 bond with

PdFe(111) surface compared to pure Pd (111) surface. This is consistent with much larger increase of C1-O1 bond length on PdFe(111) surface than on Pd(111) surface (see Table B.1). It is therefore expected that the cleavage of C-O bond in furfuryl alcohol is much easier on PdFe(111) surface than on Pd (111) surface. The beneficial effect of Fe can be attributed to its oxyphilicity and downshift of d-band center with respect to pure Pd(111) surface, i.e., -2.01 vs -1.56eV (see Figure B.1(d)), leading to enhanced electronic interaction with O of C1-O1 bond but repulsion against the furan ring in furfuryl alcohol, methylfuran, and furan.

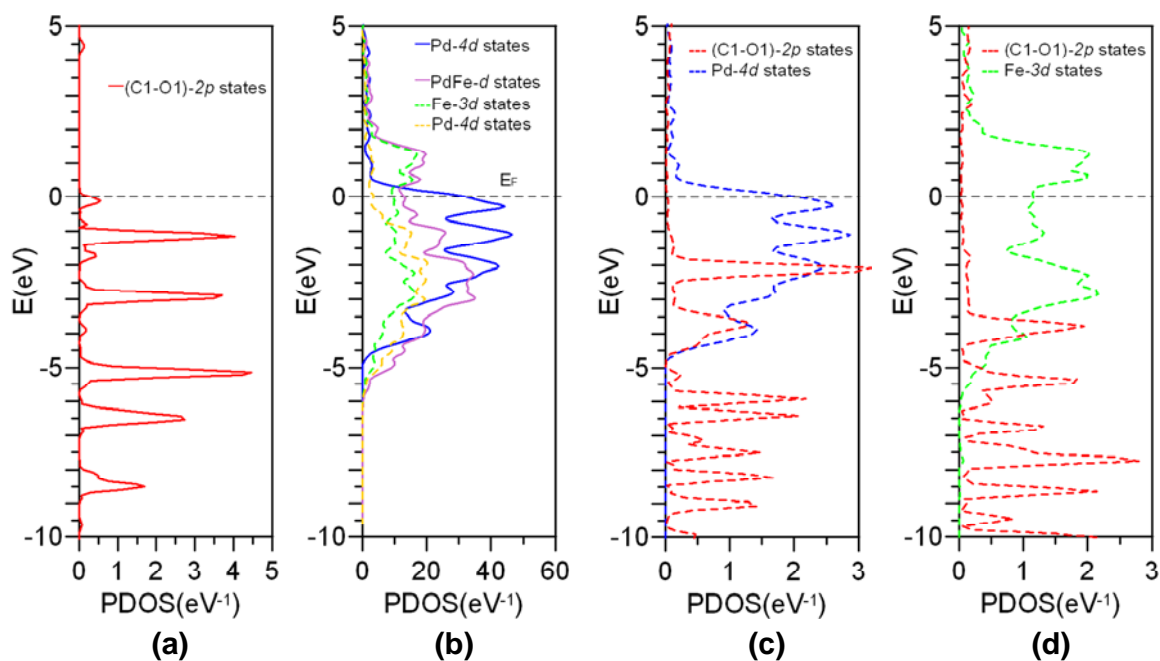


Figure B.4 Calculated PDOS for gas-phase FOL (a) clean surface (b) and FOL adsorbed on Pd(111) surface (c) and on PdFe(111) surface (d). Calculated d-band center for pure Pd(111) surface and PdFe(111) surface is -1.56 and -2.01eV, respectively.

It is well known that energetics, e.g., binding energy of a chosen species, is commonly used as a simple “descriptor” of activity for similar type of catalyst, which is governed by Brønsted-Evans-Polanyi (BEP) relation [9-12]. However, for a reaction involved complex reactant with multi-functional groups (e.g., C=O, C-OH, C=C in furfural and furfuryl alcohol) but only one specific reaction (e.g., selective cleavage of C-O bond) is of particular interest, such an energetics “descriptor” may

not be appropriate. It can be seen that the energy diagram in Figure B.3 does not follow BEP relation very well. Here, we propose that the change in bond length of a specific bond (with respect to gas phase molecule) can be used as a simple "descriptor" of activity when the activation of such a bond is of particular interest. By employing such a simple "descriptor", the trend of activity for similar catalyst can be predicted for a reaction involved complex reactants without explicit calculations on activation barrier.

References

- [1] Kresse, G.; Hafner, J. *Phys. Rev. B* 1993, 48, 13115-13118.
- [2] Kresse, G.; Furthmuller, J. *Phys. Rev. B* 1996, 54, 11169-11186.
- [3] Perdew, J. P.; Burke, K.; Ernzerhof, M. *Phys. Rev. Lett.* 1996, 77, 3865-3868.
- [4] Blochl, P. E. *Phys. Rev. B* 1994, 50, 17953-17979.
- [5] Kresse, G.; Joubert, D. *Phys. Rev. B* 1999, 59, 1758-1775.
- [6] Shao, M. H.; Liu, P.; Zhang, J. L.; Adzic, R. J. *Phys. Chem. B* 2007, 111, 6772-6775.
- [7] Ruban, A. V.; Skriver, H. L.; Norskov, J. K. *Phys. Rev. B* 1999, 59, 15990-16000.

- [8] Sitthisa, S.; An, W.; Resasco, D. E. *J. Catal.* 2011, 284, 90-101.
- [9] Logadottir, A.; Rod, T. H.; Norskov, J. K.; Hammer, B.; Dahl, S.; Jacobsen, C. J. H. *J. Catal.* 2001, 197, 229-231.
- [10] Norskov, J. K.; Bligaard, T.; Logadottir, A.; Bahn, S.; Hansen, L. B.; Bollinger, M.; Bengaard, H.; Hammer, B.; Sljivancanin, Z.; Mavrikakis, M.; Xu, Y.; Dahl, S.; Jacobsen, C. J. H. *Journal of Catalysis* 2002, 209, 275-278.
- [11] Cheng, J.; Hu, P. *J. Am. Chem. Soc.* 2008, 130, 10868-10869.
- [12] Cheng, J.; Hu, P.; Ellis, P.; French, S.; Kelly, G.; Lok, C. M. *J. Phys. Chem. C* 2008, 112, 1308-1311.

APPENDIX C

Conversion of Furfural over Pd/TiO₂

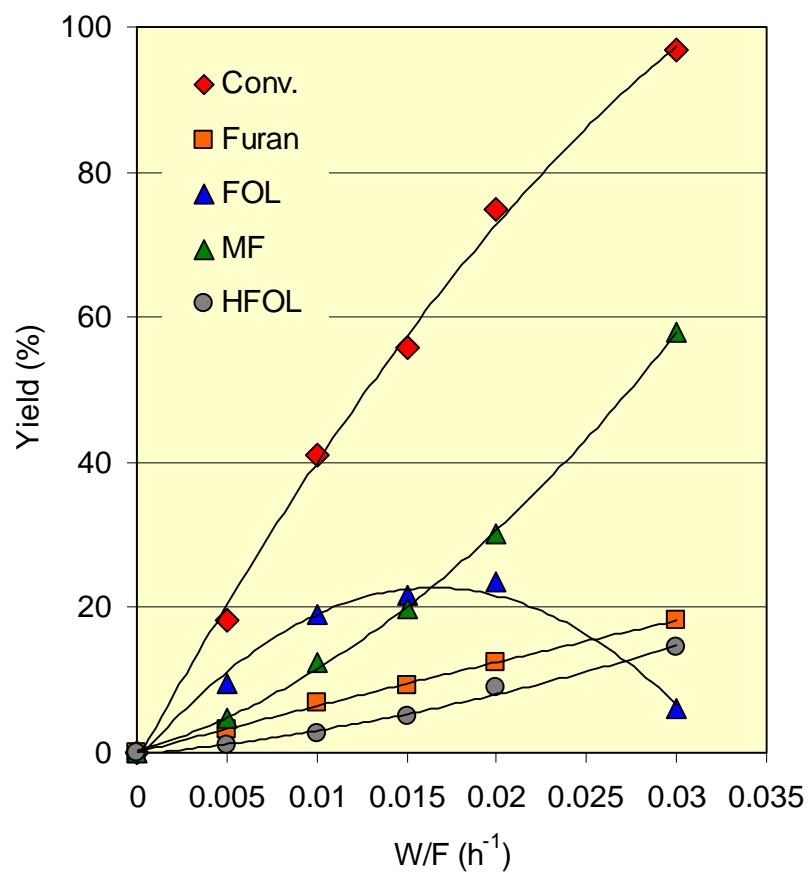


Figure C.1 Yield of products as a function W/F from the conversion of furfural over 1%Pd/TiO₂. Reaction condition: Temp. = 250°C, H₂/Feed ratio = 25, pressure = 1 atm

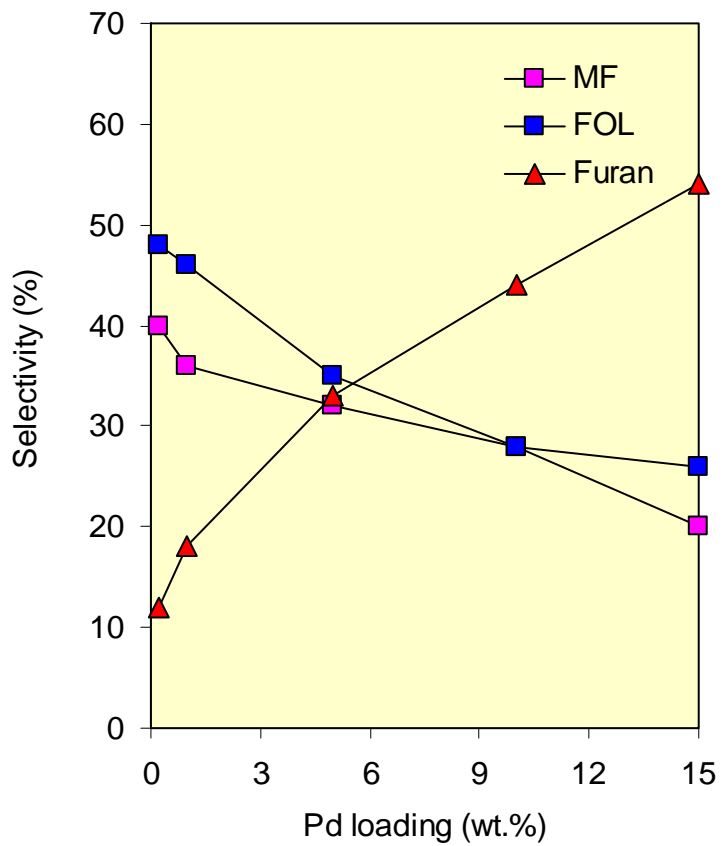


Figure C.2 Selectivity of products (conv. ~80%) as a function of Pd loading from the conversion of furfural. Reaction condition: Temp. = 250°C, H₂/Feed ratio = 25, pressure = 1 atm

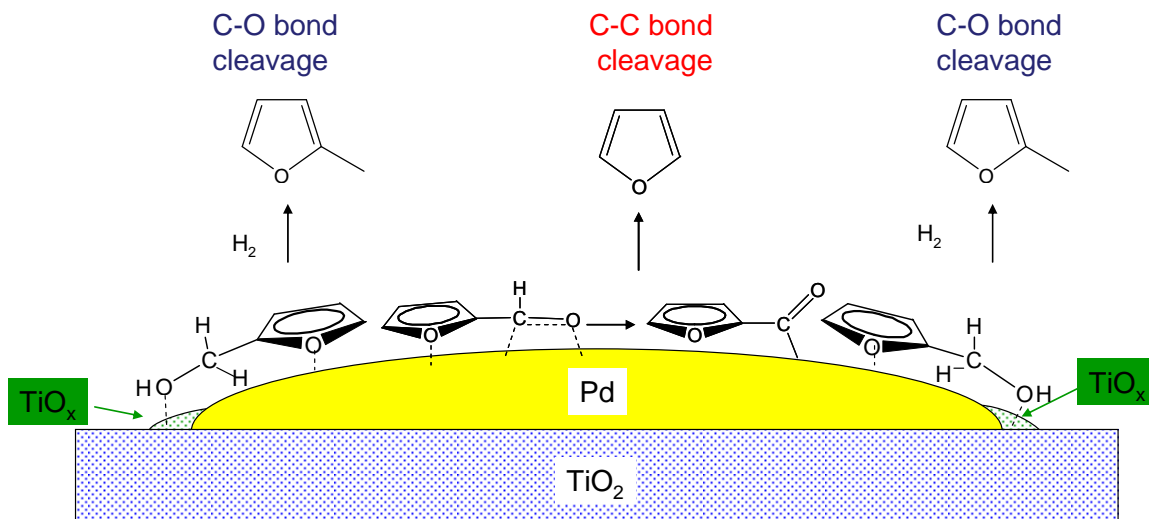


Figure C.3 Proposed reaction mechanism for conversion of furfural over Pd/TiO₂ catalysts

Comments:

As shown in chapter 6, it is clearly seen that the conversion of furfural over Pd/SiO₂ yields primarily furan via decarbonylation and shows no formation of 2-methylfuran. The results reported here suggest that monometallic Pd promotes much more C-C scission reactions of furfural compared to C-O scission reactions since we can observe a relatively high yield of furan and no formation of 2-methylfuran which could be a product derived from C-O hydrogenolysis of furfuryl alcohol.

As shown in Figure C.1, a remarkable change in product selectivity is observed over 1%Pd/TiO₂ catalyst. It is clear that the main products from the reaction of furfural over 1%Pd/TiO₂ catalyst at high W/F is 2-methylfuran which is not observed over 1%Pd/SiO₂. The observed formation of 2-methylfuran seems to be catalyzed by TiO_x sites at metal-support boundary (see Figure C.3). However, more catalyst characterization is needed to confirm the presence of this surface species.